Summer 8-15-2022

Fate of metals in presence of minerals and mineral-organic assemblages

Neha Sharma
Washington University in St. Louis

WASHINGTON UNIVERSITY IN ST. LOUIS

McKelvey School of Engineering
Department of Energy, Environmental and Chemical Engineering

Dissertation Examination Committee:
Daniel Giammar, Chair
Alexander Bradley
Jeffrey Catalano
Kimberly Parker
Yinjie Tang

Fate of Metals in Presence of Minerals and Mineral-Organic Assemblages

by

Neha Sharma

A dissertation presented to
the McKelvey School of Engineering
of Washington University in
partial fulfillment of the
requirements for the degree
of Doctor of Philosophy

December 2022
St. Louis, Missouri

Table of Contents

List of Figures

List of Tables

Acknowledgments

Writing the dissertation, I look back to the long journey of my Ph.D. and recall the names of the individuals who provided assistance, encouragement, and guidance, and without whom I would not have succeeded. I am very grateful to those people who have given me so much of their time, love, and energy.

First and foremost, I would like to express my gratitude to my advisor Dr. Daniel Giammar for his valuable guidance, consistent support, and insightful suggestions that have helped me in conducting my research in an efficient and planned way. His immense knowledge and critical thinking have helped me in improving my research outlook. I thank him for his kind gesture to accept me in his group in the middle of the year and for supporting my decision to continue my research at Washington University in St. Louis. I am extremely thankful to him for providing me with many collaboration opportunities, which broadened my research horizons and helped me secure a wonderful postdoctoral position. I cannot have imagined a better Ph.D. advisor than him, and I can never forget the exciting and enriching experience under his guidance.

I would also like to thank Dr. Jeffrey Catalano for providing me amazing opportunities to work on collaborative projects. I thank him for helping me identify interesting research questions in our collaborative project and for his wonderful discussions which improved the impact of my research. His constructive feedback on my manuscripts helped me improve their quality substantially. His vigor towards research motivated me to pursue topics in the field of environmental geochemistry.

I also express my gratitude towards Dr. Kimberly Parker for her great mentoring during my Ph.D. Through a collaborative project with her student Anamika Chatterjee, I got a chance to use

my skills in organic chemistry which was relatively a new field for me. I am thankful for her to be a part of my committee and for her insightful suggestions during my proposal defense and annual review meetings. I really appreciate her support during my search for the postdoctoral position.

I would also like to thank my committee members, Dr. Alexander Bradley and Dr. Yinjie Tang for their valuable suggestions during my proposal defense and annual review meetings. I would also like to thank Dr Fortner and Anushree Ghosh for helping me in synthesizing rhamnolipid-coated iron oxide nanoparticles in their lab. I would also like to thank our collaborators Dr Elaine Flynn and Dr Jinshu Yan from Earth and Planetary Sciences for helping me in characterizing the samples collected from different sites.

I must express my sincere gratitude to Dr. Sanmathi Chavalmane at Nano Research and Environmental Facility for training me on the sophisticated instruments. I would also like to thank the administrative staff at EECE for taking care of all the administrative requirements and documentation related to graduate studies and finances. They did a commendable job for the department, especially during the COVID-19 outbreak.

I thank the McDonnell International Scholars Academy for funding my fellowship during my doctoral research. I thank the Department of Energy (DOE) for funding major portions of my thesis research aimed at understanding the bioavailability of trace metals in natural aquatic systems by evaluating their interactions with minerals and organic matter.

Being a graduate student during COVID-19 period, the sudden lockdown made this journey difficult at times. Thus, I sincerely thank my small group of friends Yashika, Sukrant, Weiyi, Rohit, Priya, Girish, Anshuman, Nishit, and Piyush, who were always there for me during tough times. I would always cherish the weekend game nights and potlucks with them.

A positive working environment makes the job easier. I thank my lab mates and friends, Anushka Mishrra, Anshuman Satpathy, Elmira Ramazanova, Weiyi Pan, Xicheng He, Yao Ma, Yeunook Bae, and Yihang Yuan for maintaining a positive work attitude and for their constant motivation. They always cared for my well-being and were always eager for discussions. I loved talking to them about their amazing culture and foods. I will always be grateful for this lifelong friendship.

In the end, I would like to thank my parents and brother for their continuous love and support. They always believed in me in every phase of my life. They were always there to enjoy my successes and to motivate me during hard times.

Finally, a very special thanks to my husband and best friend Shubham for his unconditional love and support. He always motivated me during the ups and downs of my PhD journey. He ensured that I remained motivated throughout the research journey and postdoctoral position search. He celebrated my achievements with even more enthusiasm than I. I am lucky to find a perfect partner during my Ph.D. journey, and I cannot imagine walking this journey without him.

Neha Sharma

Washington University in St. Louis

December 2022

Dedicated to my family

ABSTRACT OF THE DISSERTATION

Fate of Metals in Presence of Minerals and Mineral-Organic Assemblages

by

Neha Sharma

Doctor of Philosophy in Energy, Environmental and Chemical Engineering

Washington University in St. Louis, 2022

Professor Daniel Giammar, Chair

Metals can enter aquatic systems from natural and anthropogenic processes associated with weathering, sediment re-suspension, industrial activities, and atmospheric deposition. Metals pose health and environmental risks at high concentrations due to their potential toxicity and bioaccumulation, but many trace metals also serve as essential micronutrients for biogeochemical processes in natural aquatic systems. Biogeochemical processes such as methanogenesis, denitrification, and mercury methylation require transition metals such as nickel (Ni), cobalt (Co), copper (Cu), and molybdenum (Mo) for completion. These biogeochemical processes can be substantial contributors of greenhouse gases, such as methane (CH_4) and nitrous oxide (N_2O), into the atmosphere. The behavior, mobility, and bioavailability of metals in water systems are controlled by their interactions with mineral phases and mineral-organic assemblages. Understanding the reactivity of metals with minerals and organic moieties will not only help in developing effective removal techniques but will also aid in developing robust fate and transport models to predict metal mobility in environmental systems. The knowledge of how metals reactivity affects their bioavailability in environmental systems can be important in improving the

accuracy of ecosystem models to estimate greenhouse gas emissions from natural landscapes. The dissertation pursued four main objectives to understand dominant reaction mechanisms controlling metals mobility in natural and engineered systems: (i) to optimize the reaction conditions for removing uranium from water systems by using synthesized biosurfactant-coated iron oxide nanoparticles, (ii) to elucidate the factors governing the fate of trace metals added in dissolved form to soils and sediments collected from three different natural aquatic systems, (iii) to determine the role of available Cu in a biogeochemical process in natural aquatic systems, and (iv) to understand the mobility behavior of trace metals from wetland soils and stream sediments upon fluctuating redox conditions.

Based on tunable properties, engineered nanoparticles hold significant promise for water treatment technologies. Motivated by concerns regarding toxicity and non-biodegradability of some nanoparticles, we explored engineered magnetite (Fe_3O_4) nanoparticles with a biocompatible coating. These were prepared with a coating of rhamnolipid, a biosurfactant primarily obtained from *Pseudomonas aeruginosa*. By optimizing synthesis and phase transfer conditions, particles were observed to be monodispersed and stable in water under environmentally relevant pH and ionic strength values. The rhamnolipid-coated iron oxide nanoparticles (IONPs) showed high sorption capacities for U(VI) removal under different pH and dissolved inorganic carbon concentrations. Equilibrium sorption behavior was interpreted using surface complexation modeling (SCM). Two models (diffuse double layer and non-electrostatic) were evaluated for their ability to account for U(VI) binding to the carboxyl groups of the rhamnolipid coating as a function of the pH, total U(VI) loading, and dissolved inorganic carbon concentration. The diffuse double layer model provided the best simulation of the adsorption data and was sensitive to U(VI) loadings as it accounted for the change in the surface charge associated with U(VI) adsorption.

Natural aquatic systems can act as a sink for trace metals through adsorption, precipitation, and complexation. We conducted batch experiments under anoxic conditions on soils and sediments collected from three different natural aquatic systems to understand their response to influxes of dissolved Cu, Ni and Zn. X-ray absorption spectroscopy indicated that the speciation of the freshly added metals taken up by the solids differs substantially from the speciation of the metals originally present in unamended samples. Cu speciation was dominated by sulfides at low loadings (1 μmol/g), whereas complexation to thiol groups and formation of metallic Cu governed speciation at high loadings (10 μmol/g). For Ni and Zn, adsorption to mineral surfaces and organic matter governed their speciation in materials from most sites. Our findings imply that geochemical processes controlling trace metal speciation may vary considerably with metal loading in different natural systems.

Laboratory studies of pure cultures have highlighted that the availability of Cu, required for the multicopper enzyme nitrous oxide reductase, can limit nitrous oxide (N_2O) reduction during denitrification. However, in natural aquatic systems, the role of Cu in controlling denitrification had not been well understood. Our study indicated that natural systems with background Cu concentrations below or around geological levels (40 - 280 nmol g^{-1}) may lack sufficient bioavailable Cu to carry out the conversion of N_2O to nitrogen (N_2). By providing Cu at dissolved concentrations of 10-300 nM, the conversion of N_2O to N_2 can be enhanced substantially. Our results indicated that including Cu bioavailability in ecosystem models could improve the accuracy of estimates of N_2O emissions from natural landscapes.

Wetland soils and hyporheic zones of stream beds undergo fluctuating redox conditions due to microbial activity, varying water saturation levels, and nutrient dynamics. With fluctuating redox conditions, trace metals can be mobilized or sequestered in response to changes in iron and

sulfur speciation and the concentrations and lability of organic carbon. We conducted systematic studies to examine the effect of redox fluctuations on samples collected from a riparian wetland and a stream. Water-saturated soils and sediments were incubated under three cycles of anoxic-oxic conditions (τ_{anoxic}:τ_{oxic} = 3) spanning 24 days to observe the change in dissolved and bioavailable metal concentrations. We observed that the trace metal dynamics in microcosms with materials from natural environments under events of redox fluctuations is strongly coupled to solid-phase speciation of the trace metals and the redox status of the recent past. This study illustrated that different trace metals display distinct bioavailability patterns during redox fluctuations in soils and sediments.

The information gained from the research projects improved our understanding of metal interactions with engineered nanoparticles and soils and sediments from natural aquatic subsurface systems. We believe that with effective optimization methods, biodegradable engineered materials can be successfully implemented in water treatment systems for the removal of potent contaminants using environmentally benign materials. The insights from the studies broadened our knowledge of the factors controlling trace metal speciation and bioavailability in natural systems. High association of trace metals to iron oxides, sulfide minerals, and dissolved organic matter decreased the bioavailability of trace metals in wetland soils and hyporheic zones of streams for biogeochemical processes.

Chapter 1: Introduction

1.1 Background and Motivation

Metals occur in all ecosystems, although their concentrations vary depending on their natural geologic conditions and surrounding human activities. In addition to metals intrinsically present from the geology of a particular system, metals can enter environmental systems from a wide variety of natural and anthropogenic sources, such as sediment re-suspension, mining operations, industrial processes, agricultural activities, and atmospheric deposition.[1,2] While metals can be toxic at high concentrations, some metals serve as essential micronutrients for biogeochemical processes.[1–6] Metal transport and availability in engineered and natural water systems depend on processes of adsorption/desorption, oxidation/reduction, dissolution/precipitation, and ligand complexation.[7–10] A comprehensive understanding of the interactions of metals with mineral surfaces and mineral-organic moieties is essential for developing effective remediation strategies and removal techniques. Insights into the speciation of metals and their bioavailability will also help advance understanding of the roles of metals in the biogeochemical cycling of nutrients.

1.1.1 Uranium Removal using Engineered Nanoparticles

Uranium contamination of water resources and terrestrial ecosystems is primarily associated with past mining and milling operations and waste disposal activities associated with the development of materials for nuclear energy and weapons.[11] Considering chronic health impacts due to chemical toxicity and potential radiotoxicity of uranium, the maximum contaminant level (MCL) for uranium in drinking water in the United States is set to 30 µg/L. However, groundwater concentrations in many regions across the United States exceed the MCL.[12] Therefore, techniques

that can effectively remove uranium from water sources without themselves contaminating the environment are necessary.

Uranium predominantly exists in oxidation states of IV and VI with U(VI) dominating in oxic environments. U(VI) is generally more mobile than U(IV). Depending upon the pH and dissolved inorganic carbon concentrations, U(VI) can exist as the uranyl ion (UO_2^{2+}) and aqueous complex complexes of uranyl with hydroxide and carbonate. Processes involving redox reactions, dissolution-precipitation, and adsorption-desorption reactions underpin uranium mobility in natural and engineered systems.[13]

Iron-containing minerals such as amorphous iron hydroxide, ferrihydrite, goethite, and hematite have been studied extensively for the adsorption of U(VI).[13,14] Recently, there has been an increase in the use of iron oxide nanoparticles (IONPs) in the fields of biomedical, health care and agriculture, due to their large specific surface area, tunable surface chemistries, biocompatibility and unique magnetic properties, for removal of U(VI).[15–19] IONPs, synthesized through the thermal decomposition method, are highly crystalline with uniform size and shape, but they are only dispersible in apolar solvents.[15,16,20,21] Various synthetic organic surface coatings, including lauric acid, stearic acid, sodium dodecylbenzenesulfonate, and polymers,[22–24] have been explored for stabilization of IONPs synthesized through non-hydrolytic routes and have shown tremendous potential in the removal of metals and metalloids from water systems.[25,26] However, these coatings can be toxic and non-biodegradable and hence their use in water treatment can introduce new environmental risks.

Recent studies have focused on using naturally derived coatings and biosurfactants for the stabilization of nanoparticles.[27–31] Biodegradability and lower toxicity of naturally available

coatings have encouraged their use in the removal of toxic contaminants, such as heavy metals, metalloids and organic compounds, from environmental systems.[32–34] Another emerging application of biosurfactants is their use in the stabilization of nanomaterials as they counter the attractive (magnetic and van der Waals) interparticle forces with repulsive steric or electrostatic forces and prevent aggregation of nanoparticles.[27,28,35] A well-known biosurfactant rhamnolipid, being a nontoxic and biodegradable surface modifier[29,36] may have less impact on the environment as compared to other synthetic coatings used for stabilizing IONPs. To develop an efficient environmental-friendly technique for removing uranium from water systems, we have explored the use of rhamnolipids to stabilize IONPS (possible mechanism of removal shown in Figure 1.1)

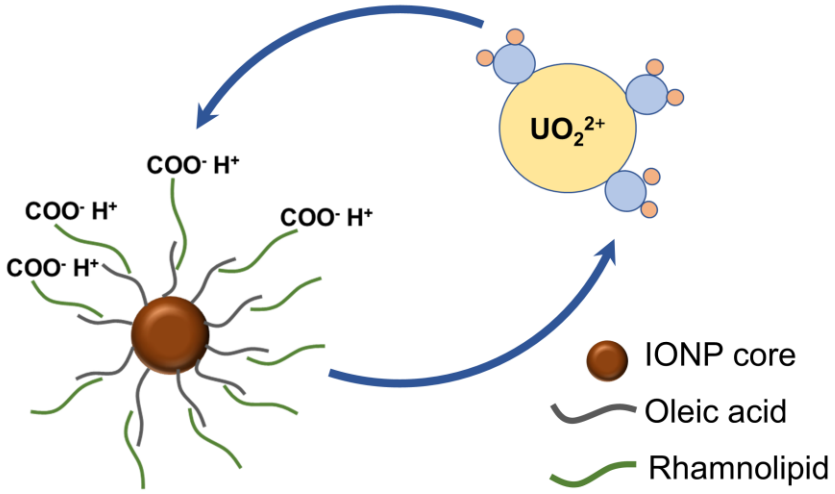

Figure 1.1: Interaction between uranium and surfactant-coated iron oxide nanoparticles

1.1.2 Trace Metal Role in Biogeochemical Cycling

Natural aquatic systems are active centers for carbon and nitrogen cycling making them substantial sources of the greenhouse gases methane (CH_4), and nitrous oxide (N_2O). The latest estimates indicate that 60-80% of emitted CH_4 comes from wetlands, and ~58% of emitted N_2O comes from soils with ~36% contribution from natural soils.[37] Understanding the biogeochemical processes

associated with CH_4 and N_2O emissions is essential for predicting future emission levels and developing mitigation strategies for their minimization.

The dominant biogeochemical processes responsible for CH_4 and N_2O emissions are methanogenesis and denitrification, respectively. Recent studies have shown that CH_4 and N_2O emission rates depend on soil properties, water chemistry, and temperature.[38–41] However, the roles that trace metal micronutrients (Cu, Ni, Co, and Mo) play in these emissions had been rarely investigated. Specifically, copper (Cu) and molybdenum (Mo) are essential for the transformation of N_2O[3,42,43], and free nickel (Ni) and cobalt (Co) are required for CH_4 formation.[3] The bioavailability of trace metal micronutrients is critical to the biogeochemical cycling of nutrients in subsurface systems.

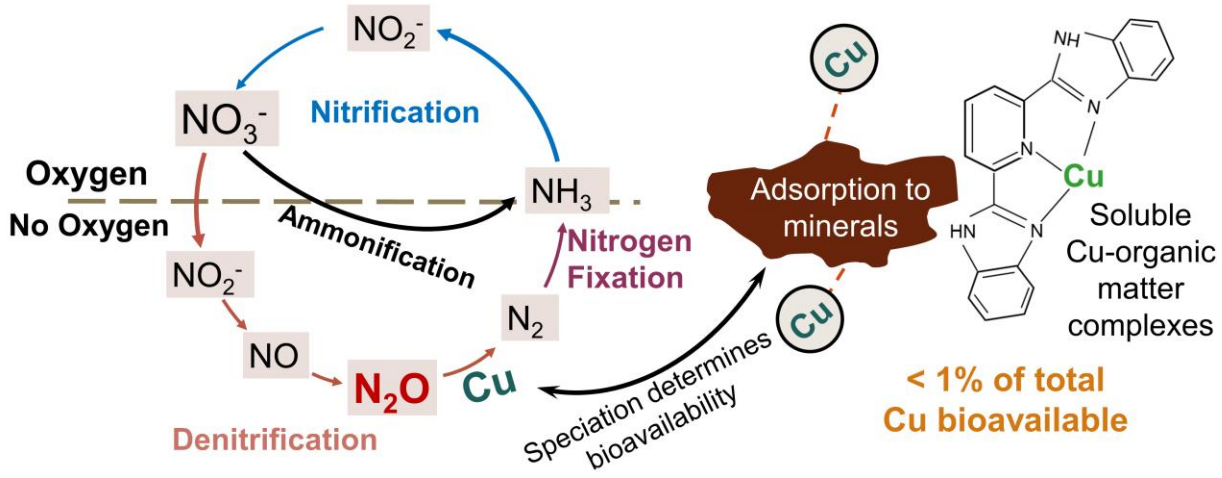

Figure 1.2: Role of Cu in N_2O emissions from natural aquatic systems and processes affecting Cu bioavailability

The scope of this dissertation is limited to the role of Cu in nitrogen cycling in natural aquatic systems. Denitrification is an anaerobic process carried out by heterotrophs to convert NO_3^- to N_2 through a series of intermediate steps producing NO and N_2O (Figure 1.2).[44] The global importance of this process lies in its contribution to global warming as a result of N_2O release in

the atmosphere due to the incomplete conversion of N_2O to N_2. Wetlands receiving high concentrations of nitrate exhibit high denitrification rates and therefore may be significant contributors to atmospheric N_2O.[45] The global warming potential of N_2O is 310 times higher than that of CO_2. Many studies have reported the impact of temperature, pH, presence of oxygen, nitrogen availability, and organic carbon content on denitrification in soil systems,[46,47] but the effect of trace metal limitations on completion of this process is not completely understood.

The reduction of nitrogen oxides to nitrogen is catalyzed by various metalloenzymes present in denitrifying bacteria.[42,48] The final step of denitrification, i.e. conversion of N_2O to N_2 (Figure 1.2), depends on a copper reductase enzyme.[42,48] Unavailability of Cu can decrease the percent conversion of N_2O to N_2 and can result in the accumulation of N_2O and its release into the atmosphere.[49] Recent laboratory studies on pure cultures have demonstrated that Cu limitation resulted in N_2O accumulation.[42,43] In natural aquatic systems, Cu availability will vary considerably with its speciation depending upon the type of mineral-phases present and the concentrations of dissolved organic matter.[7,50–52]. Thus, it becomes crucial to determine the role that Cu plays in nitrogen cycling in environmental systems.

1.1.3 Trace Metal Dynamics in Response to Redox Fluctuations

In soils and sediments, the bioavailability of metals is controlled by association with solid phases, such as minerals and organic matter, and by aqueous phase speciation.[7,50] Natural aquatic systems undergo fluctuating redox conditions due to microbial activity and varying water saturation levels. As conditions cycle between oxic/anoxic conditions, trace metals can be mobilized/sequestered in response to changes in iron and sulfur speciation and the concentrations and lability of dissolved organic carbon (Figure 1.3).[53,54] The exposure of anoxic sediments to oxic conditions favors the degradation of organic matter and the oxidation of sulfides, thus increasing the porewater

concentrations of any metals that had been associated with those phases (Figure 1.3).[55–58] Conversely, microbial reduction of Fe-Mn oxyhydroxides under anoxic conditions can mobilize metals associated with these mineral phases.[7,55,59,60] Microbial communities responsible for the biogeochemical processes may respond strongly to changing biogeochemical dynamics in these natural systems due to changes in metal availability patterns. Thus, it is imperative to elucidate the processes governing trace metal dynamics in natural environments to predict the extent of carbon and nitrogen cycling.

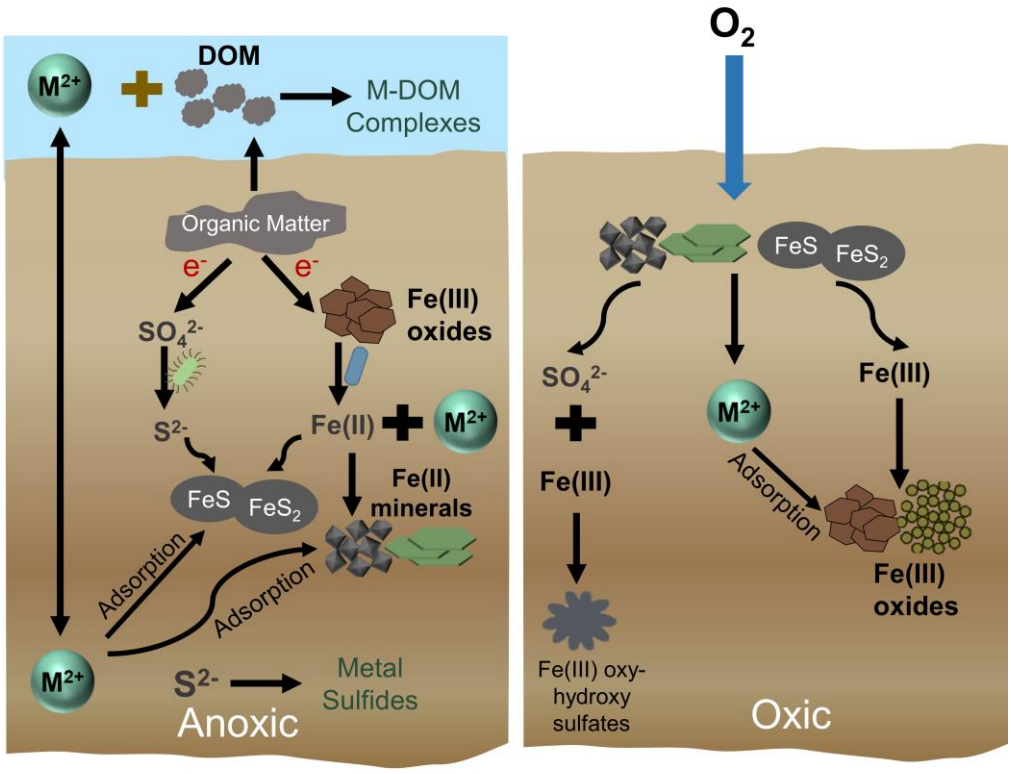

Figure 1.3: Schematic of dominant processes controlling metal mobilization in natural aquatic systems under redox fluctuations

1.2 Research Objectives

The dissertation sought to provide a detailed understanding of the mobilization/sequestration of metals in aquatic systems by studying their associations with natural/engineered minerals and organic matter. In this regard, I have divided my research into four main objectives schematically described in Figure 1.4.

Objective 1: Develop a predictive understanding of U(VI) adsorption to rhamnolipid-coated engineered IONPs

To achieve the outlined objective, we synthesized water-stabilized superparamagnetic magnetite nanoparticles using rhamnolipid, a biocompatible ligand. With the help of a phase-transfer technique, we optimized rhamnolipid concentrations required for stabilizing monodisperse iron oxide nanoparticles. Extensive characterization techniques, dynamic light scattering, transmission electron microscopy, and total organic carbon analysis, were used to determine the stability of the bilayer-coated nanoparticles. We evaluated the efficacy of this coating by using rhamnolipid-coated nanoparticles for U(VI) sorption under varying conditions of pH and dissolved inorganic carbon (DIC). Rhamnolipid-coated iron oxide nanoparticles demonstrated high efficiency to adsorb the contaminant U(VI) at environmentally relevant concentrations and aqueous chemistry.

Objective 2: To understand the relationship between the extents of trace metal uptake and their speciation in wetland soils and stream sediments

We selected three different natural aquatic systems- marsh wetland soils, riparian wetland soils, and stream sediments to determine the fate and the speciation of trace metals introduced to environmental systems in dissolved forms. Batch experiments were conducted with different trace

metals (Cu, Ni, and Zn) at varied loadings to obtain their uptake trends on different soils and sediments. We investigated trace metal speciation using X-ray absorption spectroscopy (XAS) to determine the major components associated with metal uptake at the selected sites at low and high loadings. This approach provided an understanding of the differences between the speciation of added metals and those originally present in the soils and sediments. This study suggested that the background speciation of trace metals in natural aquatic systems is a poor indicator of the speciation and lability of metals introduced to terrestrial aquatic systems from anthropogenic or natural sources.

Objective 3: To determine the effect of copper limitation on nitrogen cycling in wetland soils and stream sediments

Natural systems with background Cu concentrations below or similar to crustal abundances were selected to evaluate the role of Cu in denitrification. We conducted incubation experiments on samples collected from marsh wetlands, riparian wetlands, and stream sediments at three different conditions were studied: no Cu added (control), low Cu loading, and high Cu loadings. The different Cu loadings were selected based on preliminary Cu uptake experiments. We also developed a kinetic model to quantify the effect of Cu addition on N_2O conversion to N_2. We observed that conversion of N_2O to N_2 is substantially limited by low bioavailable Cu concentrations in control samples. The reduction rate of N_2O to N_2 was enhanced in Cu-amended systems. With the help of speciation modeling, we noted that the presence of dissolved organic matter in these water systems decreased the availability of Cu substantially which resulted in limited N_2O to N_2 conversion. Our study demonstrated that pristine natural aquatic systems may have incomplete reduction of N_2O to N_2 due to limited availability of Cu. Additionally,

incorporating the bioavailability of Cu in ecosystem models could improve the accuracy of estimates of N_2O emissions from natural landscapes.

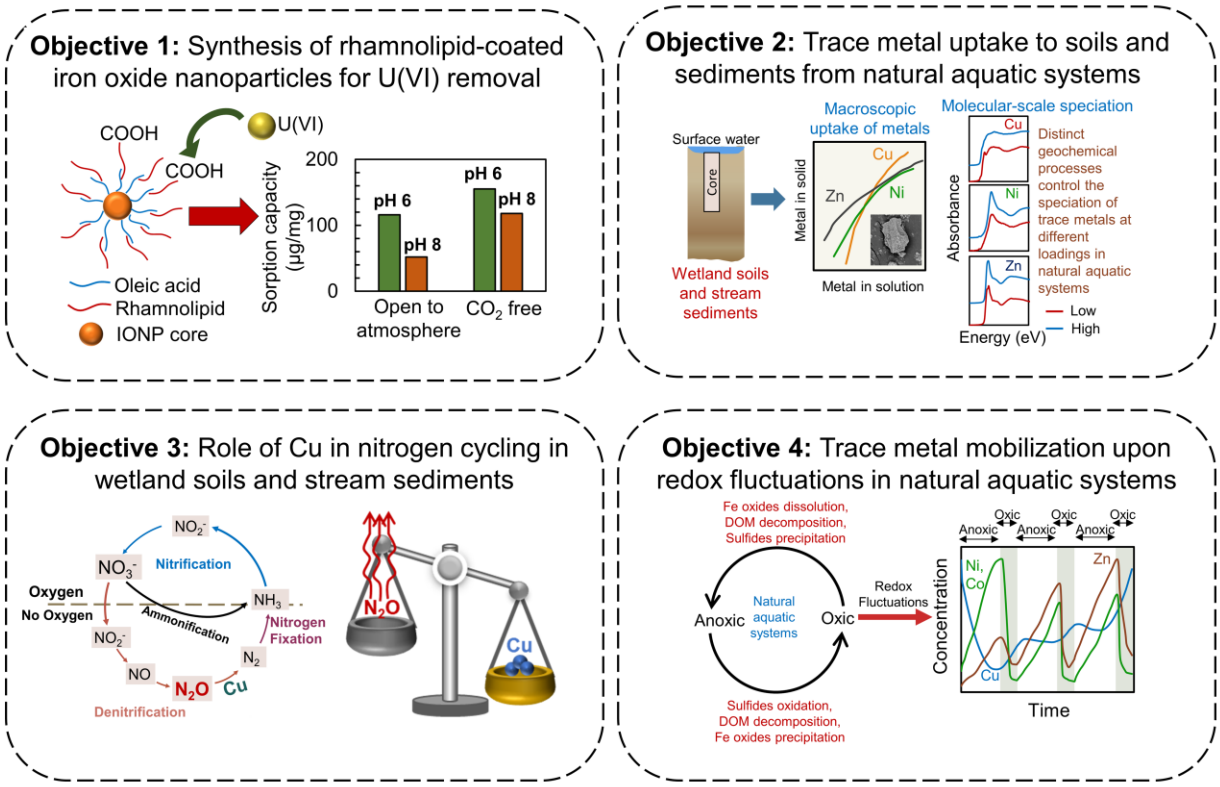

Figure 1.4: Overview of research objectives and their associated research tasks

Objective 4: Quantify variability in trace metal availability under fluctuating redox conditions

With fluctuating redox conditions, trace metals undergo speciation and mobility changes in response to transformations of iron and sulfur-bearing minerals, and organic matter. In order to understand metal mobility behavior under varying redox conditions, wetland soils and stream sediments were subjected to three alternating cycles of anoxic-oxic fluctuations over a time period of 24 days. We also monitored the change in the bioavailable concentrations of trace metals upon redox fluctuations by using in-situ passive samplers. We observed that the mobilization behavior

of trace metals in response to redox fluctuations varied between different systems due to inherent differences in solid-phase speciation of metals, mineral composition, sulfur contents, and organic matter concentrations.

1.3 Dissertation Outline

The dissertation presents work done to improve the understanding of interactions of metals with mineral surfaces and mineral-organic moieties in engineered and natural systems. With this enhanced understanding, we identify a path to developing an environmentally-benign way to remove U(VI) from water systems. Additionally, we obtained a deeper understanding of the roles that trace metals play in biogeochemical cycling in natural aquatic systems. The following four chapters describe the tasks performed toward achieving the objectives of the dissertation. Each chapter is self-contained containing an introduction, methodology, results, discussion, and conclusion sections. **Chapter 2:** outlines the systematic approach taken to synthesize biosurfactant-coated iron oxide nanoparticles which were subsequently tested for their efficiency to remove U(VI) from water systems. In this study, we explored a biosurfactant, rhamnolipid, as a coating for dispersing hydrophobic iron oxide nanoparticles in water, and the stability of these bilayer-coated nanoparticles was explored under a variety of pH and ionic strength conditions. Using batch experiments, we tested the impact of pH, initial loading of U(VI), presence and absence of dissolved inorganic carbon on the removal of U(VI) from water using bilayer-coated nanoparticles. The observed equilibrium partitioning was interpreted using surface complexation modeling to account for U(VI) binding to the carboxyl groups in the rhamnolipid. **Chapters 3, 4 and 5** discuss experiments conducted to understand the dynamics and role of trace metals in wetland soils and hyporheic zones at the base of streams. **Chapter 3:** indicates the experiments conducted to evaluate trace metal (Cu, Ni, and Zn) uptake behavior on soils and sediments under

varied loadings. The results were corroborated by X-Ray based characterization of solid-phases. **Chapter 4:** describes the incubation experiments conducted to understand the role of Cu in nitrogen cycling, especially the conversion of N_2O to N_2, in wetland soils and stream sediments. **Chapter 5:** presents laboratory-based incubation experiments conducted to understand the response of metal mobility to fluctuating redox conditions in soils and sediments. **Chapter 6:** provides the major conclusions from the thesis followed by direction for the scientific community to pursue research in the field of metal mobilization and fate in engineered and natural aquatic subsurface systems. The above five chapters are followed by a list of all the references cited in the dissertation.

There are six appendices attached to the dissertation. **Appendices A–D** contains supplementary information for Chapters 2 – 5, respectively. **Appendix E** includes the results of a field deployment of in-situ passive samplers to estimate the bioavailable concentrations of trace metals in stream sediments of East Fork Poplar Creek at Oak Ridge National Laboratory. These results helped us check the applicability of in-situ samplers for determining bioavailable concentrations of metals in systems containing metal contents similar to geological levels. The results also helped us determine that the majority of trace metals are bound strongly to the mineral phases and are not readily available for biogeochemical processes in the studied stream sediments.

Chapter 2: Rhamnolipid-Coated Magnetite Nanoparticles for U(VI) Sorption

This chapter has been published in – Sharma, N., Ghosh, A., Fortner, J. D., & Giammar, D. E. (2020). "Modeling performance of rhamnolipid-coated engineered magnetite nanoparticles for U (VI) sorption and separation." Environmental Science: Nano, *7(7), 2010-2020.*

2.1 Introduction

Uranium can be introduced into aquatic systems via a number of anthropogenic pathways, including discharge from mining and milling operations, leading to public health concerns.[61] Considering chronic health effects associated with uranium, the current U.S. EPA maximum contaminant level (MCL) for uranium in drinking water is 30 µg/L. Uranium predominantly exists at oxidation states of +IV and +VI, U(VI) being the more mobile form and the dominant one present under oxidizing conditions.[62] The fate of U(VI) in aquatic environments strongly depends on the pH, redox potential, presence of divalent cations, and dissolved inorganic carbon.[62,63] Processes involving redox, dissolution-precipitation and adsorption-desorption reactions underpin uranium mobility in natural and engineered systems.[13]

Strategies for removal of uranium under oxidizing conditions often rely on adsorption processes. Recently, a variety of nanomaterial adsorbents, including aluminium oxides, iron oxides, titanium oxides and graphene oxides have been developed and evaluated for their efficacy towards uranium removal from water systems.[26,64–74] Iron oxide nanoparticles (IONPs) are one of the promising materials for the removal of contaminants from water systems due to their large

specific surface area, tunable surface chemistries and potential biocompatibility.[15,16,64,74] A number of studies have focused on the use of magnetite nanoparticles for contaminant removal due to their unique magnetic properties which allow easy removal and collection from water systems by application of an external magnetic field.[15,16,22,69,72,73,75]

Synthesis of water-dispersible IONPs has been achieved by chemical co-precipitation, microemulsion and hydrothermal routes.[16] These methods produce poorly crystalline and aggregated nanoparticles. This has encouraged the use of non-hydrolytic routes (organic phase synthesis) for the synthesis of IONPs, allowing for reproducible and highly crystalline nanostructures with uniform size and shape.[15,16,76] Typically, nanoparticles obtained from these routes are stable in nonpolar solvents and are capped with nonpolar moieties (e.g. oleic acid) to lower surface energies and prevent aggregation.[15,16,76] Surface coatings reduce particle aggregation as they counter the attractive interparticle forces with repulsive steric or electrostatic forces.[35]

For successful application of IONPs dispersed in nonpolar solvents to water treatment, the outer hydrophobic coating needs to be modified to be hydrophilic.[15] Ligand exchange and ligand addition methods are used for surface modification of as-synthesized IONPs.[15,76] In the ligand exchange method, the original coating is replaced by the desired amphiphile or surfactant that has an affinity for both the nanoparticle surface and the water interface. In the case of ligand addition, a hydrophobic tail of the selected amphiphile interacts with the original coating while the hydrophilic tail is oriented towards the water, yielding a stable aqueous suspension of the nanoparticles.[15,24] Various synthetic organic surface coatings, including oleic acid, humic acid, stearic acid and polymers,[22–24,72,77,78] have been explored for stabilization of IONPs synthesized through non-hydrolytic routes. These stabilized IONPs have shown tremendous potential in the removal of metals and metalloids from water.[25,26,67,75] However, these coatings are often toxic or

non-biodegradable, and they may pose environmental risks if the particles are not retained in the treatment unit. Recent studies have explored naturally derived coatings and biosurfactants for the stabilization of the nanoparticles.[27,32,66,79–81] The addition of micro-algal exudate as a biosurfactant in the preparation of polyethene nanoparticles reduced their aggregation in the salt solutions.[82] The performance of nanoparticles for contaminant removal can also be significantly improved by the addition of naturally-derived coatings.[66,83] The use of chitosan in a nanocomposite with graphene oxide enhanced the sorption capacity for U(VI) removal.[83,84] Cyclodextrin-modified maghemite nanocomposites showed remarkable stability as no change in their efficiency for U(VI) removal was observed even after four cycles of adsorption/desorption.[72]

Biosurfactants are amphiphilic molecules produced by microorganisms to reduce interfacial tension in the process of utilization of various substrates. As compared to their synthetic counterparts, biosurfactants are typically less toxic and more biodegradable.[85,86] An emerging application of biosurfactants is in the stabilization of nanomaterials as they reduce the surface energy at the interface and prevent aggregation of nanoparticles.[36] Rhamnolipids are glycolipids (biosurfactants) produced primarily by *Pseudomonas aeruginosa* at relatively high concentrations extracellularly, and they consist of a rhamnose moiety and a 3-(hydroxyalkanoyloxy) alkanoic acid fatty acid tail.[32] Recent studies show that rhamnolipids act as an effective stabilizer for palladium-coated nanoscale zero-valent iron (nZVI) nanoparticles and prevent their aggregation.[27,35,87] Another study observed that the inclusion of rhamnolipid in the synthesis of chitosan nanoparticles improved their stability and monodispersity.[81] Rhamnolipids also enhanced soil deliverability and reactivity of nZVI for in situ remediation.[30] Rhamnolipids have also been used as capping agents in several studies for the synthesis of stabilized nanoparticles.[28,31,79–81,88] However, the potential of

rhamnolipids to stabilize magnetite nanoparticles had not previously been observed; consequently, the use of rhamnolipid-coated IONPs as adsorbents for metals is also unexplored.

Surface complexation modeling (SCM) is a robust approach to model the partitioning of sorbates between solid and solution phases as a function of pH, solute concentration, and ionic strength. The prediction of U(VI) adsorption on sorbents is confounded by complexities of U(VI) speciation under different dissolved inorganic carbon conditions.[13,14,62] In carbonate-containing systems, U(VI) adsorption to sorbents is affected by the formation of stable soluble U(VI)-CO_3 complexes at higher pH values.[13,14,65] SCM has been previously applied to engineered nanomaterials to model sorption of U(VI) over a wide pH range and different carbonate conditions.[26,65,89–92] As model parameters will be different for different adsorbents, we aimed to understand if SCM could interpret metal binding to IONPs coated with rhamnolipid. The model can also yield insight into the mechanism of U(VI) binding onto these rhamnolipid-coated IONPs.

In this work, we have explored rhamnolipids as potential biocompatible ligands for stabilizing superparamagnetic magnetite nanoparticles in water. The efficiency of this coating was then evaluated by using rhamnolipid-coated nanoparticles for U(VI) sorption under varying conditions of pH and dissolved inorganic carbon (DIC). The three primary objectives of the study were to (i) optimize conditions for coating as-synthesized magnetite nanoparticles with rhamnolipids for stabilizing them in water suspensions, (ii) evaluate the performance of rhamnolipid-coated IONPs for U(VI) adsorption under varying conditions of pH and carbonate, and (iii) develop a surface complexation model to interpret U(VI) adsorption performance onto these engineered nanoparticles.

2.2 Experimental Section

2.2.1 Materials and Methods

Iron(III) oxide (hydrated, catalyst grade, 30–50 mesh), oleic acid (technical grade, 90%), 1-octadecene (technical grade, 90%), sodium chloride (ACS reagent, 99.0%), magnesium chloride hexahydrate (ACS reagent, 99%), sodium hydroxide (ACS reagent 99.0%), sodium bicarbonate (ACS reagent 99.0%), sodium carbonate (ACS reagent 99.0%) and nitric acid (trace metal grade) were purchased from Sigma-Aldrich. Hexane, acetone, and ethanol were also purchased from Sigma-Aldrich and were used without purification. Rhamnolipid (90%) standard was purchased from AGAE Technologies. A U(VI) stock solution was prepared from uranyl nitrate ($UO_2(NO_3)_2 \cdot 6H_2O$).

2.2.2 Nanoparticle Synthesis Process and Phase Transfer

Monodispersed IONPs (~8nm) were synthesized using a published method.[24,76] Briefly FeOOH powder (0.178 g, finely ground), oleic acid (2.26 g) and 1-octadecene (5.0 g) were thermally decomposed at 320°C to form brown-black colloids that were further purified using acetone and hexane to obtain 8-nm IONPs dispersible in apolar solvents. Purified IONPs were collected in hexane and stored in the dark at room temperature. To make the IONPs suitable for water treatment applications, these were phase transferred from hexane to water by a bilayer ligand addition method using a probe sonicator. For optimizing phase-transfer conditions, varying amounts of IONPs and rhamnolipids were used. Specifically, IONPs in hexane (400 µL – 800 µL) were combined with 8 mL of rhamnolipids (60 mg/L -100 mg/L) in aqueous solution combined in a 20 mL glass vial and probe sonicated (UP 50H, Dr. Hielscher, GMHB) under different conditions of time and amplitude (details in Appendix A, Table A-1). The suspension was kept in a fume hood

for 24 hours to remove residual hexane. Unstable particles were removed from the aqueous phase by centrifugation, stirred cell filtration (Ultrafiltration cellulose membranes, 100 kDa MWCO), and filtration through a 0.22 μm membrane filter. The optimum parameters were selected based on phase transfer efficiency and hydrodynamic diameter (details in Appendix A, Table A-1). A stock suspension of IONPs coated with rhamnolipids was then prepared using optimized parameters.

2.2.3 Characterization of IONPs

IONPs core sizes before and after phase transfer were determined using transmission electron microscopy (TEM, FEI Tecnai G2 Spirit) operated at 120 kV. Sample preparation was done by placing 20 μL of diluted IONP suspension on a carbon-coated copper grid. After drying the grid at room temperature, the images were observed using TEM. The average diameter of the suspended particles was calculated by counting 2000 randomly chosen IONPs from the TEM micrographs using ImageJ software (National Institutes of Health). The phase transfer efficiency was estimated by analyzing dissolved Fe concentrations before and after phase transfer with inductively coupled plasma optical emission spectroscopy (ICP-OES, Perkin Elmer ELAN DRC). Suspensions were prepared for ICP-OES analysis by digesting IONPs suspensions in 10% nitric acid on a hot plate at 100 °C.

The number of rhamnolipid molecules attached per nanoparticle was estimated using the total organic carbon (TOC) content in the aqueous suspension before and after ultracentrifugation.[25] TOC analysis was performed using a total organic carbon analyzer (TOC-L, Shimadzu Scientific Instrument, Inc., MD; 680 °C). The hydrodynamic diameter and zeta potential of IONPs in the aqueous phase were estimated using dynamic light scattering (Zetasizer, Malvern Nano ZS, UK). For both measurements, pH was varied from 4-11 to determine the stability of

aqueous suspension over the desired range. The mean value and standard deviation for hydrodynamic diameter and zeta potential were based on triplicate samples and at least 10 readings for each sample. The aggregation kinetics of IONPs in aqueous suspension were determined using time-resolved DLS in the presence of NaCl and $MgCl_2$ over a range of concentrations. All the measurements were done at pH 7.5± 0.1 and in accordance with a previously reported procedure.[24] The attachment efficiency (α) for IONPs was calculated by the following equation[93]:

$$\alpha = \frac{k}{k_{fast}} \quad \textbf{(1)}$$

where k is the initial aggregation rate constant at an examined condition and k_{fast} is the aggregation rate constant under diffusion-limited (fast) aggregation conditions. Slow aggregation occurs at lower salt concentrations due to a repulsive energy barrier, and an increase in salt concentration in this regime generally results in an increase in aggregation rate.[35,93] The minimum salt concentration beyond which there is no effect on aggregation rate is called the critical coagulation concentration (CCC), and k_{fast} is the aggregation rate constant above this point.[27,35,93]

2.2.4 U(VI) Sorption Studies

Adsorption edges: Sorption efficiency of rhamnolipid-coated engineered magnetite nanoparticles was evaluated at different pH values (5.5-11.50) at two fixed U(VI) loadings and under three different carbonate conditions (open to atmosphere, carbonate-free system and 1 mM fixed DIC system). U(VI) loadings of 1 µM and 10 µM were selected based on preliminary calculations in MINEQL+ V5.0 that identified conditions that would avoid any possible precipitation of U(VI). For open to atmosphere adsorption experiments, ultrapure water was adjusted to target pH values (5.5-11.5) by 0.1 M HNO_3 and 0.1 M NaOH and continuously stirred to attain equilibrium with atmospheric CO_2. For achieving equilibrium at higher pH values (> 9), predetermined amounts of

sodium carbonate and sodium bicarbonate were added to obtain a DIC concentration closer to the value that would be achieved once equilibrium with atmospheric CO_2 was reached at the desired pH.[26] Carbonate-free experiments were performed in a glove box (Coy Laboratory Products Inc., MI) under an N_2 atmosphere where the gas in the glove box was bubbled through a concentrated NaOH solution to remove any traces of CO_2. For adsorption experiments with 1 mM fixed DIC, the amount of acid/base required at desired experimental conditions (pH and U(VI) loading) was predetermined to minimize the contact with the atmosphere.

Adsorption isotherms: The sorption capacity of rhamnolipid-coated nanoparticles was explored at pH 6 and 8 under open to atmosphere and carbonate-free conditions. Two different pH values (6 and 8) were selected as the speciation of U(VI) at the selected pH values varies significantly. For open to atmosphere system, at pH 6, UO_2CO_3 and $(UO_2)_2CO_3(OH)_3^-$ dominate, whereas at pH 8, $UO_2(CO_3)_3^{-4}$, $UO_2(CO_3)_2^{-2}$ and $(UO_2)_2CO_3(OH)_3^-$ are in the majority. However, in carbonate free system, UO_2OH^+ and $(UO_2)_3(OH)_5^+$ exist in the majority at pH 6 whereas $(UO_2)_3(OH)_5^+$, $UO_2(OH)_3^-$ and $(UO_2)_3(OH)_7^-$ dominate at pH 8. U(VI) loading was varied between 0.1 µM and 25 µM at selected carbonate conditions and equilibrated for 24 hours.

For each set of U(VI) adsorption experiments, the suspensions were continuously mixed by end-overend rotation for 24 hours, and the pH was readjusted after 4, 8 and 12 hours. Control experiments without nanoparticles were conducted to monitor any loss of U(VI) throughout the procedure. Similarly, control experiments with only nanoparticles were performed to observe the stability of IONPs at desired pH values. The suspensions from each set of conditions were ultracentrifuged (Sorvall WX Ultra 80, Thermo scientific, T1270) at 40000 rpm for 2 hours to separate IONPs, and the supernatant was collected for uranium (U) analysis (ICP-MS,

PerkinElmer). The concentration of Fe in the supernatant was also measured to monitor the leaching of iron from nanoparticles due to U(VI) adsorption.

2.2.5 Surface Complexation Modeling

SCM was used to describe sorption of U(VI) to rhamnolipid-coated IONPS over a wide range of pH at three different carbonate conditions and with two different U(VI) initial loadings. The carboxyl group on the rhamnolipid was considered as the main site for UO_2^{2+} sorption. Similar to aqueous complexation, surface complexation reactions predict sorption on the basis of equilibrium complexation of a metal and surface-associated functional groups.[94] The diffuse layer model (DLM) and non-electrostatic model (NEM) were selected to evaluate the impact of pH, DIC and initial U(VI) loadings on the sorption of U(VI) onto rhamnolipid coated IONPs. NEM does not consider electrostatic interactions and simulates surface complexation reactions in a similar way as the corresponding aqueous complexation reactions, however, DLM considers both electrostatic and chemical contributions to adsorption. Before fitting the models to adsorption edge and adsorption isotherm data, surface characteristics (specific surface area, site density and surface acidity constant) of the IONPs were estimated. Potentiometric titration was performed using 30 mg/L of IONPs suspension, and the data were fitted using NEM and DLM models by varying the surface acidity constant, specific surface area and site density. The best fit was obtained by minimizing the residual sum of squares between experimental and modeled data. The optimized parameters were used in DLM and NEM models to fit the adsorption edge and adsorption isotherm data. The optimal fits for both the models were obtained by varying the logK values of surface reactions using MINEQL+ V5.0 (Environmental Research Software) and MINFIT.[95] The full set of aqueous reactions (details in Table A-2) along with the U(VI) surface complexation reactions were considered.

2.3 Results and Discussion

2.3.1 Synthesis and Characterization of Rhamnolipid-Coated Nanoparticles

Nanoparticles obtained after the thermal decomposition method were highly uniform, spherical and had an average size of 9.0 ± 0.8 nm as shown in TEM micrographs (Figure 2.1a). XRD patterns identified the crystal structure to be face centered cubic (FCC), as expected for Fe_3O_4, which is a spinel ferrite.[67,76] Single domain Fe_3O_4 of this size also displays superparamagnetic characteristics at room temperature, which allows for low energy separation from the aqueous phase by applying a magnetic field.[67,76]

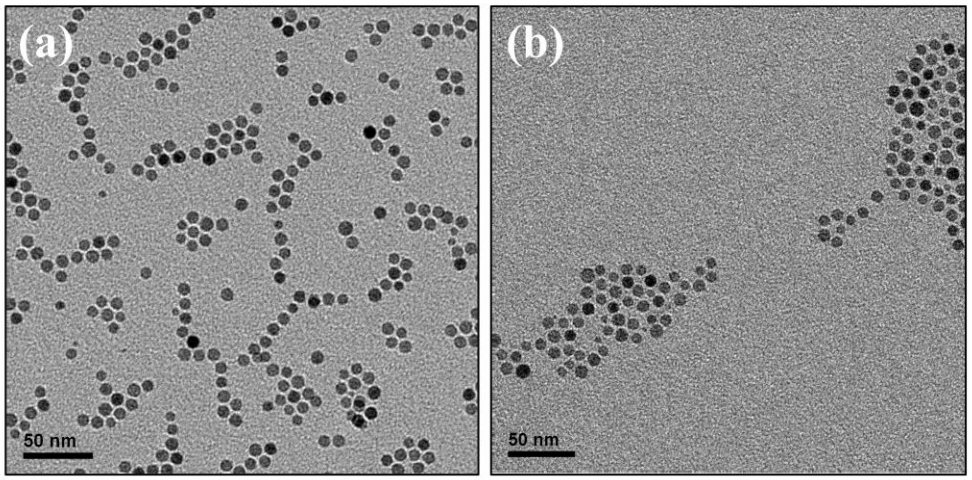

Figure 2.1: Transmission electron micrographs for (a) Oleic acid-coated nanoparticles in hexane (b) Rhamnolipid (bilayer) stabilized nanoparticles in water. Scale bars are 50 nm.

As particles were synthesized through a nonhydrolytic route using oleic acid as a capping agent; they were only stable in nonpolar solvents and required a passivating layer for water transfer. For this, a mixture of monorhamnolipid and dirhamnolipid was employed. The hydrophobic tail of oleic acid associates with the hydrophobic tail of the rhamnolipid (via hydrophobic and dispersive van der Waals forces), and the hydrophilic tail of the rhamnolipid

(possessing carboxylic groups) interacts with water molecules to render IONPs stable in water systems.[75] The details of the conditions considered for optimizing phase transfer conditions are shown in Table A-1. The sonication amplitude used for phase transfer ranged between 80% and 100%. The phase transfer efficiency decreased significantly when the amplitude was less than 80% (Table A-1). The average time required for efficient phase transfer was 10-12 minutes, and IONPs volume was varied from 400 µL to 600 µL (2.2 – 3.3 mg as Fe). Hydrodynamic diameter of 27.6 nm obtained from DLS measurements show that rhamnolipid forms a thin coating around the nanoparticles at a concentration of 100 mg/L. Maximum phase transfer efficiency of 91% was achieved by taking 600 µL of IONPs and 100 mg/L of rhamnolipid. The yield is higher than other optimized coatings (for similar materials), including oleic acid (70%), dodecyl trimethylammonium bromide (47%), sodium dodecyl benzenesulfonate (68%) and sodium dodecyl sulfate (79%).[24] TEM micrographs (Figure 2.1b) confirmed that at the selected conditions, rhamnolipid did not alter the monodispersity and core size of IONPs.

The hydrodynamic diameter of IONPs in the stock suspension used for sorption studies was 27.6 ± 3.4 nm. Zeta potential measurements (Figure 2.2a) found that the coated IONPs were negatively charged at pH above 5.5, which is consistent with the pK_a value (4.5-5.5) of rhamnolipids.[96] No significant change in hydrodynamic diameter was observed with the change in pH > 5.5, whereas at pH < 5.5, destabilization followed by aggregation of nanoparticles was observed. All the experiments described (characterization and sorption) were conducted at pH > 5.5. Aggregation kinetics of IONPs were studied to understand the response of nanoparticle suspensions to salt (NaCl and $MgCl_2$) addition (Figure 2.3). The aggregation increased with increasing salt concentration until the aggregation rate reached the diffusion-limited regime (α=1). The critical coagulation concentration was obtained when the attachment efficiency reached unity.

The CCC values for rhamnolipid-coated NPs were found to be 62.5 mM and 3 mM for NaCl and $MgCl_2$, respectively. The stability of the suspension can be attributed to the hydrophobic interactions between the first and second layer coatings and steric stabilization induced by rhamnolipid moieties.[24,35,79,80] The CCC values of rhamnolipid-coated IONPs were close to the CCC values obtained using synthetic anionic surfactants with shorter carbon chain lengths (decanoic acid and lauric acid) and containing complex functionalities (sodium dodecyl sulfate and sodium dodecyl benzenesulfonate).[24]

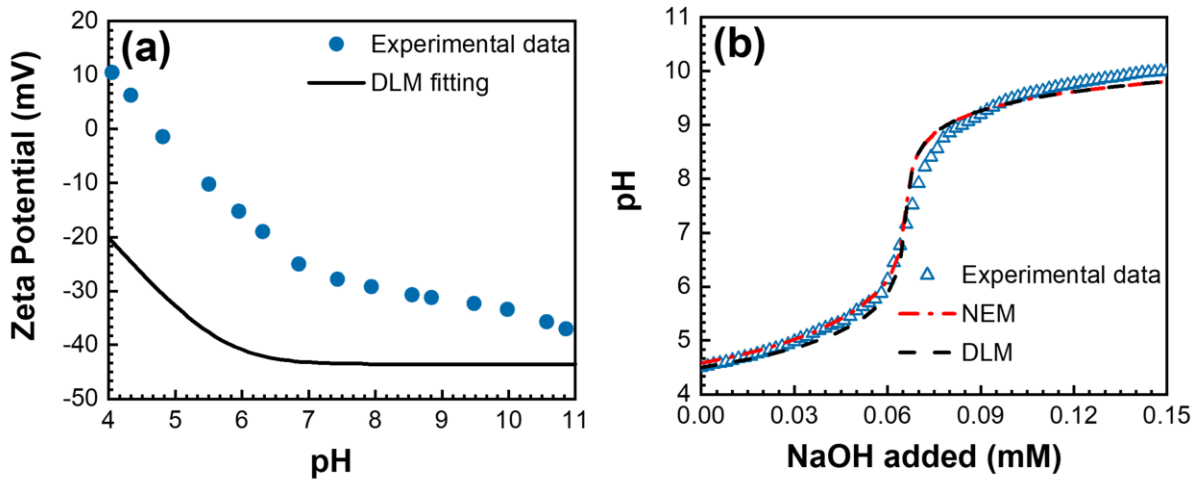

Figure 2.2: (a) Zeta potential of rhamnolipid-stabilized IONPs as a function of pH at a nanoparticle concentration of 30 mg/L and (b) titration curves for rhamnolipid-coated nanoparticle suspensions

From TOC analysis, the total amount of carbon attached to the nanoparticles was obtained. The number of rhamnolipids attached per nanoparticle was estimated by assuming that one molecule of rhamnolipid attaches to two molecules of oleic acid. From previous studies, it has been shown that the IONPs obtained through thermal decomposition method are in the form of magnetite.[21,67] Assuming a density of 5 g/cm^3 (for magnetite) and average diameter of 9 nm, it

was estimated that 186 rhamnolipid molecules are attached to one nanoparticle upon phase transfer, thus providing a site density of 0.73 sites/nm^2 (detailed calculations in the section A1).

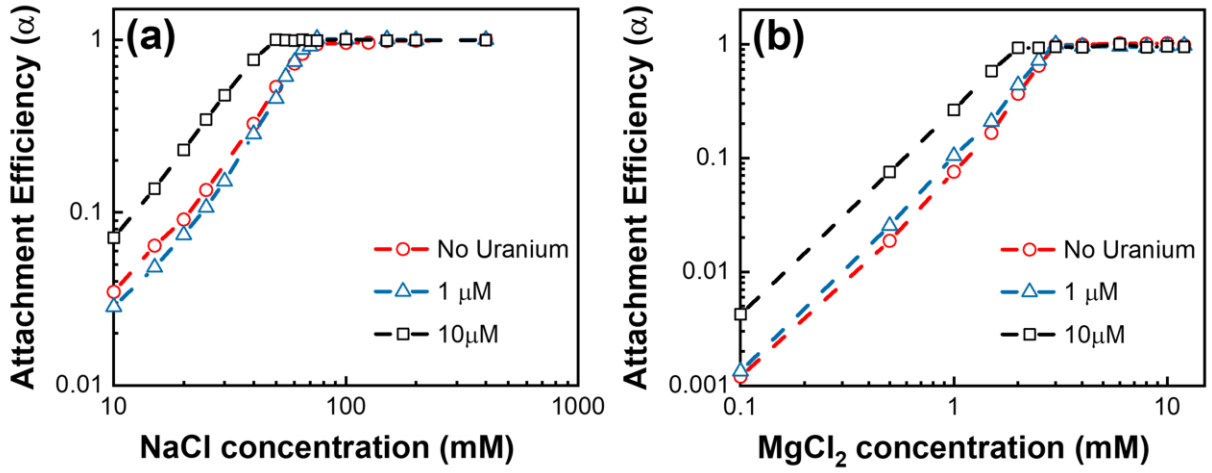

Figure 2.3: Effect of U(VI) loading (1 µM and 10 µM) on CCC evaluated using (a) NaCl and (b) $MgCl_2$. The experiment was performed at pH= 7.5 and nanoparticle concentration of 30 mg/L.

To understand the effect of U(VI) loading on the stability of IONPs, aggregation kinetics in the presence of U(VI) (1 µM and 10 µM) were studied. There was no effect on CCC values when U(VI) loading was 1 µM, whereas the CCC value reduced to 50 mM and 2 mM in presence of NaCl and $MgCl_2$, respectively, when loading was increased to 10 µM (Figure 2.3). The aggregation of nanoparticles was likely promoted by adsorption of UO_2^{2+}, which resulted in the reduction of the effective surface charge of IONPs. This can be observed from zeta potential measurements (Figure A-5) where a decrease in effective surface charge of nanoparticles was observed upon U(VI) adsorption at pH values above 6.

Table 2.1: Coefficients for Langmuir and Freundlich models obtained by fitting adsorption isotherm studies

Condition	pH	Langmuir		Freundlich	
		q_{max} (µg/mg)	K (L/µg)	K ((µg/g)(L/µg)$^{1/n}$)	n
Open to atmosphere	6	116	0.0045	8.61	2.99
	8	52	0.0071	8.03	4.35
Carbonate free system	6	155	0.0080	14.70	3.16
	8	118	0.0154	16.00	3.68

2.3.2 Equilibrium Adsorption Experiments

For evaluating U(VI) sorption capacity, adsorption isotherms were obtained for rhamnolipid-coated nanoparticles (Figure 2.4) under a variety of conditions. The calculated sorption capacities for different carbonate and pH conditions are shown in Table 2.1. For open (atmosphere) system conditions, the maximum sorption capacity (q_{max}) decreased significantly as the pH increased from 6 to 8. At pH 6, positively charged species such as UO_2^{2+}, $(UO_2)_2(OH)_2^{2+}$, UO_2OH^+ and $(UO_2)_3(OH)_5^+$ favor adsorption of U(VI) to negatively charged (Figure 2.4) rhamnolipid-coated nanoparticles due to electrostatic interactions. However, at pH 8, the sorption capacity was lower owing to the formation of negatively charged stable U(VI) carbonate complexes ($UO_2(CO_3)_3^{4-}$, $UO_2(CO_3)_2^{2-}$ and $(UO_2)_2CO_3(OH)_3^-$) that do not adsorb to surfaces and that effectively lower the activity of UO_2^{2+}. Even at pH 6, the adsorption capacity for open to atmosphere conditions is less (116 µg/mg) than in the carbonate-free system (155 µg/mg) due to the formation of negatively charged stable uranyl carbonate complexes. For the carbonate-free system, at pH 8, the activity of UO_2^{2+} is much higher as compared to in the open to the atmosphere conditions, which resulted in the favorable adsorption of U(VI) to rhamnolipid-coated IONPs. In addition to the surface

complexation models ability to fit the data (discussed below), both Langmuir and Freundlich models were also fitted to experimental data. The plots in Figure 2.4show that the Langmuir model provides a better fit to the data under all conditions.

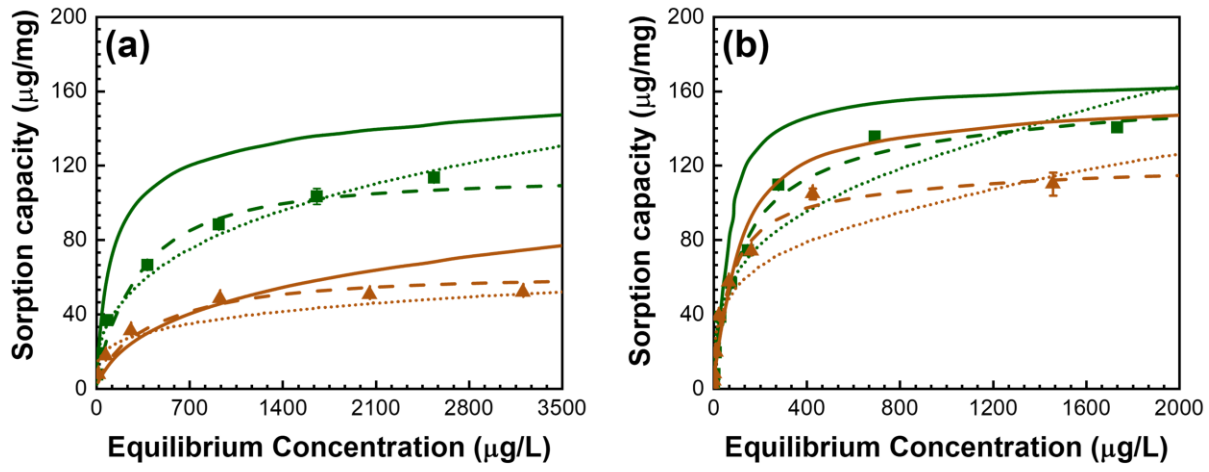

Figure 2.4: Adsorption Isotherm at pH=6 and pH=8 in (a) open to atmosphere conditions and (b) carbonate-free system. ▲ represent points obtained at pH =8 and ■ represent data points obtained at pH=6. Dashed lines show the Langmuir fitting and dotted lines represent the Freundlich fitting. DLM parameters were also fitted to the isotherm data and solid lines represent DLM fitting at pH 6 and pH 8.

The adsorption of U(VI) on rhamnolipid-coated nanoparticles was observed over the range of pH values from 5.5 to 11.5 at two different loadings (1 µM and 10 µM) and three different carbonate conditions (carbonate-free, open to atmosphere, fixed DIC) in 0.01 M $NaNO_3$ (shown in Figure 2.5). The two U(VI) loadings were selected as they were below the values at which precipitation of uranyl species might occur. The adsorption edges obtained for each set of conditions are shown in Figure 2.5.

For the carbonate free system, both 1 µM and 10 µM loadings showed almost 100% sorption until pH~10. At pH > 10, sorption efficiency reduced dramatically owing to the steep

decrease in UO_2^{2+} availability (shown in Appendix, Figure A-1) in the system. The favorable adsorption at pH values down to pH 5.5 can also be attributed to the presence of positively charged aqueous species that favor adsorption to the negatively charged adsorbent through electrostatic interactions (Figure A-2).

For adsorption studies with the suspensions equilibrated with the atmosphere, the fraction of total U(VI) adsorbed decreased when loading was increased from 1 µM to 10 µM (Figure 2.5). For both loadings adsorption onto IONPs decreased as pH increased above pH 7 due to the formation of stable U(VI) carbonate complexes that lowered the available UO_2^{2+} in the system.

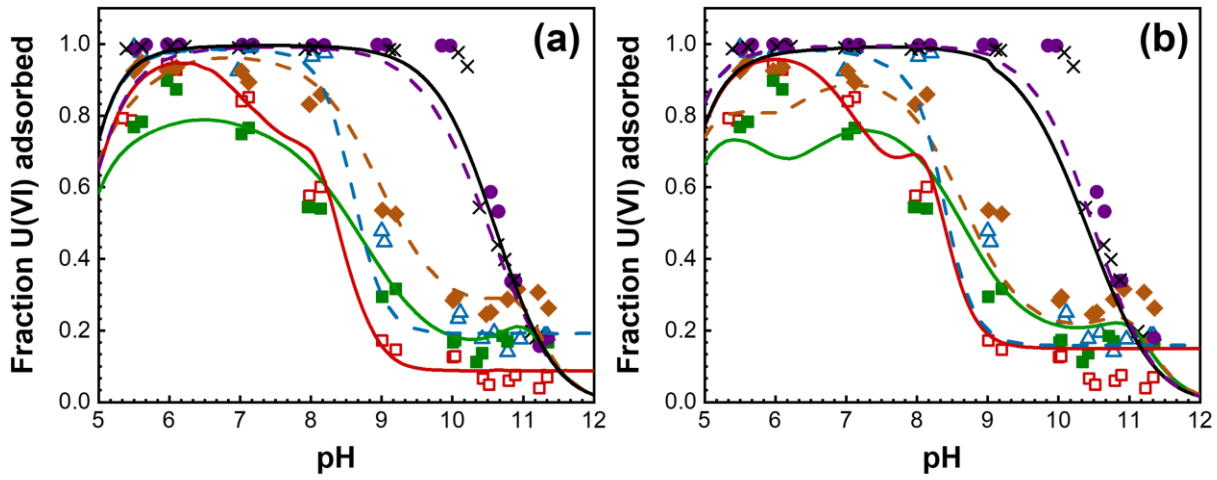

Figure 2.5: Comparison of experimental U(VI) adsorption data and output of surface complexation models using (a) the diffuse double layer model (DLM) and (b) a non-electrostatic (NEM) model. The markers represent the experiment data points and lines represent fitting obtained using SCM modeling. X:- 10 µM Carbonate-free system; ●:-1 µM Carbonate-free system; ♦:- 1 µM Fixed DIC system; ■:- 10 µM Fixed DIC system; □:- 10 µM Open to atmosphere and Δ:- 1 µM Open to atmosphere.

Adsorption edges obtained at 1 mM fixed DIC conditions followed the same trend observed in open to atmosphere conditions with the adsorption percentage decreasing dramatically at higher pH values for the reasons discussed above. However, at lower pH values (< 8), the fixed DIC system showed lower adsorption percentages as compared to the open to atmosphere conditions due to less availability of UO_2^{2+} in the fixed DIC system (as shown in Figure A-1). At pH > 8, the trend reversed, owing to more availability of UO_2^{2+} in fixed DIC system because the supply of CO_3^{2-} for complexing UO_2^{2+} was limited in the fixed DIC system while it continued to increase with increasing pH in the system that was open to uptake of CO_2 from the atmosphere.

Although there is theoretically the possibility of U(VI) reduction to U(IV) due to interaction with Fe(II) in the magnetite nanoparticles, this will only happen if U(VI) diffuses through the rhamnolipid coating. At low U(VI) loadings, as in this case, U(VI) will adsorb on the outer layer before it has a chance to diffuse through the layer to where it could contact the magnetite surface. The absence of dissolved Fe in the supernatant obtained after ultracentrifugation in adsorption studies confirmed that the leaching of iron from rhamnolipid-coated magnetite nanoparticles did not occur at the experimental conditions studied. As the IONPs were stable under all the experimental conditions considered, it is not expected that there was any opportunity for U(VI) to interact directly with the magnetite nanoparticles. Recent studies on U(VI) using bilayer coated IONPs showed that U(VI) reduction was observed only at much higher U(VI) loadings.[67,75] At these higher loadings, the nanoparticles became destabilized, which resulted in changes in the possible diffusion and contact pathway of U(VI) to the surface of nanoparticles.[26,67,75]

2.3.3 Interpretation of U(VI) Adsorption by Surface Complexation Modeling

A surface complexation model was developed to account for U(VI) adsorption to rhamnolipid-coated IONPs in a reaction-based framework that could account for variation in pH, U(VI) loading,

and carbonate condition with a single set of surface complexation reactions. The first step in model development was the determination of nanoparticle surface properties (specific surface area, surface site density and acid-base equilibrium constants). Rhamnolipid-coated nanoparticles can only be neutral or positively charged as the charge is solely decided by protonation/deprotonation of carboxyl groups in the rhamnolipid structure. The charge and pH-dependence of charge is also evident from zeta potential measurements (Figure 2.2). Consequently, the SCM was developed with only protonated (SITEOH) and deprotonated ($SITEO^-$) forms of the surface site.

Potentiometric acid-base titration was performed to determine the surface acidity constant of IONPs. As the pK_a of rhamnolipid lies between 4.3-5.5[96], rhamnolipid-coated IONPs provided effective buffering from pH 4.5-6.0 (Figure 2.2b). The specific surface area was not calculated experimentally as the surface of the magnetite cores of the IONPs may not represent the surface area of the rhamnolipid-coated nanoparticles in aqueous suspension. The optimized values of pK_a, specific surface and site density were determined by minimizing the squares of the residuals between model outputs and experimentally obtained titration curve (Figure 2.2b). The best fit was obtained for a specific surface area of 150 m^2/g and site density of 0.73 sites/nm^2. For DLM, the best fit was obtained for a pK_a of 3.6, whereas for NEM the pK_a value obtained was 5.6 (Table 2.2). The surface site concentration obtained at the optimized values for 30 mg/L of Fe_3O_4 nanoparticles using optimized values from the titration curve was 22.4 µM. This site concentration value is close to the value of 20.16 µM obtained using TOC analysis. The optimized parameters were used for fitting the adsorption edge and adsorption isotherm data. The obtained surface characteristics were also used to fit the zeta potential measurements obtained using DLS. The Gouy-Chapman equation was used to obtain the surface potential of nanoparticles as a function of pH as shown in Figure 2.2a. The model was able to capture the trend of zeta-potential

measurements. Zeta potential value is the value obtained on the imaginary slipping plane (where particles interact with each other or other entities), which is less than the actual surface potential of the nanoparticles.[97]

Based on the nanoparticle properties obtained above, DLM was fitted to adsorption edge data (Figure 2.4a) obtained at U(VI) loadings of 1 µM and 10 µM and for three sets of carbonate conditions. The best-fitting was obtained using the set of surface complexation reactions shown in Table 2.2. Aqueous reactions were set at values from a critically-reviewed database (Table A-2). In addition to the surface deprotonation reaction (Reaction 1) discussed previously, four additional reactions (Reactions 2-5) were included for UO_2^{2+} binding to the rhamnolipid carboxyl groups on the IONPs. The logK values were obtained using MINFIT, which interacts with MINEQL+ to optimize equilibrium constants by minimizing the residual sum of squares between experimental and modeled data.[95]

Reactions 2 and 3 were first used to fit the carbonate-free system, and their logK values were estimated. Reaction 4 was then added to Reactions 2-3 to model the systems with fixed DIC and open to the atmosphere. Various combinations of just two of the reactions in the set that included Reactions 2-4 were attempted for fitting, but none of these provided as good of a fit as that provided with all three present, especially for fixed DIC conditions. Consequently, the combination of Reactions 2-4 was selected and optimized log K values for each reaction were obtained using MINFIT. The addition of Reaction 4 provided a good fit for carbonate-containing systems at pH values < 8, but it underestimated the adsorption percentages at higher pH values. This necessitated the inclusion of another surface complexation reaction that could better describe the fixed DIC and open to atmosphere systems at higher pH values. Reaction 5 was added to the earlier set of reactions and an optimum set of constants was obtained. The inclusion of Reaction 5

in the set of reactions reduced the residual sum of squares between experimental data and modelled data by 50%.

Table 2.2: Reactions and Parameters for Diffuse Double Layer (DLM) and Non-Electrostatic Model (NEM)

	Reactions	DLM logK	NEM
1	$SITEOH = SITEO^- + H^+$	-3.60	-5.60
2	$UO_2^{2+} + H_2O + SITEOH = SITEOUO_2OH + 2H^+$	-4.45	-4.12
3	$UO_2^{2+} + 2H_2O + SITEOH = SITEOUO_2OH_2^- + 3H^+$	-8.55	-10.55
4	$UO_2^{2+} + 2CO_3^{2-} + SITEOH = SITEOUO_2(CO_3)_2^{3-} + H^+$	24.60	18.00
5	$UO_2^{2+} + 3CO_3^{2-} + SITEOH = SITEOUO_2(CO_3)_3^{5-} + H^+$	33.50	19.80

NEM was also fitted to adsorption edge data following the same approach used for DLM fitting (Figure 2.5b). The model was able to describe the carbonate-free system, but it was not able to capture all the features of the systems with dissolved inorganic carbon. The model was also not able to differentiate between the difference in adsorption percentages obtained at different U(VI) loadings, which was prominent in DLM. The main reason for this was that NEM does not consider the change in surface characteristics of the adsorbent (e.g., change in surface charge) as those are altered by adsorption.

The developed models (DLM and NEM) were also used to fit the adsorption isotherms. The results obtained for the DLM model are shown in Figure 2.4, and the fitting obtained for NEM model is shown in Figure A-4. The developed SCM models, NEM and DLM were able to describe the trends observed for both open to atmosphere and carbonate-free systems, however, the maximum sorption capacities were overpredicted by the models. The overprediction may be

attributed to bidentate inner-sphere complexation of UO_2^{2+} with rhamnolipid moieties. The actual mode of UO_2^{2+} adsorption to the rhamnolipid-coated IONPs may involve binding to two rhamnolipid functional groups, which would result in a decrease of the maximum sorption capacity of U(VI). Earlier studies on U(VI) sorption to mineral surfaces suggest that both monodentate and bidentate surface complexes are favorable under different pH and carbonate conditions.[13,90,98]

2.4 Conclusions

Based on the optimized particle systems described here, rhamnolipid is a highly effective, biocompatible coating for stabilizing engineered iron oxide nanoparticles. The use of naturally occurring biosurfactant coatings may be developed as an environmentally benign and cost-effective way for stabilizing nanoparticles in water. The data also show that rhamnolipid-coated nanoparticles act as strong sorbents for U(VI) and can be used for its removal from water over a broad range of water chemistries. The set of four reactions included in SCM were able to predict the adsorption behavior of U(VI) over a wide range of pH and at three different carbonate conditions and two total U(VI) loadings. Excellent agreement between experimental and SCM-predicted sorption values indicate that both electrostatic and chemical interactions are important to U(VI) removal using rhamnolipid-coated IONPs. While these results are promising, further research is needed to systematically investigate the efficiency of these rhamnolipid-coated nanoparticles in real water systems. There is also a need to explore the efficacy of other biosurfactants for the stabilization of these and similar nanoparticles being considered for treatment processes, among other aqueous-based technologies.

Chapter 3: Trace Metals Uptake to Soils and Sediments from Natural Aquatic Systems

3.1 Introduction

Trace metals can enter aquatic environments from natural and anthropogenic sources. Natural phenomena responsible for trace metal addition in environmental systems are weathering, soil erosion, sediment re-suspension, and airborne transport following volcanic eruptions.[1,99] Trace metals can also be introduced anthropogenically from influxes of waters enriched in metals from industrial and municipal activities, application of metal-bearing solids, and atmospheric deposition.[99,100] Understanding the response of wetlands and stream sediments to metal addition can help predict the fate of metals following both natural and anthropogenic metal inputs.

The behavior, fate, and transport of metals in wetlands and stream sediments is governed by binding to mineral surfaces and organic matter and coprecipitation as minerals.[7,60,101] Sulfide minerals serve as important hosts for metals. Zn and Cu can displace iron from FeS and can form separate sulfide mineral phases such as covellite (CuS) and sphalerite (ZnS).[7,60] Iron minerals can immobilize trace metals through adsorption and co-precipitation mechanisms.[8,60] Additionally, Fe(II)-bearing minerals and reactions of Fe(II) on mineral surfaces may alter the mobility of metals by chemically reducing them.[102] Particulate organic matter has a high affinity for trace metals and alters their speciation and bioavailability through complexation.[103] Sediments containing clay minerals, especially smectites, bind metals due to their active surfaces and ion-exchange sites.[60,104–107] Clay minerals in the fine fraction of sediments can sorb high concentrations of metals

due to their large specific surface area, chemical and mechanical stability, and high cation exchange capacity.[104–106,108]

Trace metals pose health and ecosystems risks at high concentrations due to their potential toxicity and bioaccumulation, but many trace metals also serve as essential elements for biogeochemical processes.[3,5,42,43] Biogeochemical processes such as methanogenesis and anaerobic methane oxidation require transition metals, mainly Co and Ni, for completion. Aerobic methanotrophy and nitrous oxide (N_2O) production in denitrification are dependent on the availability of Fe, Mo, and Cu.[3,5,42] Laboratory studies on pure cultures have indicated that optimum availability of Cu promotes N_2O reduction to N_2 during denitrification.[42,43] Similarly, the growth of methanogens is substantially increased when Ni and Co are sufficiently available.[3,5] Trace metals can adsorb to solid phases and coprecipitate as sulfides in wetland soils and stream sediments, which can limit their availability in the pore water to serve as trace nutrients for biogeochemical processes such as denitrification and methanogenesis.[109,110]

A more complete understanding of the reactivity of trace metals in aquatic systems can enable more accurate predictions of metal transport in subsurface systems and improved models for estimating greenhouse gas emissions from natural landscapes.[111] Insight into the molecular-level speciation of the trace metals in soils and sediments can help predict their bioavailability in natural systems.[112] Our recent study on trace metal speciation in uncontaminated wetland soils and stream sediments found that the majority of trace metals were associated with sulfides or other mineral phases, and hence have limited availability for biogeochemical processes.[113] This study indicated that diverse aquatic systems with substantial differences in location and mineralogy showed similar trace metal speciation.[113] This previous study motivated the present study's interest

in determining whether or not the speciation of trace metals at different loadings reflected the speciation at geological background levels.

The objective of this study was to understand the factors governing the fate of trace metals added in dissolved form to three different natural aquatic systems. We quantified Cu, Zn and Ni uptake trends on samples collected from wetland soils and stream sediments and assessed the relationship between uptake and the characteristics of the soils and sediments. We investigated metal speciation using X-ray absorption spectroscopy (XAS) to determine the major components associated with metal uptake at the selected sites at low and high loadings. This approach provided an understanding of the differences between the speciation of added metals and those originally present in the soils and sediments.

3.2 Materials and Methods

3.2.1 Materials

Copper chloride dihydrate (99.99%), nickel chloride hexahydrate (99.99%) and zinc chloride (98%) salts used to prepare stock solutions were purchased from Sigma Aldrich. All other salts (sodium chloride, potassium chloride, sodium nitrate, sodium sulfate, magnesium chloride hexahydrate, magnesium sulfate, calcium sulfate dihydrate, ammonium chloride and disodium phosphate) used for preparing artificial water for conducting uptake studies were purchased from Thermo Fisher Scientific and were of reagent grade. Nitric acid (trace metal grade) purchased from Thermo Fisher Scientific was used for acidifying samples for dissolved metal analysis.

3.2.2 Site Description and Sampling Information

The samples for the study were collected from three different natural aquatic systems: marsh wetlands at Argonne National Laboratory (ANL), Illinois USA, stream sediments at East Fork Poplar Creek (EFPC) at Oak Ridge National Laboratory, Tennessee USA, and riparian wetlands of Tims Branch (TB) at Savannah River National Laboratory, South Carolina USA. Two sampling locations were selected at each of the three sites. These six locations are referred to as Marsh 1, Marsh 2, Stream 1, Stream 2, Riparian 1, and Riparian 2 in further discussion. Information on the location of the sampling sites and the detailed procedure for the collection of the soils and sediments are in our recent study[113] and in the appendix (Section B.1).

3.2.3 Characterization

The concentrations of Cu, Ni and Zn in water samples collected from the sites were determined by inductively coupled plasma-mass spectrometry (ICP-MS, PerkinElmer Elan DRC II, details in appendix B.1). Total metal concentrations in the soils and sediments were determined using a microwave digestion method followed by elemental analysis (details in section B.2).[114] Specific surface areas were measured using BET N_2 adsorption (Quantachrome Nova 2000e), and total organic carbon (TOC) contents were determined using the solid sample analysis module of a total organic carbon analyzer (Shimadzu TOC-L CPH/CPN). For TOC analysis, sediments were dried and then combusted at 900°C to determine the total carbon content. The inorganic carbon content in the samples was determined by heating them at 200°C in a total inorganic carbon chamber. The organic carbon was obtained as the difference between the total and inorganic carbon contents. The total sulfur content was determined using an Elementar Vario MACRO cube CHNS analyzer.[113]

3.2.4 Metal Uptake

Batch Cu, Zn and Ni uptake experiments were performed in an anaerobic chamber on soils and sediments collected from the three anoxic subsurface aquatic systems. These soils and sediments were always maintained under anaerobic conditions before conducting the studies to maintain original metal speciation. For each experiment, wet soil (0.2 g equivalent dry mass) obtained from the top 0-5 cm of each soil or sediment core was added to 15 mL polypropylene tubes that were then filled with 10 mL of deoxygenated simulated site water (recipes in Table B-1 in Appendix B). The dry mass was determined on a separate portion of soil/sediment by drying at 120°C until a constant mass was achieved. The initially added metal concentrations were varied from 0.5 µM to 1000 µM, and the samples were equilibrated for 24 hours with mixing provided by end-over-end rotation. The water was deoxygenated by bubbling N_2 gas through ultrapure water for 4-5 hours, followed by bubbling in an anaerobic chamber in sequence through a ferrous chloride/KOH solution and deionized water for 3 hours. The pH was adjusted to target values of ~7.0 for marsh and riparian sites and maintained at ~7.6 for stream sites using HCl and NaOH solutions. For riparian wetland soils, the uptake studies were also conducted at pH 5 to determine uptake at actual field conditions (pH of the surface water at riparian sites is approximately 5).[113] Control experiments were conducted to monitor any loss of metals from the solution in the absence of soil or sediment. Equilibrium solubility calculations were conducted in MINEQL+ V5.0 to determine the conditions at which precipitation might occur **(**Figure B-1**)**.[115] These calculations indicated that Ni and Zn will not form precipitates at any of the conditions studied but that Cu precipitation might occur at loadings > 10 µM in marsh wetland soils and stream sediments. To avoid precipitation, Cu was added in steps of 10 µM in metal uptake studies conducted on marsh wetland soils and stream sediments. The tubes were wrapped in aluminum foil to prevent any photochemical

reactions. The pH was readjusted after 4 hours and 8 hours. After 24 hours of equilibration, the final pH was measured, and the samples were filtered using 0.22 µm MCE filters and were diluted and acidified to 1% HNO_3 (trace metal grade) for dissolved metal analysis using ICP-MS. In a previous study with materials from these sites, we determined that equilibrium solid-water partitioning of Cu was reached within 12 h.[116]

3.2.5 Spectroscopic Analysis

X-ray absorption spectroscopy (XAS) is a well-established tool for determining the chemical speciation of metals in soils and sediments. XAS was performed on the samples collected from Marsh 1, Stream 1, Riparian 1, and Riparian 2 after metal uptake experiments to determine the speciation of Cu, Ni and Zn recently taken up by the soils and sediments. For Riparian 1 and Riparian 2 soils, spectra were collected on samples from uptake studies performed at pH 5. Two doses, 50 µM (1 µmol/g) and 500 µM (10 µmol/g) were considered for each metal in this study. The soils or sediments (0.5 g dry mass) were equilibrated with these doses for 24 hours, and samples were then collected on membrane filters (MCE) for XAS. The supernatants were collected and acidified for dissolved metal analysis using ICP-MS. The metal-loaded soils and sediments were added as wet pastes to polycarbonate sample holders using Kapton tape and heat-sealed in polyethylene bags to preserve anaerobic conditions before analysis. Each polyethylene bag contained a piece of laboratory tissue moistened with ultrapure water to prevent desiccation. A set of Zn, Ni and Cu standards were also prepared for measuring XANES spectra **(**Figure B-2-Figure B-4).

Fluorescence-yield XANES spectra of unamended samples, as well as samples with added metals, were collected at the Stanford Synchrotron Radiation Lightsource (SSRL) beamline 11-2. The incident beam energy was selected using a Si(220) double crystal, variable-exit

monochromator with phi = 90° orientation. Three to ten scans were collected for each sample and then averaged to reduce the noise level; no scan-to-scan variations in edge position or features were observed. Metal foils were used to calibrate the incident beam energy and the K-edges were set to 8979 eV, 9659 eV, and 8333 eV for Cu, Zn, and Ni, respectively. XANES spectra obtained at SSRL were background subtracted and averaged using SIXPACK and were further normalized and analyzed using ATHENA.[117,118] Principal component analysis (PCA) was used to determine the minimum number of components required to explain all the features of the XANES region of the spectra.[8,117,119] Target transformation (TT) analysis was then performed on a set of standards to select the model compounds most likely to occur in a set of samples. These selected model compounds were further used in linear combination fitting (LCF) to determine the abundance of the components in the samples analyzed.[8,117,119] We used the combinational LCF approach, where all combinations of the spectra of relevant standards identified by TT were fit to the sample spectra**.** The fit with the lowest chi-squared value was selected as the optimum. Fitted components were grouped into specific categories **(**Table B-2-Table B-4**)** representing the species governing trace metal uptake at the evaluated sites.

3.3 Results and Discussion

3.3.1 Solid Phase Characterization

The total concentration of trace metals in the unamended soils and sediments followed the trend Zn > Cu > Ni **(**Table B-5**).** The wetland soils from Marsh 1 had the highest solid-phase Cu (730 nmol/g), Zn (2100 nmol/g) and Ni (420 nmol/g), and the Riparian 1 soils from riparian wetlands had the lowest solid-phase trace metals concentrations (Cu: 30 nmol/g; Ni: 40 nmol/g; Zn: 100

nmol/g). The total concentrations of the metals in the soils and sediments lie in the typical ranges expected for uncontaminated natural aquatic systems.[120]

The organic carbon content, specific surface area (SSA), iron content, and sulfur content of soil samples were determined **(**Table B-5**).** Marsh 1 soils are rich in organic carbon (Marsh 1: 10.26% and Marsh 2: 9.83%) and sulfur (Marsh 1: 2.57 mg/g and 3.12 mg/g) as compared to the riparian soils and stream sediments. The total iron contents of the samples were similar at all the sites (20-35 mg/g), except for the wetland soil at Riparian 1 where the concentration of Fe was 10-fold less than at other sites. The values of specific surface area (SSA) lie within the range typically observed for sediments.[121,122] The SSA was measured so that metal uptake results could be normalized to surface area for comparing metal uptake across different sites. The details on the mineral composition and metal concentrations in the surface water are indicated in our previous study[113] and in the appendix (section B.3).

3.3.2 Macroscopic Metal Uptake

Cu, Zn, and Ni uptake by soils and sediments was measured following their additions to suspensions in dissolved forms **(**Figure 3.1**).** All the soils and sediments took up large fractions of the added metals. The control experiments with metal addition but no soils or sediments confirmed that there was no precipitation of metals from solution or adsorption to the walls of the tubes at the experimental conditions. Based on the amount of metals taken up by the solids, stream sediments and riparian wetland soils follow the order Cu > Zn > Ni at all the loadings studied. For marsh wetland soils, Zn uptake is higher than Cu and Ni at low loadings, however, at high loadings, the same trend as stream sediments and riparian wetland soils (i.e., Cu > Zn > Ni) was observed.

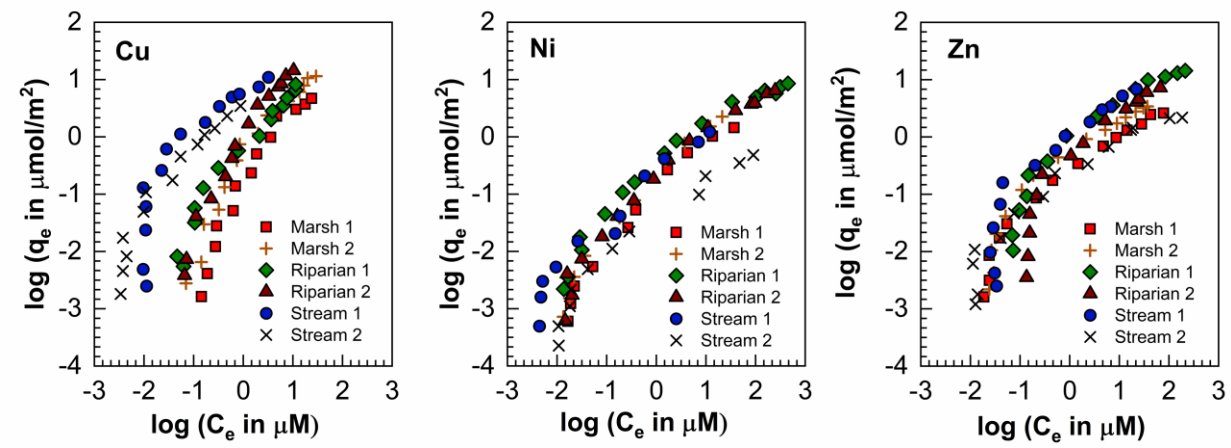

Figure 3.1: Solid-water partitioning of (a) Cu (b) Ni and (c) Zn on soils and sediments collected from different sites. pH considered for Marsh 1 and Marsh 2 is 7, Stream 2 and Stream 1 is 7.6 and Riparian 1 and Riparian 2 is 7. The equilibration time is 24 hours.

Even after normalization to the specific surface area of sediments, there was significant variation in the metal uptake across materials from different sites, especially for Cu **(**Figure 3.1a**).** For Cu uptake, stream sediments had more uptake than wetland soils at all studied loadings. This may be related to the stream sediments containing the highest amount of elemental sulfur of the materials studied; the reaction of the dissolved metals with elemental sulfur can result in precipitation of metal sulfides, such as CuS.[113] Maximum Ni uptake was similar across the marsh wetland soils and riparian wetland soils **(**Figure 3.1b**).** The uptake behavior of Ni on stream sediments was different from other sites. Stream 1 sediments showed more Ni uptake at low loadings, and the uptake capacity of Stream 2 sediments was substantially lower than other sites at high loadings. Riparian wetland soils adsorbed less Zn at low loadings as compared to marsh soils and stream sediments, however, this trend was reversed at high Zn addition. The variability in uptake behavior of metals suggests that different moieties in the solid phases governed metal immobilization in different locations of the selected natural aquatic systems.

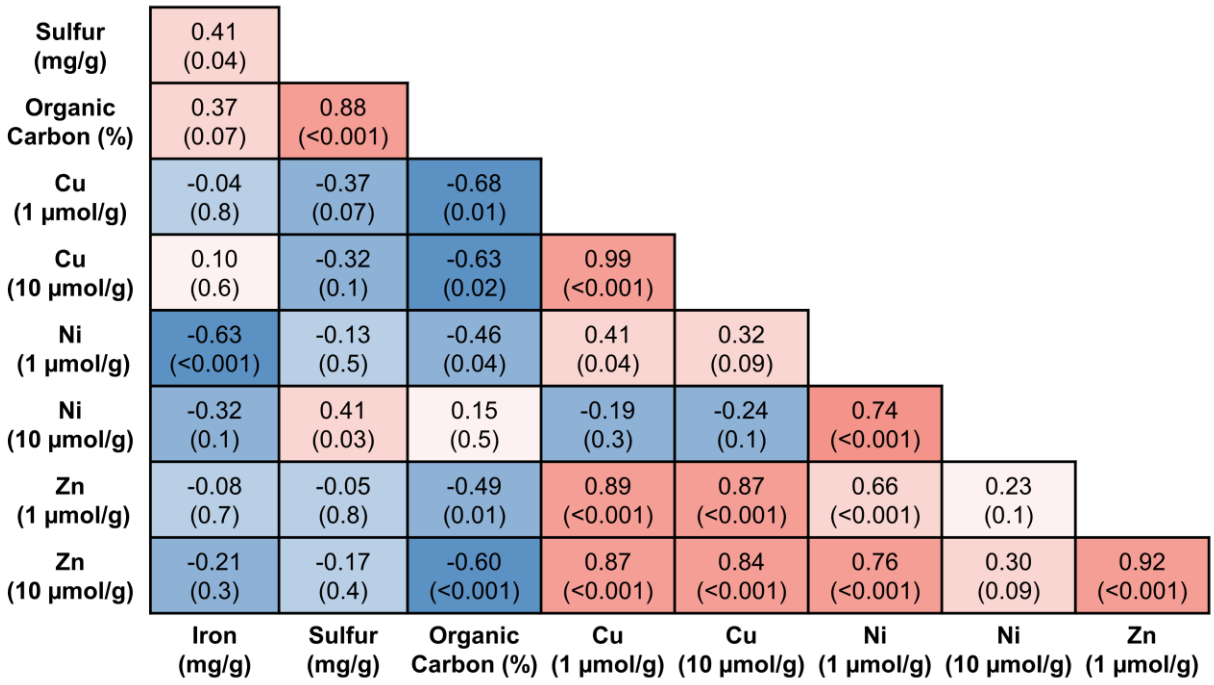

Figure 3.2: Correlation coefficients (r) between K_D and solid-phase composition for different soils and stream sediments. The values in parentheses indicate the significance level (p-values).

The effect of changing the pH from 7 to 5 on the metal uptake of the riparian wetland soil was evaluated to understand the uptake behavior at field conditions **(**Figure B-5**,**Figure B-6**).** The shift in pH from 7 to 5 substantially affected Cu uptake on Riparian 1 soils, indicating lower adsorption on mineral phases at low pH values. At a loading of 10 µmol/g, Cu uptake was 1.3% lower in Riparian 2 soils and 45% lower in Riparian 1 soils at pH 5 than at pH 7. Zn uptake was also lower at pH 5 than at pH 7 with 10.3% and 8.8% less uptake at 10 µmol/g loading in Riparian 2 and Riparian 1 soils, respectively. The differences in Ni uptake between pH 5 and 7 were negligible at both Riparian 1 and Riparian 2 locations.

To examine the correlation between metal uptake and total iron, sulfur, and organic carbon in the samples, a single quantitative measure of metal uptake was needed. We chose K_D $\left(\frac{\text{solid-phase concentration}}{\text{solute concentration}}\right)$ values for this measure, and these were determined at low (1 µmol/g)

and high metal (10 µmol/g) loadings **(**Table B-6**).** To account for SSA in determining K_D, the solid phase concentrations were calculated in terms of µmol/m^2. The K_D values obtained were used to determine correlation coefficients (r) between metal uptake and major elements (Fe, S, and organic carbon) in the soils and sediments **(**Figure 3.2**).** We did not observe any correlation between Fe, S, and organic carbon contents in the samples and metal uptake trends, suggesting that the total Fe, S, and organic carbon contents at the sites do not provide insight into the processes controlling metal uptake by the soils and sediments. Further information on chemical speciation is required to determine the factors driving metal uptake at the selected sites.

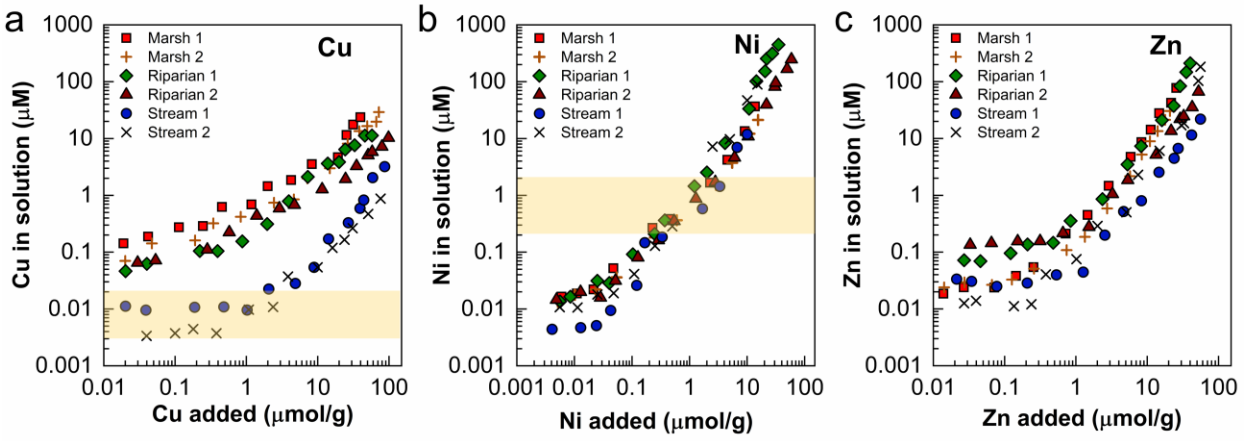

Figure 3.3: Amount of (a) Cu (b) Ni and (c) Zn remaining in the supernatant at the end of the uptake experiments. pH considered for Marsh 1 and Marsh 2 is 7, Stream 2 and Stream 1 is 7.6 and Riparian 1 and Riparian 2 is 7. The equilibration time is 24 hours. Shaded areas indicate optimum Cu and Ni concentrations required for denitrification and methanogenesis, respectively.

The correlation coefficients indicated relationships in the binding behavior of trace metals studied. The K_D values of Cu and Zn were strongly correlated ($r > 0.80$) with each other at low and high loadings, whereas Ni correlated poorly with Cu and Zn, especially at high loadings. For all the sites, Ni showed lower adsorption as compared to Cu and Zn as high Ni concentrations were observed in the dissolved phase at similar trace metal amendments **(**Figure 3.3**)** causing a poor

correlation between K_D values of Ni and Cu/Zn. With increased loading i.e. from 1 µmol/ g to 10 µmol/g, K_D values of Ni and Zn decreased, whereas the K_D values increased in the case of Cu. High K_D values at high Cu loadings indicate a stronger affinity of soils/sediments towards Cu as compared to Ni and Zn.

3.3.3 Implications of Metal Uptake for Biogeochemical Processes

The metal uptake trends provided information on the metal amendments required to raise concentrations to optimum levels required for biogeochemical processes occurring in natural environments **(**Figure 3.3**)**. Even after 1 µmol/g Cu addition to Stream 1 and Stream 2 sediments, the resulting Cu concentrations in the supernatant after uptake are less than the optimum (0.003 µM -0.020 µM, shaded area in Figure 3.3a) required for denitrification in pure cultures.[42,43] The limited availability of Cu might inhibit N_2O reduction to N_2, which makes these sites potential sources of N_2O to the atmosphere. At riparian and marsh wetland sites, background dissolved Cu concentrations in the water samples (50-100 nM) are above the optimum range (3 nM -10 nM) required for the completion of denitrification in pure cultures. However, changes in redox and hydrological conditions and phenomena such as sulfide scavenging and adsorption of Cu to Fe/Mn oxides and organic matter present in soils can limit Cu bioavailability. In our recent study on the role of Cu in N_2O reduction to N_2 in natural aquatic systems, we observed transient as well as permanent accumulation of N_2O in microcosms with riparian wetland soils (Riparian 1 and Riparian 2), Stream 1 sediments, and Marsh 1 soils.[116] Upon addition of Cu to obtain dissolved concentrations in the range of 10-300 nM, we noted decreased N_2O accumulation in all the systems.[116] Because of complexation of Cu by dissolved organic matter that limits the bioavailability of a portion of the dissolved Cu, the dissolved Cu concentrations needed to alleviate Cu limitations of microbial reduction of N_2O were somewhat higher than in experiments with pure

cultures and simple aqueous solutions. Similarly, the concentration of Ni in the supernatant after uptake **(**Figure 3.3b**)** suggests that 0.5-1 µmol/g Ni addition is required at all sites to raise the dissolved Ni concentration to optimum levels for methanogenesis (0.2- 2µM, shaded area in Figure 3.3b). Thus, the limitation of Ni and Cu can be an important factor in governing greenhouse gas emissions from the studied soils and sediments.

3.3.4 Interpretation of Metal Uptake Data using XANES Analysis

XAS was employed to determine the solid-phase metal speciation in the soils after uptake. PCA combined with target transformation analysis was performed on model compounds **(**Figure B-2-Figure B-4**)** and each metal spectra set **(**Figure B-7Figure B-9**)** to identify the number of components and then select the relevant model compounds for LCF.[117,119] LCF was then used to obtain the speciation of the added metals at both low (1 µmol/g) and high metal loadings (10 µmol/g).[123,124] The speciation of the metals in the unamended soils was obtained from our previous study.[113] For Cu speciation after uptake we selected five different categories: Cu precipitated as sulfides (CuS and Cu_2S), amine bound, thiol bound, adsorbed, and Cu(0) **(**Table B-2**).** The adsorbed Cu category included the spectra of aqueous Cu(II) ions because the spectra of aqueous ions are indistinguishable from those adsorbed at cation exchanges species on clay minerals **(**Figure B-2**).** For understanding Ni speciation in soils and sediments after uptake, five categories were also used: NiS, amine bound, adsorbed, thiol bound, and clay structures **(**Table B-3**).** The clay structure fraction included metals substituted into octahedral sheets in phyllosilicates and related phases. The clay structures category is a separate grouping from adsorbed and refers to the Ni incorporated in the clay structure, which has spectra distinct from that of cation exchanged Ni **(**Figure B-3**).** Five categories were also used for Zn speciation after uptake: ZnS, thiol bound, ZnO, adsorbed, and clay structures **(**Table B-4**).** The spectra of Zn bound to carboxylic acids was similar

to aqueous and cation-exchanged Zn and hence was included in the adsorbed Zn category **(**Figure B-4**)**.

3.3.5 Cu Speciation following Cu Addition to Soils and Sediments

The speciation of Cu did not vary substantially between unamended samples and soils and sediments following Cu addition at low loading (1 µmol/g) **(**Figure 3.4**)**. Cu was predominantly present in a form similar to covellite (CuS) in all the unamended soils and sediments, except in Riparian 1 where the adsorbed fraction and Cu_2S solid also occurred as a significant proportion. The mass concentration of each species **(**Figure B-10**)** before and after Cu uptake shows that the background Cu retained its original speciation when additional Cu was added to all samples, with an exception of Riparian 1 soils. In Riparian 1 soils, the addition of Cu at low loading altered the speciation of Cu originally present in the soils as Cu initially in the adsorbed form in unamended soils either converted into Cu(0) or Cu_2S upon Cu addition. At 1 µmol/g loading, the added Cu predominantly binds to the soils by forming a stable CuS-like or Cu_2S solid species for all sites. The observation of added Cu associated with reduced sulfur highlights the importance of the presence of sulfides or sulfate-reducing conditions in the studied soils and sediments **(**Figure 3.4a-d**).** Previous studies of Cu speciation in soils and sediments also observed the presence of Cu sulfides due to their high thermodynamic stability under sulfate-reducing conditions.[109,110] Reactive sulfide species, such as FeS and aqueous sulfides are known for binding high concentrations of trace metals under anoxic conditions.[125,126]

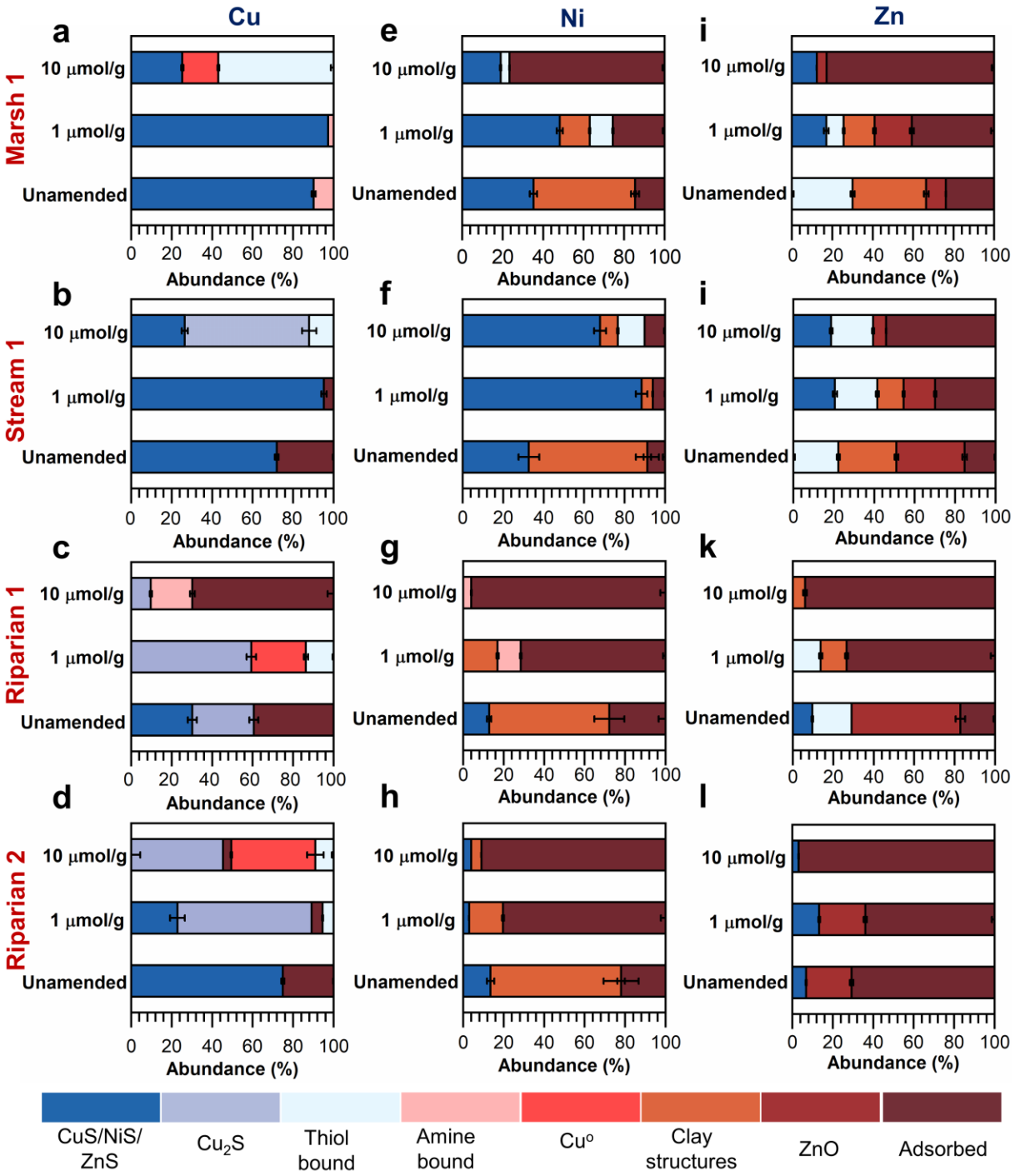

Figure 3.4: Linear combination fitting results of XANES spectra for metals in unamended soils and sediments and after uptake for (a-d) Cu, (e-f) Ni, (i-l) Zn through i-l for the Marsh 1 wetland soils (a, e, and i), Stream 1 sediments (b, f, j), Riparian 1 wetland soils (c, g, and k), and Riparian 2 wetland soils (d, h, l).

High Cu in soils and sediments was taken up by the solids in forms different than those observed in unamended samples and at low Cu loadings **(**Figure 3.4 a-d**).** At high Cu loadings, the speciation of Cu also varied significantly between the different sites. The dominant Cu species at high Cu loading included Cu_2S-like species in stream sediments and Riparian 2 soils, thiol bound Cu in Marsh 1 soils, and adsorbed Cu in Riparian 1 soils. The formation of stable Cu_2S-like species at high Cu loading in Stream 1 sediments suggests the presence of sulfides to sequester high concentrations of dissolved Cu.[109,110,127,128] In Marsh 1 and Riparian 2 samples, the percentage of added Cu that binds to sulfides decreased at high loading, however, the amount present in the form of Cu(0) and that bound to thiol groups on organic matter increased. Under anoxic conditions and in low sulfide environments, Cu(II) can undergo reduction to Cu(I) by reaction with Fe(II) or redox-active functional groups of organic matter or by the action of microorganisms.[129–132] The Cu(I) species may form strong complexes with thiol groups of organic matter (R-SH)[133] or may be further reduced to metallic Cu(0).[132,134] Metallic Cu(0), often in nanoparticulate form, has been observed in earlier studies in the roots of wetland plants, organic-rich bog soils and contaminated soils upon flooding.[135–137] Photoreduction of Cu(II) from X-ray beams during data collection, which has been observed during earlier studies of organic Cu complexes,[138–140] did not occur for these samples. Individual scans of samples containing Cu(0) did not display progressive changes in XANES features during data collection, Further, a wide array of samples of similar composition showed no Cu(0), and elemental copper was not observed to form in unamended wetland soils and stream sediment samples during data collection under similar conditions.[113]

3.3.6 Ni Speciation following Cu Addition to Soils and Sediments

The added Ni dominantly bound to the soils and sediments in adsorbed forms or as nickel sulfide (NiS) **(**Figure 3.4 e-h**)**. In the unamended soils and sediments, Ni associated with clay

mineral structures was the dominant fraction (46-60%) in all the samples. The fraction of Ni associated with clays decreased significantly when additional Ni was introduced to the soils and sediments. The freshly added Ni was taken up by the solid phase as NiS or bound to reduced sulfur groups on the organic matter with a significant fraction also present in the adsorbed form. The Ni mass balance before and after uptake **(**Figure B-11**)** showed that the Ni speciation in unamended soils was retained even after the addition of Ni at low and high loadings. In marsh wetland soils and stream sediments, sulfide moieties controlled Ni speciation at low loading **(**Figure 3.4 e-f**)** as most of the added Ni (61% for Marsh 1 and 88% for Stream 1) was taken up either in the form of NiS or bound to thiol groups on organic matter. At high loading, the presence of reactive sulfide species still dominated Ni uptake by stream sediments (81%), however, in marsh wetland soils the added Ni was primarily taken up in the form of the adsorbed fraction (80%). In the case of riparian wetland soils **(**Figure 3.4 g-h**),** the adsorbed fraction played a dominant role in immobilizing Ni at low and high loadings. The speciation results indicated that Ni showed more affinity to adsorb onto mineral phases than forming sulfide precipitates in the wetland soils.

3.3.7 Zn Speciation following Cu Addition to Soils and Sediments

Similar to Cu and Ni, the speciation of added Zn varied in unamended samples and Zn-loaded soils and sediments. The speciation of the Zn originally present in the soils, except for the zinc oxide component, was conserved even after the addition of Zn at both low and high concentrations **(**Figure B-12**).** The observation of ZnO in the solid-phases is associated with contamination from beamline components **(**section B.4**)**.[113] In marsh wetland soils and stream sediments, Zn speciation in unamended samples as well as after Zn addition at low loading was similar **(**Figure 3.4 i-j**).** At low loading, the speciation of Zn taken up on marsh wetland soils and stream sediments consisted of adsorbed species, Zn associated with the structures of clay minerals,

and Zn co-precipitated in the form of sulfides or complexed to thiol moieties. At high loading, the samples lacked a clay-associated component in both the marsh wetland soils and the stream sediments. Zn uptake at high loadings was dominated by the adsorbed fraction for the marsh wetland soils; however, adsorption, complexation to thiol groups and co-precipitation as sulfide minerals are possible mechanisms responsible for decreasing the dissolved Zn in the stream sediments. The fraction of Zn bound in the form of sulfides or complexed to thiol groups of organic matter is significantly higher in the stream sediments than in marsh wetland soils at low as well as high loading.

In unamended riparian wetland soils, clay-associated Zn was absent, and the samples contained Zn associated with sulfides. The thiol bound fraction was absent in Riparian 2 unamended soils and the Zn speciation was dominated by the adsorbed fraction. Upon addition of Zn at low and high concentrations, the speciation is dominated by adsorbed forms in Riparian 1 and Riparian 2 soils, however, very small fractions became associated with clays and sulfides present in the Riparian 1 and Riparian 2 soils, respectively.

3.3.8 Dominant Mechanisms of Metal Uptake

The metal speciation determined using XAS helped identify the mechanisms driving Cu, Ni and Zn uptake at different loadings on soils and sediments collected from three different natural systems **(**Table B-7**).** Reaction with sulfide species to form CuS/Cu_2S dominated Cu uptake at low loadings in all the systems, which indicates sufficient reduced sulfur species to sequester Cu in the form of Cu sulfides. Cu(II) has more affinity towards sulfur moieties than the other trace metals (Ni, Co, and Zn) and forms a variety of sulfide precipitates.[110,141,142] Due to the higher affinity of Cu to form sulfides, we observed a high abundance of CuS/Cu_2S even in Riparian 1 wetland soils

with very low total sulfur content (0.091%). In sulfur-limited systems, such as the wetland soils and stream sediments evaluated in this study (total sulfur < 0.3%), the formation of Cu(0) and Cu(I) complexation to thiol groups on organic matter are important mechanisms for decreasing the mobility of Cu.[126,143] Due to limited availability of reduced sulfur moieties to precipitate Cu sulfides at high loadings, the formation of Cu(0) and thiol-bound Cu was observed in riparian and marsh wetland soils. Reaction with sulfide species and adsorption decreased Ni availability in marsh wetland soils; sulfide moieties dominated Ni uptake in stream sediments, and only adsorption controlled Ni uptake in riparian wetland soils. Zn uptake is dominated by reactive sulfide species and adsorption in marsh wetland and stream sediments sites, and similar to Ni only adsorption affected uptake of Zn in riparian wetland soils.

Metal speciation information from XANES helped us interpret the differences in Cu uptake behavior among the different soils and sediments. Metal uptake **(**Figure 3.1**)** results revealed that stream sediments showed more Cu uptake than soils at the marsh and riparian wetlands which may signify different binding mechanisms. The difference in the uptake can be attributed to the limited availability of reactive sulfide species in the marsh and riparian wetland soils to bind added Cu, and competition from other metal cations for reaction with a limited amount of sulfide present in the soils.[137] Formation of Cu(0) and associations with thiol-containing ligands at high loading in the case of Marsh 1 and Riparian 2 further support the limited availability of reduced sulfur species to form Cu sulfide precipitates in these soils. Riparian wetlands, Riparian 1 and Riparian 2, show substantially different Cu uptake trends at pH 5 **(**Figure B-5**)** as Riparian 2 soils showed more uptake of Cu especially at the high loadings. The reason for substantial difference in Cu uptake at high loadings on these riparian wetland soils can be interpreted from their speciation results

(Figure 3.4 c-d**).** Cu is dominantly taken up in the adsorbed fraction in Riparian 1 soils, whereas at Riparian 2 site, formation of sulfide precipitates or Cu(0) governed Cu immobilization.

The variation in dominant speciation at different sites provided insight into the differences observed in Ni and Zn uptake behavior. Ni uptake trends showed that Stream 1 sediments bind more Ni at lower loadings than other studied sites **(**Figure 3.1b**).** This high uptake capacity at low loadings can be attributed to the fact that sulfides dominate Ni uptake in Stream 1, whereas at other sites Ni is also substantially bound to the adsorbed fraction. Previous studies indicate that chalcophile metals easily precipitate with sulfides under anoxic conditions to form sulfide precipitates,[110,141] and hence availability of sulfur to sequester Ni increased Ni uptake in Stream 1 at low loadings. Zn uptake was similar across the marsh wetland soils and stream sediments at low loadings, which can be attributed to the similar binding mechanisms **(**Figure 3.4 i-j**)** as revealed by LCF results. The decrease in Zn uptake at high loading in marsh wetland soils may be due to the lower affinity of Zn for the mineral phases present in the soils because at high loading Zn uptake is driven by binding to mineral phases rather than by association with sulfides **(**Figure 3.4i**).** The uptake of Zn on riparian wetland soils was less than on the materials from other sites at lower loadings, and this trend can be attributed to the absence of reactive sulfide species in riparian wetland soils.

3.4 Environmental Implications

The speciation of the added metals varied substantially from the speciation originally present in unamended soils and sediments. This observation indicates that the background speciation of metals is not an appropriate predictor of the lability of freshly added metals to these terrestrial aquatic systems. The dominant mechanisms governing the availability of added metals strongly

depend on the solid-phase characteristics (mineralogy, organic matter composition, and speciation of sulfur moieties) of the soils and sediments. The differences in uptake processes, such as formation of Cu(0) in wetland soils and not in stream sediments, indicate such differences in reactive entities of natural aquatic systems. The combined metal uptake and XANES results indicate consistent differences in speciation of different trace metals. While presence of sulfur moieties played an important role in immobilizing Cu, Zn was dominantly taken up in the adsorbed fraction for most sites. These observations showed that distinct geochemical processes are responsible for immobilizing Cu, Ni, and Zn in the studied wetland soils and stream sediments. The different binding mechanisms of trace metals will govern their availability under varying hydrological and environmental conditions. The release of metals from the adsorbed pools and sulfide precipitates strongly depends upon the pH and redox status of the aquatic systems. However, decomposition/degradation of organic matter due to microbial activity can mobilize metals bound to thiol/amine groups on organic matter.[7,53,144]

Metal uptake results on the selected natural samples suggest that the stream sediments might lack optimum Cu for carrying out complete reduction of N_2O to N_2 during denitrification. Similarly, limited availability of Ni can inhibit methanogenesis in all the studied natural systems. Metal uptake trends can provide information on the amendments of trace metals required to raise the concentrations to optimum levels for biogeochemical processes.

Chapter 4: Role of Copper in Nitrous Oxide Accumulation in Natural Aquatic Systems

This chapter has been published in – Sharma, N., Flynn, E. D., Catalano, J. G., & Giammar, D. E. (2022). Copper availability governs nitrous oxide accumulation in wetland soils and stream sediments. Geochimica et Cosmochimica Acta, 327, 96-115.

4.1 Introduction

Nitrous oxide (N_2O) is a potent greenhouse gas whose global warming potential per unit mass is 265–298 times that of carbon dioxide (CO_2) for a 100-year timescale.[145,146] Global N_2O emissions in the decade between 2007-2016 averaged 17 Tg N yr^{-1}, of which 57% (9.7 Tg N yr^{-1}) were from natural soils and oceans and ~22% (3.8 Tg N yr^{-1}) were from agricultural soils.[37] Denitrification, an anoxic process in which nitrate (NO_3^-) is reduced to N_2, is a key biogeochemical process that regulates the amount of N_2O released from both terrestrial and aquatic ecosystems into the atmosphere.[37,147,148] Natural aquatic systems, especially those that display vertical redox gradients, such as wetlands and hyporheic zones in streams, are active sites for denitrification.[40,148–150] Oxic regions above redox transition zones favor the oxidation of ammonia (NH_3) to NO_3^- via nitrification, and the anoxic regions below redox transition zones promote denitrification with NO_3^- being reduced to nitrite (NO_2^-), nitric oxide (NO), N_2O, and N_2. The incomplete conversion of NO_3^- and NO_2^- to N_2 causes N_2O to be released from the aquatic systems to the atmosphere.[43,151]

An array of metalloenzymes that contain Fe, Cu, and Mo are involved in reducing nitrate and intermediate species to N_2 during denitrification.[152–154] The transformation of NO_3^- to NO_2^- is

catalyzed by respiratory nitrate reductase (Nar), which requires Fe and Mo for complete conversion.[153,155] Depending on the type of microorganism, reduction of NO_2^- to NO is catalyzed by either an iron-containing nitrite reductase (NirS) or a Cu-containing nitrite reductase (NirK).[152,154] NO is rapidly transformed to N_2O with an Fe-bearing nitric oxide reductase (cNOR), and in the final step, N_2O is reduced to N_2 by a Cu-rich nitrous oxide reductase (Nos).[156]

A scarcity of available Cu can limit the conversion of N_2O to N_2. Laboratory studies of pure cultures have demonstrated that Cu limitation resulted in N_2O accumulation.[42,157,158] Granger and Ward (2003) conducted a study with *Pseudomonas stutzeri* and *Paracoccus denitrificans* in an artificial seawater medium to evaluate the effect of Cu on denitrification. They observed that Cu concentrations of approximately 3 nM caused N_2O to accumulate, whereas 10 nM Cu resulted in increased growth rates and complete conversion of N_2O to N_2. The growth of denitrifying microorganisms, *Alcaligenes* sp. NGIB 11015, *Alcaligenes faecalis* lAM 1015, and *P. stutzeri* was also stimulated by the addition of Cu in the range of 0.5 to 80 µM.[157,158]

In soils and sediments, high concentrations of Cu can inhibit denitrification, whereas low availability of Cu can limit microbial activity causing accumulation of intermediate nitrogen species. In estuarine sediments, the addition of 79 µg g^{-1} Cu inhibited microbial activity by 85% and specifically increased the accumulation of NO_2^- and N_2O [159]. Similarly, the addition of Cu at high loadings of 250-1000 µg g^{-1} increased N_2O emissions from soils and wetland sediments [160,161]. In these three studies, the associated dissolved Cu concentrations were not measured. While the three studies just noted had increased accumulation of N_2O associated with high Cu, two other studies found that the addition of Cu to systems with initially low Cu decreased N_2O accumulation. A recent study of freshwater wetland sediments that initially had 37.8 µg g^{-1} Cu and were amended with $CuSO_4$ to have 26 µM dissolved Cu showed an increased abundance of nitrite and nitrous

oxide reductase genes that enhanced the conversion of N_2O to N_2 [151]. Similarly, a study of freshwater sediments collected from central Indiana also showed that N_2O accumulation decreased when the sediments were amended with 50-100 μg g^{-1} Cu [162]. On the other hand, the addition of 100 μg L^{-1} Cu did not have any effect on N_2O emissions release in freshwater wetland sediments [163]. Copper concentrations in uncontaminated environments are typically low [158,164], and hence limited Cu bioavailability in such settings may significantly affect N_2O conversion via denitrification.

In natural aquatic systems, the relationship between the total Cu amount in the sediments and the bioavailable concentration of dissolved Cu is controlled by the presence of solid phases, such as sulfide minerals, particulate organic carbon, iron and manganese oxyhydroxides, and clay minerals [7,50–52]. Changes in aquatic phase parameters, including pH, redox potential, and the concentration of ligands, can mobilize/immobilize metals from solid phases, thus affecting their bioavailability [7,50]. Dissolved Cu is present as a free hydrated ion (Cu^{2+}) and complexes with hydroxides, inorganic ligands (carbonates and chlorides), and organic ligands (humic and fulvic acids) depending on the water composition.[165] Strong organic Cu-chelates, such as complexes with humic acids and fulvic acids, are inert and hence not readily bioavailable, but inorganic hydroxy and carbonate complexes are labile and might be toxic to some microorganisms at concentrations as low as 10 μg L^{-1}.[52,166–168] Several studies have reported that Cu has a high affinity for dissolved organic carbon and exists predominantly as Cu-organic ligand complexes in natural waters [169–172]. Thus, even dissolved Cu concentrations that would be expected to be optimal for N_2O conversion (>10 nM) might exert a limiting effect on denitrification in natural environments if the Cu is predominantly complexed in non-bioavailable forms.

In natural environments, nitrogen cycling can also occur via processes other than biological denitrification. These processes include dissimilatory nitrate reduction to ammonium (DNRA), anaerobic ammonium oxidation (anammox), chemoautotrophic denitrification, and abiotic photochemical and thermochemical processes [148,173,174]. Other elemental cycles, such as those of iron and sulfur, play important roles in nitrogen cycling in natural environments. Autotrophic and mixotrophic denitrifiers can gain energy from mediating the reduction of NO_3^- by inorganic electron donors that include sulfur compounds (S^o, S^{2-}, $S_2O_3^2$), pyrite (FeS_2), Fe^{2+}, Fe^0, and Mn^{2+} [175–179]. Additionally, abiotic reduction of NO_3^-/NO_2^- by dissolved Fe(II) or Fe(II)-bearing minerals has been studied extensively as a pathway for N_2O or N_2 formation under anoxic conditions [177,180–187]. Fe(II)-rich flooded soils showed decreased N_2O emissions because high Fe(II) concentrations favored the complete conversion of NO_3^- to N_2 [188]. A recent study of marine sediments found that ~15-25% of the total N_2O released was produced by abiotic nitrite reduction in the presence of Fe(II) [189].

The effects of redox conditions, substrate availability, temperature, and pH on denitrification have been widely studied [38–41,190]. There has also been significant progress in understanding the toxic effects of elevated Cu levels on the denitrification pathway, but only limited studies have investigated the effect of Cu availability on N_2O accumulation in uncontaminated aquatic systems [43,151]. A broader understanding of how Cu affects N-cycling in natural systems can improve the accuracy of ecosystem models, such as the Dynamic Land Ecosystem Model (DLEM) [37], used to estimate N_2O emissions. The objectives of this study were to (1) investigate the effect of trace concentrations of dissolved Cu on nitrate reduction and the formation of reaction products (NO_2^- and N_2O) with soils and sediments from three different natural aquatic systems and (2) develop a kinetic model for the denitrification reactions that can

quantify the effect of Cu addition on the transformation and accumulation of nitrogen species in environmental systems.

4.2 Materials and Methods

4.2.1 Description of Sites

To investigate the effect of Cu on denitrification, we selected three separate natural aquatic systems: marsh wetlands at Argonne National Laboratory (ANL) in Lemont, Illinois; riparian wetlands in the Tims Branch (TB) watershed at the Savannah River Site in Aiken County, South Carolina; and East Fork Poplar Creek (EFPC) at Oak Ridge National Laboratory (ORNL) in Oak Ridge, Tennessee. Detailed information on the sampling sites, sampling techniques, and soil characterization can be found in our recent study on trace metal speciation at these sites [191]. Briefly, soil/sediment and surface water samples were collected from two different locations at each aquatic system. To identify locations within the sites, we used the labels "Riparian 1" and "Riparian 2" for Tims Branch riparian wetland soils; "Stream 1" and "Stream 2" for Oak Ridge stream sediment sites, and "Marsh 1" and "Marsh 2" for Argonne marsh wetland soils.

4.2.2 Sampling and Characterization

Soil or sediment cores were collected in polycarbonate tubes. Cores from the marsh wetland and riparian wetland were shipped on ice to Washington University in St. Louis, where they were extruded from the tubes and immediately transferred to an anaerobic chamber (Coy Laboratory Products, 3% H_2/97% N_2, with Pd catalyst) to maintain anaerobic conditions. The cores from the stream sediment site were extruded at ORNL within 1 h of sampling, impulse sealed in polyethylene pouches in an anaerobic chamber, and stored in a refrigerator at 4°C before being shipped on ice to Washington University, where they were stored in an anaerobic chamber.

Surface water samples were filtered using 0.22 µm mixed cellulose ester (MCE) syringe filters. A portion was immediately acidified to 2% nitric acid (HNO_3), and the rest of the filtered water was stored at 4 ^oC prior to anion and nutrient analysis. The acidified surface water samples were analyzed to quantify the dissolved major elements (sodium, magnesium, aluminum, silicon, potassium, and calcium) and trace metals (cobalt, nickel, copper, and zinc). The major elements were quantified using a Thermo Scientific iCap 7400 Duo inductively-coupled plasma optical emission spectrometer (ICP-OES), and the trace metals were quantified with an inductively coupled plasma mass spectrometer (PerkinElmer Elan DRC II). The unacidified water samples were used to measure the concentrations of dissolved anions (Br^-, Cl^-, F^-, and SO_4^{2-}) using a Thermo Scientific Dionex Integrion high-pressure ion chromatograph (IC) with a conductivity detector. The major elements and trace metals were extracted from the soils/sediments by microwave-assisted digestion and were analyzed using ICP-OES and ICP-MS, respectively [191]. The extractable nutrients (nitrate, ammonium, and phosphate) in the soils and sediments were obtained using a 2 M potassium chloride extraction method adapted from previous studies[192,193] and were measured using a Seal Analytical AQ300 Discrete Multi-Chemistry Analyzer.

4.2.3 Reagent Preparation

All the solutions were prepared in an anaerobic chamber (3% H_2/97% N_2, with Pd catalyst) using deoxygenated deionized water (>18.2 MΩ cm). Deoxygenated water was prepared by bubbling N_2 gas through it for 4-5 h, followed by bubbling the water in an anaerobic chamber for 3 h with a filtered stream of the anaerobic chamber atmosphere that had been passed in sequence through solutions of ferrous chloride and KOH to remove traces of oxygen and carbon dioxide. A colorimetric assay (CHEMets test kit K-7511) was used to ensure that the dissolved oxygen level in the deoxygenated water was below the detection limit (2 µg/L). Copper chloride dihydrate

(99.99%, Sigma Aldrich) was used to vary the Cu loading in denitrification studies. All other salts (sodium chloride, potassium chloride, sodium sulfate, magnesium chloride hexahydrate, magnesium sulfate, calcium sulfate dihydrate, ammonium chloride, and disodium phosphate) used for preparing simulated site water were purchased from Thermo Fisher Scientific and were of reagent grade. Sodium nitrate and potassium nitrate (99.9%, Sigma Aldrich) were used for preparing a stock solution of nitrate. Nitric acid (trace metal grade, Thermo Fisher Scientific) was used to acidify samples for dissolved metal analysis. Reagents and calibration standards for nutrient analysis were prepared using reagent grade chemicals.

4.2.4 Laboratory Incubation Experiments

The incubation studies were conducted with the samples from the riparian wetlands (Riparian 2 and Riparian 1), the stream (Stream 2 and Stream 1) and the marsh wetlands (Marsh 1). The two locations in riparian wetland soils and stream sediments had different total carbon, sulfur, and metal contents and exhibited different solid-phase speciation of Cu. Both the locations in the marsh wetland soils showed similar characteristics [191], so the samples from only one marsh wetland location (Marsh 1) were used in further studies. Cu uptake experiments were performed to determine the Cu concentration range to consider in the incubation studies. The soils and sediments were completely homogenized before uptake experiments. These experiments were conducted in 15 mL polypropylene tubes containing 1-200 µM $CuCl_2$ and 10 mL of simulated site water, maintained at the desired pH (5.0 for Riparian 1 and Riparian 2, 7.6 for Stream 1 and Stream 2, and 7.0 for Marsh 1) and 0.5 g of soil/sediment. The recipe for the simulated water included the major cations and anions analyzed in the water samples (Table C-1 in Appendix C). Samples were rotated end-over-end for 24 h to ensure complete mixing. After 4 h and 8 h of rotation, the pH values were readjusted to the original values, using 1M NaOH and 2M HCl solutions. The

suspension was then immediately filtered using disposable 0.22 µm MCE syringe filters and acidified to 1% HNO_3. Dissolved Cu concentrations were measured by ICP-MS (PerkinElmer, NexION 2000).

Incubation experiments were initiated under anaerobic conditions in 100 mL serum bottles containing 2.5 g of homogenized soil/sediment along with 50 mL of simulated site water. The simulated water only contained major cations and anions and lacked trace metals or Fe and Mn (Table C-1). The pH of the slurries was adjusted to 5.0 for Riparian 1 and Riparian 2, 7.6 for Stream 1 and Stream 2, and 7.0 for Marsh 1, using NaOH and HCl solutions. For each site, three different conditions were studied: no Cu added (control), low Cu loading, and high Cu loading (loading details are in Table 4.1). The different Cu loadings were selected based on the Cu uptake experiments discussed above. The selection of loadings was done so that the dissolved concentrations after 24 h of equilibration ranged between 10-100 nM and 100-2500 nM for low and high Cu loadings, respectively (Figure 4.1). After 24 h of equilibration, 1 mM NO_3^- was added, and the bottles were sealed with a 20 mm butyl stopper and aluminum cap. Immediately after the addition of NO_3^-, 1 mL of the fluid was sampled to determine the concentrations of dissolved metals and nutrients. The bottles were removed from the anaerobic chamber after NO_3^- addition and were flushed for 10 minutes with ultrapure N_2 to remove trace amounts of O_2 and H_2 from the headspace.

To determine N_2O concentrations, headspace gas samples were taken from each serum bottle at 24 h intervals and were transferred to 3 mL pre-evacuated glass vials (Exetainer®, Labco, United Kingdom) using a gas-tight syringe. The vials were stored upside down to prevent gas leakage from the septum. To separate the dissolved phase, 1 mL of slurry from each serum bottle was sampled and centrifuged (Spectrafuge 16M) for 5 min at 5000 rpm. The supernatant obtained

was divided into three parts, 300 µL was acidified to 1% HNO_3 for dissolved metal analysis, 400 µL was stored for nutrient analysis, and the remaining supernatant was used to estimate the pH using Whatman pH indicator strips. At the end of incubation experiments, the final pH value was recorded using a pH electrode. The water was filtered and stored at 4°C to determine the dissolved organic carbon (DOC) concentration at the end of incubation experiments.

4.2.5 Analytical Techniques

N_2O concentrations in the samples were measured using a gas chromatograph (GC) (Thermo Scientific GC TRACE 1310). Specifically, 1000 µL of the gas sample was injected (split injection at the split rate of 10:1) into the GC inlet (heated to 130 °C) using a TriPlus RSH (Thermo Scientific) autosampler equipped with a 2500 µL headspace syringe. The temperature of the column (Supelco Carboxen 1010 PLOT, 30 m x 0.32 mm) was maintained at 50 °C for 7.5 min, after which it was ramped to 130 °C using a rate of 20 °C/min and then kept at this temperature for 2 min. Helium was used as the carrier gas at a flow rate of 30 mL/min. A pulse discharge detector (PDD) at 150 °C was used for the analysis of N_2O. The concentration of the standards varied from 10 ppmv to 0.1% N_2O and were prepared using a certified gas standard from Airgas. The concentration of N_2O dissolved in the fluid was determined using the ideal gas law and Henry's gas solubility law. The value of Henry's constant at 25 °C used for determining dissolved N_2O was $2.4*10^{-4}$ mol m^{-3} Pa^{-1} [194]. The total N_2O present in the microcosm at the time of sampling was the sum of the gas in the headspace and the gas dissolved in the water.

The dissolved metal concentrations (Cu, Fe, and Mn) were measured using inductively coupled plasma mass spectrometer (PerkinElmer Elan DRC II). DOC concentrations were determined using a total organic carbon analyzer (Shimadzu TOC-L). The nutrient concentrations (NO_3^-, NO_2^- and NH_4^+) were obtained spectrophotometrically using a discrete multi-chemistry

analyzer (Seal Analytical AQ300). The samples used for nutrient analysis were frozen and then thawed overnight at 4°C before analysis. Nitrite was measured by the reaction of the sample with sulfanilamide in dilute phosphoric acid to form a diazonium compound which binds to N-(1-naphthyl)-ethylenediamine dihydrochloride to form an azo dye detected at 520 nm [195]. To determine the nitrate concentration, NO_3^- was first reduced to NO_2^- by cadmium and then the NO_2^- was measured. Ammonium present in the samples was determined by reacting the samples with hypochlorite liberated from dichloroisocyanurate in an alkaline solution followed by a reaction with salicylate in the presence of nitroferricyanide to form a blue indophenol dye, which was measured at 660 nm [196].

4.2.6 Complexation of Dissolved Cu by DOC

To estimate the speciation of Cu in the presence of organic carbon in the incubation experiments, the nonideal competitive adsorption-Donnan (NICA-Donnan) model in Visual MINTEQ 3.1[115] was used. The model is a combination of NICA which enables simulation of metal complexation to humic substances, and a Donnan model describing nonspecific electrostatic interactions between ions and humic substances [171,197,198]. Although humic substances might not truly represent the dissolved organic matter present in aquatic systems [199,200], we used the NICA-Donnan model to estimate the aqueous speciation of Cu because this model has previously provided accurate predictions of metal speciation and availability in natural systems [201,202]. NICA considers competitive binding between protons and metals to humic substances by accounting for binding site heterogeneity and ion-specific nonideality [197]. The generic parameters obtained in previous studies for Cu and proton binding to humic material were used [203–205]. Water chemistry parameters (pH, total dissolved elements (Table C-1)), dissolved Cu, Fe, and Mn, and dissolved organic carbon (DOC) were used as the input parameters for determining dissolved Cu speciation. Three

sets of conditions were used to account for Cu speciation at different total dissolved Cu concentrations corresponding to the control, low Cu loading, and high Cu loading experiments. The combined NICA-Donan model provides the amount of Cu bound to humic substances by using equations S1 and S2 shown in supplementary material (details of the methodology and parameters used are provided in C1 and Table C-3). Under anoxic environments, as in our incubation experiments, Cu(II) can be reduced to Cu(I) by microorganisms, inorganic reductants, and redox-active functional groups on dissolved organic matter [176,206,207]. Cu(I) can form stable complexes with inorganic ligands or thiol groups of organic matter [132,206,208]. In our speciation calculations, we have not accounted for the formation of these Cu(I)-thiol complexes, and dissolved Cu is assumed to be in Cu(II) form.

4.2.7 Kinetic Model

A kinetic model was developed to quantify the effect of Cu on denitrification. Michaelis-Menten expressions were used to describe the evolution of NO_3^-, NO_2^-, N_2O, and N_2 during denitrification (Eq 1-4).

$$\frac{d[NO_3^-]}{dt} = -V_{max}\frac{[C_{NO_3^-}]}{K_{NO_3^-} + [C_{NO_3^-}]} \quad (1)$$

$$\frac{d[NO_2^-]}{dt} = V_{max}\left(\frac{[C_{NO_3^-}]}{K_{NO_3^-} + [C_{NO_3^-}]} - \frac{[C_{NO_2^-}]}{K_{NO_2^-} + [C_{NO_2^-}]}\right) - k_{ab}[C_{NO_2^-}] \quad (2)$$

$$\frac{d[N_2O]}{dt} = V_{max}\left(\frac{[C_{NO_2^-}]}{K_{NO_2^-} + [C_{NO_2^-}]} - \frac{[C_{N_2O}]}{K_{N_2O} + [C_{N_2O}]}\right) \quad (3)$$

$$\frac{d[N_2]}{dt} = V_{max}\left(\frac{[C_{N_2O}]}{K_{N_2O} + [C_{N_2O}]}\right) + k_{ab}[C_{NO_2^-}] \quad (4)$$

Here, V_{max} denotes the maximum reaction rate under unlimited substrate supply (mmol-N L^{-1} day^{-1}), C_y are the concentrations of N-containing species (mmol-N L^{-1}), and K_y values are Michaelis-Menten parameters (mmol-N L^{-1}) describing the substrate concentration at which the reaction rate is half V_{max} [209,210]. For model development, the concentration of N_2 was calculated from the mass balance on nitrogen species. As discussed earlier, abiotic nitrite reduction to N_2 by inorganic electron donors, such as inorganic sulfur compounds (S^o, S^{2-}, $S_2O_3^{2-}$), pyrite (FeS_2), thiocyanate (SCN^-), and ferrous ion (Fe^{2+}), is a pathway in N-cycling [178,189,211,212]. Therefore an additional reaction, accounting for the abiotic reduction of NO_2^- to N_2, was included in the model. A pseudo first-order reaction was used to define the abiotic reduction of NO_2^- in the system (incorporated in Eq 2 and 4), where k_{ab} (day^{-1}) is the pseudo first-order rate constant assuming that the reductants are in excess [186,187], and $C_{NO_2^-}$ is the concentration of NO_2^- in the dissolved phase. Using the ODE45 function in MATLAB R2018a,[213,214] the unknown parameters were calculated. We optimized the parameters by minimizing the residuals using a non-linear least-squares method. Specifically, the value of V_{max} was first determined using Eq 1 and data on the change in nitrate concentration with time. Further, the value of V_{max} was fixed to determine the rate parameters defined in Eq 2-4 for control, low-Cu and high-Cu systems. A constant value of V_{max} can be employed when organic carbon is present in excess of NO_3^- [210]. The total organic carbon present in the systems studied far exceeded the amount of NO_3^- added (Section C.2 in appendix). In separate optimizations in which we allowed the values of V_{max} to be different in equations 1-4, the values were all in the narrow range of range 0.25 – 0.5 mmol-N L^{-1} day^{-1}. The uncertainity estimates were obtained by determining 95% confidence intervals (using "nlparci" function in MATLAB) for the nonlinear least squares parameter fitting on the Michaelis-Menten parameters. We conducted a one-way analysis of variance (ANOVA) combined with a post-hoc test (Tukey-HSD) on the replicates to

statistically evaluate the effect of Cu addition on Michaelis-Menten parameters within each site. Additionally, we performed ANOVA on all the five sites to evaluate if Cu addition effect can be generalized to different natural aquatic systems.

4.3 Results

4.3.1 Characterization of Soils and Sediments

Both the surface water samples, and the soils and sediments were characterized to determine their total carbon, sulfur, metals, and nutrient concentrations. The detailed results are presented in our recent study focused on trace metal micronutrient speciation in wetland soils and stream sediments.[191] The surface water in the marsh wetlands (Marsh 1) and stream sediments (Stream 1 and Stream 2) had pH values ranging from 7.5-8.1, and they contained high concentrations of calcium, magnesium, and sulfate. However, the riparian wetland surface water samples (Riparian 1 and Riparian 2) were at pH 5.5-6.0 with substantially lower concentrations of major elements.

The mineralogy at all of the studied sites is dominated by quartz, with variations in minor phases [191]. The total organic carbon content of aquatic systems varies with location: the marsh wetland site (Marsh 1) contained the highest carbon content (9.0%), whereas Stream 2 exhibited the lowest carbon content (0.5%) (Table C-2). The sulfur content was low at all sites (below 0.24%), following the trend Marsh 1 > Riparian 2 ≈ Stream 1 > Riparian 1 ≈ Stream 2. The total Fe concentration in the solid phases was similar at all the sites (200 to 460 μmol/g), except for Riparian 1, which contained an order of magnitude less Fe than the other soils/sediments. The concentration of Mn was two to three orders less than the Fe content, with the highest values observed in stream sediments. Extractable ammonium in soils/sediments was greater than

extractable NO_3^- and NO_2^- at all the locations, which may indicate denitrification and/or ammonium retention via cation exchange (Table C-2).

4.3.2 Selection of Cu loadings

The total solid-phase concentrations of Cu were well below the crustal abundance (428 ± 61 nmol/g) [215] at all the studied sites. The marsh wetland soil (Marsh 1) and Riparian 2 location in the riparian wetlands contained higher concentrations of solid-phase Cu than the other locations. The dissolved Cu concentrations were less than 50 nM at the selected locations (Table 4.1), indicating that Cu at these sites is predominantly associated with mineral and organic solid phases and might not be bioavailable to microorganisms for N-cycling. Cu uptake experiments were used to determine the Cu loadings to use in incubation experiments to target particular dissolved Cu concentrations (Figure 4.1). The selected loadings resulted in dissolved Cu concentrations in the range of 15-300 nM and 50-2300 nM for low and high Cu amendments, respectively in the incubation experiments (Table 4.1).

Table 4.1: Cu loadings used for conducting incubation experiments, and dissolved Cu concentrations in the fluid during incubation experiments

Site	Control		Low loading		High loading	
	Cu added (µmol/g)	Dissolved conc. (nM)	Cu added (µmol/g)	Dissolved conc. (nM)	Cu added (µmol/g)	Dissolved conc. (nM)
Riparian 1	N.A	29±10	0.25	280±60	1.3	2300±500
Riparian 2	N.A	41±9	0.25	97±10	2.5	560±40
Stream 1	N.A	3±1	0.25	16±2	2.5	53±7
Stream 2	N.A	6±2	0.50	52±6	5.0	590±30
Marsh 1	N.A	48±5	0.13	290±10	0.63	1400±100

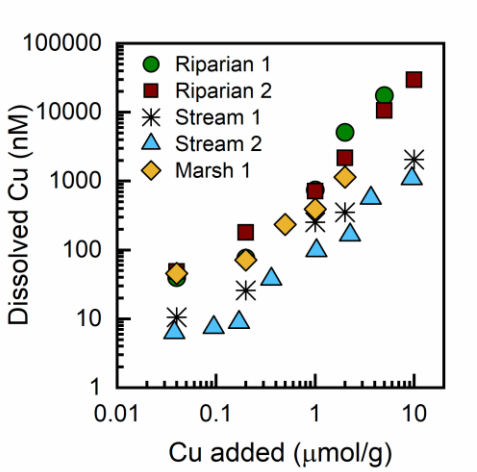

Figure 4.1: Experimentally determined values of Cu uptake by wetland soils and stream sediments, for use in determining Cu loading in microcosm experiments. Here, Riparian 2 and Riparian 1 represent selected locations from the riparian wetland soil, Marsh 1 from marsh wetland soil, and Stream 2 and Stream 1 are locations from a stream sediment site.

4.3.3 Effect of Cu on Evolution of Nitrogen Species during Incubation

The controls and the low-Cu amended sets showed similar NO_3^- reduction profiles in all the systems studied (Figure 4.2). In controls and low-Cu amended systems, the complete reduction of 1 mM added NO_3^- occurred within 16, 5, and 6 days for Riparian 2, Stream 1, and Marsh 1, respectively. In Riparian 1 and Stream 2 experiments, complete reduction of NO_3^- did not occur, even after 27 days and 20 days of incubation, respectively. A small delay in NO_3^- reduction after Cu addition was observed at high Cu loading in Riparian 1, Riparian 2, and Stream 2 incubation experiments (Figure 4.2 a, e, and m, Figure C-1 in Appendix C).

The presence of detectable NO_2^- was transient and showed a brief appearance followed by a rapid decline in concentration in Riparian 2, Stream 1, and Marsh 1 incubations. In Riparian 1 soils, the dissolved NO_2^- concentrations were below the detection limit (0.0005 mmol-N L^{-1}) throughout the experiment, suggesting rapid conversion of NO_2^- in these soils (Figure 4.2b). In the

case of Riparian 2 and Stream 2 systems, Cu addition affected NO_2^- formation/reduction because more NO_2^- was detected in controls as compared to Cu-amended sets.

For all the systems studied, less N_2O transiently accumulated in the sets amended with Cu. We did not observe persistent accumulation of N_2O in the case of Riparian 1 soils (Figure 4.2c), however, the maximum concentration of N_2O (control: 0.040 mmol-N L^{-1} at 14 days, low-Cu: 0.032 mmol-N L^{-1} at 10 days, and high-Cu: 0.021 mmol-N L^{-1} at 12 days) decreased as the dissolved Cu concentration increased. For Riparian 1 controls and low-Cu amended microcosms, N_2O started to accumulate after 3 days of incubation, whereas in high-Cu amended sets, N_2O accumulation was only observed after 6 days of incubation. The complete reduction of N_2O to N_2 was fast in low-Cu amended Riparian 1 sets; we did not observe N_2O after 14 days in low-Cu added sets, whereas it took 29 and 23 days to completely reduce N_2O in high-Cu added and control sets, respectively. In the Riparian 2 control, N_2O accumulated in the headspace and persisted until the end of the experiment at 30 days, whereas the N_2O concentration first increased and then decreased after 10 days and 16 days in Riparian 2 sets amended with low Cu and high Cu, respectively (Figure 4.2g). For Riparian 2, relative to controls, the maximum N_2O concentration decreased by 38.6% in low Cu-added sets and by 70.1% in high Cu-added sets. In the case of the stream sediments, Stream 1 showed a significant effect of Cu addition on N_2O reduction; with respect to controls, the peak N_2O concentration decreased by 2.6 times and 7.8 times in sets with low and high Cu loading, respectively (Figure 4.2k). In Stream 2 and Marsh 1 systems, we were able to measure detectable N_2O in the headspace of only the controls; in the Cu-amended sets, any N_2O generated was rapidly reduced before the N_2O reached detectable levels (Figure 4.2 n, r).

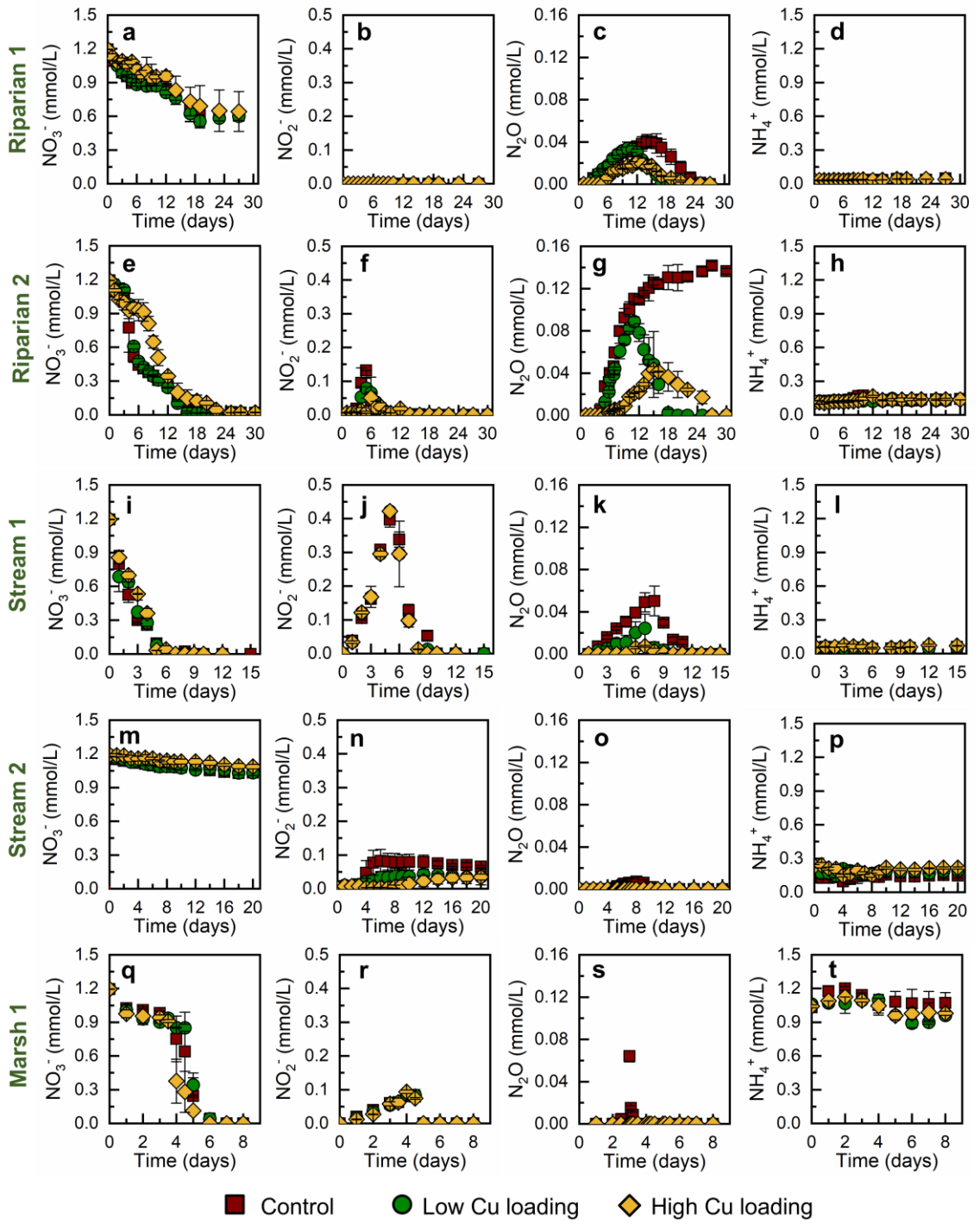

Figure 4.2: Variation in the concentrations of different N- species (mmol-N L^{-1}) during the incubation experiments for (a-d) Riparian 1, (e-h) Riparian 2, (i-l) Stream 1, (m-p) Stream 2 and (q-t) Marsh 1. In case of low Cu loading, 0.25 µmol/g Cu was added in incubation experiments for Riparian 1, Riparian 2, and Stream 1 samples, 0.50 µmol/g for Steam 2 and 0.13 µmol/g for Marsh 1 incubations. High Cu loading amendments for incubation experiments were 5.0 µmol/g for Riparian 1 and Stream 1, 1.3 µmol/g for Riparian 2, 5.0 µmol/g for Stream 2, and 0.63 µmol/g for Marsh 1.

The concentration of dissolved ammonium (NH_4^+) remained relatively constant throughout the experiment for all the treatments (control, low loading, and high loading) in the systems studied (Figure 4.2). Dissolved NH_4^+ was highest in Marsh 1, at 1.039 ± 0.048 mmol-N/L. Riparian 2 and Riparian 1, contained 0.130 ± 0.004 mmol-N/L and 0.033 ± 0.004 mmol-N/L NH_4^+, respectively. The dissolved NH_4^+ concentrations in stream sediments averaged 0.053 ± 0.005 mmol-N/L and 0.172 ± 0.019 mmol-N/L in the Stream 1 and Stream 2 samples, respectively.

4.3.4 Variation in Dissolved Metal (Cu, Fe, and Mn) Concentrations

Dissolved Cu, Fe, and Mn were monitored throughout the incubation experiments (Figure 4.3). The dissolved Cu concentrations in the unamended control microcosms followed the trend Marsh 1 > Riparian 2 > Riparian 1 > Stream 2 > Stream 1. The dissolved Cu concentration remained relatively constant throughout the experiment for Riparian 2, Stream 2, and Stream 1 experiments. However, a decrease in Cu concentration was observed in all Riparian 1 sets, and controls and low-Cu amended Marsh 1 sets in the initial days of incubation (Figure 4.3 d,m).

A decrease in dissolved Fe concentration was observed during the experiment for the riparian wetland soils (Riparian 1 and Riparian 2) and stream sediments (Stream 1 and Stream 2), whereas, in marsh wetland soil (Marsh 1), dissolved Fe concentration did not fluctuate during the 8 days of incubation (Figure 4.3). In the Riparian 1 and Riparian 2 experiments, the dissolved Mn concentration remained constant and was similar for all treatments (control, low and high Cu-loadings). However, in Stream 1 and Marsh 1, we observed a decrease in the concentration of Mn until 7 days and 4 days, respectively and then it remained constant (Figure 4.3 i,o). Mn concentrations in Stream 2 experiments amended with high Cu were greater than the concentrations in controls and low Cu-loading experiments (Figure 4.3l).

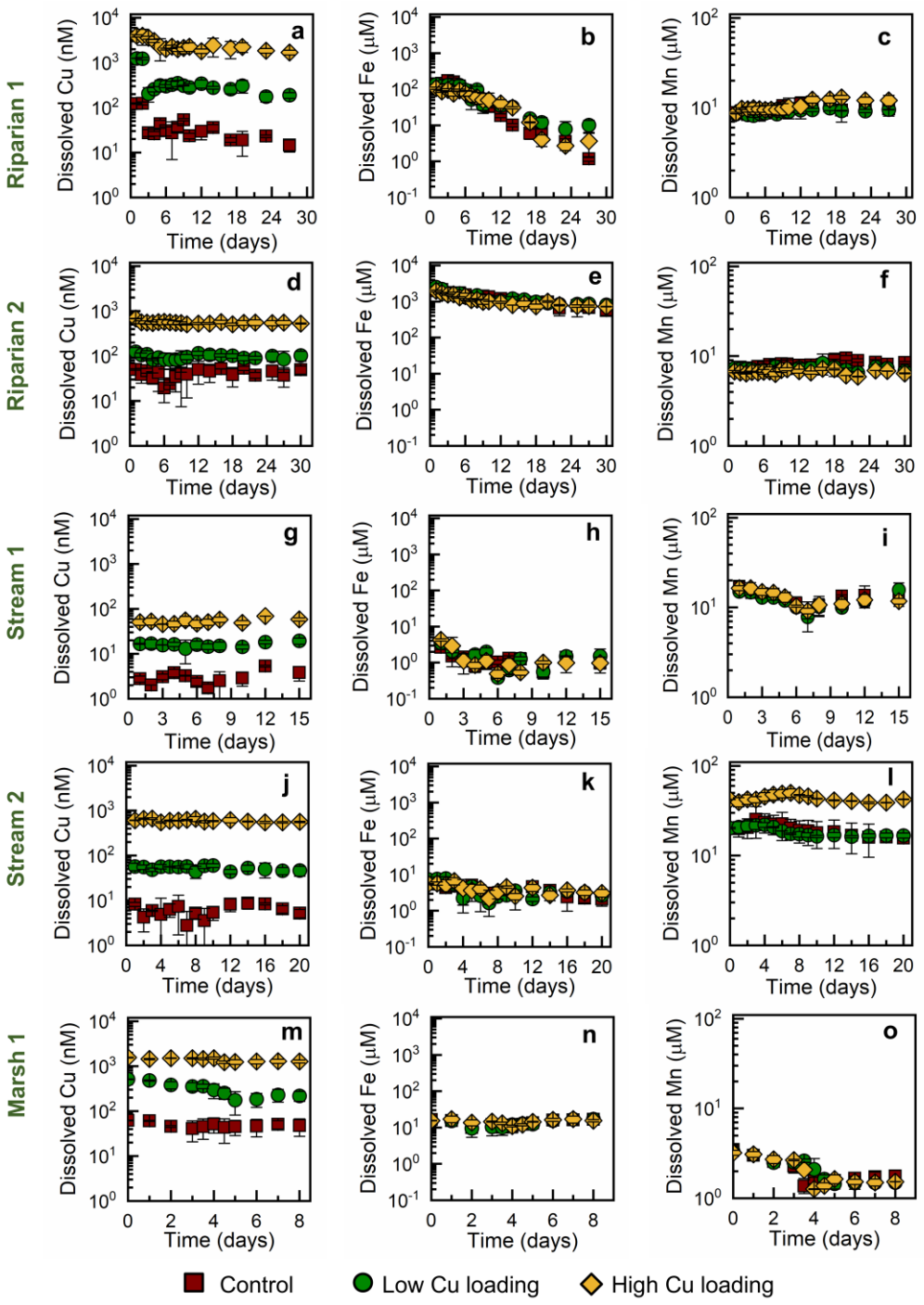

Figure 4.3: Variation in the concentrations of Cu, Fe and Mn during the incubation experiments for (a-c) Riparian 2, (d-f) Riparian 1, (g-i) Stream 1, (j-l) Stream 2 and (m-o) Marsh 1. In case of low Cu loading, 0.25 µmol/g Cu was added in incubation experiments for Riparian 1, Riparian 2, and Stream 1 samples, 0.50 µmol/g for Steam 2 and 0.13 µmol/g for Marsh 1 incubations. High Cu loading amendments for incubation experiments were 5.0 µmol/g for Riparian 1 and Stream 1, 1.3 µmol/g for Riparian 2, 5.0 µmol/g for Stream 2, and 0.63 µmol/g for Marsh 1.

4.3.5 Effect of Cu Addition on Denitrification Rate

The effect of Cu on denitrification was quantified with the help of the kinetic model. We obtained Michaelis-Menten parameters (Table 4.2) and the abiotic rate constant for the set of differential equations defined earlier (Eq 1-4). Here, $K_{NO_3^-}$, $K_{NO_2^-}$, and K_{N_2O} values reflect the ability of the microbial community present in the soils and sediments to reduce NO_3^- to NO_2^-, NO_2^- to NO, and N_2O to N_2, respectively under the conditions studied. NO is rapidly transformed to N_2O, hence the conversion of NO to N_2O was assumed to not be rate-limiting. The rate constant for abiotic reduction of NO_2^- to N_2 by inorganic donors in the system is defined by k_{ab}, and inclusion of this reaction helped us reproduce the major features of all the experiments (Figure 4.4). The abiotic reduction of NO_2^- to N_2O is also a possible pathway, but the incorporation of this reaction into the kinetic model did not improve the fit to experimental data. Michaelis-Menten parameters have an inverse relationship with rates, unlike rate constants; the smaller the value of K_y, the faster the forward reaction; whereas the greater the value of k_{ab}, the faster the rate of abiotic nitrite reduction.

With the help of the kinetic model, we were able to describe the major features in the evolution of the concentrations of different nitrogen species for all the sites except for Marsh 1. For the Marsh 1 site, we observed a lag in NO_3^- reduction in all the incubation experiments. Our model does not account for the acclimatization time of microorganisms after NO_3^- addition, which could have caused poor fitting of data from the Marsh 1 experiments. ANOVA results showed that Cu addition significally affected N_2O transformation in all the systems (Table 4.2 with p-values in brackets). ANOVA results on the full dataset of three Cu levels and five different sites indicated that for a 5% significance level, the Michaelis-Menten parameters are not statistically different for control, low Cu loading, and high Cu loading systems (Section C.4). For the exact values of the

Michaelis-Menten parameters, there is more variability associated with the differences in sites than in the Cu levels. This was expected as the selected natural systems varied substantially in total metal contents, mineralogy, organic matter, and sulfur concentrations.

The modeled $K_{NO_3^-}$ values show that NO_3^- reduction is fastest in Stream 1 sediments followed by Marsh 1, Riparian 2, Riparian 1, and Stream 2. The parameter $K_{NO_3^-}$ was similar for control and low Cu-loading in all the systems studied. However, the modeled value increased (Table 4.2) in high Cu-loading sets initiated with Riparian 1, Riparian 2, and Stream 2 sediments, indicating that the reduction of NO_3^- to NO_2^- is slower in these sets amended with a high concentration of Cu.

Cu addition decreased NO_2^- accumulation in Riparian 2 and Stream 2 samples. The value of $K_{NO_2^-}$ was less in Cu-amended Riparian 2 experiments (control: 0.68 mmol-N L^{-1}; low Cu: 0.22 mmol-N L^{-1}; and high Cu: 0.33 mmol-N L^{-1}), which signified that Cu enhanced the rate of NO_2^- reduction in Riparian 2 soils. Similarly, in Stream 2 sediments, the modeled $K_{NO_2^-}$ values show a substantial decrease in Cu-amended sets (control: 0.079 mmol-N L^{-1}; low Cu: 0.0067 mmol-N L^{-1}; and high Cu: 0.0035 mmol-N L^{-1}).

The rate of N_2O to N_2 conversion, as indicated by the K_{N_2O} parameter, increased upon Cu addition in the Riparian 1, Riparian 2, Stream 1, and Stream 2 locations. In the marsh wetland soil, K_{N_2O} remained relatively constant in the control and Cu-amended experiments. The effect of Cu addition on N_2O reduction was greatest in the Riparian 1 and Riparian 2 soils; in Riparian 2 soils, the value of K_{N_2O} decreased from 11000 mmol-N L^{-1} in unamended control experiments to 0.48 mmol-N L^{-1} and 0.21 mmol-N L^{-1} in low-Cu loading and high-Cu loading experiments, respectively. Similarly, in Riparian 1 soils, Cu addition increased the N_2O conversion significantly;

K_{N_2O} values decreased from 6900 mmol-N L^{-1} to 24 mmol-N L^{-1} and 3.5 mmol-N L^{-1} at low and high Cu loadings, respectively.

The rate of abiotic NO_2^- to N_2 reduction was greater in Riparian 1 and Riparian 2 wetland soils than in the other three systems; all microcosms incubated with Stream 2 sediments and Marsh 1 soils showed negligible k_{ab} values. NO_2^- was not detected in any Riparian 1 incubation experiments (Figure 4.2b); the abiotic rate constant for NO_2^- to N_2 reduction is high in Riparian 1 soils, which could have prevented NO_2^- accumulation in these soil incubations. The values of k_{ab} were similar for all the different incubation studies (controls, low-Cu, and high-Cu loading) of a location, signifying that this step is not affected by the presence of Cu.

4.3.6 Labile Concentration of Cu in Soil/Sediment Incubations

To understand Cu bioavailability as a nutrient and as a toxic element, we estimated the speciation of dissolved Cu using Visual MINTEQ 3.1 and the NICA-Donnan model at the studied experimental conditions and in the presence of dissolved organic carbon (Figure 4.5). The calculations predict that DOC substantially decreased the lability of Cu in the systems studied. Here, the labile Cu concentration is defined as the sum of Cu^{2+}, $Cu(OH)^+$, and $Cu(OH)_{2(aq)}$. In riparian wetland controls, Riparian 1 and Riparian 2, in the studied pH range (5-6), Cu is predominantly present as Cu-organic matter complexes (Figure 4.6), and the labile Cu concentration (Table C-4), is < 3 nM. Similarly, in Stream 1 controls, the total labile Cu concentration is < 1 nM in the experimental pH range (7.6-9.0). Due to a lower concentration of DOC in Stream 2 (Figure 4.5), ~80% of dissolved Cu is present as labile Cu in Stream 2 controls. High DOC in Marsh 1 samples complexed ~84% of dissolved Cu(II), and only 7.6 nM remained as labile concentration in the fluid of controls. In all the Cu-amended experiments, the lability of

Cu was greater than the optimum concentration (3-10 nM) determined to complete N_2O to N_2 conversion in pure culture studies and lake systems [42,43]. Additionally, in high-Cu amended experiments, labile Cu in Riparian 1, Riparian 2, and Stream 2 was substantially higher (> 350 nM), which could inhibit biological denitrification due to toxic effect [165,166,168].

4.4 Discussion

4.4.1 Role of Labile Cu in Nitrogen Cycling

The trends in nitrogen species transformation with and without Cu addition varied between different sites as discussed in section 3.3. The labile concentration of Cu rather than the total dissolved concentration helped us understand the evolution of nitrogen species at different sites. This study found that high dissolved Cu concentrations decreased the rate of NO_3^- reduction in the riparian wetland soils (Riparian 1 and Riparian 2) and from the Stream 2 sediments. This observation is in line with previous results: higher concentrations of Cu can inhibit denitrification by causing a shift in the community composition of denitrifiers [159,216,217]. A recent study that focused on evaluating the toxic effects of copper oxide (CuO) nanoparticles on denitrification in soils observed that the Cu ions (Cu^{2+}) released upon nanoparticle application can decrease nitrate reductase (Nar) activity by 21.1- 42.1%, causing an 11-times decrease in NO_3^- reduction [217]. Elevated Cu^{2+} concentrations (> 500 μg g^{-1} in solid-phase and ~0.95 mg L^{-1} in dissolved form) can decrease biological denitrification by inhibiting extracellular or intracellular enzymes [160,218,219]. At high Cu loadings in the above-mentioned locations (Riparian 1, Riparian 2, and Stream 2), the labile Cu concentrations estimated using the NICA-Donnan model were higher (> 350 nM) than in Stream 1 (28 nM) and Marsh 1 (150 nM) locations (Table C-4), and the higher concentratons could have inhibited NO_3^- reduction during the incubation experiments.

Table 4.2: The values of Michaelis-Menten parameters of different reactions involved in carrying out denitrification at different sites as well as the pseudo first-order rate constant for abiotic reduction of NO_2^- to N_2

Site	Condition	V_{max} (mmol L^{-1} day^{-1})	$K_{NO_3^-}$ (mmol L^{-1})	k_{ab} (day^{-1})	$K_{NO_2^-}$ (mmol L^{-1})	K_{N_2O} (mmol L^{-1})
Riparian 1	Control	0.41±0.02	12±0.5	99±2	0.072±0.004	6900±4
	Low loading	0.41±0.05	11±0.7 (0.11)	99±4 (0.96)	0.072±0.006 (0.56)	24±0.2 (<0.001)
	High loading	0.41±0.03	15±0.3 (0.003)	98±5 (0.82)	0.068±0.002 (0.82)	3.5±0.4 (0.001)
Riparian 2	Control	0.25±0.08	1.1±0.1	2.2±0.3	0.68±0.08	11000±8
	Low loading	0.25±0.07	1.1±0.3 (0.52)	2.2±0.9 (0.99)	0.22±0.06 (0.012)	0.48±0.1 (<0.001)
	High loading	0.25±0.03	1.7±0.3 (0.003)	2.2±0.4 (0.51)	0.33±0.07 (<0.001)	0.21±0.09 (<0.001)
Stream 1	Control	0.39±0.06	0.39±0.09	0.69±0.1	9.1±2	3.7±1
	Low loading	0.39±0.07	0.41±0.1 (0.87)	0.71±0.2 (0.08)	9.7±2 (0.33)	0.72±0.4 (<0.001)
	High loading	0.39±0.01	0.49±0.01 (0.062)	0.64±0.5 (0.29)	9.5±1 (0.81)	0.00078±0.0003 (<0.001)
Stream 2	Control	0.37±0.2	39±3	0.015±0.002	0.079±0.001	0.0085±0.0009
	Low loading	0.37±0.7	40±4 (0.97)	0.015±0.007 (0.96)	0.0067±0.002 (0.004)	0.0024±0.0004 (0.003)
	High loading	0.37±0.02	71±7 (0.002)	0.015±0.001 (0.44)	0.0035±0.001 (0.003)	0.0032±0.0007 (0.006)
Marsh 1	Control	0.27±0.07	0.47±0.2	0.00024±0.0001	0.058±0.008	0.14±0.04
	Low loading	0.27±0.09	0.55±0.2 (0.31)	0.00027±0.0001 (0.95)	0.067±0.002 (0.74)	0.037±0.02 (<0.001)
	High loading	0.27±0.04	0.38±0.2 (0.18)	0.00029±0.0001 (0.68)	0.047±0.009 (0.24)	0.018±0.01 (<0.001)

The values in brackets for control samples indicates the significance level (p-values) for one-way ANOVA followed by post-hoc analysis. p-values < 0.05 imply that there was significant difference in Michaelis-Menten parameters in controls and Cu-amended systems (low-Cu and high-Cu). The error estimates on the Michealis-Menten parameters were obtained using a function "nlparci" in MATLAB which provides 95% confidence intervals on the parameters.

Incomplete reduction of NO_3^- was observed in incubation experiments using Riparian 1 soils and Stream 2 sediments even when Cu was not added and had low labile concentrations. This suggests that denitrification was limited by the low total organic carbon content at these sites [190].

While the total organic carbon present in the soils/sediments exceeded the amount stoichiometrically required for complete reduction of NO_3^- (Section C.2), not all of the organic carbon will be available to denitrifying microorganisms [220]. The biodegradability of the organic matter depends upon molecular characteristics of the organic matter; carbohydrates, proteins, and organic acids are easily degradable, whereas, aromatic and hydrophobic organic entities are recalcitrant to microbial activity.[221,224,226] The low degradability of organic matter is probably limiting NO_3^- reduction in Riparian 1 and Stream 2 sites. In future investigations the CO_2 respiration rate could be measured during the incubation experiments to assess the association between organic matter oxidation and denitrification.

The dissolved Cu concentration in the Riparian 2 control (41 ± 9 nM) was higher than the optimum concentration required for N_2O to N_2 conversion in pure culture studies (3 to 10 nM) [3,42,43]. However, N_2O accumulation was observed at the Riparian 2 site, suggesting that the dissolved Cu may not have been completely bioavailable to the microorganisms that convert N_2O to N_2. The high DOC (47 mg C/L) at Riparian 2 (Figure 4.5) indicated the presence of soluble organic ligands. These ligands may form soluble complexes with Cu, thus decreasing Cu availability [7,50]. The free Cu^{2+} and the Cu(II)-hydroxo complexes concentrations control the bioavailability of Cu rather than the total dissolved concentration [52,164]. The labile Cu concentration in Riparian 2 control experiments, shown as the sum of Cu^{2+}, $Cu(OH)^+$, and $Cu(OH)_{2(aq)}$ (Table C-4), is ~ 1.4 nM which is less than the optimum Cu concentration (3-10 nM) [3,42,43] required for conversion of N_2O to N_2 in pure culture studies. Thus, the low lability of Cu in Riparian 2 control sets could have caused persistent N_2O accumulation in the headspace.

In Riparian 1 soils, both the background dissolved Cu concentration (29.3 nM) and the solid-phase-associated Cu (48.3 nmol/g) were less than the Cu concentration in Riparian 2 soils

(dissolved: 41 nM; solid-phase: 262.3 nmol/g), but N_2O did not accumulate persistently in the headspace of Riparian 1 soils. This observation suggests that bioavailable Cu for N_2O to N_2 conversion is more abundant in Riparian 1 soils. Riparian 1 soils have less dissolved organic carbon (23 mg C/L) than Riparian 2 soils, and thus are less able to decrease the bioavailability of Cu by forming soluble complexes of organic matter with Cu. The speciation results corroborated the hypothesis because in the pH range studied, the dissolved labile Cu in Riparian 1 controls (2.8 ± 0.9 nM) was greater than Riparian 2 controls (1.4 ± 0.8 nM). Prior study on a lake system indicated that the presence of 3 nM dissolved Cu decreased N_2O accumulation during denitrification relative to systems containing no Cu [43]. Although the rate of N_2O to N_2 conversion was slow in Riparian 1 controls as compared to Cu-amended sets (Table 4.2), the labile-Cu concentration closer to optimum range (3-10 nM) prevented persistent N_2O accumulation in the headspace.

The concentration of accumulated N_2O in the headspace of Stream 1 controls was greater than the Stream 2 controls. Both stream sediment sites contained low concentrations of dissolved Cu in the control sets (3.1 ± 1 nM at Stream 1, and 6.2 ± 1.9 nM at Stream 2), however, substantial N_2O accumulation was only observed at Stream 1 location. This finding suggests that the low Cu concentrations of ~ 6 nM were sufficient to enable the N_2O to N_2 conversion in Stream 2 sediments. The dissolved organic carbon concentration is lower at the Stream 2 location (2.1 mg C/L, Figure 4.5) which indicated that the fraction of dissolved Cu that is labile (i.e., not complexed with organic ligands) would be higher for Stream 2 (labile Cu in Stream 1: 0.55 nM and Steam 2: 4.8 nM). Thus, the presence of un-complexed Cu(II) at a concentration of ~ 4.8 nM enabled N_2O to N_2 conversion in Stream 2 controls.

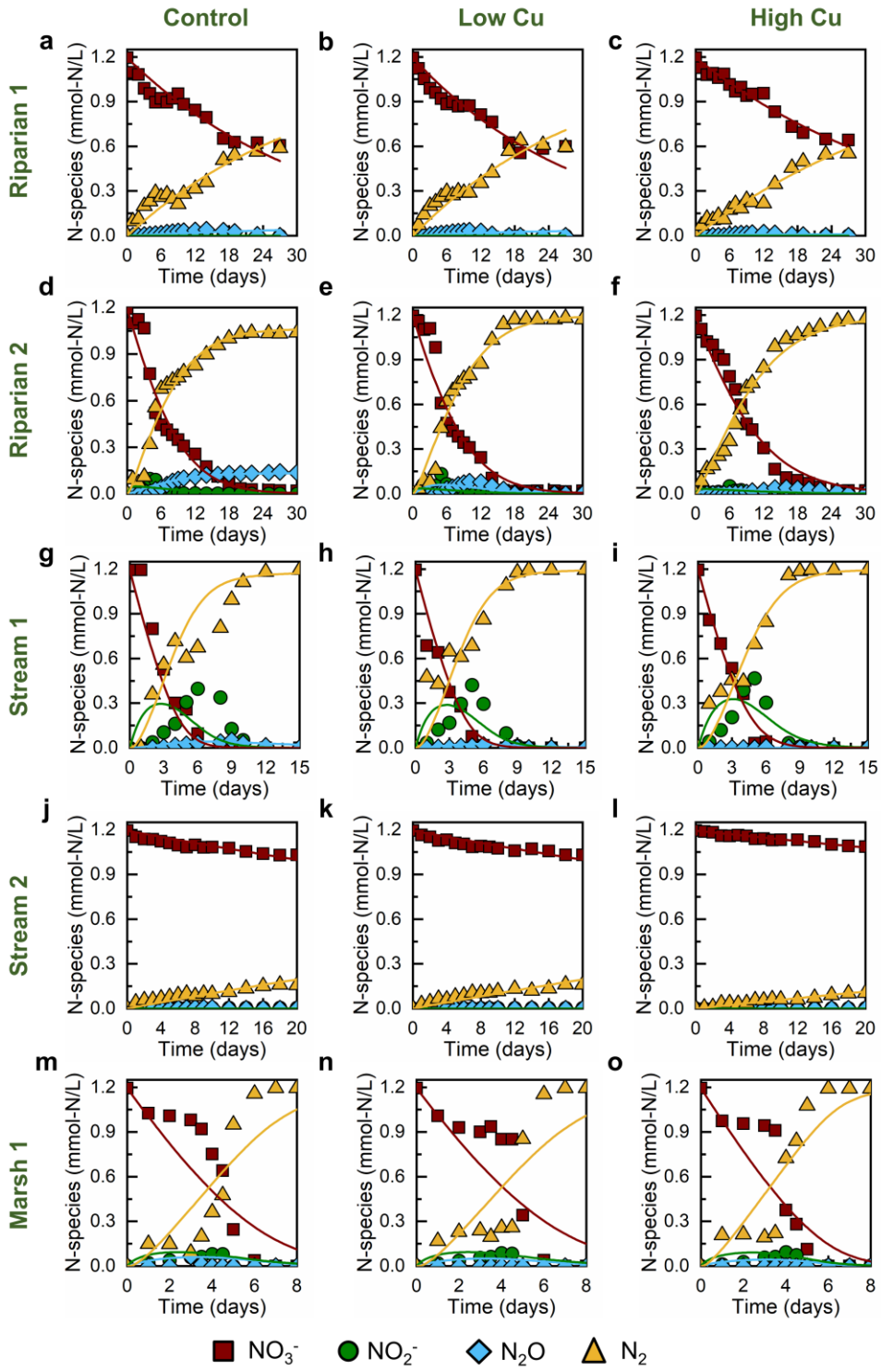

Figure 4.4: Experimental data together with the output of the optimized kinetic model for the evolution of N-containing species during the incubation experiments using the parameters obtained from the kinetic model for (a-c) Riparian 1, (d-f) Riparian 2, (g-i) Stream 1, (j-l) Stream 2 and (m-o) Marsh 1

N_2O was not detected in the headspace of Marsh 1 Cu-amended microcosms, however, we observed accumulation of N_2O in unamended control experiments in the initial days of incubation (max N_2O: 0.064 mmol-N/L). This observation suggests that the rate of N_2O to N_2 conversion was promoted by Cu amendment in Marsh 1 site (Figure 4.2s). The dissolved Cu concentration in the control samples was 48 nM, which is higher than the optimal range (3 to 10 nM) for N_2O transformation in pure culture studies [3,42]. The dissolved organic carbon (32 mg C/L) at the site is calculated to have decreased the bioavailability of Cu substantially (labile Cu in controls: 7.6 ± 5 nM) in the pH range studied, thus resulting in the transient N_2O accumulation in the headspace of the unamended controls.

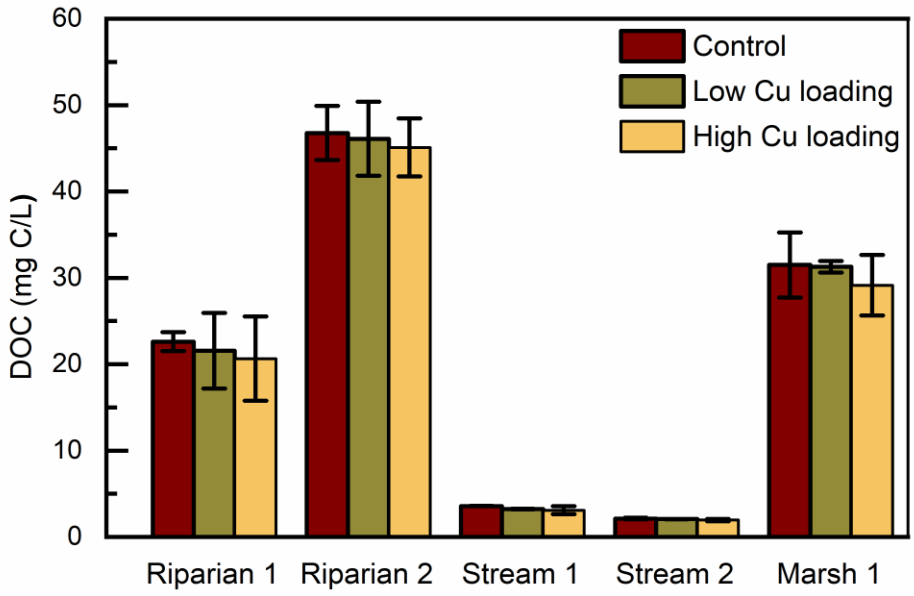

Figure 4.5: Final dissolved organic carbon concentrations in the incubation experiments with soils and sediments of different natural aquatic systems.

4.4.2 Ammonium Release during the Incubations

In all the locations studied, a substantial amount of NH_4^+ was detected in the dissolved phase and remained constant throughout the experiment (Figure 4.2). Exchangeable NH_4^+ can be

released from the solid phase to the fluid because of changes in the water-to-solid ratio, pH, and ionic strength. Alternatively, the NH_4^+ can result from the microbially-mediated dissimilatory nitration reduction to ammonium (DNRA) [222,223,225,227,228]. The ammonium was released into the fluid phase even before the onset of NO_3^- reduction (Figure 4.2), and the concentration of NH_4^+ remained constant throughout the experiment. This observation indicated that most of the released NH_4^+ was due to exchange from the soils/sediments and not due to biological nitrate reduction. Additionally, the mass balance of extractable ammonium in soils/sediments indicates that the soils/sediments have the capacity to release the amounts of NH_4^+ observed in the fluid (Riparian 1: 0.05 mmol-N L^{-1}, Riparian 2: 0.14 mmol-N L^{-1}, Stream 1: 0.15 mmol-N L^{-1}, Stream 2: 0.14 mmol-N L^{-1}, and Marsh 1: 1.04 mmol-N L^{-1}).

4.4.3 Relationship between pH, Dissolved Metal Content, and Denitrification

During the initial 2-3 days of incubation, the pH increased from 5.0 to ~ 6.5 for Riparian 1 and Riparian 2 soils, from 7.6 to ~ 8.9 for Stream 1 and Stream 2 sediments, and from 7.0 to ~ 8.2 for Marsh 1 soils, and then remained relatively constant. The increase in pH values can be attributed to NO_3^- and NO_2^- reduction during denitrification. Previous study on riparian soils indicated that the pH increased from 5 to 7 and 5 to 9 in unbuffered NO_3^- reduction experiments with low (111 µmol N g^{-1}) and high (500 µmol N g^{-1}) nitrogen loadings, respectively [229]. In contrast, pH variation was limited (± 0.5) when denitrification occurred in carbonate-buffered lowland soils from Northern Italy [230]. Our previous study on the studied natural aquatic systems indicated that these soils and sediments lacked carbonate minerals [191]; hence, the buffering capacity of the soils/sediments was likely inadequate to prevent the increase in pH upon NO_3^- and NO_2^- reduction.

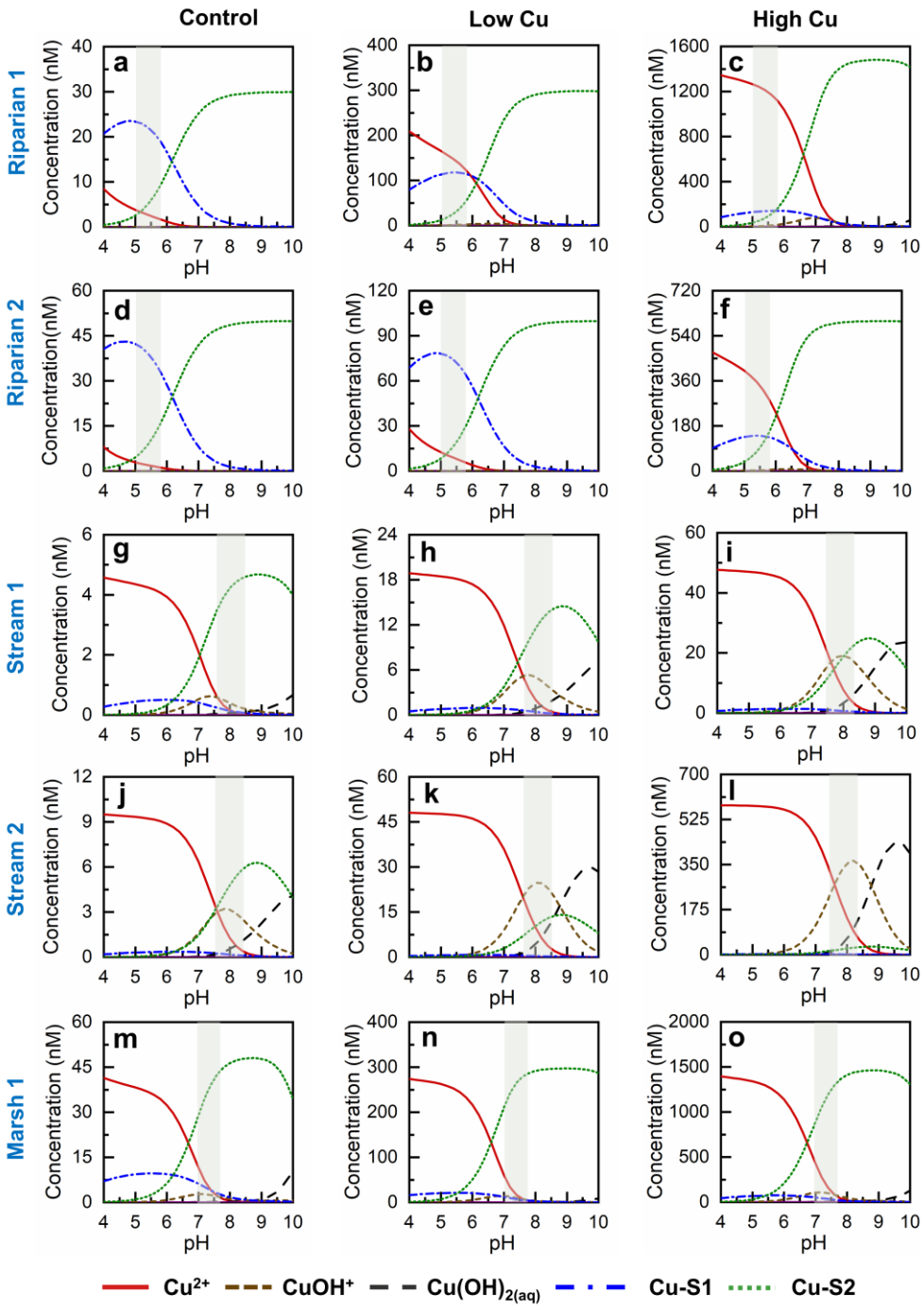

Figure 4.6: Speciation of dissolved Cu at different concentrations for (a-c) Riparian 2 (d-f) Riparian 1 and (g-i) Stream 2 (j-l) Stream 2 and (m-o) Marsh 1. The concentrations of Cu selected for determining the speciation are based on the dissolved concentration of Cu in the incubation experiments (Table 4.1). Here, Cu-S1 shows Cu bound to carboxylic acids of organic carbon and Cu-S2 is the Cu bound to phenolic groups on organic carbon. Shaded areas indicate the pH range over the course of the experiment.

The dissolved concentrations of Cu, Fe, and Mn were indirectly affected by nitrogen cycling in the incubation experiments. Due to a pH increase driven by denitrification, adsorption of metals to minerals phases increased and caused the dissolved concentrations of Cu, Fe, and Mn to decrease with time [7,231] . The decrease in Cu concentrations in Riparian 1 systems and controls and low-Cu amended sets of Marsh 1 soils (Figure 4.3 a, d, and m) likely resulted from an increase in Cu adsorption with increasing pH. We also observed that substantial amounts of Fe and Mn were released into the water in all of the incubation experiments after 24 h of incubation, indicating the reductive dissolution of Fe/Mn oxyhydroxides under anaerobic conditions [7]. The change in the ionic strength and pH of the soils/sediments during the preparation of the slurries could have also caused dispersion of colloidal Fe and Mn [232]. The released Fe decreased over time in the Riparian 1, Riparian 2, Stream 1, and Stream 2 sites. Under the conditions studied, dissolved Fe predominantly exists as Fe(II); the extent of Fe(II) sorption on clays, silica, and metal-oxide phases increases with an increase in pH [231,233,234]. Additionally, Fe(II) may serve as an electron donor for the abiotic reduction of NO_3^- and NO_2^- to form N_2 in soils and sediments (Eq 5-6) [173,184,189,223,235–237].

$$NO_3^- + 5Fe^{2+} + 12H_2O \rightarrow \frac{1}{2}N_{2(g)} + 5Fe(OH)_3 + 9H^+ \quad (5)$$

$$NO_2^- + 3Fe^{2+} + 7H_2O \rightarrow \frac{1}{2}N_{2(g)} + 3Fe(OH)_3 + 5H^+ \quad (6)$$

Although the abiotic reduction of NO_3^- to N_2 in the presence of Fe(II) is thermodynamically feasible, studies indicate that NO_3^- can only be directly reduced by Fe(II) in the presence of mixed-valence Fe-bearing solids (green-rusts), or a catalyst, such as Cu(II), Sn(II), and Ag(I) [175,180,181]. Fe(II) adsorbed to iron-oxide surfaces is a stronger reducing agent than Fe(II) in dissolved form [175,238], hence adsorbed Fe(II) might promote NO_3^- reduction in the studied systems. Additionally,

biological oxidation of structural Fe(II) in clay minerals, such as illite and nontronite, can be coupled with reduction of NO_3^- to N_2 [239,240]. In our incubation studies, the dissolved Fe concentration decreased until 27, 18, and 6 days in Riparian 1, Riparian 2, and Stream 1 systems, respectively and then remained almost constant through the end of the experiments. Decreases in Fe concentration were only observed until the NO_3^-/NO_2^- were completely consumed in these systems indicating that Fe(II) oxidation to Fe(III) oxides/hydroxides is coupled abiotically or biotically to NO_3^-/NO_2^- reduction at Riparian 1, Riparian 2, and Stream 1 sites. Mass balance calculations indicated that NO_3^- concentrations were sufficient to allow for consumption of Fe(II) in Riparian 1, Riparian 2, and Stream 1 systems to react with Fe(II) (Section C.3 in appendix). The values of k_{ab} relative to $K_{NO_2^-}$ were high in Riparian 1, Riparian 2, and Stream 1 systems, suggesting that the reaction involving abiotic NO_2^- reduction is substantial in these systems. On the other hand, the decrease in the Fe(II) concentration in Stream 2 experiments aligned with the pH increase during the initial 2-3 days of incubation, so the decrease in Fe concentration could also be due to increased adsorption at higher pH.

The addition of Cu affected Mn concentrations in Stream 2 experiments; the release of Mn was greater in sets amended with high Cu (Figure 4.3l). In stream 2 incubation experiments with high Cu loading, 250 µM Cu was added and only 0.60 µM remained in the dissolved phase after 24 h equilibration; the competitive adsorption of Cu(II) onto active sites of mineral-phases could have mobilized Mn(II) (~ 40 µM in this case) to the water. Prior studies have also observed the release of Mn(II) in the presence of Cu due to competitive adsorption [241,242]. In Stream 1 and Marsh 1 studies, the concentration of dissolved Mn decreased with time (Figure 4.3 i,o). Mn adsorption has been found to increase with pH on clay minerals, iron oxides/hydroxides and aluminum oxides.

In reducing NO_3^-, Mn^{2+} can also serve as an electron donor (Eq 7) to autotrophic denitrifiers belonging to the genera *Acinetobacter* and *Pseudomonas* [243,244].

$$Mn^{2+} + 0.4NO_3^- + 0.8H_2O \rightarrow MnO_2 + 0.2N_2 + 1.6H^+ \quad (7)$$

Thus, the decrease in the concentration of Mn observed in Stream 1 and Marsh 1 samples can result from increased adsorption caused by a shift in pH or from Mn consumption by autotrophic denitrifiers.

4.4.4 Comparison of Nitrogen Cycling with Materials from Different Systems

The studied aquatic systems, even different locations of the same site, showed varied trends in the reduction of nitrogen species in the incubation experiments. The total dissolved Cu concentrations in both locations of EFPC stream sediments (Stream 1 and Steam 2) were very low (3-10 nM), but transient N_2O accumulation only occurred in their unamended controls, whereas TB riparian wetland soils (Riparian 1 and Riparian 2) showed substantial N_2O accumulation despite having much higher dissolved background Cu concentrations of 30-50 nM. This disparity suggests that the speciation of Cu, and hence its bioavailability, plays a more important role than the total Cu content in controlling N_2O to N_2 conversion in the studied environmental systems.

Even after Cu addition, the accumulated concentrations of N_2O in the riparian wetland samples were higher than in the other locations. One possible explanation is that the riparian wetland incubation experiments were conducted at pH 5, whereas the incubations for marsh wetland soils (Marsh 1) and stream sediments (Stream 1 and Stream 2) were performed at neutral pH conditions. Acidic soils decrease the activity of the nitrous oxide reductase enzyme, leading to N_2O accumulation [245–248]. Optimal N_2O reduction has been observed in the pH range of 7.5-8.0; previous studies have observed substantial N_2O accumulation in the pH range of 6.0-6.5 [247,248].

Although the pH in the riparian wetland soils increased to ~ 6.5 in the first two days of incubation, i.e., before the onset of N_2O accumulation, it was in the range where a decrease in the activity of nitrous reductase enzyme has been observed [247,248]. Thus, Riparian 1 and Riparian 2 wetland soils could be a significant source of N_2O, not only because the bioavailable Cu is limited but also because they are acidic.

4.5 Geochemical Significance and Implications

Most pristine natural aquatic systems contain low solid-phase Cu, and hence they may have low availability of Cu for microbial denitrification. The limited set of studies on natural aquatic systems containing Cu at concentrations less than or equal to crustal abundances (441±63 nmol g^{-1}) support our major finding that increased Cu concentrations can increase the extent of conversion of N_2O to N_2. At 26 µM dissolved Cu, Giannopoulos et al. (2020) concluded that greater availability of Cu led to less N_2O accumulation and higher abundance of Cu-dependent enzymes in wetland soils. A study on agricultural soils indicated that the application of organic fertilizer modified with 130 mM $CuSO_4$ decreased N_2O emissions substantially [249]. However, these above-mentioned studies evaluated Cu concentrations that are relatively higher than the optimum range (3-10 nM) required for N_2O to N_2 transformation in pure culture studies. The concentrations of dissolved Cu in natural environments are typically low (< 200 nM), and the presence of inorganic/organic ligands can further decrease the bioavailability of Cu causing incomplete denitrification with N_2O accumulation. Our results indicated that without Cu amendment, substantial N_2O accumulation can take place in soils and sediments.

The selected sites represent different aquatic systems in geologically-distinct regions and contain low solid-phase and dissolved Cu (solid-phase: 45-280 nmol g^{-1} and dissolved: 3-48 nM).

Despite the differences in mineralogy, elemental composition, and aqueous-phase characteristics, the presence of dissolved Cu at trace levels (10-500 nM) decreased N_2O accumulation in all the sites. The response of riparian wetland soils (Riparian 1 and Riparian 2) to Cu addition was less pronounced than that of other studied sites, which highlights that the systems with acidic conditions like Riparian 1 and 2 can be substantial contributors of N_2O emissions even in the abundance of Cu.

Our study provides greater insight into the importance of Cu speciation on cycling of nitrogen species in environmental systems The effect of Cu on N_2O accumulation was more closely associated with estimated labile-Cu concentrations than with total dissolved Cu concentrations. Dissolved Cu in the porewater of soils and sediments was substantially lower than the total solid-phase associated concentration, and its lability is lowered by its interactions with dissolved organic matter [7,52].

For systems with Cu limitations of complete denitrification, our results indicate that the addition of minor amounts of Cu can increase the rate of N_2O conversion in natural aquatic systems Natural soils have been recognized as an important source of N_2O to the atmosphere and are estimated to release up to 5.6 Tg N_2O-N yr^{-1} [37]. Current ecosystem models, such as DLEM, incorporate multiple environmental factors, including moisture content, temperature, nitrate and dissolved organic carbon concentration, and pH, in the estimation of N_2O emissions from terrestrial systems [250]. These models do not account for the effect of trace metal micronutrient availability (Cu, Ni, Zn, Co, and Mo) on biogeochemical processes responsible for the release of greenhouse gas emissions. The inclusion of Cu as an additional parameter can help improve the accuracy of existing ecosystem models to predict N_2O emissions from soils and sediments. Addition of Cu at micronutrient levels to natural aquatic systems could potentially decrease N_2O release to the

atmosphere. Addition of $CuSO_4$ in lakes is commonly practiced to inhibit algal growth. Previous studies indicate that Cu concentrations above 100 nM can decrease algal and bacterial populations in surface waters [251]. Hence, addition of Cu at micronutrient levels (10-30 nM) is not expected to be toxic to aquatic organisms. Changes in Cu speciation in wetlands and stream sediments associated with hydrologic variation could also influence net N_2O emissions.

4.6 Conclusions

Through a combination of incubation experiments and a kinetic model we determined the effect of dissolved Cu at trace levels (10-500 nM) on the rate of N_2O reduction. Only the systems containing estimated labile Cu < 10 nM had substantial N_2O accumulation. Even with a small increase in dissolved Cu concentration, as observed in low-Cu-loaded incubation experiments, the rate of N_2O to N_2 conversion was significantly enhanced. The contribution of the abiotic reduction of NO_2^- to N_2 by Fe(II) was significant at Riparian 1, Riparian 2, and Stream 1 locations. Riparian wetland soils showed higher N_2O accumulation than the other sites studied, indicating that the acidic pH conditions can enhance N_2O emissions from natural environments. The sites containing high concentrations of DOC (Riparian 1, Riparian 2, and Marsh 1) had less concentrations of dissolved Cu that were labile and showed greater N_2O accumulation. Our results indicate that including Cu bioavailability in ecosystem models could improve the accuracy of estimates of N_2O emissions from natural landscapes.

Chapter 5: Metal Mobilization upon Redox Fluctuations in Natural Aquatic Systems

This chapter has been published in – Sharma, N., Wang, Z., Catalano, J. G., & Giammar, D. E. (2022). Dynamic Responses of Trace Metal Bioaccessibility to Fluctuating Redox Conditions in Wetland Soils and Stream Sediments. ACS Earth and Space Chemistry.

5.1 Introduction

Wetland soils and hyporheic zones in streams display vertical redox gradients that make them active sites for biogeochemical processes, such as methanogenesis, denitrification, and aerobic and anaerobic methanotrophy.[154,252,253] These processes serve as substantial sources of the greenhouse gases nitrous oxide (N_2O) and methane (CH_4). Wetlands are the dominant natural source of CH_4 emissions (60-80%) to the atmosphere, and ~58% of total N_2O emissions are contributed by natural and agricultural soils.[37,250] Microorganisms involved in carrying out biogeochemical processes require trace metal micronutrients as cofactors in key enzymes. Methanogens require Ni-containing hydrogenases and Co-bearing methyltransferase to carry out methanogenesis, and denitrifiers utilize the Cu-containing nitrous oxide reductase for reduction of N_2O during dentification. Laboratory studies have demonstrated that low availability of trace metal micronutrients may limit these microbial processes,[254–256] while at high concentrations some trace metals can be toxic to microorganisms driving biogeochemical processes.[160,257,258] Optimal methanogenic growth occurs at 0.2- 2µM Ni and 0.1- 2µM Co, and Cu concentration required for nitrous oxide conversion to nitrogen via denitrification lies in the range of 3-10 nM.[253,255] Thus,

trace metal concentrations in the porewater of soils and sediments can potentially influence biogeochemical processes in these natural systems.

In environmental systems, the bioavailability of trace metals is controlled by processes including adsorption/desorption onto solid phases, such as iron and manganese (oxyhydr)oxides, clay minerals, aluminum oxides, and iron sulfides, co-precipitation with sulfides and phosphates, and complexation with soluble and solid-phase organic matter.[7,50,141,259–262] The bioavailability of dissolved metals is also affected by aqueous phase parameters (pH, inorganic ligands, and organic ligands). Complexation of trace metals by dissolved organic matter (DOM) occurs widely in natural aquatic systems and lowers metal bioavailability.[130,259,263–265] Studies have shown that Fe/Mn oxyhydroxides, aluminum oxides, clay minerals, and soil organic matter control the dissolved concentrations of Zn, Ni, and Co under aerobic conditions.[50,264,266,267] Changes in soil and sediment geochemistry can result in the transformation of trace metals into forms that are more bioavailable to and potentially more toxic to microorganisms than metals occluded in the crystal lattices of minerals.[7,268,269]

Anoxic systems containing high sulfur concentrations may immobilize trace metals by co-precipitating them with Fe-sulfides or by forming distinct metal sulfides.[110,270,271] The available sulfide is consumed in the order of most insoluble to more soluble metal sulfides (Cu, Zn, Ni, Co, Fe).[141] In a laboratory-based microcosm study on sulfur-limited riparian floodplain soils, Cu was completely sequestered in the form of sulfides, whereas Zn, Ni, and Fe remained in the dissolved phase.[141] Due to the redox-active nature of Cu, the mobility of Cu in anoxic conditions can also be affected by the formation of Cu(0) and association of Cu(I) with reduced sulfur groups on organic matter.[272] Upon oxidation, dissolution of reduced Cu species causes mobilization of Cu; in a sulfate-limited system, Cu release was more pronounced due to rapid oxidation of Cu(0).[132]

Chalcophile trace metals can also form metal sulfide nanoparticles that may persist over several weeks in oxic environments.[136,143] Additionally, soils subjected to redox variability can form sulfide colloids that enhance the mobility of trace metals through colloid-mediated transport.[141]

Anoxic conditions favor the reductive dissolution of iron and manganese oxyhydroxides, which may release adsorbed trace metals into the porewater.[50,54,144,270] An influx of dissolved oxygen can oxidize Fe(II) and Mn(II) causing the rapid formation of iron(III) and manganese(III/IV) oxyhydroxides, which decreases the bioavailability of many trace metals by sorption or coprecipitation mechanisms.[7,50,144,271] Fe(II) mobilized under anoxic conditions may form Fe(II)-bearing minerals, such as siderite ($FeCO_3$), vivianite ($Fe_3(PO_4)_2 \cdot 8H_2O$), and mackinawite (FeS).[54,102,273] These minerals can immobilize trace metals through adsorption or co-precipitation[102,270] and may alter the mobility of trace metals by chemically reducing them.[274,275] Cu is much less mobile in reduced forms due to Cu(0) precipitation or complexation of Cu(I) by reduced organic sulfur groups.[132,272]

Soil organic matter is another crucial constituent controlling trace metal mobility in natural environments. Under anoxic conditions, dissolved organic matter (DOM) can be released into the porewater due to the production of organic metabolites in microbial processes, release of organic matter upon reductive dissolution of Fe/Mn oxides, and desorption of organic matter from soil minerals upon a pH increase that accompanies reduction reactions.[265] The increase in DOM concentration can mobilize sorbed/complexed trace metals. Previous studies indicate an increase in Ni mobility due to DOM release in reducing conditions in soils and sediments.[276,277] In systems that are rich in soil organic matter, Cu mobility is restricted by adsorption to soil organic matter under oxic conditions; however, under suboxic conditions, Cu mobility is expected to increase due to limited Cu-sulfide formation and Cu-dissolved organic matter complex formation.[278]

The effect of redox fluctuations on Fe, metalloids (As, Cr), and radionuclides (U) has been widely explored,[279–283] but only a few studies have focused on changes in the availability of trace metals (Cu, Zn, Ni, and Co) upon variability in redox conditions.[284,285] The repeated cycling of redox conditions affects the crystallinity of Fe(III)-oxyhydroxides,[279,286] modifies the properties of Fe-rich clays,[287–289] and can decrease the reduction capacity of natural aquatic systems.[290,291] The modifications in Fe-rich clays upon redox fluctuations include changes in Fe coordination environment and oxidation state, cation exchange capacity, and swelling capacity.[287–289] The impact of the changes noted above on trace metal mobility in complex environmental systems, such as wetland soils and hyporheic zones of stream sediments, under fluctuating redox conditions remains unclear.

The objectives of this study were to (1) quantify the responses of trace metal (Cu, Ni, Co, and Zn) mobility to fluctuating redox conditions in wetland soils and stream sediments and (2) connect those responses with controls on mobility exerted by Fe/Mn oxyhydroxides, organic matter, and sulfur species. The selected sites varied from each other in aspects of total iron, sulfur, and organic carbon concentrations. We subjected the wetland soils and stream sediments to three cycles of redox fluctuations in laboratory microcosms and observed the variation in the dissolved concentration of trace metals. To determine the change in the bioavailable concentrations of trace metals as a result of a change in redox state and with cumulative redox cycles, passive samplers based on the diffusive gradient in thin film technique (DGT) were deployed in the microcosms after each redox fluctuation.

5.2 Materials and Methods

5.2.1 Description of Sites and Sampling Information

Samples from two natural aquatic systems, a riparian wetland and a stream, were investigated to observe the effect of fluctuating redox conditions on trace metal availability (details of the locations in Figure D-1 in the appendix). Soil samples were collected in October 2020 from a riparian wetland in the Tims Branch watershed at the Savannah River Site in Aiken County, South Carolina. The site has flooded and dried several times during the last decade.[292] It lacks surface water during the summer but quickly, within hours, recharges during extreme weather events. Tims Branch also experiences high beaver activity causing ponding. Stream sediments were sampled from East Fork Poplar Creek (EFPC) in Oak Ridge, Tennessee in September 2020. The creek has a history of mercury contamination and currently receives treated wastewater from the City of Oak Ridge Wastewater Treatment Facility (ORWTF).[293] The overlying surface water at Tims Branch site was acidic (~5.0), whereas stream water at Oak Ridge was slightly basic (~7.6). The mineral composition at both the sites was dominated by quartz with slight variation in minor phases. The wetland soils contained gibbsite in addition to K-feldspar, kaolinite, chlorite, and illite.[294]

Solids (~ 15 kg from each site) from the top layer of soils and sediments (~ 0-10 cm depth) were collected from the selected locations. The samples were stored at 4°C in large polyethylene pouches before being shipped to Washington University in St. Louis. The samples were shipped to St. Louis on ice packs within 24 h of sampling, where they were immediately transferred to an anaerobic chamber, and then impulse-sealed in polyethylene pouches. To maintain anaerobic conditions during storage in the laboratory, an oxygen scavenging sachet (BD GasPak™ EZ

anaerobic container system sachets with indicator) was added to the secondary pouch. The secondary bag was also impulse sealed, and the samples were stored at 4°C for ~3 months before initiating redox fluctuations experiments.

5.2.2 Experimental Layout

The soils and sediments were completely homogenized, and debris was removed manually before initiating the microcosm studies. Wetland soils and stream sediments were subjected to three cycles of anoxic and oxic fluctuations for 24 days (Figure 5.1, Table D-1 in appendix). Separate soil microcosms were maintained at constant anoxic or oxic conditions for the entire duration of the experiment. Anoxic cycles were conducted in an anaerobic chamber (Coy Laboratory Products, 3% H_2/97% N_2, with Pd catalyst), whereas oxic cycles were performed on the bench-top under atmospheric conditions.

For each site, 12 microcosms containing 30 g of soil/sediment and 100 mL of simulated site water (Table D-2) were initiated under anoxic conditions in an anaerobic chamber. To replicate the field conditions, the microcosms were initiated at pH 5.0 and pH 7.6 for wetland soil and stream sediments, respectively. The pH of the microcosms was readjusted to the original values using 1 M NaOH and 1 M HCl solutions throughout the experiment. In an effort to focus on the effects of dissolved oxygen independent of changes in pH, we chose to readjust the pH to the target value in these experiments. The slurries were agitated on an end-over-end shaker to ensure homogeneity. At the end of the first anoxic fluctuation (i.e., 6 days), two microcosms were used for analyzing the supernatant composition, the bioavailable concentration of the metals, and the speciation of metals in the solid phase (details of analysis below). The remaining microcosms were transferred to oxic conditions where they were sparged with air for 1 h to increase the dissolved oxygen concentration to at least 9.0 mg/L. The dissolved oxygen concentration was monitored using a DO

probe (EcoSense ODO200). The microcosms were aerated after 1, 3, 6, 12, 24, 30, and 36 h by sparging with air for ~ 45 min. After an additional 2 days of incubation in oxic conditions, two microcosms were used for analysis whereas the remaining microcosms were shifted to anoxic conditions by sparging with N_2 for 1 h. The procedure was repeated to complete three sets of anoxic-oxic fluctuations. The time-intervals of anoxic conditions and oxic conditions (τ_{anoxic}:τ_{oxic} = 3) were chosen based on those used in previous studies focusing on multiple cycles of redox fluctuations.[280,295] We did not encounter any unexpected or unusually high safety hazards while conducting the incubation experiments.

Water samples were collected to determine the concentrations of dissolved metals, sulfate, and dissolved organic carbon (DOC) in the water during different cycles of redox fluctuations. For stream sediments, water samples were collected at the end of each anoxic and oxic step, however, in the case of riparian wetland microcosms, we collected water samples every 24 h to examine the kinetics of trace metal uptake/release in anoxic and oxic conditions. Water samples were filtered using 0.22 µm mixed cellulose ester (MCE) syringe filters; ~ 2 mL of filtered water sample was acidified to 1% HNO_3 to determine dissolved metal concentrations, and ~ 5 mL unacidified filtered sample was stored in the refrigerator prior to measurement of the DOC and sulfate concentrations. DGT samplers were then deployed in the microcosms to estimate the bioavailable concentration of metals. The DGT samplers were removed after a 24 h incubation time. Previous studies indicated that 24 h was sufficient for establishing steady-state conditions and measuring labile trace metal species.[296,297] The resin gels were retrieved from the DGT samplers and immersed in 1 mL of 1 M HNO_3 for at least 24 h to extract the metals bound to the gel. The labile concentrations of metals bound to the gel were estimated using the equations shown in Section D.1.

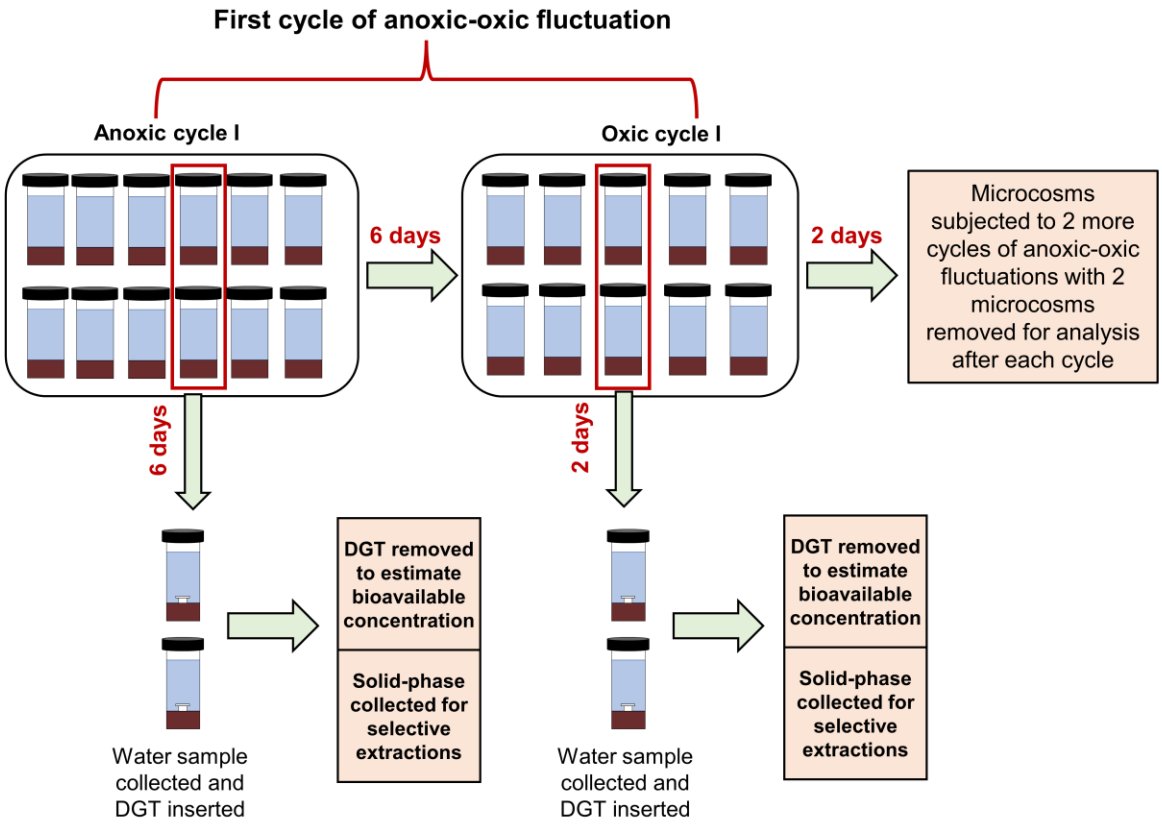

Figure 5.1: Experimental layout for redox fluctuation experiments. Separate microcosms maintained at constant oxic or anoxic conditions were also initiated and run in parallel to those with fluctuations.

Following the DGT sampler retrieval, the excess supernatant was discarded, and the solid phase was collected for selective extractions that probed the metal fraction bound to oxidizable and reducible solid-phases (details of extraction technique in Section D.4 in appendix). Dissolved metal (Cu, Ni, Zn, Co, Fe, and Mn) concentrations were quantified using inductively coupled plasma mass spectrometry (ICP-MS, PerkinElmer NexION 2000). The detection limits of the method were 0.31 ± 0.10 nM, 0.28 ± 0.10 nM, 0.18 ± 0.05 nM, 8.7 ± 2 nM, 0.14 ± 0.05 nM, and 62 ± 5 nM for Cu, Ni, Co, Zn, Mn, and Fe, respectively. The accuracy of the method was monitored by using check standards at regular intervals during the analysis. The concentrations of the check

standards varied by < 5% during the analysis. A total organic carbon analyzer (Shimadzu TOC-L) was used for determining the DOC concentration; and the concentration of sulfate was quantified with ion chromatography (Dionex Integrion HPIC, Madison, WI, USA) with an IonPac AS18 column.

5.2.3 DGT Sampler Development

DGT samplers contain three layers, a filter membrane, a diffusion gel, and a resin gel. Labile trace metals, including free and weakly-bound species, diffuse across the membrane and through the diffusion gel and accumulate on the resin gel. The diffusion gel and the binding gels for DGT samplers were prepared according to the procedure published by Zhang and Davison.[298] The gel solution used for preparing diffusion and binding gels contained 15% by volume acrylamide and 0.3% by volume N,N-methylenebisacrylamide crosslinker. Freshly prepared ammonium persulfate (10%) was used as an initiator for polymerization and N,N,N',N'-tetramethylethylenediamine (TEMED) served as a catalyst. For the preparation of 10 mL of diffusion gel, 70 µL of ammonium persulfate and 20 µL of TEMED were added. The pore size of the diffusion gel used is ~ 2 nm which will prevent the entry of colloids and nanoparticles.[298,299] The resin gel contained 2 g of Chelex 100 (Na form, 200-400 mesh) in 10 mL of gel solution. We added less ammonium persulfate (50 µL) and TEMED (15 µL) to the resin gel solution than to the diffusion gel to prolong the setting process and allow the Chelex to settle by gravity. After 45 minutes of setting time, the gels were removed from the casting assembly and hydrated in ultrapure water for 24 hours. The water was periodically changed to remove any trace metal contamination. The diffusion gels were stored in $NaNO_3$ (0.01 M), and resin gels were stored in ultrapure water at 4°C. Prior to storage, the gels were cut into 25 mm discs for use in DGT samplers. DGT samplers

were assembled 1-2 days before deployment in the microcosms and were stored in re-sealable storage bags along with a few drops of 0.01 M NaCl to prevent the gels from drying out.

5.3 Results and Discussion

5.3.1 Characterization of the Samples

Stream sediments had higher total concentrations of most metals than the riparian wetland soil; the one exception was Cu, which was more abundant in the wetland soil (Table D-3, methods used in Section D.2). Overall, trace metals followed the trend Zn > Cu > Ni > Co at both sites. The concentrations of the trace metals in natural aquatic systems studied were similar to or below geological background levels of 440±60 nmol g^{-1} Cu, 800±200 nmol g^{-1} Ni, 290±10 nmol g^{-1} Co, and 1000±90 nmol g^{-1} Zn.[300] Total organic carbon contents were similar at both the sites (3.6% for the wetland soil and 3.0% for the stream sediments); however, the stream sediment contained more sulfur (31 µmol/g versus 18 µmol/g). Surface water samples at the riparian wetland were slightly acidic with pH values ~5.0; the stream water samples had pH values ranging from 7.5-8.1.[294] The low pH at riparian wetlands soils is due to high dissolved CO_2. The mineral composition at both sites is dominated by quartz; carbonate minerals were not detected at either site.

5.3.2 Redox-Induced Dynamics of pH and DO

We monitored the pH throughout the experiment; the pH values were readjusted to 5.0 ± 0.5 and 7.6 ± 0.5 daily for riparian wetland soils and stream sediments, respectively (Table D-4). Due to pH adjustments, the change in ionic strength over different cycles (Table D-5) is negligible to cause mobilization of trace metals in the studied systems. In actual environments, the pH would not be readjusted and would increase during anoxic conditions and decrease during oxic conditions. The magnitude of the pH change in natural systems experiencing redox fluctuations

may not be as large as in the laboratory-scale microcosms because of the flow of water in and out of the system (as opposed to closed batch microcosms) and to a higher solid-water ratio (solid to water loading in microcosms is 300 g L^{-1}) that would allow greater pH buffering from clays, organic matter, and other mineral phases.[301–304]

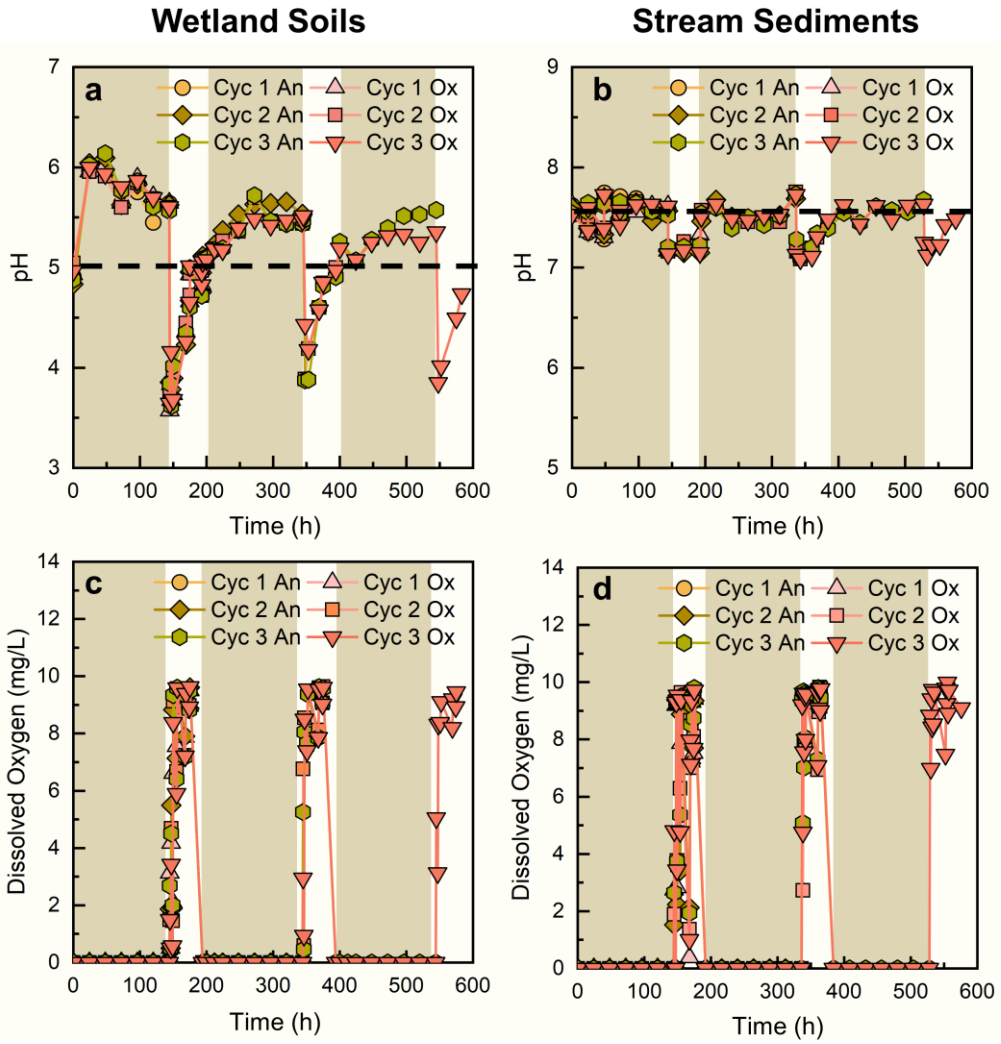

Figure 5.2: Effect of anoxic and oxic fluctuations on the pH (a-b) and dissolved oxygen (c-d) in the different microcosms initiated with riparian wetland soils and stream sediments. Shaded areas indicate anoxic cycles and unshaded areas are oxic cycles. The dashed line represents the pH at which microcosms were initiated and the value to which they were readjusted every 24 h. The results are shown for six replicate microcosms; the labels in the legend refer to the cycle and the

condition (An for anoxic and Ox for oxic) after which the microcosm were sacrificed for analysis. Because one microcosm was sacrificed after each change in redox status for analysis of solid phases, the total number of replicates decreased with increasing experiment time.

Greater fluctuations in pH were observed in wetland soils (5.0 ± 1.5) than in the stream sediments (7.6 ± 0.5) during the redox cycles. For riparian wetland soils, even after daily pH readjustment, pH values increased from 5.0 to ~6.0 in 24 h during the first anoxic cycle; the magnitude of the pH increase in the second and third anoxic cycles was smaller (Figure 5.2a). Upon shifting the wetland soil microcosms to oxic conditions, we observed a reverse trend as the pH values dropped to ~3.8 after sparging air into the system for 45 min. In microcosms initiated with the stream sediments, the pH remained stable at ~7.6 in anoxic conditions, whereas a decrease in pH from 7.6 to ~7.0 was observed under oxic conditions (Figure 5.2b). The microcosms maintained under sustained anoxic and oxic conditions showed the same trend in pH change as observed in the microcosms subjected to redox fluctuations (Figure D-2). The increase in pH under anoxic conditions in wetland soils can be attributed to the reduction of sulfate and Fe oxides and the consumption of organic matter in anaerobic microbial processes (methanogenesis and denitrification). On the other hand, the decrease in pH under oxic conditions in both the systems suggests the formation of Fe oxides and oxidation of reduced sulfur-containing species, such as elemental sulfur and sulfide minerals.[7,50,54] The greater stability in pH of stream sediment microcosms under anoxic conditions may be due to either greater buffering capacity of clays and organic matter or to limited dissolution of Fe/Mn (hydr)oxides under anoxic conditions.

In wetland soils and stream sediments, the amount of oxygen consumed (Table D-6) decreased with each subsequent oxidation cycle (Figure 5.2 c,d). When oxygen is added to anoxic microcosms, it can be consumed either in the microbial processes involving degradation of organic matter or in the biotic or abiotic oxidation of sulfides, Fe(II), and Mn(II).[53,54,238,282,305] The decrease

in oxygen demand in subsequent oxic cycles may be due to a decline in microbial activity caused by the death of anaerobic/anoxic microorganisms and depletion of the labile portion of organic matter in the first oxic cycle.

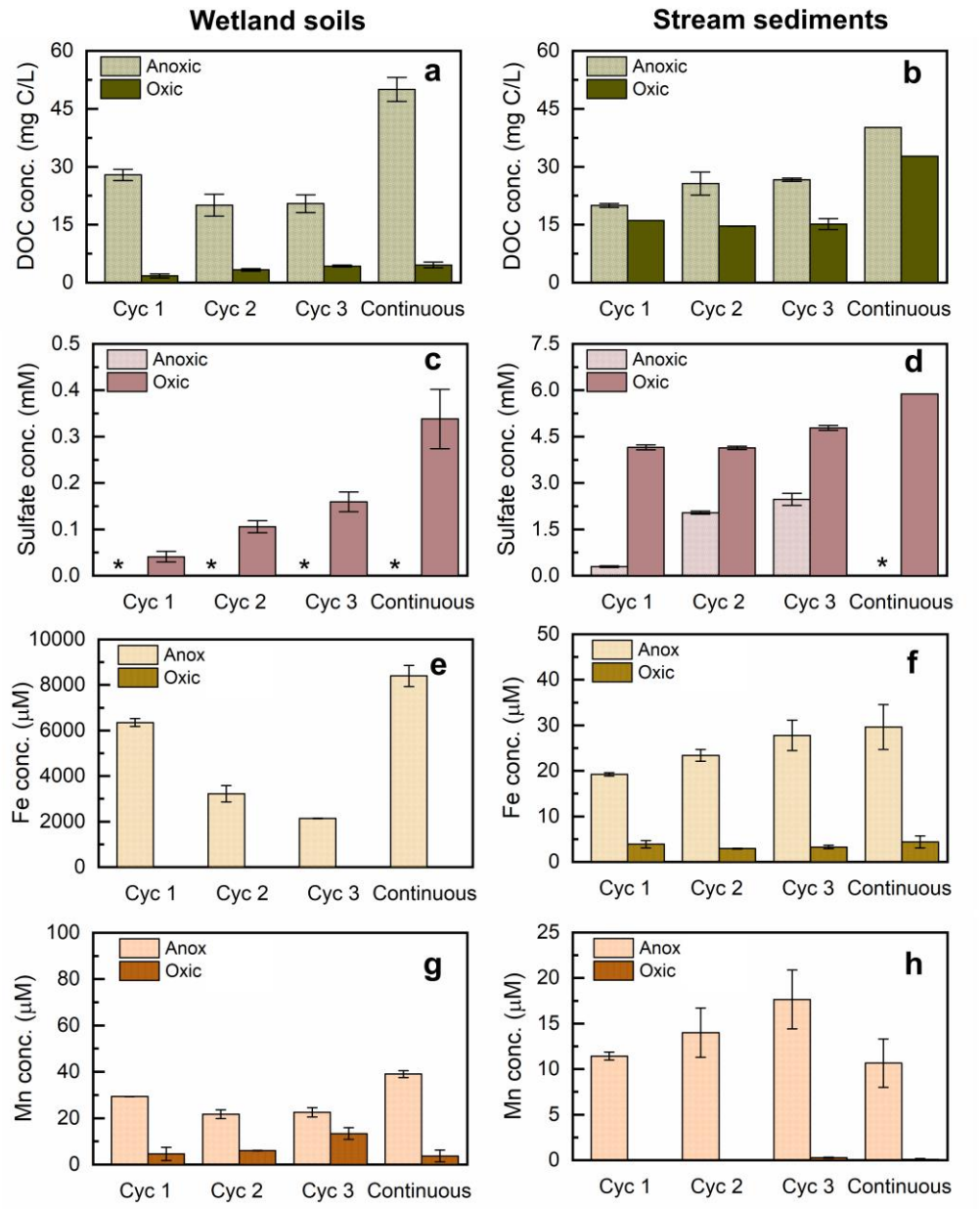

Figure 5.3: Variation in the concentration of DOC (a-b), sulfate (c-d), total dissolved Fe (e-f) and total dissolved Mn (g-h) after each anoxic and oxic cycle of redox fluctuation in riparian wetland soils and stream sediments. The results labeled "Continuous" are from the parallel microcosms that were sustained at oxic and anoxic conditions. (*) indicates that the sulfate concentration is below

the detection limit (0.1 mg/L). Error bars indicate the standard deviation in the duplicate microcosms.

5.3.3 Responses of DOC and Sulfate to Alternating Anoxic-Oxic Cycles

In both wetland soils and stream sediments, DOC concentrations under anoxic conditions were higher than under oxic conditions (Figure 5.3). Under anoxic cycles, DOC may be released due to either degradation of complex organic matter by reductive fermentation and hydrolysis or from desorption of organic matter upon reductive dissolution of Fe(III)/Mn(III) phases.[9,53,265,306] Additionally, increase in pH associated with Fe(III) (hydr)oxides dissolution under anoxic conditions may cause dispersion of colloids, increasing DOC concentrations.[306,307] Low DOC values in oxic cycles suggest resorption of organic matter on iron oxides,[265] organic carbon consumption by aerobic organisms, or abiotic degradation of organic carbon by hydroxyl radicals generated during oxidation of Fe(II) by O_2.[308,309]

Sulfate concentrations responded to changing redox conditions in both wetland soil and stream sediment microcosms (Figure 5.3 c,d) with high values at the end of the oxic cycles and low values after anoxic cycles. During anoxic cycles, sulfate was not observed in the supernatant of riparian wetland soil microcosms, indicating the conversion of sulfate into reduced forms of sulfur as observed in earlier studies.[7,50,54,110,310] During the redox fluctuations with stream sediments, lower sulfate concentrations were observed during anoxic cycles than during oxic cycles, but the concentration during anoxic cycles increased with successive fluctuations. Sulfate concentrations observed in stream sediment microcosms exceeded the amount (~ 10 fold) observed in wetland soil experiments. The complete oxidation of sulfur would release up to 16.3 mM and 27.8 mM sulfate in wetland soils and stream sediments, respectively. However, the concentration of sulfate released in the sustained oxic microcosms was much lower (wetland soil: 0.34 mM and stream

sediment: 5.9 mM), indicating the presence of appreciable amounts of stable sulfur species that were resistant to oxidation by dissolved oxygen or the formation of other intermediate S species, such as sulfite, thiosulfate, and elemental sulfur. Sulfur bound to soil organic matter can also be oxidized and released as sulfate upon organic matter mineralization in oxic cycles.[311] Sulfate released via organic matter mineralization cannot be reversibly incorporated back with organic matter in subsequent anoxic cycles, thus, progressive organic matter mineralization could have caused high sulfate concentrations in the second and third anoxic cycles of stream sediments.

5.3.4 Redox Fluctuation Effects on Metal Concentrations

Wetland soils: Water samples were collected periodically to monitor the variation in the concentration of dissolved metals due to fluctuating redox conditions. For riparian wetland soils (Figure 5.4), we observed that Ni, Co, and Zn behaved similarly upon alternating redox fluctuations; their concentrations increased under anoxic conditions and decreased under oxic conditions. The decrease in the dissolved Ni, Co, and Zn concentration aligned with the decrease in dissolved Fe concentrations, which suggests the sorption of these trace metals on freshly formed Fe precipitates. Under low sulfur conditions, like those of the riparian wetland soils, Zn, Ni, and Co may not be sequestered in sulfide precipitates. During redox fluctuations, dissolved concentrations of both Ni and Co were positively correlated with DOC (r values of 1.00 or Ni and 0.99 for Co) (Figure 5.5), indicating that these trace metals and DOC might undergo the same mechanisms of mobilization/sequestration under redox fluctuations. In anoxic cycles, reductive dissolution of iron oxyhydroxides can release sorbed DOC and trace metals,[53,312] however, under oxic cycles, resorption of both DOC and trace metals could have caused the decrease in their dissolved concentrations. Increase in DOC and trace metals (Ni, Co, and Zn) under anoxic cycles

can also be associated with colloidal and nanoparticle dispersion upon pH increase caused by iron (hydr)oxides dissolution.

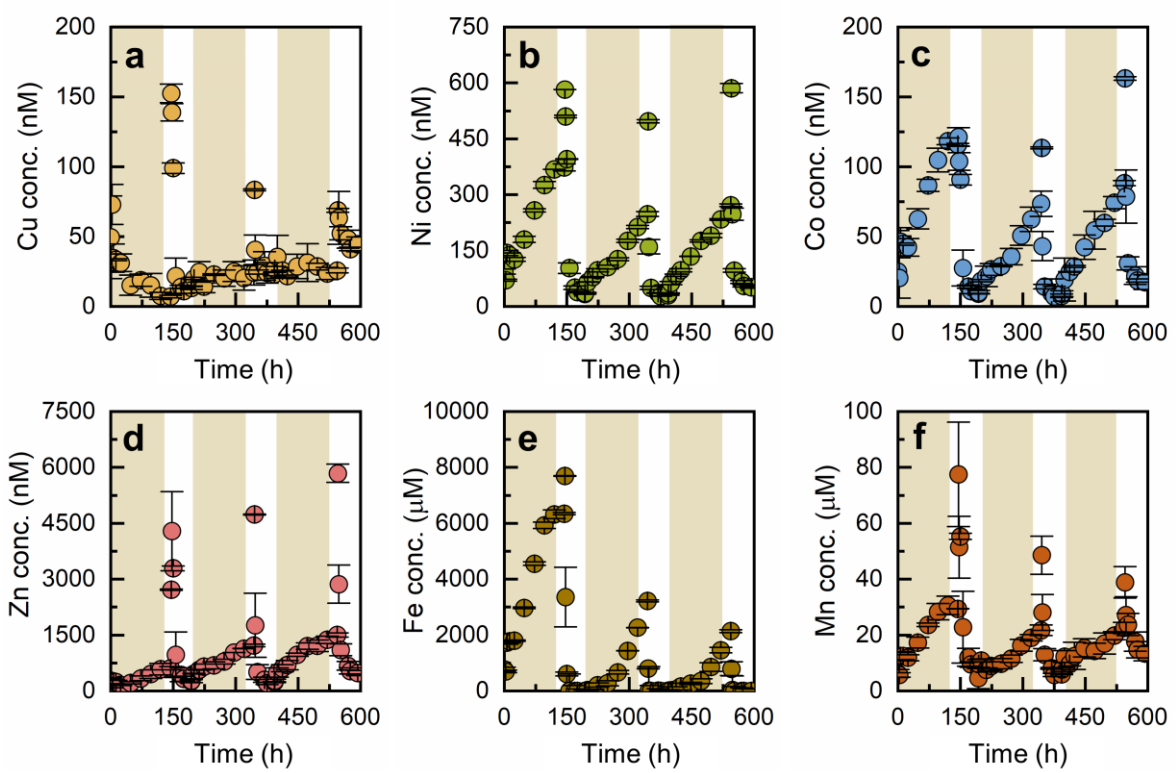

Figure 5.4: Time series of (a) Cu (b) Ni (c) Co (d) Zn (e) Fe and (f) Mn during three different cycles of redox fluctuations spanning 24 days in riparian wetland soil microcosms. The data plotted shows the dissolved concentrations in the microcosms after each anoxic and oxic fluctuation. Shaded areas indicate anoxic cycles and unshaded areas are oxic cycles. Error bars indicate the standard deviation in the duplicate microcosms

Fe and Mn concentrations were substantially lower in oxic conditions (Figure 5.4 e,f). As oxygen is introduced, dissolved Fe(II) and Mn(II) oxidize to form oxides/hydroxides that can serve as sorption sites for metals.[271,313] The decrease in dissolved Fe and Mn concentrations with increasing oxygen concentration indicated the formation of Fe and Mn oxides/hydroxides. At the pH conditions studied (~5), the rate of abiotic Fe(II) oxidation by dissolved O_2 is very slow (10^{-12}-10^{-10} mol L^{-1} s^{-1});[314–316] however, Fe (hydr)oxide formation can be microbially-mediated (10^{-8}-

10^{-5} mol L^{-1} s^{-1}) even at slightly acidic pH.[315–317] Additionally, the presence of mineral surfaces, such as iron oxyhydroxides, increases the rate of Fe(II) oxidation (10^{-8}-10^{-7} mol $L^{-1}s^{-1}$) in the pH range 4.5-5.5.[318,319] The rate of Fe(II) oxidation in oxic cycles in our study (10^{-8} mol $L^{-1}s^{-1}$) suggests that either mineral surfaces are catalyzing the Fe(II) oxidation or that the oxidation is microbially mediated. As the amount of Fe bound to oxidizable phases (Figure D-3) did not vary substantially under oxic cycles, only dissolved Fe was used to calculate the oxidation rates. Similarly, the abiotic oxidation of Mn(II) by dissolved oxygen in homogeneous systems is kinetically inhibited at pH < 8[305,320]; heterogeneous oxidation of Mn(II) on mineral surfaces, such as iron (oxyhydr)oxides, has not been observed at pH values < 6.[321–323] Thus, it is likely that at the pH 5 conditions of the microcosms that Mn(II) oxidation occurred due to the action of microorganisms.[324,325]

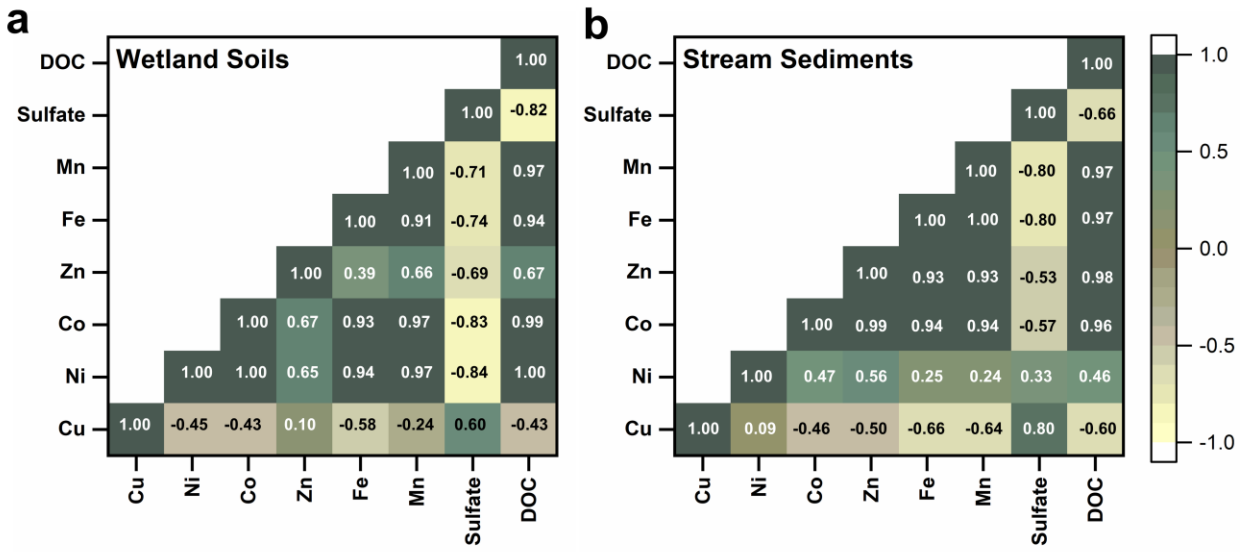

Figure 5.5: Pearson correlation coefficient (r) between different components obtained by using their concentration in the supernatant after each anoxic and oxic fluctuation for (a) riparian wetlands and (b) stream sediments. The values are rounded to two decimal places.

Under anoxic conditions, Fe/Mn (hydr)oxides are microbially reduced and release Fe(II) and Mn(II) into the porewater.[54,280] Fe can form iron sulfide phases in reducing environments.[110] The high concentration of dissolved Fe in anoxic cycles of the microcosms of this study suggested limited or no formation of Fe sulfides. The solution Fe:S ratio in the three anoxic cycles (> 30) indicates that the total available sulfur is not enough to form substantial amounts of iron sulfides. Any Fe sulfide that did form would most likely be FeS and not FeS_2 because the formation of FeS_2 is very slow under normal temperature and low sulfur conditions.[326,327] Our recent study also indicated that riparian wetland soils from this site contained very little FeS (< 5%).[294] The dissolved Fe concentration is substantially lower in the second and third anoxic cycles, which indicates that the extent of Fe (hydr)oxide reduction decreased in subsequent anoxic fluctuations. The limited availability of reducing species, i.e., labile organic matter, could have resulted in less reduction of Fe (hydr)oxides as the fluctuation progressed in the later anoxic cycles.

Cu behavior was different from that of other trace metals in the wetland soils with its concentration decreasing during anoxic conditions (Figure 5.4). Cu(II) has more affinity towards sulfur moieties than the other trace metals (Ni, Co, and Zn) and forms a variety of sulfide precipitates.[110,141,142] Cu(II) can also be reduced to Cu(I) or Cu(0) in reducing conditions by various electron donors (Fe(II), natural organic matter, and sulfide moieties), further decreasing its solubility.[130,328] Metallic Cu(0), often in nanoparticulate form, has been observed in other studies in the roots of wetland plants, organic-rich bog soils and contaminated soils upon flooding.[135,136,141] XANES analysis of soil samples collected from this same wetland indicated that Cu(0) was absent in these soils,[294] however redox fluctuations could have enabled the formation of Cu(0) or Cu(I), thus decreasing the solubility of Cu in anoxic cycles. The Cu concentration decreased with time in the anoxic stage of the first cycle (73 nM to 7 nM) and then increased slightly in consecutive oxic

and anoxic cycles. The decrease in Cu concentrations during anoxic cycles indicate precipitation in the form copper sulfides, such as CuS. Metals adsorbed to sulfides are rapidly released upon exposure to oxic conditions; however, sulfide minerals, such as crystalline CuS, are more stable and are unlikely to be oxidized in short durations.[110,271] Under the timescale considered for the anoxic cycles in our study, it is likely that CuS is present in an amorphous or nanoparticulate form;[126,329,330] amorphous CuS can easily oxidize under oxic cycles;[331] however, nanoparticulate CuS is stable and can persist under oxic conditions for weeks.[329] The low release of Cu in oxic cycles may indicate the presence of nanoparticulate CuS.

For all the metals, there was a transient increase in concentration immediately following the shift to oxic conditions. In the first few hours of each oxic cycle (8-12 h), the pH was 3.5-4.0. The low pH values would result in desorption of trace metals from clays, aluminum oxides, and organic matter and low sorption of released trace metals to freshly formed Fe/Mn (hydr)oxides under acidic conditions.[50,313,332] Upon pH readjustment, a decrease in the dissolved concentration of Ni, Co, and Zn was observed due to enhanced sorption as the pH increased back toward the target value of 5.0 (Figure 5.4).

We used DGT samplers to estimate the bioavailable concentration of metals (equations 1-4 in Section D.1 in appendix) in the microcosms at the end of each stage of redox fluctuation (Figure 5.6). The bioavailable concentrations of Ni, Co, and Fe were lower under oxic conditions, whereas the bioavailable concentrations of Cu and Mn were higher under oxic conditions. At low pH conditions (~4), Mn(III) in minerals can disproportionate to Mn(II) and M(IV), increasing the dissolved concentration of Mn(II) in oxic conditions.[333] Due to lower concentrations of DOC in oxic cycles to complex Mn(II), the estimated bioavailable concentrations of Mn could have been higher in oxic fluctuations. For Zn, the DGT-estimated concentration was similar in the first two

cycles of anoxic and oxic fluctuations; however, the bioavailable concentration of Zn increased substantially following the oxic condition of the third redox cycle. For all the trace metals, the ratio of DGT-estimated concentration to total dissolved concentration (C_{DGT}/C_{diss}) (Table D-9) is < 0.30 under anoxic cycles (Cu: 0.16 ± 0.09, Ni: 0.28 ± 0.03, Co: 0.15 ± 0.05, Zn: 0.21 ± 0.09). C_{DGT}/C_{diss} was higher (Cu: 0.65 ± 0.20, Ni: 0.89 ± 0.05, Co: 0.65 ± 0.10, Zn: 0.86 ± 0.10) under oxic cycles. Our speciation results (estimated using NICA-Donnan model in Table D-7, details in Section D.3) showed that DOC was not able to complex Ni, Co, and Zn under anoxic cycles, indicating that these trace metals might be present in colloidal or nanoparticulate form which prevented their diffusion inside DGTs.

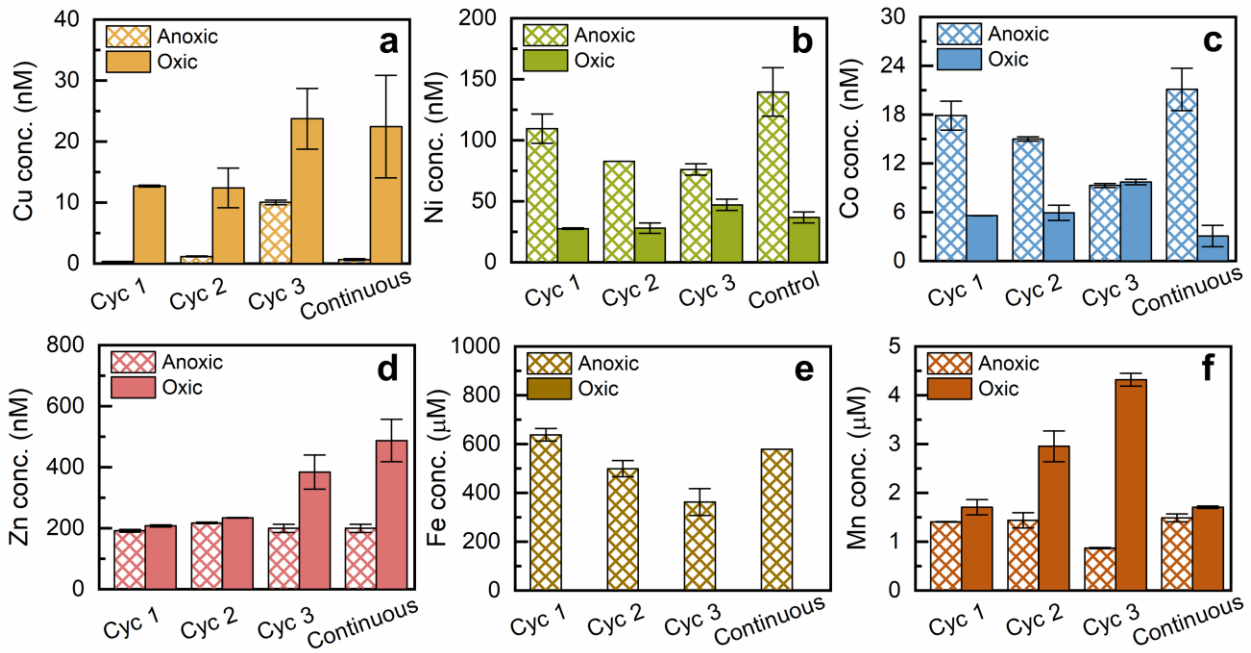

Figure 5.6: Variability in the bioavailable concentration of (a) Cu (b) Ni (c) Co (d) Zn (e) Fe and (f) Mn in riparian wetland soil microcosms during three cycles of redox fluctuations determined by DGT samplers. Each subplot also contains the bioavailable fraction of metal determined in microcosms that were sustained at oxic and anoxic conditions as indicated by the "Continuous" label. Error bars indicate the standard deviation in the duplicate microcosms.

With successive redox fluctuations, the bioavailable concentrations (Figure 5.6) of Cu and Zn increased, whereas bioavailable concentrations of Ni and Co decreased. In microcosms with sustained oxic conditions, the bioavailable concentration of Co was substantially lower than in the microcosms subjected to redox fluctuations. Similarly, a sustained anoxic environment resulted in less bioavailable Cu than in the microcosms subjected to redox fluctuations. The formation of more crystalline and stable minerals under longer flooding or drying periods has been observed to lower the bioavailability of metals and decrease their accumulation in benthic organisms.[312,334] In contrast, Ni and Co dissolved (Figure D-5) and bioavailable concentrations (Figure 5.6) in completely anoxic microcosms were higher than in microcosms subjected to fluctuations. The amount of Fe released in sustained anoxic conditions (8400 µM) was higher than Fe released in anoxic cycles (cycle 1: 6300 µM, cycle 2: 3200, and cycle 3: 2100 µM), thus, higher dissolution of iron (hydr)oxides could have caused more release of Ni and Co.

Stream sediments: Like the wetland soils, the trace metals in stream sediments displayed distinct trends when subjected to fluctuating redox conditions (Figure 5.7). Fluctuating redox conditions increased the amounts of Co, Zn, Fe, and Mn released to the supernatant upon successive anoxic cycles, whereas the Cu concentration increased in consecutive oxic cycles. Ni behavior was different than in wetland soils; dissolved Ni (Figure 5.7b) increased in the first oxic fluctuation and then remained almost constant (~40 nM) in the subsequent oxic cycles.

The solid-phase speciation of Cu and Ni in the studied sediments likely affected their dynamics during redox fluctuations. XANES speciation results for the stream sediments collected from the same site in our earlier study[294] indicated that Cu is present in a CuS-like form,[294] and the oxidation of a CuS-like fraction could have released Cu under oxic cycles. Further, in sulfur-limited systems, the formation of Cu(0) and Cu(I) complexation to thiol groups on organic matter

are important mechanisms for decreasing the solubility of Cu.[126,136] Thus, oxidation of Cu(0) and mineralization of organic carbon under oxic conditions can also release Cu to the solution.[132] Similarly, approximately 30% of Ni is associated with sulfides in stream sediments collected from Oak Ridge,[294] the oxidation of the sulfide-associated fraction in the first oxic cycle might have mobilized Ni, and this process may not have been sufficiently reversible to resequester Ni during the anoxic cycles

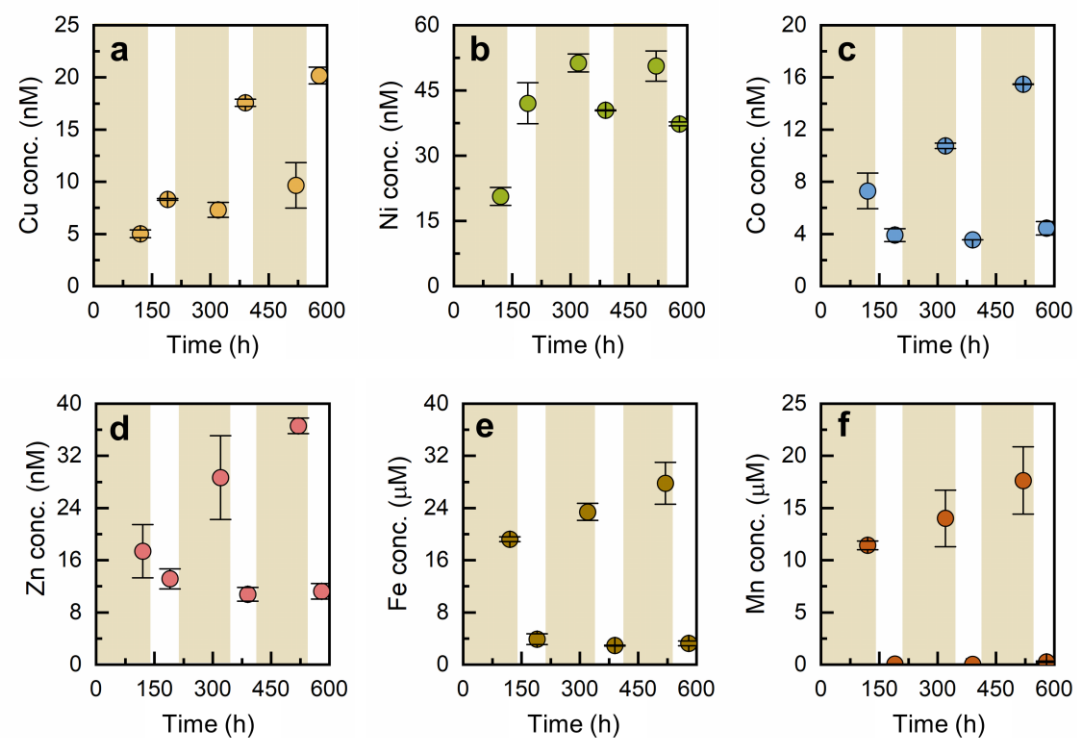

Figure 5.7: Dissolved concentrations of (a) Cu (b) Ni (c) Co (d) Zn at the end of three different cycles of redox fluctuations spanning 24 days in stream sediment microcosms. Error bars indicate the standard deviation in the duplicate microcosms. Shaded areas indicate anoxic cycles and unshaded areas are oxic cycles.

Co, Zn, Fe, and Mn behaved similarly in the stream sediments, and their dissolved concentrations decreased during oxic cycles of redox fluctuations (Figure 5.7c,e,f). The strong correlation between dissolved Co/Zn/Mn and dissolved Fe (Figure 5.5) might indicate that the Co

and Zn concentrations are governed by the dissolution of Fe (hydr)oxides in stream sediments. In all three oxic cycles, negligible Fe and Mn remained in the supernatant, indicating either the formation of Fe/Mn oxides and hydroxides[54,271] or association of manganese with the iron oxyhydroxides.[335–337]

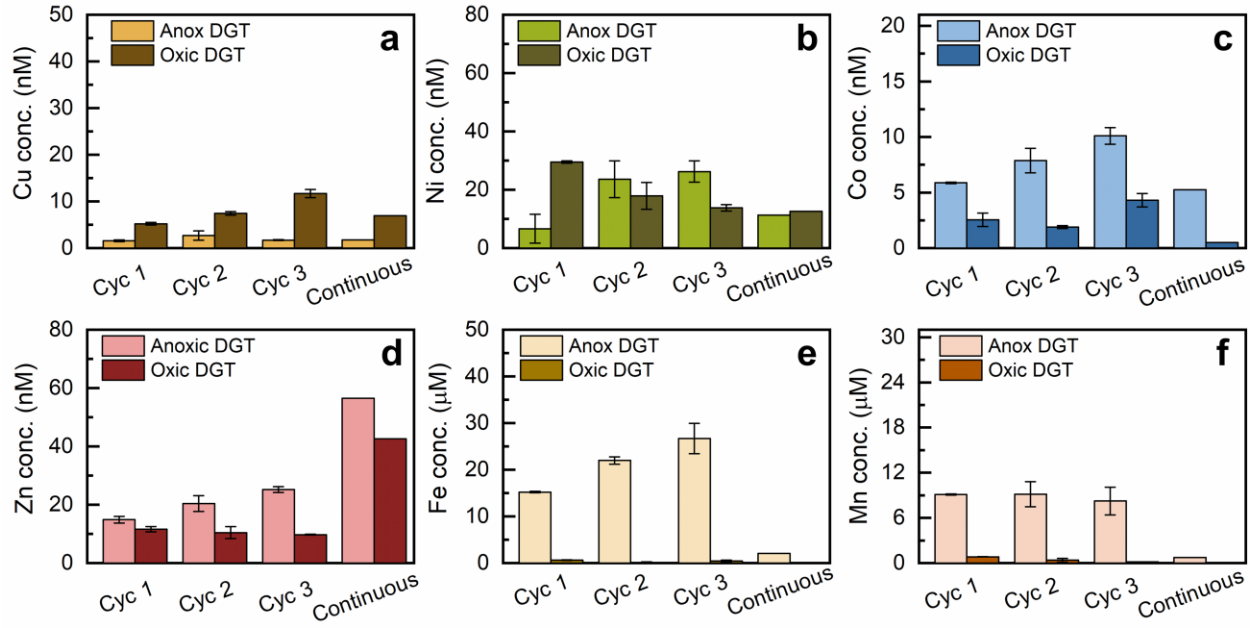

Figure 5.8: Variability in the bioavailable concentrations of metals due to redox fluctuations shown in (a) Cu (b) Ni (c) Co (d) Zn (e) Fe and (f) Mn during three cycles of redox fluctuations spanning 24 days on the sediments collected from a stream. The results labeled "Continuous" are from the parallel microcosms that were sustained at oxic and anoxic conditions. DGTs were deployed for a time period of 24 h at the end of each redox fluctuation. The equations used for estimating the bioavailable concentration of metals are listed in the methods section. Error bars indicate the standard deviation in the duplicate microcosms.

Sustained oxic and anoxic environments showed different extents of trace metal mobilization than did the cyclic redox conditions. As compared to microcosms which experienced redox fluctuations, higher concentrations of Cu were released in sustained oxic conditions. On the other hand, less Ni and Co were released during sustained anoxic conditions than after three anoxic

cycles. Selective extraction results showed that differences in solid-phase speciation between microcosms subjected to redox cycling and maintained under sustained conditions caused a variation in the extent of trace metal mobilization. In sustained oxic microcosms, Cu associated with oxidizable solid phases decreased (Figure D-4, determined using selective extractions) increasing the concentration of Cu in the dissolved phase. Similarly, in sustained anoxic conditions, the abundance of Ni and Co bound to oxidizable solid phases is greater than in the microcosms after 3 cycles of anoxic fluctuations (Figure D-4) which could have resulted in greater immobilization of these metals.

After multiple cycles of redox fluctuations, the bioavailable concentrations in the stream sediments increased for all the metals with each successive fluctuation (Figure 5.8 g-l). Bioavailable Cu was more abundant in oxic cycles, whereas bioavailable concentrations of Zn and Co were higher during anoxic cycles. For Ni, the bioavailable concentration increased upon a shift to oxic conditions in the first redox cycle and then decreased in subsequent oxic cycles. The bioavailable concentration in sustained oxic/anoxic microcosms showed the same trend for all trace metals with the exception of Ni; for Ni, the bioavailable concentration was similar in sustained anoxic and oxic conditions. Unlike, wetland soils, we did not observe a substantial difference in C_{DGT}/C_{diss} values in different redox cycles in stream sediments (Table D-9). The ratio of C_{DGT} to C_{diss} for Cu was lower than for other trace metals, which suggests the presence of soluble Cu-organic matter complexes with low bioavailability. This is consistent with the trend observed in our speciation results obtained through NICA-Donnan, where freely available Cu was less as compared to other trace metals due to complexation with DOC (Table D-8). Previous studies also indicate a higher affinity of dissolved organic ligands for Cu as compared to Ni, Cd, and Zn.[171,338] In both sustained oxic and sustained anoxic microcosms, DGT-estimated Zn concentrations were

greater than the dissolved concentrations measured in the supernatant. Resin gels can be contaminated with Zn during casting and assembly procedures due to leaching from common labware items[339] which might have caused high DGT-estimated Zn concentrations.

5.3.5 Comparison between Wetland Soils and Stream Sediments

The riparian wetland soil has lower total metal concentrations as compared to the stream sediments (Table D-3), but it released greater amounts of trace metals during fluctuating redox conditions (percent mobilized with respect to total content in Table D-10). In stream sediments, the percent of trace metals released was 0.01% - 0.06%, with Zn < Cu ≈ Co < Ni. The percent of Cu released in wetland soils was similar to stream sediments, however, mobilized percentages of Ni, Co, and Zn were substantially higher in wetland soils, especially under anoxic cycles.

Due to the differences in total iron content, pH conditions, and solid-phase speciation of Fe, S, and trace metals between the two sites, the effects of multiple redox fluctuations on the extent of trace metal mobilization in wetland soils and stream sediments were different. Reduction of Fe/Mn (hydr)oxides released Ni, Co, and Zn during anoxic cycles of riparian wetland soil microcosms. The abundance of Ni, Co, and Zn bound to the oxidizable fraction was substantially lower in wetland soils as compared to stream sediments (Figure D-3Figure D-4). In our recent study, we observed that the proportion of sulfur that is elemental sulfur in wetland soils is lower (~20%) than the proportion for the stream sediments (~70%).[294] Hence, the limited availability of free sulfide moieties in wetland soils to sequester Ni, Co, and Zn under anoxic cycles probably increased their dissolved concentrations in the supernatant. The amount of Cu mobilized during the oxic stages with respect to total Cu present in the sediments was very low in both the systems studied (Table D-10), owing to the high affinity of Cu for sulfide phases and to complexation with thiol groups on organic matter; even in oxic cycles, substantial amounts of Cu (> 75%) are present in the form

of oxidizable fraction (estimated through selective extractions) in both the wetland soil and stream sediment.

In stream sediments, dissolved concentrations of trace metals increased substantially with each successive anoxic stage of the anoxic-oxic fluctuations. Sulfur is predominantly present as elemental sulfur (~70%) in stream sediments collected from ORNL,[294] and ~16% of total sulfur was oxidized in oxic cycles (indicated by the formation of sulfate). The complete reduction of sulfate did not take place in consecutive anoxic cycles (Figure 5.3); thus, the reductive dissolution of Fe (hydr)oxides and limited formation of reduced sulfur minerals for immobilizing trace metals could have increased dissolved trace metals in the second and third anoxic stages. On the other hand, in wetland soils, the concentrations of mobilized Ni and Co decreased in the second and third anoxic cycles; dissolved Zn and Cu concentrations increased with multiple redox fluctuations. XANES analysis on previously collected soils from the wetland site indicated that this site contained very little FeS (< 5%) and had abundant Fe(III) (hydr)oxides.[294] In the first anoxic cycle, ~17% of total Fe dissolved, however, only ~6% and ~4% of the total Fe released in second and third anoxic cycles, respectively. Thus, the limited dissolution of Fe(III) oxides under fluctuating reducing conditions would have limited the mobilization of Ni and Co in second and third anoxic cycles.

5.3.6 Implications of Redox Fluctuations for Biogeochemical Processes

The focus of this study on the dynamics of trace metals under fluctuating redox conditions in systems containing low sulfur and organic matter and trace metal concentrations similar to or below crustal abundances has implications for the roles of trace metals as micronutrients that affect carbon and nitrogen cycling. The bioavailability of trace metal micronutrients, Cu, Ni, and Co, is critical to denitrification and methanogenesis.[253–255] Both methanogenesis and denitrification occur

under anoxic conditions; fluctuating redox conditions might not only affect these processes due to the variation in redox status but also due to a change in the bioavailability of trace metals.

This study illustrates the cumulative effects of multiple cycles of redox fluctuations on the bioavailability of trace metals in wetland soils and stream sediments. In wetland soils, the bioavailable concentrations of Ni and Co decreased with multiple anoxic-oxic cycles; however, in stream sediments, the bioavailability of Ni and Co increased with redox fluctuations. These observations suggest that depending on the solid-phase speciation of trace metals and redox status of the recent past, periodic changes in redox status might inhibit/promote methanogenesis in the natural aquatic systems. In both systems studied, fluctuating redox conditions increased the bioavailability of Cu. DGT estimated Cu concentrations in sustained anoxic conditions and the first anoxic cycle of wetland soils were very low (< 1 nM); such low concentrations can cause nitrous oxide accumulation in the anoxic zones of riparian wetland soils because of limited bioavailability of Cu as a trace nutrient required for reduction of nitrous oxide to N_2. Our recent study focused on evaluating the effect of Cu denitrification under completely anoxic conditions concluded that nitrous oxide accumulated in riparian wetland soils due to limited availability of Cu.[116] Due to multiple cycles of redox fluctuations, bioavailable Cu increased in both stream sediments and wetland soils, indicating that redox fluctuations might promote nitrous oxide to nitrogen conversion in these natural aquatic systems when Cu is the limiting factor. Hence, soils that are prone to flooding and drying events might produce less nitrous oxide than environmental systems with static anoxic conditions because the bioavailability of Cu as a micronutrient is important for the biological reduction of N_2O to N_2.

5.4 Conclusions

This study quantified responses of dissolved and bioavailable trace metal concentrations to changes between oxic and anoxic conditions as well as the cumulative effects of successive redox fluctuations. For both systems, the amount of metals released upon redox fluctuations constituted less than 2% of the total solid-phase associated metals, indicating that only a fraction of metals is susceptible to mobilization in the events of flooding and drying. The study suggests that trace metal mobilization in natural environments under events of redox fluctuations is strongly coupled to solid-phase speciation of the trace metals and the redox status of the recent past. Natural systems containing high sulfur and iron contents will immobilize more trace metals and may release lesser amounts of trace metals under fluctuating redox conditions. Our results can be extended to other natural environments with similar characteristics, such as low organic matter and sulfur content, to predict trends in the bioavailability of trace metals under dynamic redox environments. Further, our study suggests that redox fluctuations may alter the rates of metal-dependent biogeochemical processes in natural environments by varying the bioavailable concentrations of trace metal micronutrients.

Chapter 6: Conclusions and Future Outlook

6.1 Conclusions

This doctoral thesis investigated the mobility and bioaccessibility of metals in natural and engineered water systems by specifically evaluating their interactions with mineral phases and mineral-organic assemblages. The research provided fundamental information about dominant interaction pathways between different metals (U, Cu, Ni, Zn, and Co) and iron oxides/sulfides/organic matter under environmentally-relevant conditions. With the help of this knowledge, we were able to develop an environmental-friendly technique for removing uranium from water systems. A deeper understanding of the geochemical cycles of iron and sulfur helped us determine the bioavailability of trace metals for biogeochemical processes in wetland soils and stream sediments. With the knowledge of the speciation of metals under different aqueous chemistry conditions, we were able to predict the fate and mobility of contaminants in engineered and natural systems.

In our study on uranium removal using magnetite nanoparticles, we provided evidence that biosurfactants can be effectively used to coat and stabilize iron oxide nanoparticles in aqueous suspension. Biosurfactants such as rhamnolipids are biodegradable, and their use raises fewer environmental concerns than the use of their synthetic counterparts. Due to their stability under environmentally relevant pH and ionic strength conditions, these engineered materials can be successfully implemented in water treatment systems for the removal of potent contaminants without causing any further downstream pollution. Rhamnolipid-coated iron oxide nanoparticles were demonstrated to be able to adsorb the environmentally significant contaminant U(VI), and

the effects of water chemistry on adsorption were successfully modeled within a reaction-based surface complexation modeling framework. The formation of stable anionic U(VI) carbonate complexes decreased U(VI) adsorption onto the negatively-charged rhamnolipid-magnetite system. The study indicated that both electrostatic and chemical interactions between U(VI) and rhamnolipid-coated nanoparticles contributed to U(VI) removal.

In our study on trace metal uptake behavior of different natural systems, we observed that fresh inputs of trace metals to wetland soils and stream sediments resulted in substantial immobilization in the solid phase with speciation differing substantially from that of the metals originally present. There were substantial differences in trace metal uptake trends between different sites, especially for Cu, which can be described by solid-phase characteristics (mineralogy, organic matter composition, and speciation of sulfur moieties) of the soils and sediments. This study suggested that the background speciation of metals in natural aquatic systems cannot be used to determine the speciation and lability of metals introduced to terrestrial aquatic systems from anthropogenic or natural processes.

With our study on the role of Cu in nitrogen cycling in wetland soils and stream sediments, we established that natural systems with total Cu concentrations similar to crustal abundances may lack sufficient Cu to carry out denitrification. In the laboratory-based incubation experiments on soils and sediments, we observed that N_2O accumulated permanently or transiently in all microcosms lacking Cu amendment. With Cu added to provide dissolved concentrations at trace levels (10-300 nM), the reduction rate of N_2O to N_2 in the wetland soils and stream sediments was enhanced. Our kinetic model could account for the trends in nitrogen species by combining the reactions for microbial reduction of NO_3^- to $NO_2^-/N_2O/N_2$ and abiotic reduction of NO_2^- to N_2. The model revealed that the rate of N_2O to N_2 conversion increased significantly in the presence of Cu.

For riparian wetland soils and stream sediments, the kinetic model also suggested that overall denitrification is driven by abiotic reduction of NO_2^- in the presence of inorganic electron donors. These results suggest that natural aquatic systems containing low background Cu may display an incomplete reduction of N_2O to N_2 that would cause N_2O accumulation and release into the atmosphere. Thus, the addition of Cu at micronutrient levels to natural aquatic systems could potentially decrease N_2O release into the atmosphere. We also believe that the inclusion of Cu as an additional input to ecosystem models can help improve their accuracy for predicting N_2O emissions from soils and sediments.

In our redox fluctuation incubation experiments, we observed varied mobilization behavior for different trace metals. For both natural systems, riparian wetland soils and stream sediments, reduction of iron oxides under anoxic conditions caused Co and Zn release. In contrast, oxidation of sulfides mobilized Cu under oxic conditions in both sites. In wetland soils, dissolution of Fe (hydr)oxides increased Ni solubility; however, in stream sediments, Ni release occurred when sulfides or organic matter were oxidized. The mobilization behavior in the events of changing redox conditions can be directly associated with the solid-phase speciation of metals and the redox status of the recent past. For stream sediments, each subsequent redox cycle increased the bioavailability of trace metals. Redox fluctuations in wetland soils increased bioavailable Zn and Cu and decreased bioavailable Ni and Co. The bioavailability of trace metal micronutrients (Cu, Ni, and Co) is critical to biogeochemical processes, such as denitrification and methanogenesis. Thus, the biogeochemical cycling of nutrients in systems with redox fluctuations may also be influenced by the trace metal availability patterns in addition to the availability of electron donors and acceptors. Our results can be extended to other natural systems with similar characteristics,

such as low organic matter (<10%) and sulfur content (<3%), to predict trends in the bioavailability of trace metals under events of flooding and drying.

The results from the dissertation provided insights into the fundamental processes which govern metal speciation and hence their bioaccessibility in water systems. The understanding of these processes will not only help in optimizing removal processes for the contaminants but will also aid in developing fate and transport models to predict metal mobilization in environmental systems. We also established that availability of Cu may be an important factor in the release of N_2O emissions via denitrification in wetland soils and stream sediments. The conducted research provided in-depth knowledge of the role of mineral surfaces/mineral-organic assemblages in metal uptake and release under a variety of environmental conditions. However, a few important aspects still need to be evaluated which are discussed below.

6.2 Recommendations for Future Research

Based on tunable properties, engineered nanoparticles (NPs) hold significant promise for water treatment technologies. There are numerous concerns regarding the toxicity and non-biodegradability of nanoparticles in environmental systems. Our study on rhamnolipid-coated nanoparticles provided evidence that biosurfactant-coated nanoparticles are stable over a prolonged period. Further, these nanoparticles can be used to remove inorganic contaminants under environmentally-relevant conditions without having a significant impact on their stability. While these results are promising, further research is required to systematically investigate the efficiency of these rhamnolipid-coated nanoparticles in real water systems containing other metals and organic moieties. The presence of divalent cations such as Ca^{2+} and Mg^{2+} could cause nanoparticle aggregation decreasing their efficiency to remove contaminants from water

systems.[340] Further, metals and organic matter could also compete for adsorption at the carboxylic groups of rhamnolipid. It would be interesting to study the desorption of uranium from the bilayer-coated nanoparticles which can indicate their reusability for potential water treatment applications. There is also a need to explore the efficacy of other biosurfactants, such as surfactin and dextran, for the stabilization of these and similar nanoparticles considered for treatment processes, among other aqueous-based technologies.

Most pristine natural aquatic systems contain low solid-phase trace metals, and hence they will have low availability of trace metals for biogeochemical processes. Optimal methanogenic growth occurs at 0.2-2µM Ni and 0.1-2µM Co, while the Cu concentration required for N_2O to N_2 via denitrification lies in the range of 3-10 nM.[3,43,341] Current ecosystem models, such as Dynamic Land Ecosystem Model, do not account for the effect of trace metal micronutrient availability (Cu, Ni, Zn, Co, and Mo) on biogeochemical processes responsible for the release of greenhouse gas emissions. Thus, we need to collaborate with the groups working on quantification of greenhouse gas emissions from natural sources to incorporate our new scientific understanding into existing ecosystem models. These efforts will need extensive field-based measurement of greenhouse gas emissions under the presence/absence of optimum bioavailable trace metal nutrients.

The wetland soils and stream sediments evaluated in our studies contained low organic matter (<10%) and sulfur contents (<1%). In environments with high organic matter or sulfur concentrations, trace metal availability will be lower than in the systems investigated in this research due to the formation of metal-sulfide precipitates or adsorption onto the organic matter.[9,110,265] Additionally, metals can form complexes with dissolved organic matter which can further lower their availability for microbial processes.[111,134] Thus, a broader understanding of the bioavailability of metals in ecosystems with high concentrations of organic matter and sulfur

concentrations is needed to completely identify the roles trace metal micronutrients play in biogeochemical processes.

Agricultural soils are significant contributors of N_2O emissions (~22% of total global N_2O) due to the application of nitrogenous fertilizers and manure. Various studies have indicated that the physicochemical properties of soils, crop type, and climate zone are significant factors contributing to N_2O release from agricultural soils.[342,343] The common mitigation strategies to limit N_2O release from agricultural soils focus primarily on optimizing N application rate, organic matter stabilization, and the use of nitrification inhibitors to limit NO_3^- formation.[343] The use of Cu to limit N_2O release in agricultural soils is yet to be evaluated. Cu is a vital micronutrient required to maximize crop yield and quality; however, high Cu contents (> 500 nmol g^{-1}) will result in adverse effects on plant growth.[344] Cu supplements could be applied either as soil amendments or fertilizers (e.g. in the form of $CuSO_4$) to minimize N_2O release.[345] Investigating the trade-off between the effect of Cu on N_2O emissions and plant growth is an important aspect which needs to be explored.

Methane oxidizing bacteria (MOB) responsible for decreasing CH_4 fluxes from natural aquatic systems via aerobic methanotrophy also require metalloenzymes for catalyzing the first step of CH_4 oxidation to CH_3OH.[48] The most prevalent metalloenzyme is Cu-dependent (pMMO); however, some MOB are also able to express the iron-containing, soluble (sMMO) under conditions of copper scarcity. The relation between Cu availability and methane oxidation in environmental systems is poorly understood. Some studies indicate that methanotrophic activity is not limited by Cu bioavailability because some MOBs can access mineral-bound and organic-bound Cu with the help of small Cu-binding peptides, such as methanobactin.[346,347] However, Morton et al. (2000) showed that the increased surface site concentrations on mineral surfaces

(goethite, clays, and ferrihydrite) and the presence of strong binding chelates (ethylenediamine tetraacetic acid, ethylene glycol, and nitrilotriacetic acid) decreased Cu bioavailability to *M. trichosporium* OB3b for carrying out aerobic methanotrophy.[348] The geochemistry of natural systems influences Cu bioavailability substantially, thus, careful investigation is needed to determine the optimum bioavailable Cu concentrations required by MOBs to carry out CH_4 oxidation in terrestrial aquatic systems.

In our study on Cu effect on denitrification in wetland soils and stream sediments, we used the Michaelis-Menten equation to quantify the nitrogen-species reduction rates. Michaelis-Menten kinetics is used to describe a process catalyzed by a single enzyme. In complex natural systems, where multiple enzyme systems and substrates might be involved in carrying out reduction of nitrogen species, Michaelis-Menten equations might capture the overall rates of reactions for the environmentally system without describing the specific mechanism associated with a single enzyme. Monod kinetics describes both the growth of microorganisms and microbial degradation of substrate during biogeochemical processes.[349] Thus, by accounting for the microbial growth and decay using the Monod equation, we may be able to improve the fit of the kinetic model to the data while better representing the actual transformations processes occurring in the microcosms.

Redox fluctuation experiments provided evidence that trace metal availability may change substantially under events of flooding and drying due to the change in the metal speciation caused by the formation/dissolution of minerals. The biogeochemical cycling of nutrients in systems with redox fluctuations may be influenced by these trace metal availability patterns in addition to the availability of electron donors and acceptors. The bioavailability of trace metal micronutrients, Cu, Ni, and Co, is critical to biogeochemical processes such as denitrification, methanogenesis, and mercury methylation.[253–255] These biogeochemical processes can experience promotion/inhibition

depending upon changes in trace metal bioavailability. Thus, future work is needed to quantify the responses of CH_4 production and N_2O production to dynamic changes in trace metal bioavailability during redox fluctuations in natural aquatic systems. By incorporating the results from these experiments, we can develop a predictive model to estimate the release of greenhouse gas emissions from these natural sources under changing climatic conditions.

In our incubation experiments with redox fluctuations, we varied the redox status of the microcosms by sparging with oxygen and nitrogen for oxic and anoxic cycles, respectively. Additionally, we also adjusted the pH continuously throughout the incubations to focus on the effects of dissolved oxygen independent of changes in pH. In actual field conditions, redox fluctuations are induced by wetting-drying cycles which will be accompanied by pH variations caused by oxidation and reduction reactions. The column experiments with varying water saturation levels are required to investigate the dynamics of trace metal micronutrients under events of flooding and drying.

In our incubation experiments on samples from natural systems, the change in the microbial community composition was not investigated. We observed that at high dissolved Cu concentrations (~500 nM) there was a lag in NO_3^- reduction owing to the toxicity induced to the microorganisms by high metal concentrations. The abundance of functional genes associated with denitrification (*nirS*, *nirK*, *nosZ*), dissimilatory nitrate reduction to ammonium (DNRA; *nrfA*), and methanogenesis (*mcrA*) can also change upon trace metal amendments to natural soils and sediments.[4] Additionally, microbial communities can respond quickly to redox fluctuations which can show a varied response to trace metal availability. Thus, systematic investigation to study microbial community changes upon metal amendments and changing seasons is necessary to develop a predictive understanding of biogeochemical dynamics.

We used in-situ passive samplers to obtain an estimate of the bioavailable concentrations of trace metals in pristine natural environments. The diffusion-based devices provided us with high-resolution profiles of trace metal bioaccessibility with depth. But this information along with analysis of other entities like sulfur content and dissolved organic matter concentrations can enhance our understanding of these complex environments. Additionally, the cost of conducting an in-situ sampler-based campaign is considerably high after accounting for sampler development, sampler deployment, and postmortem analysis. The existing equilibrium-based models (NICA-Donnan and WHAM) that predict the bioavailability of metals in water systems by accounting for metal ion adsorption to humic substances often over-estimate the labile metal concentrations.[171,296,350] In order to improve the ability of the models to predict labile metal concentrations under different aqueous chemistry conditions, there is a need to optimize the equilibrium constants that determine the amount of metals bound to organic matter.

References

1. Tchounwou, P.B., Yedjou, C.G., Patlolla, A.K., and Sutton, D.J. (2012). Molecular, clinical and environmental toxicicology Volume 3: Environmental Toxicology. Mol. Clin. Environ. Toxicol. *101*, 133–164.

2. Briffa, J., Sinagra, E., and Blundell, R. (2020). Heavy metal pollution in the environment and their toxicological effects on humans. Heliyon *6*, e04691.

3. Glass, J.B., and Orphan, V.J. (2012). Trace metal requirements for microbial enzymes involved in the production and consumption of methane and nitrous oxide. Front. Microbiol. *3*, 1–20.

4. Giannopoulos, G., Hartop, K.R., Brown, B.L., Song, B., Elsgaard, L., and Franklin, R.B. (2020). Trace Metal Availability Affects Greenhouse Gas Emissions and Microbial Functional Group Abundance in Freshwater Wetland Sediments. Front. Microbiol. *11*, 1–12.

5. Jansen, S., Gonzalez-Gil, G., and Van Leeuwen, H.P. (2007). The impact of Co and Ni speciation on methanogenesis in sulfidic media-Biouptake versus metal dissolution. Enzyme Microb. Technol. *40*, 823–830.

6. Chatterjee, A., Zhang, K., Rao, Y., Sharma, N., Giammar, D.E., and Parker, K.M. (2022). Metal-Catalyzed Hydrolysis of RNA in Aqueous Environments. Environ. Sci. Technol. *56*, 3564–3574.

7. Zhang, C., Yu, Z.G., Zeng, G.M., Jiang, M., Yang, Z.Z., Cui, F., Zhu, M.Y., Shen, L.Q., and Hu, L. (2014). Effects of sediment geochemical properties on heavy metal bioavailability. Environ. Int. *73*, 270–281.

8. Merrot, P., Juillot, F., Noël, V., Lefebvre, P., Brest, J., Menguy, N., Guigner, J.M., Blondeau, M., Viollier, E., Fernandez, J.M., et al. (2019). Nickel and iron partitioning between clay minerals, Fe-oxides and Fe-sulfides in lagoon sediments from New Caledonia. Sci. Total Environ. *689*, 1212–1227.

9. Schulz-Zunkel, C., Rinklebe, J., and Bork, H.R. (2015). Trace element release patterns from three floodplain soils under simulated oxidized-reduced cycles. Ecol. Eng. *83*, 485–495.

10. Bae, Y., Crompton, N.M., Sharma, N., Yuan, Y., Catalano, J.G., and Giammar, D.E. (2022). Impact of dissolved oxygen and pH on the removal of selenium from water by iron electrocoagulation. Water Res. *213*, 118159.

11. Nolan, J., and Weber, K.A. (2015). Natural Uranium Contamination in Major U.S. Aquifers Linked to Nitrate. Environ. Sci. Technol. Lett. *2*, 215–220.

12. Ayotte, J.D., Gronberg, J.A.M., and Apodaca, L.E. (2011). Trace elements and radon in groundwater across the United States, 1992-2003. Sci. Investig. Rep. (United States Geol.

Surv., i–xi, 1–115.

13. Wang, Z., Lee, S.W., Catalano, J.G., Lezama-Pacheco, J.S., Bargar, J.R., Tebo, B.M., and Giammar, D.E. (2013). Adsorption of uranium(VI) to manganese oxides: X-ray absorption spectroscopy and surface complexation modeling. Environ. Sci. Technol. *47*, 850–858.

14. Barnett, M.O., Jardine, P.M., and Brooks, S.C. (2002). U(VI) adsorption to heterogeneous subsurface media: Application of a surface complexation model. Environ. Sci. Technol. *36*, 937–942.

15. De Palma, R., Peeters, S., Van Bael, M.J., Van Den Rul, H., Bonroy, K., Laureyn, W., Mullens, J., Borghs, G., and Maes, G. (2007). Silane ligand exchange to make hydrophobic superparamagnetic nanoparticles water-dispersible. Chem. Mater. *19*, 1821–1831.

16. Laurent, S., Forge, D., Port, M., Roch, A., Robic, C., Vander Elst, L., and Muller, R.N. (2008). Magnetic Iron Oxide Nanoparticles: Synthesis, Stabilization, Vectorization, Physicochemical Characterizations, and Biological Applications. Chem. Rev. *108*, 2064–2110.

17. Vallabani, N.V.S., and Singh, S. (2018). Recent advances and future prospects of iron oxide nanoparticles in biomedicine and diagnostics. 3 Biotech *8*, 1–23.

18. Ali, A., Zafar, H., Zia, M., ul Haq, I., Phull, A.R., Ali, J.S., and Hussain, A. (2016). Synthesis, characterization, applications, and challenges of iron oxide nanoparticles. Nanotechnol. Sci. Appl. *9*, 49–67.

19. Chourpa, I., Douziech-Eyrolles, L., Ngaboni-Okassa, L., Fouquenet, J.F., Cohen-Jonathan, S., Soucé, M., Marchais, H., and Dubois, P. (2005). Molecular composition of iron oxide nanoparticles, precursors for magnetic drug targeting, as characterized by confocal Raman microspectroscopy. Analyst *130*, 1395–1403.

20. Li, W., Lee, S.S., Wu, J., Hinton, C.H., and Fortner, J.D. (2016). Shape and size controlled synthesis of uniform iron oxide nanocrystals through new non-hydrolytic routes. Nanotechnology *27*, 1–7.

21. Yu, W.W., Falkner, J.C., Yavuz, C.T., and Colvin, V.L. (2004). Synthesis of monodisperse iron oxide nanocrystals by thermal. Chem. Commun., 2306–2307.

22. Jiang, W., Cai, Q., Xu, W., Yang, M., Cai, Y., Dionysiou, D.D., and O'Shea, K.E. (2014). Cr(VI) adsorption and reduction by humic acid coated on magnetite. Environ. Sci. Technol. *48*, 8078–8085.

23. Ge, S., Agbakpe, M., Wu, Z., Kuang, L., Zhang, W., and Wang, X. (2015). Influences of surface coating, UV irradiation and magnetic field on the algae removal using magnetite nanoparticles. Environ. Sci. Technol. *49*, 1190–1196.

24. Li, W., Hinton, C.H., Lee, S.S., Wu, J., and Fortner, J.D. (2016). Surface engineering superparamagnetic nanoparticles for aqueous applications: Design and characterization of tailored organic bilayers. Environ. Sci. Nano *3*, 85–93.

25. Kim, C., Lee, S.S., Lafferty, B.J., Giammar, D.E., and Fortner, J.D. (2018). Engineered superparamagnetic nanomaterials for arsenic(v) and chromium(VI) sorption and separation: Quantifying the role of organic surface coatings. Environ. Sci. Nano *5*, 556–563.

26. Pan, Z., Li, W., Fortner, J.D., and Giammar, D.E. (2017). Measurement and Surface Complexation Modeling of U(VI) Adsorption to Engineered Iron Oxide Nanoparticles. Environ. Sci. Technol. *51*, 9219–9226.

27. Bhattacharjee, S., Basnet, M., Tufenkji, N., and Ghoshal, S. (2016). Effects of Rhamnolipid and Carboxymethylcellulose Coatings on Reactivity of Palladium-Doped Nanoscale Zerovalent Iron Particles. Environ. Sci. Technol. *50*, 1812–1820.

28. Singh, B.N., Rawat, A.K.S., Khan, W., Naqvi, A.H., and Singh, B.R. (2014). Biosynthesis of stable antioxidant ZnO nanoparticles by Pseudomonas aeruginosa Rhamnolipids. PLoS One *9*.

29. Kiran, G.S., Selvin, J., Manilal, A., and Sujith, S. (2011). Biosurfactants as green stabilizers for the biological synthesis of nanoparticles. Crit. Rev. Biotechnol. *31*, 354–364.

30. Zhao, X., Liu, W., Cai, Z., Han, B., Qian, T., and Zhao, D. (2016). An overview of preparation and applications of stabilized zero-valent iron nanoparticles for soil and groundwater remediation. Water Res. *100*, 245–266.

31. Hazra, C., Kundu, D., Chaudhari, A., and Jana, T. (2013). Biogenic synthesis, characterization, toxicity and photocatalysis of zinc sulfide nanoparticles using rhamnolipids from Pseudomonas aeruginosa BS01 as capping and stabilizing agent. J. Chem. Technol. Biotechnol. *88*, 1039–1048.

32. Mulligan, C.N. (2009). Recent advances in the environmental applications of biosurfactants. Curr. Opin. Colloid Interface Sci. *14*, 372–378.

33. Mulligan, C.N., Yong, R.N., and Gibbs, B.F. (1999). On the use of biosurfactants for the removal of heavy metals from oil-contaminated soil. Environ. Prog. *18*, 50–54.

34. Karlapudi, A.P., Venkateswarulu, T.C., Tammineedi, J., Kanumuri, L., Ravuru, B.K., Dirisala, V. ramu, and Kodali, V.P. (2018). Role of biosurfactants in bioremediation of oil pollution-a review. Petroleum *4*, 241–249.

35. Basnet, M., Ghoshal, S., and Tufenkji, N. (2013). Rhamnolipid biosurfactant and soy protein act as effective stabilizers in the aggregation and transport of palladium-doped zerovalent iron nanoparticles in saturated porous media. Environ. Sci. Technol. *47*, 13355–13364.

36. Singh, P., Ravindran, S., Suthar, J.K., Deshpande, P., Rokhade, R., and Rale, V. (2017). Production of biosurfactant stabilized nanoparticles. Int. J. Pharma Bio Sci. *8*, 701–707.

37. Tian, H., Xu, R., Canadell, J.G., Thompson, R.L., Winiwarter, W., Suntharalingam, P., Davidson, E.A., Ciais, P., Jackson, R.B., Janssens-Maenhout, G., et al. (2020). A comprehensive quantification of global nitrous oxide sources and sinks. Nature *586*, 248–256.

38. Nowicki, B.L. (1994). The effect of temperature, oxygen, salinity, and nutrient enrichment on estuarine denitrification rates measured with a modified nitrogen gas flux technique. Estuar. Coast. Shelf Sci. *38*, 137–156.

39. Koponen, H.T., Flojt, L., and Martikainen, P.J. (2004). Nitrous oxide emissions from agricultural soils at low temperatures: A laboratory microcosm study. Soil Biol. Biochem. *36*, 757–766.

40. Nag, S.K., Liu, R., and Lal, R. (2017). Emission of greenhouse gases and soil carbon sequestration in a riparian marsh wetland in central Ohio. *189*, 1–12.

41. Baeseman, J.L., Smith, R.L., and Silverstein, J. (2006). Denitrification potential in stream sediments impacted by acid mine drainage: Effects of pH, various electron donors, and iron. Microb. Ecol. *51*, 232–241.

42. Granger, J., and Ward, B.B. (2003). Accumulation of nitrogen oxides in copper-limited cultures of denitrifying bacteria. Limnol. Oceanogr. *48*, 313–318.

43. Twining, B.S., Mylon, S.E., and Benoit, G. (2007). Potential role of copper availability in nitrous oxide accumulation in a temperate lake. Limnol. Oceanogr. *52*, 1354–1366.

44. Payne, W.J. (1976). Denitrification. Trends Biochem. Sci. *1*, 220–222.

45. Nag, S.K., Liu, R., and Lal, R. (2017). Emission of greenhouse gases and soil carbon sequestration in a riparian marsh wetland in central Ohio.

46. Sirivedhin, T., and Gray, K.A. (2006). Factors affecting denitrification rates in experimental wetlands : Field and laboratory studies. *26*, 167–181.

47. Herrman, K.S., Bouchard, *Æ*.V., and Moore, R.H. (2008). Factors affecting denitrification in agricultural headwater streams in Northeast Ohio , USA. 305–314.

48. Glass, J.B., and Orphan, V.J. (2012). Trace metal requirements for microbial enzymes involved in the production and consumption of methane and nitrous oxide. Front. Microbiol. *3*, 1–20.

49. Koponen, H.T., Flöjt, L., and Martikainen, P.J. (2004). Nitrous oxide emissions from agricultural soils at low temperatures: A laboratory microcosm study. Soil Biol. Biochem. *36*, 757–766.

50. Du Laing, G., Rinklebe, J., Vandecasteele, B., Meers, E., and Tack, F.M.G. (2009). Trace metal behaviour in estuarine and riverine floodplain soils and sediments: A review. Sci. Total Environ. *407*, 3972–3985.

51. Campana, O., Simpson, S.L., Spadaro, D.A., and Blasco, J. (2012). Sub-lethal effects of copper to benthic invertebrates explained by sediment properties and dietary exposure. Environ. Sci. Technol. *46*, 6835–6842.

52. Bourgeault, A., Ciffroy, P., Garnier, C., Cossu-Leguille, C., Masfaraud, J.F., Charlatchka, R., and Garnier, J.M. (2013). Speciation and bioavailability of dissolved copper in different

freshwaters: Comparison of modelling, biological and chemical responses in aquatic mosses and gammarids. Sci. Total Environ. *452–453*, 68–77.

53. Bhattacharyya, A., Campbell, A.N., Tfaily, M.M., Lin, Y., Kukkadapu, R.K., Silver, W.L., Nico, P.S., and Pett-Ridge, J. (2018). Redox Fluctuations Control the Coupled Cycling of Iron and Carbon in Tropical Forest Soils. Environ. Sci. Technol. *52*, 14129–14139.

54. Karimian, N., Johnston, S.G., and Burton, E.D. (2018). Iron and sulfur cycling in acid sulfate soil wetlands under dynamic redox conditions: A review. Chemosphere *197*, 803–816.

55. Chuan, M.C., Shu, G.Y., and Liu, J.C. (1996). Solubility of heavy metals in a contaminated soil: Effects of redox potential and pH. Water. Air. Soil Pollut. *90*, 543–556.

56. De Jonge, M., Teuchies, J., Meire, P., Blust, R., and Bervoets, L. (2012). The impact of increased oxygen conditions on metal-contaminated sediments part I: Effects on redox status, sediment geochemistry and metal bioavailability. Water Res. *46*, 2205–2214.

57. Choppala, G., Bush, R., Moon, E., Ward, N., Wang, Z., Bolan, N., and Sullivan, L. (2017). Oxidative transformation of iron monosulfides and pyrite in estuarine sediments: Implications for trace metals mobilisation. J. Environ. Manage. *186*, 158–166.

58. Baldwin, D.S., and Mitchell, A. (2012). Impact of sulfate pollution on anaerobic biogeochemical cycles in a wetland sediment. Water Res. *46*, 965–974.

59. Rieuwerts, J.S., Thornton, I., Farago, M.E., and Ashmore, M.R. (1998). Factors influencing metal bioavailability in soils: Preliminary investigations for the development of a critical loads approach for metals. Chem. Speciat. Bioavailab. *10*, 61–75.

60. Du Laing, G., Rinklebe, J., Vandecasteele, B., Meers, E., and Tack, F.M.G. (2009). Trace metal behaviour in estuarine and riverine floodplain soils and sediments: A review. Sci. Total Environ. *407*, 3972–3985.

61. Gavrilescu, M., Pavel, L.V., and Cretescu, I. (2009). Characterization and remediation of soils contaminated with uranium. J. Hazard. Mater. *163*, 475–510.

62. Tournassat, C., Tinnacher, R.M., Grangeon, S., and Davis, J.A. (2018). Modeling uranium(VI) adsorption onto montmorillonite under varying carbonate concentrations: A surface complexation model accounting for the spillover effect on surface potential. Geochim. Cosmochim. Acta *220*, 291–308.

63. Sharma, N., Ghosh, A., Fortner, J.D., and Giammar, D.E. (2020). Modeling performance of rhamnolipid-coated engineered magnetite nanoparticles for U(vi) sorption and separation. Environ. Sci. Nano *7*, 2010–2020.

64. Huang, X., Hou, X., Zhang, X., Rosso, K.M., and Zhang, L. (2018). Facet-dependent contaminant removal properties of hematite nanocrystals and their environmental implications. Environ. Sci. Nano *5*, 1790–1806.

65. Wan, T., Cheng, W., Ren, J., Wu, W., Wang, M., Hu, B., Jia, Z., and Sun, Y. (2018). The

influence of nanoscale size on the adsorption-desorption of U(vi) on nano-Al oxides. Environ. Sci. Nano *5*, 2731–2741.

66. Guo, X., Chen, R., Liu, Q., Liu, J., Zhang, H., Yu, J., Li, R., Zhang, M., and Wang, J. (2018). Superhydrophilic phosphate and amide functionalized magnetic adsorbent: A new combination of anti-biofouling and uranium extraction from seawater. Environ. Sci. Nano *5*, 2346–2356.

67. Li, W., Mayo, J.T., Benoit, D.N., Troyer, L.D., Lewicka, Z.A., Lafferty, B.J., Catalano, J.G., Lee, S.S., Colvin, V.L., and Fortner, J.D. (2016). Engineered superparamagnetic iron oxide nanoparticles for ultra-enhanced uranium separation and sensing. J. Mater. Chem. A *4*, 15022–15029.

68. Alqadami, A.A., Naushad, M., Alothman, Z.A., and Ghfar, A.A. (2017). Novel Metal-Organic Framework (MOF) Based Composite Material for the Sequestration of U(VI) and Th(IV) Metal Ions from Aqueous Environment. ACS Appl. Mater. Interfaces *9*, 36026–36037.

69. Das, D., Sureshkumar, M.K., Koley, S., Mithal, N., and Pillai, C.G.S. (2010). Sorption of uranium on magnetite nanoparticles. J. Radioanal. Nucl. Chem. *285*, 447–454.

70. Lee, S.S., Li, W., Kim, C., Cho, M., Catalano, J.G., Lafferty, B.J., Decuzzi, P., and Fortner, J.D. (2015). Engineered manganese oxide nanocrystals for enhanced uranyl sorption and separation. Environ. Sci. Nano *2*, 500–508.

71. Wazne, M., Meng, X., Korfiatis, G.P., and Christodoulatos, C. (2006). Carbonate effects on hexavalent uranium removal from water by nanocrystalline titanium dioxide. J. Hazard. Mater. *136*, 47–52.

72. Helal, A.S., Mazario, E., Mayoral, A., Decorse, P., Losno, R., Lion, C., Ammar, S., and Hémadi, M. (2018). Highly efficient and selective extraction of uranium from aqueous solution using a magnetic device: Succinyl-β-cyclodextrin-APTES@maghemite nanoparticles. Environ. Sci. Nano *5*, 158–168.

73. Tang, M., Chen, J., Wang, P., Wang, C., and Ao, Y. (2018). Highly efficient adsorption of uranium(vi) from aqueous solution by a novel adsorbent: Titanium phosphate nanotubes. Environ. Sci. Nano *5*, 2304–2314.

74. Huang, X., Hou, X., Wang, F., Guo, B., Song, F., Ling, L., Zhao, J., and Zhang, L. (2019). Molecular-scale structures of uranyl surface complexes on hematite facets. Environ. Sci. Nano *6*, 892–903.

75. Li, W., Troyer, L.D., Lee, S.S., Wu, J., Kim, C., Lafferty, B.J., Catalano, J.G., and Fortner, J.D. (2017). Engineering Nanoscale Iron Oxides for Uranyl Sorption and Separation: Optimization of Particle Core Size and Bilayer Surface Coatings. ACS Appl. Mater. Interfaces *9*, 13163–13172.

76. Li, W., Lee, S.S., Wu, J., Hinton, C.H., and Fortner, J.D. (2016). Shape and size controlled synthesis of uniform iron oxide nanocrystals through new non-hydrolytic routes.

Nanotechnology *27*, 324002.

77. Patsula, V., Kosinová, L., Lovrić, M., Ferhatovic Hamzić, L., Rabyk, M., Konefal, R., Paruzel, A., Šlouf, M., Herynek, V., Gajović, S., et al. (2016). Superparamagnetic Fe3O4 Nanoparticles: Synthesis by Thermal Decomposition of Iron(III) Glucuronate and Application in Magnetic Resonance Imaging. ACS Appl. Mater. Interfaces *8*, 7238–7247.

78. Luongo, G., Campagnolo, P., Perez, J.E., Kosel, J., Georgiou, T.K., Regoutz, A., Payne, D.J., Stevens, M.M., Ryan, M.P., Porter, A.E., et al. (2017). Scalable High-Affinity Stabilization of Magnetic Iron Oxide Nanostructures by a Biocompatible Antifouling Homopolymer. ACS Appl. Mater. Interfaces *9*, 40059–40069.

79. Xie, Y., Ye, R., and Liu, H. (2006). Synthesis of silver nanoparticles in reverse micelles stabilized by natural biosurfactant. Colloids Surfaces A Physicochem. Eng. Asp. *279*, 175–178.

80. Szymanska, A., and Sadowski, Z. (2010). Effects of biosurfactants on surface properties of hematite. Adsorption *16*, 233–239.

81. Marangon, C.A., Martins, V.C.A., Ling, M.H., Melo, C.C., Plepis, A.M.G., Meyer, R.L., and Nitschke, M. (2020). Combination of Rhamnolipid and Chitosan in Nanoparticles Boosts Their Antimicrobial Efficacy. ACS Appl. Mater. Interfaces *12*, 5488–5499.

82. Balakrishnan, G., Déniel, M., Nicolai, T., Chassenieux, C., and Lagarde, F. (2019). Towards more realistic reference microplastics and nanoplastics: preparation of polyethylene micro/nanoparticles with a biosurfactant. Environ. Sci. Nano *6*, 315–324.

83. Huang, G., Peng, W., and Yang, S. (2018). Synthesis of magnetic chitosan/graphene oxide nanocomposites and its application for U(VI) adsorption from aqueous solution. J. Radioanal. Nucl. Chem. *317*, 337–344.

84. Cai, Y., Wu, C., Liu, Z., Zhang, L., Chen, L., Wang, J., Wang, X., Yang, S., and Wang, S. (2017). Fabrication of a phosphorylated graphene oxide-chitosan composite for highly effective and selective capture of U(VI).

85. Wang, S., and Mulligan, C.N. (2009). Rhamnolipid biosurfactant-enhanced soil flushing for the removal of arsenic and heavy metals from mine tailings. Process Biochem. *44*, 296–301.

86. De, S., Malik, S., Ghosh, A., Saha, R., and Saha, B. (2015). A review on natural surfactants. RSC Adv. *5*, 65757–65767.

87. Basnet, M., Gershanov, A., Wilkinson, K.J., Ghoshal, S., and Tufenkji, N. (2016). Interaction between palladium-doped zerovalent iron nanoparticles and biofilm in granular porous media: Characterization, transport and viability. Environ. Sci. Nano *3*, 127–137.

88. Hosseinidoust, Z., Basnet, M., Van De Ven, T.G.M., and Tufenkji, N. (2016). One-pot green synthesis of anisotropic silver nanoparticles. Environ. Sci. Nano *3*, 1259–1264.

89. Qian, L., Ma, M., and Cheng, D. (2015). Adsorption and desorption of uranium on nano goethite and nano alumina. J. Radioanal. Nucl. Chem. *303*, 161–170.

90. Zeng, H., Singh, A., Basak, S., Ulrich, K.U., Sahu, M., Biswas, P., Catalano, J.G., and Giammar, D.E. (2009). Nanoscale size effects on uranium(VI) adsorption to hematite. Environ. Sci. Technol. *43*, 1373–1378.

91. Boyanov, M.I., O'Loughlin, E.J., Roden, E.E., Fein, J.B., and Kemner, K.M. (2007). Adsorption of Fe(II) and U(VI) to carboxyl-functionalized microspheres: The influence of speciation on uranyl reduction studied by titration and XAFS. Geochim. Cosmochim. Acta *71*, 1898–1912.

92. Duster, T.A., Szymanowski, J.E.S., and Fein, J.B. (2017). Experimental Measurements and Surface Complexation Modeling of U(VI) Adsorption onto Multilayered Graphene Oxide: The Importance of Adsorbate-Adsorbent Ratios. Environ. Sci. Technol. *51*, 8510–8518.

93. Chen, K.L., Mylon, S.E., and Elimelech, M. (2006). Aggregation kinetics of alginate-coated hematite nanoparticles in monovalent and divalent electrolytes. Environ. Sci. Technol. *40*, 1516–1523.

94. Waite, T.D., Davis, J.A., Payne, T.E., Waychunas, G.A., and Xv', N. (1994). Australian Nuclear Science and Technology Organisation. Environmental Science Program. Private Mail Bag I. Aust. ZUnited States Geol. Surv. *58*, 5465–5478.

95. Xie, X., Giammar, D.E., and Wang, Z. (2016). MINFIT: A Spreadsheet-Based Tool for Parameter Estimation in an Equilibrium Speciation Software Program. Environ. Sci. Technol. *50*, 11112–11120.

96. Lebrón-Paler, A., Pemberton, J.E., Becker, B.A., Otto, W.H., Larive, C.K., and Maier, R.M. (2006). Determination of the acid dissociation constant of the biosurfactant monorhamnolipid in aqueous solution by potentiometric and spectroscopic methods. Anal. Chem. *78*, 7649–7658.

97. Lowry, G. V., Hill, R.J., Harper, S., Rawle, A.F., Hendren, C.O., Klaessig, F., Nobbmann, U., Sayre, P., and Rumble, J. (2016). Guidance to improve the scientific value of zeta-potential measurements in nanoEHS. Environ. Sci. Nano *3*, 953–965.

98. Jang, J.H., Dempsey, B.A., and Burgos, W.D. (2007). A model-based evaluation of sorptive reactivities of hydrous ferric oxide and hematite for U(VI). Environ. Sci. Technol. *41*, 4305–4310.

99. Elder, J.F. (1988). Metal Biogeochemistry in Surface-Water Systems - A Review of Principles and Concepts (U.S. Geological Survey circular; 1013). 50.

100. Gimeno-García, E., Andreu, V., and Boluda, R. (1996). Heavy metals incidence in the application of inorganic fertilizers and pesticides to rice farming soils. Environ. Pollut. *92*, 19–25.

101. Tessier, A., and Campbell, P.G.C. (1987). Partitioning of trace metals in sediments: Relationships with bioavailability. Hydrobiologia *149*, 43–52.

102. Parmar, N., Gorby, Y.A., Beveridge, T.J., and Ferris, F.G. (2001). Formation of green rust and immobilization of nickel in response to bacterial reduction of hydrous ferric oxide.

Geomicrobiol. J. *18*, 375–385.

103. Strom, D., Simpson, S.L., Batley, G.E., and Jolley, D.F. (2011). The influence of sediment particle size and organic carbon on toxicity of copper to benthic invertebrates in oxic/suboxic surface sediments. Environ. Toxicol. Chem. *30*, 1599–1610.

104. Saeedi, M., Li, L.Y., Karbassi, A.R., and Zanjani, A.J. (2013). Sorbed metals fractionation and risk assessment of release in river sediment and particulate matter. Environ. Monit. Assess. *185*, 1737–1754.

105. Srinivasan, R. (2011). Advances in application of natural clay and its composites in removal of biological, organic, and inorganic contaminants from drinking water. Adv. Mater. Sci. Eng. *2011*.

106. Sdiri, A., Higashi, T., Hatta, T., Jamoussi, F., and Tase, N. (2011). Evaluating the adsorptive capacity of montmorillonitic and calcareous clays on the removal of several heavy metals in aqueous systems. Chem. Eng. J. *172*, 37–46.

107. Bhattacharyya, K.G., and Gupta, S. Sen (2008). Adsorption of a few heavy metals on natural and modified kaolinite and montmorillonite: A review. Adv. Colloid Interface Sci. *140*, 114–131.

108. Huang, B., Yuan, Z., Li, D., Zheng, M., Nie, X., and Liao, Y. (2020). Effects of soil particle size on the adsorption, distribution and migration behaviors of heavy metal(loid)s in soil: a review. Environ. Sci. Process. Impacts, 1596–1615.

109. Pattrick, R.A.D., Mosselmans, J.F.W., Charnock, J.M., England, K.E.R., Helz, G.R., Garner, C.D., and Vaughan, D.J. (1997). The structure of amorphous copper sulfide precipitates: An X-ray absorption study. Geochim. Cosmochim. Acta *61*, 2023–2036.

110. Morse, J.W., and Luther, G.W. (1999). Chemical influences on trace metal-sulfide interactions in anoxic sediments. Geochim. Cosmochim. Acta *63*, 3373–3378.

111. Martino, M., Turner, A., and Millward, G.E. (2003). Influence of organic complexation on the adsorption kinetics of nickel in river waters. Environ. Sci. Technol. *37*, 2383–2388.

112. Yang, J., Liu, J., Dynes, J.J., Peak, D., Regier, T., Wang, J., Zhu, S., Shi, J., and Tse, J.S. (2014). Speciation and distribution of copper in a mining soil using multiple synchrotron-based bulk and microscopic techniques. Environ. Sci. Pollut. Res. *21*, 2943–2954.

113. Yan, J., Sharma, N., Flynn, E.D., Giammar, D.E., Schwartz, G.E., Brooks, S.C., Weisenhorn, P., Kemner, K.M., O'Loughlin, E.J., Kaplan, D.I., et al. (2022). Consistent controls on trace metal micronutrient speciation in wetland soils and stream sediments. Geochim. Cosmochim. Acta *317*, 234–254.

114. Hassan, N.M., Rasmussen, P.E., Dabek-Zlotorzynska, E., Celo, V., and Chen, H. (2007). Analysis of environmental samples using microwave-assisted acid digestion and inductively coupled plasma mass spectrometry: Maximizing total element recoveries. Water. Air. Soil Pollut. *178*, 323–334.

115. Yan, M., and Korshin, G. V. (2014). Comparative examination of effects of binding of different metals on chromophores of dissolved organic matter. Environ. Sci. Technol. *48*, 3177–3185.

116. Sharma, N., Flynn, E.D., Catalano, J.G., and Giammar, D.E. (2022). Copper availability governs nitrous oxide accumulation in wetland soils and stream sediments. Geochim. Cosmochim. Acta *327*, 96–115.

117. Ravel, B., and Newville, M. (2005). ATHENA, ARTEMIS, HEPHAESTUS: Data analysis for X-ray absorption spectroscopy using IFEFFIT. J. Synchrotron Radiat. *12*, 537–541.

118. Webb, S.M. (2005). SIXpack: A graphical user interface for XAS analysis using IFEFFIT. Phys. Scr. T *T115*, 1011–1014.

119. Scheinost, A.C., Kretzschmar, R., Pfister, S., and Roberts, D.R. (2002). Combining selective sequential extractions, X-ray absorption spectroscopy, and principal component analysis for quantitative zinc speciation in soil. Environ. Sci. Technol. *36*, 5021–5028.

120. Smith, D.B., Cannon, W.F., Woodruff, L.G., Solano, F., and Ellefsen, K.J. (2014). Geochemical and mineralogical maps for soils of the conterminous United States: U.S. Geological Survey Open-File Report 2014–1082.

121. Rawlins, B.G., Turner, G., Mounteney, I., and Wildman, G. (2010). Estimating specific surface area of fine stream bed sediments from geochemistry. Appl. Geochemistry *25*, 1291–1300.

122. Stoliker, D.L., Kent, D.B., and Zachara, J.M. (2011). Quantifying differences in the impact of variable chemistry on equilibrium uranium(VI) adsorption properties of aquifer sediments. Environ. Sci. Technol. *45*, 8733–8740.

123. Da Silva-Cadoux, C., Zanella, L., and Gaillard, J.F. (2012). Selecting reference compounds for determining chemical speciation by X-ray absorption spectroscopy. J. Anal. At. Spectrom. *27*, 957–965.

124. Prietzel, J., Botzaki, A., Tyufekchieva, N., Brettholle, M., Thieme, J., and Klysubun, W. (2011). Sulfur speciation in soil by S K -edge XANES spectroscopy: Comparison of spectral deconvolution and linear combination fitting. Environ. Sci. Technol. *45*, 2878–2886.

125. Burton, E.D., Bush, R.T., and Sullivan, L.A. (2006). Acid-volatile sulfide oxidation in coastal flood plain drains: Iron-sulfur cycling and effects on water quality. Environ. Sci. Technol. *40*, 1217–1222.

126. Cervi, E.C., Clark, S., Boye, K.E., Gustafsson, J.P., Baken, S., and Burton, G.A. (2021). Copper transformation, speciation, and detoxification in anoxic and suboxic freshwater sediments. Chemosphere *282*, 131063.

127. Ciglenečki, I., Krznarić, D., and Helz, G.R. (2005). Voltammetry of copper sulfide particles and nanoparticles: Investigation of the cluster hypothesis. Environ. Sci. Technol. *39*, 7492–7498.

128. Luther, G.W., Theberge, S.M., Rozan, T.F., and Rickard, D.T. (2000). Evidence for aqueous clusters as intermediates during copper sulfide formation. ACS Div. Environ. Chem. Prepr. *40*, 665–666.

129. Wakatsuki, T. (1995). Metal oxidoreduction by microbial cells. J. Ind. Microbiol. *14*, 169–177.

130. Pham, A.N., Rose, A.L., and Waite, T.D. (2012). Kinetics of Cu(II) reduction by natural organic matter. J. Phys. Chem. A *116*, 6590–6599.

131. Matocha, C.J., Karathanasis, A.D., Rakshit, S., and Wagner, K.M. (2005). Reduction of Copper(II) by Iron(II). J. Environ. Qual. *34*, 1539–1546.

132. Fulda, B., Voegelin, A., Ehlert, K., and Kretzschmar, R. (2013). Redox transformation, solid phase speciation and solution dynamics of copper during soil reduction and reoxidation as affected by sulfate availability. Geochim. Cosmochim. Acta *123*, 385–402.

133. Boulegue, J., Lord, C.J., and Church, T.M. (1982). Sulfur speciation and associated trace metals (Fe, Cu) in the pore waters of Great Marsh, Delaware. Geochim. Cosmochim. Acta *46*, 453–464.

134. Leal, M.F.C., and Van Den Berg, C.M.G. (1998). Evidence for strong copper(I) complexation by organic ligands in seawater. Aquat. Geochemistry *4*, 49–75.

135. Manceau, A., Nagy, K.L., Marcus, M.A., Lanson, M., Geoffroy, N., Jacquet, T., and Kirpichtchikova, T. (2008). Formation of metallic copper nanoparticles at the soil-root interface. Environ. Sci. Technol. *42*, 1766–1772.

136. Hofacker, A.F., Voegelin, A., Kaegi, R., Weber, F.A., and Kretzschmar, R. (2013). Temperature-dependent formation of metallic copper and metal sulfide nanoparticles during flooding of a contaminated soil. Geochim. Cosmochim. Acta *103*, 316–332.

137. Weber, F.A., Voegelin, A., Kaegi, R., and Kretzschmar, R. (2009). Contaminant mobilization by metallic copper and metal sulphide colloids in flooded soil. Nat. Geosci. *2*, 267–271.

138. Manceau, A., and Matynia, A. (2010). The nature of Cu bonding to natural organic matter. Geochim. Cosmochim. Acta *74*, 2556–2580.

139. Strawn, D.G., and Baker, L.L. (2008). Speciation of Cu in a contaminated agricultural soil measured by XAFS, μ-XAFS, and μ-XRF. Environ. Sci. Technol. *42*, 37–42.

140. Yang, J., Regier, T., Dynes, J.J., Wang, J., Shi, J., Peak, D., Zhao, Y., Hu, T., Chen, Y., and Tse, J.S. (2011). Soft X-ray induced photoreduction of organic Cu(II) compounds probed by X-ray absorption near-edge (XANES) spectroscopy. Anal. Chem. *83*, 7856–7862.

141. Weber, F.A., Voegelin, A., and Kretzschmar, R. (2009). Multi-metal contaminant dynamics in temporarily flooded soil under sulfate limitation. Geochim. Cosmochim. Acta *73*, 5513–5527.

142. Cooper, D.C., and Morse, J.W. (1998). Extractability of metal sulfide minerals in acidic solutions: Application to environmental studies of trace metal contamination within anoxic sediments. Environ. Sci. Technol. *32*, 1076–1078.

143. Hofacker, A.F., Voegelin, A., Kaegi, R., and Kretzschmar, R. (2013). Mercury mobilization in a flooded soil by incorporation into metallic copper and metal sulfide nanoparticles. Environ. Sci. Technol. *47*, 7739–7746.

144. Karimian, N., Johnston, S.G., and Burton, E.D. (2017). Effect of cyclic redox oscillations on water quality in freshwater acid sulfate soil wetlands. Sci. Total Environ. *581–582*, 314–327.

145. Sovacool, B.K., Griffiths, S., Kim, J., and Bazilian, M. (2021). Climate change and industrial F-gases: A critical and systematic review of developments, sociotechnical systems and policy options for reducing synthetic greenhouse gas emissions. Renew. Sustain. Energy Rev. *141*, 110759.

146. IPCC (2014). Climate Change 2014: Impacts, Adaptation, and Vulnerability. Contribution of Working Group II to the Fifth Assessment Report of the Intergovernmental Panel on Climate Change. In.

147. Makowski, D. (2019). N2O increasing faster than expected. Nat. Clim. Chang. *9*, 909–910.

148. Martinez-Espinosa, C., Sauvage, S., Al Bitar, A., Green, P.A., Vorosmarty, C.J., and Sanchez-Perez, J.M. (2021). Denitrification in wetlands: A review towards a quantification at global scale. Sci. Total Environ. *754*.

149. Merill, L., and Tonjes, D.J. (2014). A review of the hyporheic zone, stream restoration, and means to enhance denitrification. Crit. Rev. Environ. Sci. Technol. *44*, 2337–2379.

150. Mwagona, P.C., Yao, Y., Yuanqi, S., and Yu, H. (2019). Laboratory study on nitrate removal and nitrous oxide emission in intact soil columns collected from nitrogenous loaded riparian wetland, Northeast China. PLoS One *14*, 1–21.

151. Giannopoulos, G., Hartop, K.R., Brown, B.L., Song, B., Elsgaard, L., and Franklin, R.B. (2020). Trace metal availability affects Greenhouse Gas emissions and microbial functional group abundance in freshwater wetland sediments. Front. Microbiol. *11*, 1–12.

152. Godden, A.J.W., Turley, S., Teller, D.C., Adman, E.T., Liu, M.Y., Payne, W.J., and Legall, J. (1991). The 2.3 angstrom X-Ray structure of nitrite reductase from Achromobacter cycloclastes. Science (80-.). *253*, 438–442.

153. Bertero, M.G., Rothery, R.A., Palak, M., Hou, C., Lim, D., Blasco, F., Weiner, J.H., and Strynadka, N.C.J. (2003). Insights into the respiratory electron transfer pathway from the structure of nitrate reductase A. Nat. Struct. Biol. *10*, 681–687.

154. Nojiri, M., Xie, Y., Inoue, T., Yamamoto, T., Matsumura, H., Kataoka, K., Deligeer, Yamaguchi, K., Kai, Y., and Suzuki, S. (2007). Structure and function of a hexameric copper-containing nitrite reductase. Proc. Natl. Acad. Sci. U. S. A. *104*, 4315–4320.

155. Jormakka, M., Richardson, D., Byrne, B., and Iwata, S. (2004). Architecture of NarGH reveals a structural classification of Mo-bisMGD enzymes. Structure *12*, 95–104.

156. Brown, K., Tegoni, M., Prudêncio, M., Pereira, A.S., Besson, S., Moura, J.J., Moura, I., and Cambillau, C. (2000). A novel type of catalytic copper cluster in nitrous oxide reductase. Nat. Struct. Biol. *7*, 191–195.

157. Iwasaki, H., Saigo, T., and Matsubara, T. (1980). Copper as a controlling factor of anaerobic growth under N2O and biosynthesis of N2O reductase in denitrifying bacteria. Plant Cell Physiol. *21*, 1573–1584.

158. Black, A., Hsu, P.C.L., Hamonts, K.E., Clough, T.J., and Condron, L.M. (2016). Influence of copper on expression of nirS, norB and nosZ and the transcription and activity of NIR, NOR and N2OR in the denitrifying soil bacteria Pseudomonas stutzeri. Microb. Biotechnol. *9*, 381–388.

159. Magalhaes, C., Costa, J., Teixeira, C., and Bordalo, A.A. (2007). Impact of trace metals on denitrification in estuarine sediments of the Douro River estuary , Portugal. *107*, 332–341.

160. Sakadevan, K., Zheng, H., and Bavor, H.J. (1999). Impact of heavy metals on denitrification in surface wetland sediments receiving wastewater. Water Sci. Technol. *40*, 349–355.

161. Shaaban, M., Peng, Q. an, Bashir, S., Wu, Y., Younas, A., Xu, X., Rashti, M.R., Abid, M., Zafar-ul-Hye, M., Núñez-Delgado, A., et al. (2019). Restoring effect of soil acidity and Cu on N2O emissions from an acidic soil. J. Environ. Manage. *250*, 109535.

162. Jacinthe, P.A., and Tedesco, L.P. (2009). Impact of elevated copper on the rate and gaseous products of denitrification in freshwater sediments. J. Environ. Qual. *38*, 1183–1192.

163. Doroski, A.A., Helton, A.M., and Vadas, T.M. (2019). Greenhouse gas fluxes from coastal wetlands at the intersection of urban pollution and saltwater intrusion: A soil core experiment. Soil Biol. Biochem. *131*, 44–53.

164. Black, A., McLaren, R.G., Reichman, S.M., Speir, T.W., and Condron, L.M. (2011). Evaluation of soil metal bioavailability estimates using two plant species (L. perenne and T. aestivum) grown in a range of agricultural soils treated with biosolids and metal salts. Environ. Pollut. *159*, 1523–1535.

165. Kozelka, P.B., and Bruland, K.W. (1998). Chemical speciation of dissolved Cu, Zn, Cd, Pb in Narragansett Bay, Rhode Island. Mar. Chem. *60*, 267–282.

166. Allen, H.E., and Hansen, D.J. (1996). The importance of trace metal speciation to water quality criteria. Water Environ. Res. *68*, 42–54.

167. Bruland, K.W., Rue, E.L., Donat, J.R., Skrabal, S.A., and Moffett, J.W. (2000). Intercomparison of voltammetric techniques to determine the chemical speciation of dissolved copper in a coastal seawater sample. Anal. Chim. Acta *405*, 99–113.

168. Huang, S., and Wang, Z. (2003). Application of anodic stripping voltammetry to predict the bioavailable/toxic concentration of Cu in natural water. Appl. Geochemistry *18*, 1215–

1223.

169. Skrabal, S.A., Donat, J.R., and Burdige, D.J. (2000). Pore water distributions of dissolved copper and copper-complexing ligands in estuarine and coastal marine sediments. Geochim. Cosmochim. Acta *64*, 1843–1857.

170. Chakraborty, P., Ramteke, D., and Chakraborty, S. (2015). Geochemical partitioning of Cu and Ni in mangrove sediments: Relationships with their bioavailability. Mar. Pollut. Bull. *93*, 194–201.

171. Ren, Z.L., Tella, M., Bravin, M.N., Comans, R.N.J., Dai, J., Garnier, J.M., Sivry, Y., Doelsch, E., Straathof, A., and Benedetti, M.F. (2015). Effect of dissolved organic matter composition on metal speciation in soil solutions. Chem. Geol. *398*, 61–69.

172. Waska, H., Brumsack, H.J., Massmann, G., Koschinsky, A., Schnetger, B., Simon, H., and Dittmar, T. (2019). Inorganic and organic iron and copper species of the subterranean estuary: Origins and fate. Geochim. Cosmochim. Acta *259*, 211–232.

173. Burgin, A.J., and Hamilton, S.K. (2007). Have we overemphasized the role of denitrification in aquatic ecosystems? A review of nitrate removal pathways. Front. Ecol. Environ. *5*, 89–96.

174. Doane, T.A. (2017). The Abiotic Nitrogen Cycle. ACS Earth Sp. Chem. *1*, 411–421.

175. Davidson, E.A., Chorover, J., and Dail, D.B. (2003). A mechanism of abiotic immobilization of nitrate in forest ecosystems: The ferrous wheel hypothesis. Glob. Chang. Biol. *9*, 228–236.

176. Weber, K.A., Urrutia, M.M., Churchill, P.F., Kukkadapu, R.K., and Roden, E.E. (2006). Anaerobic redox cycling of iron by freshwater sediment microorganisms. Environ. Microbiol. *8*, 100–113.

177. Melton, E.D., Swanner, E.D., Behrens, S., Schmidt, C., and Kappler, A. (2014). The interplay of microbially mediated and abiotic reactions in the biogeochemical Fe cycle. Nat. Rev. Microbiol. *12*, 797–808.

178. Di Capua, F., Pirozzi, F., Lens, P.N.L., and Esposito, G. (2019). Electron donors for autotrophic denitrification. Chem. Eng. J. *362*, 922–937.

179. Wei, J., Ibraim, E., Brüggemann, N., Vereecken, H., and Mohn, J. (2019). First real-time isotopic characterisation of N2O from chemodenitrification. Geochim. Cosmochim. Acta *267*, 17–32.

180. Moraghan, J.T., and Buresh, R.J. (1977). Chemical reduction of nitrite and nitrous oxide by ferrous iron. Soil Sci. Soc. Am. J. *41*, 47–50.

181. Ottley, C.J., Davison, W., and Edmunds, W.M. (1997). Chemical catalysis of nitrate reduction by iron(II). Geochim. Cosmochim. Acta *61*, 1819–1828.

182. Peters, B., Casciotti, K.L., Samarkin, V.A., Madigan, M.T., Schutte, C.A., and Joye, S.B.

(2014). Stable isotope analyses of NO2-, NO3-, and N2O in the hypersaline ponds and soils of the McMurdo Dry Valleys, Antarctica. Geochim. Cosmochim. Acta *135*, 87–101.

183. Buchwald, C., Grabb, K., Hansel, C.M., and Wankel, S.D. (2016). Constraining the role of iron in environmental nitrogen transformations: Dual stable isotope systematics of abiotic NO2- reduction by Fe(II) and its production of N2O. Geochim. Cosmochim. Acta *186*, 1–12.

184. Liu, T., Chen, D., Luo, X., Li, X., and Li, F. (2019). Microbially mediated nitrate-reducing Fe(II) oxidation: Quantification of chemodenitrification and biological reactions. Geochim. Cosmochim. Acta *256*, 97–115.

185. Matus, F., Stock, S., Eschenbach, W., Dyckmans, J., Merino, C., Nájera, F., Köster, M., Kuzyakov, Y., and Dippold, M.A. (2019). Ferrous Wheel Hypothesis: Abiotic nitrate incorporation into dissolved organic matter. Geochim. Cosmochim. Acta *245*, 514–524.

186. Chen, D., Yuan, X., Zhao, W., Luo, X., Li, F., and Liu, T. (2020). Chemodenitrification by Fe(II) and nitrite: pH effect, mineralization and kinetic modeling. Chem. Geol. *541*, 119586.

187. Matocha, C.J., Dhakal, P., and Pyzola, S.M. (2012). The role of abiotic and coupled biotic/abiotic mineral controlled redox processes in nitrate reduction. Adv. Agron. *115*, 181–214.

188. Wang, M., Hu, R., Zhao, J., Kuzyakov, Y., and Liu, S. (2016). Iron oxidation affects nitrous oxide emissions via donating electrons to denitrification in paddy soils. Geoderma *271*, 173–180.

189. Otte, J.M., Blackwell, N., Ruser, R., Kappler, A., Kleindienst, S., and Schmidt, C. (2019). N2O formation by nitrite-induced (chemo)denitrification in coastal marine sediment. Sci. Rep. *9*, 10691.

190. Ward, B.B., Tuit, C.B., Jayakumar, A., Rich, J.J., Moffett, J., and Naqvi, S.W.A. (2008). Organic carbon, and not copper, controls denitrification in oxygen minimum zones of the ocean. Deep. Res. Part I Oceanogr. Res. Pap. *55*, 1672–1683.

191. Yan, J., Flynn, E., Sharma, N., Giammar, D., Schwartz, G., Brooks, S., Weisenhorn, P., Kemner, K., O'Loughlin, E., Kaplan, D., et al. (2021). Consistent Controls on Trace Metal Micronutrient Speciation in Wetland Soils and Stream Sediments. Geochim. Cosmochim. Acta.

192. Pansu, M., and Gautheyrou, J. (2006). Handbook of soil analysis: Mineralogical, organic and inorganic methods. In Springer, Berlin Heidelberg.

193. Sparks, D.L., Page, A.L., Helmke, P.A., Loeppert, R.H., Soltanpour, P.N., Tabatabai, M.A., Johnston, C.T., and Sumner, M.E. (1996). Methods of soil analysis. Part 3: Chemical Methods. In Soil Science Society of America, Madison.

194. Sander, R. (2015). Compilation of Henry's law constants (version 4.0) for water as solvent. Atmos. Chem. Phys. *15*, 4399–4981.

195. Huffman, S.A., and Barbarick, K.A. (1981). Soil nitrate analysis by cadmium reduction. Commun. Soil Sci. Plant Anal. *12*, 79–89.

196. Krom, M.D. (1980). Spectrophotometric determination of ammonia: a study of a modified Berthelot reaction using salicylate and dichloroisocyanurate. Analyst *105*, 305–316.

197. Benedetti, M.F., Milne, C.J., Kinniburgh, D.G., Van Riemsdijk, W.H., and Koopal, L.K. (1995). Metal ion binding to humic substances: Application of the non-ideal competitive adsorption model. Environ. Sci. Technol. *29*, 446–457.

198. Benedetti, M.F., Van Riemsdijk, W.H., and Koopal, L.K. (1996). Humic substances considered as a heterogeneous Donnan gel phase. Environ. Sci. Technol. *30*, 1805–1813.

199. Kleber, M., and Lehmann, J. (2019). Humic substances extracted by alkali are invalid proxies for the dynamics and functions of organic matter in terrestrial and aquatic ecosystems. J. Environ. Qual. *48*, 207–216.

200. Myneni, S.C.B. (2019). Chemistry of natural organic matter—The next step: commentary on a humic substances debate. J. Environ. Qual. *48*, 233–235.

201. Han, S., Zhang, Y., Masunaga, S., Zhou, S., and Naito, W. (2014). Relating metal bioavailability to risk assessment for aquatic species: Daliao River watershed, China. Environ. Pollut. *189*, 215–222.

202. Ponthieu, M., Pourret, O., Marin, B., Schneider, A.R., Morvan, X., Conreux, A., and Cancès, B. (2016). Evaluation of the impact of organic matter composition on metal speciation in calcareous soil solution: Comparison of Model VI and NICA-Donnan. J. Geochemical Explor. *165*, 1–7.

203. Xu, J., Tan, W., Xiong, J., Wang, M., Fang, L., and Koopal, L.K. (2016). Copper binding to soil fulvic and humic acids: NICA-Donnan modeling and conditional affinity spectra. J. Colloid Interface Sci. *473*, 141–151.

204. Milne, C.J., Kinniburgh, D.G., Van Riemsdijk, W.H., and Tipping, E. (2003). Generic NICA - Donnan model parameters for metal-ion binding by humic substances. Environ. Sci. Technol. *37*, 958–971.

205. Milne, C.J., Kinniburgh, D.G., and Tipping, E. (2001). Generic NICA-Donnan model parameters for proton binding by humic substances. Environ. Sci. Technol. *35*, 2049–2059.

206. Fulda, B., Voegelin, A., Maurer, F., Christl, I., and Kretzschmar, R. (2013). Copper redox transformation and complexation by reduced and oxidized soil humic acid. 1. X-ray absorption spectroscopy study. Environ. Sci. Technol. *47*, 10903–10911.

207. Mehlhorn, J., Besold, J., Lezama Pacheco, J.S., Gustafsson, J.P., Kretzschmar, R., and Planer-Friedrich, B. (2018). Copper mobilization and immobilization along an organic matter and redox gradient - insights from a mofette Site. Environ. Sci. Technol. *52*, 13698–13707.

208. Yuan, X., Pham, A.N., Xing, G., Rose, A.L., and Waite, T.D. (2012). Effects of pH,

chloride, and bicarbonate on Cu(I) oxidation kinetics at circumneutral pH. Environ. Sci. Technol. *46*, 1527–1535.

209. Bowman, R.A., and Focht, D.D. (1974). The influence of glucose and nitrate concentrations upon denitrification rates in sandy soils. Soil Biol. Biochem. *6*, 297–301.

210. Kremen, A., Bear, J., Shavit, U., and Shaviv, A. (2005). Model demonstrating the potential for coupled nitrification denitrification in soil aggregates. Environ. Sci. Technol. *39*, 4180–4188.

211. Zhu, I., and Getting, T. (2012). A review of nitrate reduction using inorganic materials. Environ. Technol. Rev. *1*, 46–58.

212. Zhu-Barker, X., Cavazos, A.R., Ostrom, N.E., Horwath, W.R., and Glass, J.B. (2015). The importance of abiotic reactions for nitrous oxide production. Biogeochemistry *126*, 251–267.

213. Anyigor, C., and Afiukwa, J. (2013). Application of matlab ordinary differential equation function solver (ode45) in modelling and simulation of batch reaction kinetics. Am. J. Sci. Ind. Res. *4*, 285–287.

214. Shampine, L.F., Gladwell, I., and Thompson, S. (2003). Solving ODEs with MATLAB.

215. Rudnick, R.L., and Gao, S. (2003). Composition of the continental crust. The crust *3*, 1–64.

216. Wang, Z., Jiang, Y., Awasthi, M.K., Wang, J., Yang, X., Amjad, A., Wang, Q., Lahori, A.H., and Zhang, Z. (2018). Nitrate removal by combined heterotrophic and autotrophic denitrification processes: Impact of coexistent ions. Bioresour. Technol. *250*, 838–845.

217. Zhao, S., Su, X., Wang, Y., Yang, X., Bi, M., He, Q., and Chen, Y. (2020). Copper oxide nanoparticles inhibited denitrifying enzymes and electron transport system activities to influence soil denitrification and N2O emission. Chemosphere *245*, 125394.

218. Ochoa-Herrera, V., León, G., Banihani, Q., Field, J.A., and Sierra-Alvarez, R. (2011). Toxicity of copper(II) ions to microorganisms in biological wastewater treatment systems. Sci. Total Environ. *412–413*, 380–385.

219. Fu, M.H., and Tabatabai, M.A. (1989). Nitrate reductase activity in soils: Effects of trace elements. Soil Biol. Biochem. *21*, 943–946.

220. Schmidt, F., Koch, B.P., Goldhammer, T., Elvert, M., Witt, M., Lin, Y.S., Wendt, J., Zabel, M., Heuer, V.B., and Hinrichs, K.U. (2017). Unraveling signatures of biogeochemical processes and the depositional setting in the molecular composition of pore water DOM across different marine environments. Geochim. Cosmochim. Acta *207*, 57–80.

221. Marschner, B., and Kalbitz, K. (2003). Controls of bioavailability and biodegradability of dissolved organic matter in soils. Geoderma *113*, 211–235.

222. Wang, J., Wang, S., Jin, X., Zhu, S., and Wu, F. (2008). Ammonium release characteristics of the sediments from the shallow lakes in the middle and lower reaches of Yangtze River

region, China. Environ. Geol. *55*, 37–45.

223. Robertson, E.K., and Thamdrup, B. (2017). The fate of nitrogen is linked to iron(II) availability in a freshwater lake sediment. Geochim. Cosmochim. Acta *205*, 84–99.

224. Mohapatra, S., Sharma, N., Mohapatra, G., Padhye, L.P., and Mukherji, S. (2021). Seasonal variation in fluorescence characteristics of dissolved organic matter in wastewater and identification of proteins through HRLC-MS/MS. J. Hazard. Mater. *413*, 125453.

225. Zhu, Y., Jin, X., Tang, W., Meng, X., and Shan, B. (2019). Comprehensive analysis of nitrogen distributions and ammonia nitrogen release fluxes in the sediments of Baiyangdian Lake, China. J. Environ. Sci. (China) *76*, 319–328.

226. Sharma, N., Mohapatra, S., Padhye, L.P., and Mukherji, S. (2021). Role of precursors in the formation of trihalomethanes during chlorination of drinking water and wastewater effluents from a metropolitan region in western India. J. Water Process Eng. *40*, 101928.

227. Liu, R., Ma, T., Zhang, D., Lin, C., and Chen, J. (2020). Spatial distribution and factors influencing the different forms of ammonium in sediments and pore water of the aquitard along the Tongshun River, China. Environ. Pollut. *266*, 115212.

228. Wang, S., Pi, Y., Jiang, Y., Pan, H., Wang, X., Wang, X., Zhou, J., and Zhu, G. (2020). Nitrate reduction in the reed rhizosphere of a riparian zone: From functional genes to activity and contribution. Environ. Res. *180*, 108867.

229. Clement, J.C., Shrestha, J., Ehrenfeld, J.G., and Jaffe, P.R. (2005). Ammonium oxidation coupled to dissimilatory reduction of iron under anaerobic conditions in wetland soils. Soil Biol. Biochem. *37*, 2323–2328.

230. Castaldelli, G., Colombani, N., Soana, E., Vincenzi, F., Fano, E.A., and Mastrocicco, M. (2019). Reactive nitrogen losses via denitrification assessed in saturated agricultural soils. Geoderma *337*, 91–98.

231. Schultz, C., and Grundl, T. (2004). pH Dependence of ferrous sorption onto two smectite clays. Chemosphere *57*, 1301–1306.

232. Seta, A.K., and Karathanasis, A.D. (1996). Water dispersible colloids and factors influencing their dispersibility from soil aggregates. Geoderma *74*, 255–266.

233. Nano, G.V., and Strathmann, T.J. (2006). Ferrous iron sorption by hydrous metal oxides. J. Colloid Interface Sci. *297*, 443–454.

234. Zhu, Y., and Elzinga, E.J. (2014). Formation of layered Fe(II)-hydroxides during Fe(II) sorption onto clay and metal-oxide substrates. Environ. Sci. Technol. *48*, 4937–4945.

235. Klueglein, N., Zeitvogel, F., Stierhof, Y.D., Floetenmeyer, M., Konhauser, K.O., Kappler, A., and Obst, M. (2014). Potential role of nitrite for abiotic Fe(II) oxidation and cell encrustation during nitrate reduction by denitrifying bacteria. Appl. Environ. Microbiol. *80*, 1051–1061.

236. Rahman, M.M., Roberts, K.L., Grace, M.R., Kessler, A.J., and Cook, P.L.M. (2019). Role of organic carbon, nitrate and ferrous iron on the partitioning between denitrification and DNRA in constructed stormwater urban wetlands. Sci. Total Environ. *666*, 608–617.

237. Robinson, T.C., Latta, D.E., Notini, L., Schilling, K.E., and Scherer, M.M. (2021). Abiotic reduction of nitrite by Fe(ii): a comparison of rates and N 2 O production . Environ. Sci. Process. Impacts *23*, 1531–1541.

238. Stumm, W., and Sulzberger, B. (1992). The cycling of iron in natural environments: Considerations based on laboratory studies of heterogeneous redox processes. Geochim. Cosmochim. Acta *56*, 3233–3257.

239. Zhao, L., Dong, H., Edelmann, R.E., Zeng, Q., and Agrawal, A. (2017). Coupling of Fe(II) oxidation in illite with nitrate reduction and its role in clay mineral transformation. Geochim. Cosmochim. Acta *200*, 353–366.

240. Zhao, L., Dong, H., Kukkadapu, R., Agrawal, A., Liu, D., Zhang, J., and Edelmann, R.E. (2013). Biological oxidation of Fe(II) in reduced nontronite coupled with nitrate reduction by Pseudogulbenkiania sp. Strain 2002. Geochim. Cosmochim. Acta *119*, 231–247.

241. Kurdi, F., and Donner, H.E. (1983). Zinc and Copper Sorption and Interaction in Soils. Soil Sci. Soc. Am. J. *47*, 873–876.

242. Traina, S.J., and Doner, H.E. (1985). Heavy metal induced releases of manganese (II) from a hydrous manganese dioxide. Soil Sci. Soc. Am. J. *49*, 317–321.

243. Su, J.F., Zheng, S.C., Huang, T.L., Ma, F., Shao, S.C., Yang, S.F., and Zhang, L.N. (2015). Characterization of the anaerobic denitrification bacterium Acinetobacter sp. SZ28 and its application for groundwater treatment. Bioresour. Technol. *192*, 654–659.

244. Su, J.F., Luo, X.X., Wei, L., Ma, F., Zheng, S.C., and Shao, S.C. (2016). Performance and microbial communities of Mn(II)-based autotrophic denitrification in a Moving Bed Biofilm Reactor (MBBR). Bioresour. Technol. *211*, 743–750.

245. Knowles, R. (1982). Denitrification. Microbiol. Rev. *46*, 43–70.

246. Simek, M., and Cooper, J.E. (2002). The influence of soil pH on denitrification: Progress towards the understanding of this interaction over the last 50 years. Eur. J. Soil Sci. *53*, 345–354.

247. Pan, Y., Ye, L., Ni, B.J., and Yuan, Z. (2012). Effect of pH on N2O reduction and accumulation during denitrification by methanol utilizing denitrifiers. Water Res. *46*, 4832–4840.

248. Carreira, C., Nunes, R.F., Mestre, O., Moura, I., and Pauleta, S.R. (2020). The effect of pH on Marinobacter hydrocarbonoclasticus denitrification pathway and nitrous oxide reductase. J. Biol. Inorg. Chem. *25*, 927–940.

249. Shen, W., Xue, H., Gao, N., Shiratori, Y., Kamiya, T., Fujiwara, T., Isobe, K., and Senoo, K. (2020). Effects of copper on nitrous oxide (N2O) reduction in denitrifiers and N2O

emissions from agricultural soils. Biol. Fertil. Soils *56*, 39–51.

250. Tian, H., Chen, G., Lu, C., Xu, X., Ren, W., Zhang, B., Banger, K., Tao, B., Pan, S., Liu, M., et al. (2015). Global methane and nitrous oxide emissions from terrestrial ecosystems due to multiple environmental changes. Ecosyst. Heal. Sustain. *1*, 1–20.

251. Flemming, C.A., and Trevors, J.T. (1989). Copper toxicity and chemistry in the environment: a review. Water. Air. Soil Pollut. *44*, 143–158.

252. Sirajuddin, S., and Rosenzweig, A.C. (2015). Enzymatic oxidation of methane. Biochemistry *54*, 2283–2294.

253. Glass, J.B., and Orphan, V.J. (2012). Trace metal requirements for microbial enzymes involved in the production and consumption of methane and nitrous oxide. Front. Microbiol. *3*, 1–20.

254. Schönheit, P., Moll, J., and Thauer, R.K. (1979). Nickel, cobalt, and molybdenum requirement for growth of Methanobacterium thermoautotrophicum. Arch. Microbiol. *123*, 105–107.

255. Granger, J., and Ward, B.B. (2003). Accumulation of nitrogen oxides in copper-limited cultures of denitrifying bacteria. Limnol. Oceanogr. *48*, 313–318.

256. Prior, S.D., and Dalton, H. (1985). The effect of copper ions on membrane content and methane monooxygenase activity in methanol-grown cells of Methylococcus capsulatus (Bath). J. Gen. Microbiol. *131*, 155–163.

257. Paulo, L.M., Ramiro-Garcia, J., van Mourik, S., Stams, A.J.M., and Sousa, D.Z. (2017). Effect of nickel and cobalt on methanogenic enrichment cultures and role of biogenic sulfide in metal toxicity attenuation. Front. Microbiol. *8*, 1–12.

258. Schaefer, J.K., Szczuka, A., and Morel, F.M.M. (2014). Effect of divalent metals on Hg(II) uptake and methylation by bacteria. Environ. Sci. Technol. *48*, 3007–3013.

259. Antić-Mladenović, S., Rinklebe, J., Frohne, T., Stärk, H.J., Wennrich, R., Tomić, Z., and Ličina, V. (2011). Impact of controlled redox conditions on nickel in a serpentine soil. J. Soils Sediments *11*, 406–415.

260. Moore, J.N., Ficklin, W.H., and Johns, C. (1988). Partitioning of Arsenic and Metals in Reducing Sulfidic Sediments. Environ. Sci. Technol. *22*, 432–437.

261. Tessier, A., Rapin, F., and Carignan, R. (1985). Trace metals in oxic lake sediments: possible adsorption onto iron oxyhydroxides. Geochim. Cosmochim. Acta *49*, 183–194.

262. Bonten, L.T.C., Groenenberg, J.E., Weng, L., and van Riemsdijk, W.H. (2008). Use of speciation and complexation models to estimate heavy metal sorption in soils. Geoderma *146*, 303–310.

263. Dang, D.H., Layglon, N., Ferretto, N., Omanović, D., Mullot, J.U., Lenoble, V., Mounier, S., and Garnier, C. (2020). Kinetic processes of copper and lead remobilization during

sediment resuspension of marine polluted sediments. Sci. Total Environ. *698*.

264. Grybos, M., Davranche, M., Gruau, G., and Petitjean, P. (2007). Is trace metal release in wetland soils controlled by organic matter mobility or Fe-oxyhydroxides reduction? J. Colloid Interface Sci. *314*, 490–501.

265. Grybos, M., Davranche, M., Gruau, G., Petitjean, P., and Pédrot, M. (2009). Increasing pH drives organic matter solubilization from wetland soils under reducing conditions. Geoderma *154*, 13–19.

266. Bostick, B.C., Hansel, C.M., La Force, M.J., and Fendorf, S. (2001). Seasonal fluctuations in zinc speciation within a contaminated wetland. Environ. Sci. Technol. *35*, 3823–3829.

267. Schulz-Zunkel, C., and Krueger, F. (2009). Trace Metal Dynamics in Floodplain Soils of the River Elbe: A Review. J. Environ. Qual. *38*, 1349–1362.

268. Rieuwerts, J.S., Thornton, I., Farago, M.E., Ashmore, M.R., Rieuwerts, J.S., Thornton, I., Farago, M.E., and Ashmore, M.R. (1998). Factors influencing metal bioavailability in soils : preliminary investigations for the development of a critical loads approach for metals. Chem. Speciat. Bioavailab. *10*, 61–75.

269. Eggleton, J., and Thomas, K. V. (2004). A review of factors affecting the release and bioavailability of contaminants during sediment disturbance events. Environ. Int. *30*, 973–980.

270. Borch, T., Kretzschmar, R., Skappler, A., Van Cappellen, P., Ginder-Vogel, M., Voegelin, A., and Campbell, K. (2010). Biogeochemical redox processes and their impact on contaminant dynamics. Environ. Sci. Technol. *44*, 15–23.

271. Caetano, M., and Vale, C. (2003). Contaminated Sediment : Short-Term Laboratory Study. Water Sci. Technol. *143*, 23–40.

272. Shaheen, S.M., Frohne, T., White, J.R., DeLaune, R.D., and Rinklebe, J. (2017). Redox-induced mobilization of copper, selenium, and zinc in deltaic soils originating from Mississippi (U.S.A.) and Nile (Egypt) River Deltas: A better understanding of biogeochemical processes for safe environmental management. J. Environ. Manage. *186*, 131–140.

273. Pan, Y., Koopmans, G.F., Bonten, L.T.C., Song, J., Luo, Y., Temminghoff, E.J.M., and Comans, R.N.J. (2014). Influence of pH on the redox chemistry of metal (hydr)oxides and organic matter in paddy soils. J. Soils Sediments *14*, 1713–1726.

274. White, A.F., and Peterson, M.L. (1996). Reduction of aqueous transition metal species on the surfaces of Fe(II)-containing oxides. Geochim. Cosmochim. Acta *60*, 3799–3814.

275. O'Loughlin, E.J., Kelly, S.D., Kemner, K.M., Csencsits, R., and Cook, R.E. (2003). Reduction of AgI, AuIII, CuII, and Hg II by FeII/FeIII hydroxysulfate green rust. Chemosphere *53*, 437–446.

276. Rinklebe, J., and Shaheen, S.M. (2017). Redox chemistry of nickel in soils and sediments:

a review. Chemosphere *179*, 265–278.

277. Rinklebe, J., Antić-Mladenović, S., Frohne, T., Stärk, H.J., Tomić, Z., and Ličina, V. (2016). Nickel in a serpentine-enriched Fluvisol: Redox affected dynamics and binding forms. Geoderma *263*, 203–214.

278. Mehlhorn, J., Besold, J., Lezama Pacheco, J.S., Gustafsson, J.P., Kretzschmar, R., and Planer-Friedrich, B. (2018). Copper Mobilization and Immobilization along an Organic Matter and Redox Gradient - Insights from a Mofette Site. Environ. Sci. Technol. *52*, 13698–13707.

279. Chen, C., and Thompson, A. (2018). Ferrous Iron Oxidation under Varying pO2 Levels: The Effect of Fe(III)/Al(III) Oxide Minerals and Organic Matter. Environ. Sci. Technol. *52*, 597–606.

280. Ginn, B., Meile, C., Wilmoth, J., Tang, Y., and Thompson, A. (2017). Rapid Iron Reduction Rates Are Stimulated by High-Amplitude Redox Fluctuations in a Tropical Forest Soil. Environ. Sci. Technol. *51*, 3250–3259.

281. Stewart, B.D., Nico, P.S., and Fendorf, S. (2009). Stability of uranium incorporated into Fe (hydr)oxides under fluctuating redox conditions. Environ. Sci. Technol. *43*, 4922–4927.

282. Couture, R.M., Charlet, L., Markelova, E., Madé, B., and Parsons, C.T. (2015). On-off mobilization of contaminants in soils during redox oscillations. Environ. Sci. Technol. *49*, 3015–3023.

283. Han, Y.S., Park, J.H., Kim, S.J., Jeong, H.Y., and Ahn, J.S. (2019). Redox transformation of soil minerals and arsenic in arsenic-contaminated soil under cycling redox conditions. J. Hazard. Mater. *378*, 120745.

284. De Jonge, M., Teuchies, J., Meire, P., Blust, R., and Bervoets, L. (2012). The impact of increased oxygen conditions on metal-contaminated sediments part I: Effects on redox status, sediment geochemistry and metal bioavailability. Water Res. *46*, 2205–2214.

285. Frohne, T., Rinklebe, J., Diaz-Bone, R.A., and Du Laing, G. (2011). Controlled variation of redox conditions in a floodplain soil: Impact on metal mobilization and biomethylation of arsenic and antimony. Geoderma *160*, 414–424.

286. Thompson, A., Rancourt, D.G., Chadwick, O.A., and Chorover, J. (2011). Iron solid-phase differentiation along a redox gradient in basaltic soils. Geochim. Cosmochim. Acta *75*, 119–133.

287. Komadel, P., Madejová, J., and Stucki, J.W. (2006). Structural Fe(III) reduction in smectites. Appl. Clay Sci. *34*, 88–94.

288. Gorski, C.A., Aeschbacher, M., Soltermann, D., Voegelin, A., Baeyens, B., Marques Fernandes, M., Hofstetter, T.B., and Sander, M. (2012). Redox properties of structural Fe in clay minerals. 1. Electrochemical quantification of electron-donating and -accepting capacities of smectites. Environ. Sci. Technol. *46*, 9360–9368.

289. Gorski, C.A., Klüpfel, L.E., Voegelin, A., Sander, M., and Hofstetter, T.B. (2013). Redox properties of structural Fe in clay minerals: 3. Relationships between smectite redox and structural properties. Environ. Sci. Technol. *47*, 13477–13485.

290. Chacon, N., Silver, W.L., Dubinsky, E.A., and Cusack, D.F. (2006). Iron reduction and soil phosphorus solubilization in humid tropical forests soils: The roles of labile carbon pools and an electron shuttle compound. Biogeochemistry *78*, 67–84.

291. Rapin, A., Grybos, M., Rabiet, M., Mourier, B., and Deluchat, V. (2019). Phosphorus mobility in dam reservoir affected by redox oscillations: An experimental study. J. Environ. Sci. (China) *77*, 250–263.

292. Edwards, P.G., Gaines, K.F., Bryan, A.L., Novak, J.M., and Blas, S.A. (2014). Trophic dynamics of U, Ni, Hg and other contaminants of potential concern on the Department of Energy's Savannah River Site. Environ. Monit. Assess. *186*, 481–500.

293. Brooks, S.C., Lowe, K.A., Mehlhorn, T.L., Olsen, T.A., Yin, X.L., Fortner, A.M., and Peterson, M.J. (2018). Intraday Water Quality Patterns in East Fork Poplar Creek with an Emphasis on Mercury and Monomethylmercury.

294. Yan, J., Sharma, N., Flynn, E.D., Giammar, D.E., Schwartz, G.E., Brooks, S.C., Weisenhorn, P., Kemner, K.M., O'Loughlin, E.J., Kaplan, D.I., et al. (2022). Consistent Controls on Trace Metal Micronutrient Speciation in Wetland Soils and Stream Sediments. Geochim. Cosmochim. Acta *317*, 234–254.

295. King, E.K., Thompson, A., and Pett-ridge, J.C. (2019). Underlying lithology controls trace metal mobilization during redox fluctuations. Sci. Total Environ. *665*, 1147–1157.

296. Han, S., Naito, W., Hanai, Y., and Masunaga, S. (2013). Evaluation of trace metals bioavailability in Japanese river waters using DGT and a chemical equilibrium model. Water Res. *47*, 4880–4892.

297. Garmo, Ø.A., Røyset, O., Steinnes, E., and Flaten, T.P. (2003). Performance study of diffusive gradients in thin films for 55 elements. Anal. Chem. *75*, 3573–3580.

298. Zhang, H., and Davison, W. (1995). Performance Characteristics of Diffusion Gradients in Thin Films for the in Situ Measurement of Trace Metals in Aqueous Solution. Anal. Chem. *67*, 3391–3400.

299. Gao, Y., Leermakers, M., Gabelle, C., Divis, P., Billon, G., Ouddane, B., Fischer, J.C., Wartel, M., and Baeyens, W. (2006). High-resolution profiles of trace metals in the pore waters of riverine sediment assessed by DET and DGT. Sci. Total Environ. *362*, 266–277.

300. Rudnick, R.L., and Gao, S. (2013). Composition of the Continental Crust 2nd ed. (Elsevier Ltd.).

301. Curtin, D., and Trolove, S. (2013). Predicting pH buffering capacity of New Zealand soils from organic matter content and mineral characteristics. Soil Res. *51*, 494–502.

302. Breeman, N. Van, and Wielemaker, W.G. (1974). Buffer Intensities and Equilibrium pH of

Minerals and Soils: I. The Contribution of Minerals and Aqueous Carbonate to pH Buffering. Soil Sci. Soc. Am. J. *38*, 55–60.

303. Sposito, G., Skipper, N.T., Sutton, R., Park, S.H., Soper, A.K., and Greathouse, J.A. (1999). Surface geochemistry of the clay minerals. Proc. Natl. Acad. Sci. U. S. A. *96*, 3358–3364.

304. Jayalath, N., Mosley, L.M., Fitzpatrick, R.W., and Marschner, P. (2016). Addition of organic matter influences pH changes in reduced and oxidised acid sulfate soils. Geoderma *262*, 125–132.

305. Diem, D., and Stumm, W. (1984). Is dissolved Mn2+ being oxidized by O2 in absence of Mn-bacteria or surface catalysts? Geochim. Cosmochim. Acta *48*, 1571–1573.

306. Thompson, A., Chadwick, O.A., Boman, S., and Chorover, J. (2006). Colloid mobilization during soil iron redox oscillations. Environ. Sci. Technol. *40*, 5743–5749.

307. Buettner, S.W., Kramer, M.G., Chadwick, O.A., and Thompson, A. (2014). Mobilization of colloidal carbon during iron reduction in basaltic soils. Geoderma *221–222*, 139–145.

308. Kristensen, E. (2000). Organic matter diagenesis at the oxic/anoxic interface in coastal marine sediments, with emphasis on the role of burrowing animals. Hydrobiologia *426*, 1–24.

309. Goldstone, J. V., Pullin, M.J., Bertilsson, S., and Voelker, B.M. (2002). Reactions of hydroxyl radical with humic substances: Bleaching, mineralization, and production of bioavailable carbon substrates. Environ. Sci. Technol. *36*, 364–372.

310. Schippers, A. (2004). Biogeochemistry of metal sulfide oxidation in mining environments, sediments, and soils. Spec. Pap. Soc. Am., 49–62.

311. Schroth, A.W., Bostick, B.C., Graham, M., Kaste, J.M., Mitchell, M.J., and Friedland, A.J. (2007). Sulfur species behavior in soil organic matter during decomposition. J. Geophys. Res. Biogeosciences *112*, 1–10.

312. Winkler, P., Kaiser, K., Thompson, A., Kalbitz, K., Fiedler, S., and Jahn, R. (2018). Contrasting evolution of iron phase composition in soils exposed to redox fluctuations. Geochim. Cosmochim. Acta *235*, 89–102.

313. Saulnier, I., and Mucci, A. (2000). Trace metal remobilization following the resuspension of estuarine sediments: Saguenay Fjord, Canada. Appl Geochem *15*, 191–210.

314. Stumm, W., and Lee, G.F. (1961). Oxygenation of Ferrous Iron. Ind. Eng. Chem. *53*, 143–146.

315. Kirby, C.S., Thomas, H.M., Southam, G., and Donald, R. (1999). Relative contributions of abiotic and biological factors in Fe(II) oxidation in mine drainage. Appl. Geochemistry *14*, 511–530.

316. Morgan, B., and Lahav, O. (2007). The effect of pH on the kinetics of spontaneous Fe(II) oxidation by O2 in aqueous solution - basic principles and a simple heuristic description.

Chemosphere *68*, 2080–2084.

317. Larson, L.N., Sánchez-España, J., Kaley, B., Sheng, Y., Bibby, K., and Burgos, W.D. (2014). Thermodynamic controls on the kinetics of microbial low-pH Fe(II) oxidation. Environ. Sci. Technol. *48*, 9246–9254.

318. Jones, A.M., Griffin, P.J., Collins, R.N., and Waite, T.D. (2014). Ferrous iron oxidation under acidic conditions - The effect of ferric oxide surfaces. Geochim. Cosmochim. Acta *145*, 1–12.

319. Tamura, H., Kawamura, S., and Hagayama, M. (1980). Acceleration of the oxidation of Fe2+ ions by Fe(III)-oxyhydroxides. Corros. Sci. *20*, 963–971.

320. Morgan, J.J. (2005). Kinetics of reaction between O2 and Mn(II) species in aqueous solutions. Geochim. Cosmochim. Acta *69*, 35–48.

321. Lan, S., Wang, X., Xiang, Q., Yin, H., Tan, W., Qiu, G., Liu, F., Zhang, J., and Feng, X. (2017). Mechanisms of Mn(II) catalytic oxidation on ferrihydrite surfaces and the formation of manganese (oxyhydr)oxides. Geochim. Cosmochim. Acta *211*, 79–96.

322. Sung, W., and Morgan, J.J. (1981). Oxidative removal of Mn (II) from solution catalysed by the γ-FeOOH (lepidocrocite) surface. Geochim. Cosmochim. Acta *45*, 2377–2383.

323. Davies, S.H.R., and Morgan, J.J. (1989). Manganese(II) oxidation kinetics on metal oxide surfaces. J. Colloid Interface Sci. *129*, 63–77.

324. Silber, A., Bar-Yosef, B., Levkovitch, I., Kautzky, L., and Minz, D. (2008). Kinetics and mechanisms of pH-dependent Mn(II) reactions in plant-growth medium. Soil Biol. Biochem. *40*, 2787–2795.

325. Zhang, J., Lion, L.W., Nelson, Y.M., Shuler, M.L., and Ghiorse, W.C. (2002). Kinetics of Mn(II) oxidation by Leptothrix discophora SS1. Geochim. Cosmochim. Acta *66*, 773–781.

326. Berner, R.A. (1984). Sedimentary pyrite formation: An update. Geochim. Cosmochim. Acta *48*, 605–615.

327. Schoonen, M.A.A., and Barnes, H.L. (1991). Reactions forming pyrite and marcasite from solution: II. Via FeS precursors below 100 C. Geochim. Cosmochim. Acta *55*, 1505–1514.

328. Simpson, S.L., Rosner, J., and Ellis, J. (2000). Competitive displacement reactions of cadmium, copper, and zinc added to a polluted, sulfidic estuarine sediment. Environ. Toxicol. Chem. *19*, 1992–1999.

329. Luther, G.W., and Rickard, D.T. (2005). Metal sulfide cluster complexes and their biogeochemical importance in the environment. J. Nanoparticle Res. *7*, 389–407.

330. Gramp, J.P., Sasaki, K., Bigham, J.M., Karnachuk, O. V., and Tuovinen, O.H. (2006). Formation of covellite (CuS) under biological sulfate-reducing conditions. Geomicrobiol. J. *23*, 613–619.

331. Simpson, S.L., Apte, S.C., and Batley, G.E. (1998). Effect of short-term resuspension events

on trace metal speciation in polluted anoxic sediments. Environ. Sci. Technol. *32*, 620–625.

332. Tack, F.M.G. (2010). Trace elements: General soil chemistry, principles and processes. Trace Elem. Soils, 9–37.

333. Hinkle, M.A.G., Flynn, E.D., and Catalano, J.G. (2016). Structural response of phyllomanganates to wet aging and aqueous Mn(II). Geochim. Cosmochim. Acta *192*, 220–234.

334. Speelmans, M., Vanthuyne, D.R.J., Lock, K., Hendrickx, F., Du, L.G., Tack, F.M.G., and Janssen, C.R. (2007). Influence of flooding, salinity and inundation time on the bioavailability of metals in wetlands. Sci. Total Environ. *380*, 144–153.

335. Alvarez, M., Rueda, E.H., and Sileo, E.E. (2007). Simultaneous incorporation of Mn and Al in the goethite structure. Geochim. Cosmochim. Acta *71*, 1009–1020.

336. Manceau, A., Schlegel, M.L., Musso, M., Sole, V.A., Gauthier, C., Petit, P.E., and Trolard, F. (2000). Crystal chemistry of trace elements in natural and synthetic goethite. Geochim. Cosmochim. Acta *64*, 3643–3661.

337. Alvarez, M., Sileo, E.E., and Rueda, E.H. (2005). Effect of Mn(II) incorporation on the transformation of ferrihydrite to goethite. Chem. Geol. *216*, 89–97.

338. Cancès, B., Ponthieu, M., Castrec-Rouelle, M., Aubry, E., and Benedetti, M.F. (2003). Metal ions speciation in a soil and its solution: Experimental data and model results. Geoderma *113*, 341–355.

339. Kay, A.R. (2004). Detecting and minimizing zinc contamination in physiological solutions. BMC Physiol. *4*, 1–9.

340. Ghosh, A., Sharma, N., Li, W., &, and Fortner, J. (2018). Adsorption of rhamnolipid biosurfactant and its effect on the aggregation kinetics of iron oxide (Fe3O4) nanoparticles in monovalent and divalent electrolyte solutions. Abstr. Pap. Am. Chem. Soc. *256*.

341. Roy Chowdhury, T., Herndon, E.M., Phelps, T.J., Elias, D.A., Gu, B., Liang, L., Wullschleger, S.D., and Graham, D.E. (2015). Stoichiometry and temperature sensitivity of methanogenesis and CO2 production from saturated polygonal tundra in Barrow, Alaska. Glob. Chang. Biol. *21*, 722–737.

342. Shakoor, A., Shakoor, S., Rehman, A., Ashraf, F., Abdullah, M., Shahzad, S.M., Farooq, T.H., Ashraf, M., Manzoor, M.A., Altaf, M.M., et al. (2021). Effect of animal manure, crop type, climate zone, and soil attributes on greenhouse gas emissions from agricultural soils—A global meta-analysis. J. Clean. Prod. *278*, 124019.

343. Thangarajan, R., Bolan, N.S., Tian, G., Naidu, R., and Kunhikrishnan, A. (2013). Role of organic amendment application on greenhouse gas emission from soil. Sci. Total Environ. *465*, 72–96.

344. Thomson, A.J., Giannopoulos, G., Pretty, J., Baggs, E.M., and Richardson, D.J. (2012). Biological sources and sinks of nitrous oxide and strategies to mitigate emissions. Philos.

Trans. R. Soc. B Biol. Sci. *367*, 1157–1168.

345. Zhu, Q., Zhang, M., and Ma, Q. (2012). Copper-based foliar fertilizer and controlled release urea improved soil chemical properties, plant growth and yield of tomato. Sci. Hortic. (Amsterdam). *143*, 109–114.

346. Knapp, C.W., Fowle, D.A., Kulczycki, E., Roberts, J.A., and Graham, D.W. (2007). Methane monooxygenase gene expression mediated by methanobactin in the presence of mineral copper sources. Proc. Natl. Acad. Sci. U. S. A. *104*, 12040–12045.

347. Kulczycki, E., Fowle, D.A., Knapp, C., Graham, D.W., and Roberts, J.A. (2007). Methanobactin-promoted dissolution of Cu-substituted borosilicate glass. Geobiology *5*, 251–263.

348. Morton, J.D., Hayes, K.F., and Semrau, J.D. (2000). Bioavailability of chelated and soil-adsorbed copper to Methylosinus trichosporium OB3b. Environ. Sci. Technol. *34*, 4917–4922.

349. Mastrocicco, M., Colombani, N., Salemi, E., and Castaldelli, G. (2011). Reactive modeling of denitrification in soils with natural and depleted organic matter. Water. Air. Soil Pollut. *222*, 205–215.

350. Zhang, H., and Davison, W. (2000). Direct in situ measurements of labile inorganic and organically bound metal species in synthetic solutions and natural waters using diffusive gradients in thin films. Anal. Chem. *72*, 4447–4457.

351. Guillaumont, R., Fanghanel, T., Neck, V., Fuger, J., Palmer, D.A., Grenthe, I., and Rand, M.H. (2003). Update on the chemical thermodynamics of uranium, neptunium, plutonium, americium and technetium.

352. Luo, Y., Giammar, D.E., Huhmann, B.L., and Catalano, J.G. (2011). Speciation of selenium, arsenic, and zinc in Class C fly ash. Energy and Fuels *25*, 2980–2987.

353. Voegelin, A., Jacquat, O., Pfister, S., Barmettler, K., Scheinost, A.C., and Kretzschmar, R. (2011). Time-dependent changes of zinc speciation in four soils contaminated with zincite or sphalerite. Environ. Sci. Technol. *45*, 255–261.

354. Bostick, B.C., Hansel, C.M., La Force, M.J., and Fendorf, S. (2001). Seasonal fluctuations in zinc speciation within a contaminated wetland. Environ. Sci. Technol. *35*, 3823–3829.

355. Isaure, M.P., Laboudigue, A., Manceau, A., Sarret, G., Tiffreau, C., Trocellier, P., Lamble, G., Hazemann, J.L., and Chateigner, D. (2002). Quantitative Zn speciation in a contaminated dredged sediment by μ-PIXE, μ-SXRF, EXAFS spectroscopy and principal component analysis. Geochim. Cosmochim. Acta *66*, 1549–1567.

356. Gueguen, C., Clarisse, O., Perroud, A., and McDonald, A. (2011). Chemical speciation and partitioning of trace metals (Cd, Co, Cu, Ni, Pb) in the lower Athabasca river and its tributaries (Alberta, Canada). J. Environ. Monit. *13*, 2865–2872.

357. Zhang, H., and Davison, W. (2015). Use of diffusive gradients in thin-films for studies of

chemical speciation and bioavailability. Environ. Chem. *12*, 85–101.

358. Neaman, A., Waller, B., Mouélé, F., Trolard, F., and Bourrié, G. (2004). Improved methods for selective dissolution of manganese oxides from soils and rocks. Eur. J. Soil Sci. *55*, 47–54.

359. Mikutta, R., Kleber, M., Torn, M.S., and Jahn, R. (2006). Stabilization of soil organic matter: Association with minerals or chemical recalcitrance? Biogeochemistry *77*, 25–56.

360. Denney, S., Sherwood, J., and Leyden, J. (1999). In situ measurements of labile Cu, Cd and Mn in river waters using DGT. Sci. Total Environ. *239*, 71–80.

361. Xu, D., Gao, B., Gao, L., Zhou, H., Zhao, X., and Yin, S. (2016). Characteristics of cadmium remobilization in tributary sediments in Three Gorges Reservoir using chemical sequential extraction and DGT technology. Environ. Pollut. *218*, 1094–1101.

362. Sharma, N., Wang, Z., Catalano, G., and Giammar, D.E. (2022). Dynamic Responses of Trace Metal Bioaccessibility to Fluctuating Redox Conditions in Wetland Soils and Stream Sediments.

363. Gao, Y., van de Velde, S., Williams, P.N., Baeyens, W., and Zhang, H. (2015). Two-dimensional images of dissolved sulfide and metals in anoxic sediments by a novel diffusive gradients in thin film probe and optical scanning techniques. TrAC - Trends Anal. Chem. *66*, 63–71.

364. Leermakers, M., Gao, Y., Gabelle, C., Lojen, S., Ouddane, B., Wartel, M., and Baeyens, W. (2005). Determination of high resolution pore water profiles of trace metals in sediments of the Rupel River (Belgium) using DET (diffusive equilibrium in thin films) and DGT (diffusive gradients in thin films) techniques. Water. Air. Soil Pollut. *166*, 265–286.

365. Zhang, H., Davison, W., Knight, B., and Mcgrath, S. (1998). In situ measurements of solution concentrations and fluxes of trace metals in sells using DGT. Environ. Sci. Technol. *32*, 704–710.

366. Zhang, H., and Davison, W. (1999). Diffusional characteristics of hydrogels used in DGT and DET techniques. Anal. Chim. Acta *398*, 329–340.

367. Gimpel, J., Zhang, H., Davison, W., and Edwards, A.C. (2003). In situ trace metal speciation in lake surface waters using DGT, dialysis, and filtration. Environ. Sci. Technol. *37*, 138–146.

368. Davison, W. (1993). Iron and manganese in lakes. Earth Sci. Rev. *34*, 119–163.

369. Huerta-Diaz, M.A., Tessier, A., and Carignan, R. (1998). Geochemistry of trace metals associated with reduced sulfur in freshwater sediments. Appl. Geochemistry *13*, 213–233.

370. Duchart, P., Calvert, S.E., and Price, N.B. (1973). Distribution of Trace Metals in the Pore Waters of Shallow Water Marine Sediments. Limnol. Oceanogr. *18*, 605–610.

371. Man, K.W., Zheng, J., Leung, A.P.K., Lam, P.K.S., Lam, M.H.W., and Yen, Y.F. (2004).

Distribution and behavior of trace metals in the sediment and porewater of a tropical coastal wetland. Sci. Total Environ. *327*, 295–314.

372. Canavan, R.W., Van Cappellen, P., Zwolsman, J.J.G., van den Berg, G.A., and Slomp, C.P. (2007). Geochemistry of trace metals in a fresh water sediment: Field results and diagenetic modeling. Sci. Total Environ. *381*, 263–279.

373. Xu, J., Zhang, J., Huo, S., Xi, B., He, Z., and Xu, Y. (2017). High-resolution profiles of trace metals assessed by DGT techniques in lake sediment porewaters. Environ. Earth Sci. *76*, 1–10.

374. Gao, B., Gao, L., Zhou, Y., Xu, D., and Zhao, X. (2017). Evaluation of the dynamic mobilization of vanadium in tributary sediments of the Three Gorges Reservoir after water impoundment. J. Hydrol. *551*, 92–99.

375. Stockdale, A., Davison, W., Zhang, H., and Hamilton-Taylor, J. (2010). The association of Cobalt with Iron and Manganese (Oxyhydr)oxides in marine sediment. Aquat. Geochemistry *16*, 575–585.

376. Zhang, H., Davison, W., Mortimer, R.J.G., Krom, M.D., Hayes, P.J., and Davies, I.M. (2002). Localised remobilization of metals in a marine sediment. Sci. Total Environ. *296*, 175–187.

377. Zhang, T., Li, L., Xu, F., Chen, X., Du, L., and Li, Y. (2020). Assessing the environmental risk, fractions, and remobilization of copper and zinc in the sediments of the Jialing River—an important tributary of the Yangtze River in China. Environ. Sci. Pollut. Res. *27*, 39283–39296.

378. Jin, Z., Ding, S., Sun, Q., Gao, S., Fu, Z., Gong, M., Lin, J., Wang, D., and Wang, Y. (2019). High resolution spatiotemporal sampling as a tool for comprehensive assessment of zinc mobility and pollution in sediments of a eutrophic lake. J. Hazard. Mater. *364*, 182–191.

379. Kristensen, E., Ahmed, S.I., and Devol, A.H. (1995). Aerobic and anaerobic decomposition of organic matter in marine sediment: Which is fastest? Limnol. Oceanogr. *40*, 1430–1437.

380. Mackin, J.E., and Swider, K.T. (1989). Organic matter decomposition pathways and oxygen consumption in coastal marine sediments. J. Mar. Res. *47*, 681–716.

381. Naylor, C., Davison, W., Motelica-Heino, M., Van Den Berg, G.A., and Van Der Heijdt, L.M. (2004). Simultaneous release of sulfide with Fe, Mn, Ni and Zn in marine harbour sediment measured using a combined metal/sulfide DGT probe. Sci. Total Environ. *328*, 275–286.

382. Morse, J.W., and Rickard, D. (2004). Chemical Dynamics of Sedimentary Acid Volatile Sulfide. Environ. Sci. Technol. *38*, 131–136.

383. Hernández-Crespo, C., Martín, M., Ferrís, M., and Oñate, M. (2012). Measurement of Acid Volatile Sulphide and Simultaneously Extracted Metals in Sediment from Lake Albufera (Valencia, Spain). Soil Sediment Contam. *21*, 176–191.

384. Burton, E.D., Phillips, I.R., and Hawker, D.W. (2005). Reactive sulfide relationships with trace metal extractability in sediments from southern Moreton Bay, Australia Edward. Mar. Pollut. Bull. *50*, 589–595.

385. Zhang, T., Li, L., Xu, F., Chen, X., Du, L., Wang, X., and Li, Y. (2020). Evaluation of the environment risk, fractions and mobilization of nickel (Ni) in sediments of the Jialing River by sediment quality guidelines, sequential extraction and Chelex-AgI gel DGT probe. Appl. Geochemistry *118*.

Appendix A. Supporting Materials for

Chapter 2

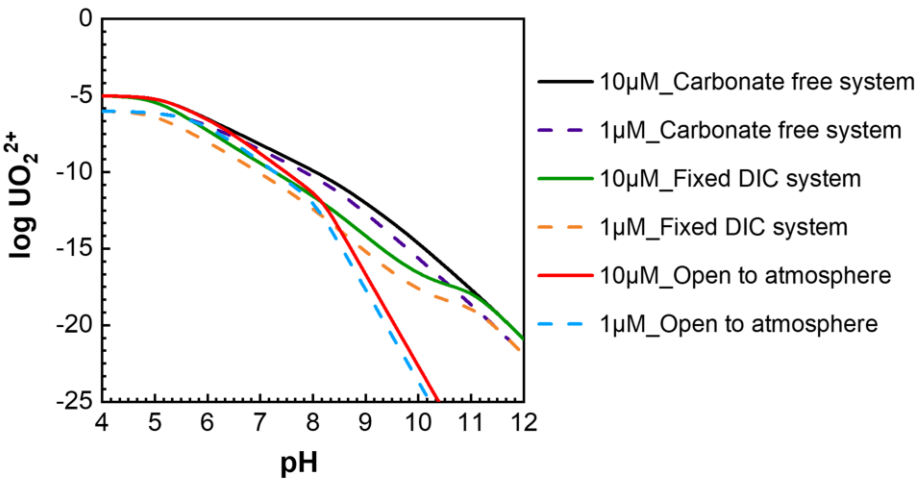

Figure A-1: Variation of log UO_2^{2+} as a function of pH. The ionic strength is fixed at 0.01 M

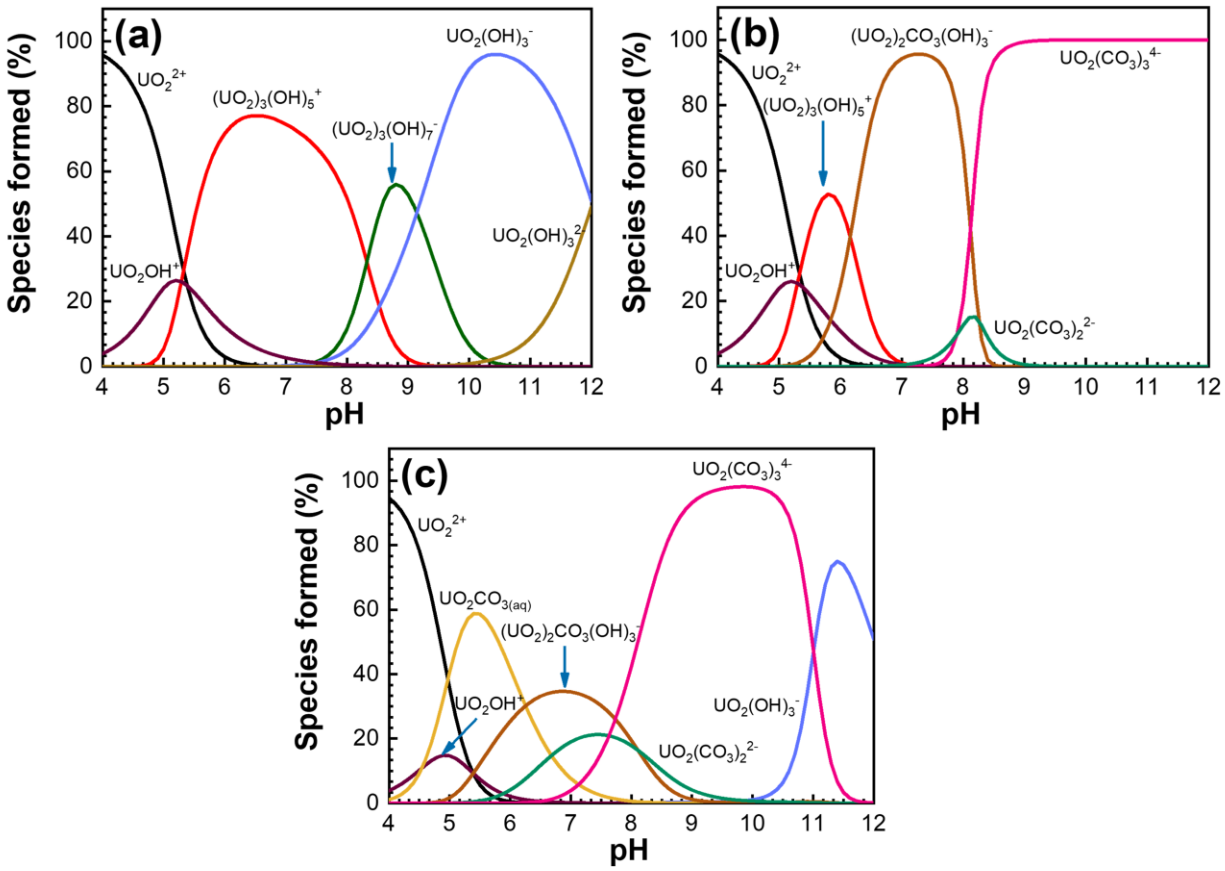

Figure A-2: Speciation of U(VI) in (a) carbonate-free system, (b) open to atmosphere system, and (c) fixed dissolved inorganic carbon (DIC) system. U(VI) loading for all carbonate conditions is 10 µM and ionic strength is 0.01 M.

Table A-1: Phase transfer efficiency achieved by variation of various parameters for obtaining aqueous stable suspensions using Rhamnolipids

Iron oxide volume (µL)	Rhamnolipid (mg/L)	Time (min)	Amplitude (%)	Numbered Mean (nm)	Efficiency (%)
400	60	5-6	60-70	61.2	26.21
400	70	5-6	60-70	38.16	28.01
400	80	5-6	60-70	41.07	39.94
400	90	5-6	60-70	47.15	36.83
400	100	5-6	60-70	49.51	32.42
500	60	5-6	60	37.86	17.87
500	70	5-6	60	37.96	25.64
500	80	5-6	60	38.27	23.29
500	90	5-6	60	37.85	24.42
500	100	5-6	60	40.35	20.67
800	60	5-6	80-90	104.4	26.7
800	70	5-6	80-90	41.21	34.57
800	80	5-6	80-90	37.5	52.12
800	90	5-6	80-90	36.24	47.46
800	100	5-6	80-90	39.2	43.48
600	60	10-12	80-100	33.76	51.79
600	70	10-12	80-100	29.86	63.71
600	80	10-12	80-100	26.1	84.78
600	90	10-12	80-100	25.66	80.33
600	100	10-12	80-100	26.29	90.57
800	60	10-12	80-100	38.23	28.5
800	70	10-12	80-100	35.1	46.82
800	80	10-12	80-100	32.59	51.43
800	90	10-12	80-100	31.14	63.05
800	100	10-12	80-100	30.42	69.93

Table A-2: Aqueous reactions considered for surface complexation modeling[351]

Reaction	log K°
$H_2O = H^+ + OH^-$	-14.00
$UO_2^{2+} + H_2O = UO_2OH^+ + H^+$	-5.25
$UO_2^{2+} + 2H_2O = UO_2(OH)_2 + 2H^+$	-12.15
$UO_2^{2+} + 3H_2O = UO_2(OH)_3^- + 3H^+$	-20.25
$UO_2^{2+} + 4H_2O = UO_2(OH)_4^{2-} + 4H^+$	-32.40
$2UO_2^{2+} + H_2O = (UO_2)_2(OH)^{3+} + H^+$	-2.70
$2UO_2^{2+} + 2H_2O = (UO_2)_2(OH)_2^{2+} + 2H^+$	-5.62
$3UO_2^{2+} + 4H_2O = (UO_2)_3(OH)_4^{2+} + 4H^+$	-11.90
$3UO_2^{2+} + 5H_2O = (UO_2)_3(OH)_5^{2+} + 5H^+$	-15.55
$3UO_2^{2+} + 7H_2O = (UO_2)_3(OH)_7^- + 7H^+$	-32.20
$4UO_2^{2+} + 7H_2O = (UO_2)_4(OH)_7^+ + 7H^+$	-21.90
$UO_2^{2+} + CO_3^{2-} = UO_2CO_3\,(aq)$	9.94
$UO_2^{2+} + 2CO_3^{2-} = UO_2(CO_3)_2^{2-}$	16.61
$UO_2^{2+} + 3CO_3^{2-} = UO_2(CO_3)_3^{4-}$	21.84
$3UO_2^{2+} + 6CO_3^{2-} = (UO_2)_3(CO_3)_6^{6-}$	54.00
$2UO_2^{2+} + 3H_2O + CO_3^{2-} = (UO_2)_2CO_3(OH)_3^- + 3H^+$	-0.86
$3UO_2^{2+} + 3H_2O + CO_3^{2-} = (UO_2)_3CO_3(OH)_3^+ + 3H^+$	0.65

A.1 Estimating Number of Rhamnolipids Attached per Nanoparticle

Before ultracentrifuge (Rhamnolipid excess +Rhamnolipid attached to IONPs + Oleic acid attached to IONPs) = 84.48 mg/L as C

After ultracentrifuge, Rhamnolipid excess = 11.16 mg/L as C

Total carbon attached to IONPs = 73.32 mg/L as C

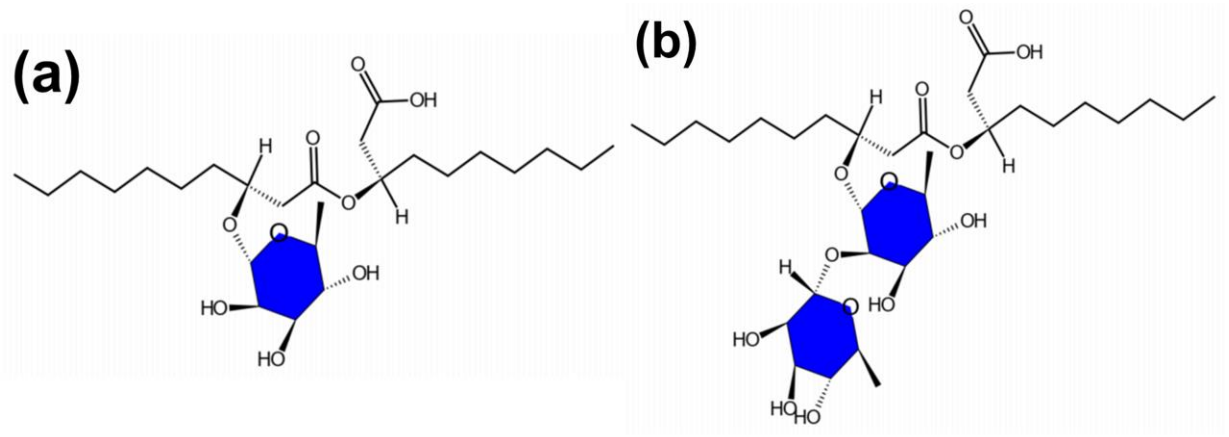

Figure A-3: Structures of (a) Monorhamnolipid and (b) Dirhamnolipid

As rhamnolipids have two hydrophobic chains so it is assumed that one molecule of rhamnolipid gets attached to two nanoparticles. This will be considered as one entity in further calculations.

The total number of carbon atoms in one entity = 65.6 carbon atoms (as the standard obtained is a mixture of monorhamnolipid (40%) and dirhamnolipid (60%))

Density of IONPs as magnetite = 5 g/cm^3

The total volume of particles in V liter of suspension = $6.16*10^{-2}$ V cm^3

Assuming the diameter of 9 nm,

Number of IONPs in suspension = 1.51 *10^{17} V

Concentration of entities in the suspension= 73.32/ (65.6*12*1000) = 9.31 * 10^{-5} M

Moles of entities in suspension of Volume V = 9.31 * 10^{-5} mol/ liter* V (liters)= 9.31 * 10^{-5} * V moles

1 mole contains 6.022 * 10^{23} entities, thus total number of entities in suspension = 56.06 x 10^{18} V

Number of entities attached per nanoparticle = 371.2 entities per nanoparticle or 185.6 rhamnolipids per nanoparticle (as 1 rhamnolipid molecule gets attached to two oleic acid molecules)

Site density estimated per surface area of magnetite nanoparticle = 0.73 sites/nm^2

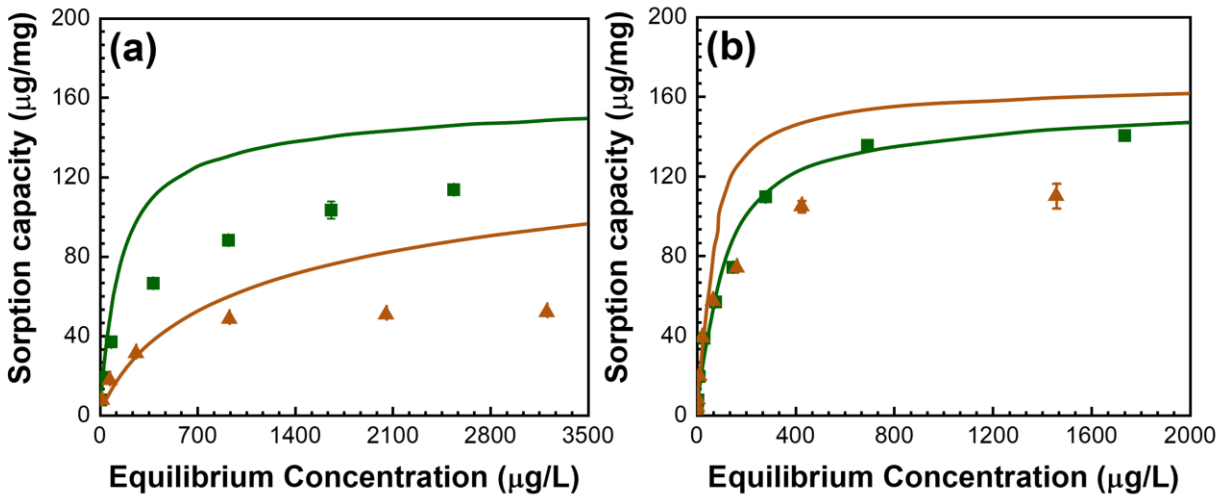

Figure A-4: Fitting SCM obtained parameters to isotherm obtained for NEM model in (a) Open to atmosphere system and (b) Carbonate-free system. ▲ represent points obtained at pH =8 and ■ represent points obtained at pH=6. Solid lines are the fitting lines obtained using NEM at pH 6 and pH 8.

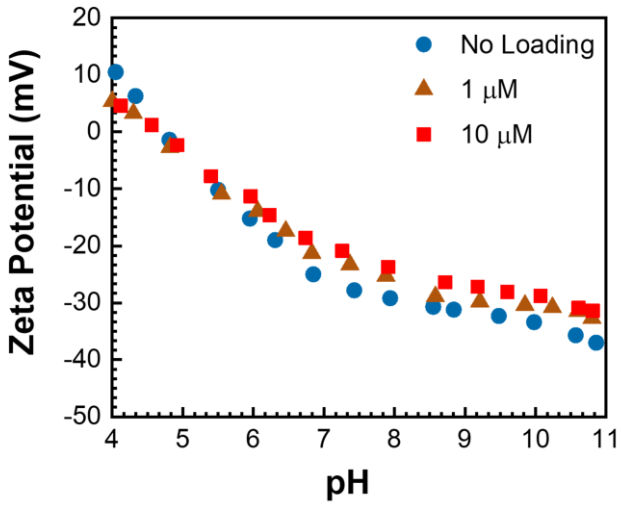

Figure A-5: Effect of uranium loading on zeta potential of rhamnolipid-coated nanoparticles

Appendix B. Supporting Materials for Chapter 3

Table B-1: Composition of simulated site water used for metal uptake study

Parameter	Marsh Wetlands	Stream Sediments	Riparian Wetlands
pH	7	7.6	5
Ionic Strength	1.65 mM	6.96 mM	0.34 mM
	Concentration (µM)		
Na^{+}	170	446	60
K^{+}	165	71	5.3
Ca^{2+}	367	1091	25
Mg^{2+}	288	389	27
Cl-	491	2690	155
SO_4^{2-}	576	256	7.6
NO_3^{-}	8	71	N.A
NH_4^{+}	N.A	0.2	N.A
PO_4^{3-}	N.A	4	N.A

* PO_4^{3-} represents the total inorganic phosphate in the water.[1]For riparian wetland sites, studies at pH 5 were also conducted. BDLindicates below detection limit. N.A indicates that the species was not present in the water samples collected from the natural aquatic systems

B.1 Sampling of Soils and Sediments

Soil and sediment cores were collected using polycarbonate tubes and were transported on ice to Washington University in St. Louis. Soil cores from marsh wetlands and riparian wetlands were extruded and divided into upper and lower sections in an anaerobic chamber (Coy Laboratory Products, 3% H_2/97% N_2 with Pd catalysts). Sediment cores from EFPC were extruded on the benchtop and immediately put in the anaerobic chamber. The soils and sediment sections were stored in an anaerobic chamber until further use to maintain an oxygen-free environment. Water samples were also collected and acidified to determine the concentration of metals at the sites. Field blanks were collected to monitor for any contamination during sampling.

B.2 Microwave Digestion of Samples

The detailed procedure used for digestion can be found in our recent study.[113] The digested samples were filtered using 0.22 µm mixed cellulose ester (MCE) filters followed by dilution to ~1% HNO_3 for dissolved metal analysis using ICP-MS. This method was able to extract almost all the trace metals present in the studied soils.[114] The efficacy of the soil digestion procedure for determining total metal contents was assessed by applying it to duplicate samples of reference materials (Montana II Soil / Standard Reference Material 2711a and Green River shale/SGR-1b) with known compositions.

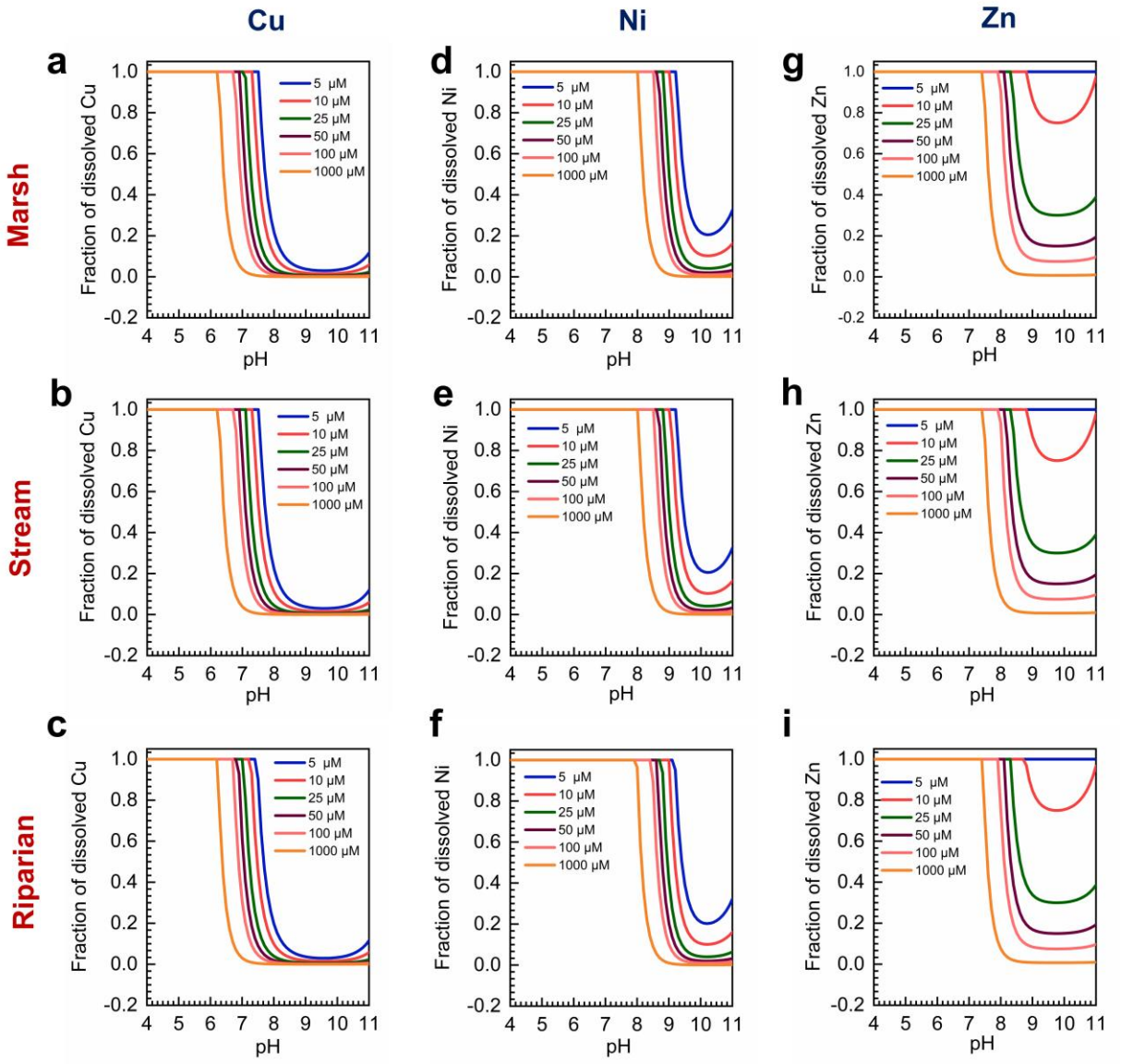

Figure B-1: Calculated equilibrium solubility for (a-c) Cu (d-f) Ni and (g-i) Zn in simulated water of marsh wetlands, stream sediments, and riparian wetlands. The solids considered for Zn include $Zn(OH)_2$, $ZnCl_2$ and $ZnSO_4$; for Cu include $CuCl_2$, $CuSO_4$ and $Cu(OH)_2$ and for Ni only $Ni(OH)_2$ is included. The fraction of dissolved metal signifies the amount remaining in the solution at equilibrium for the different total metal concentrations indicated.

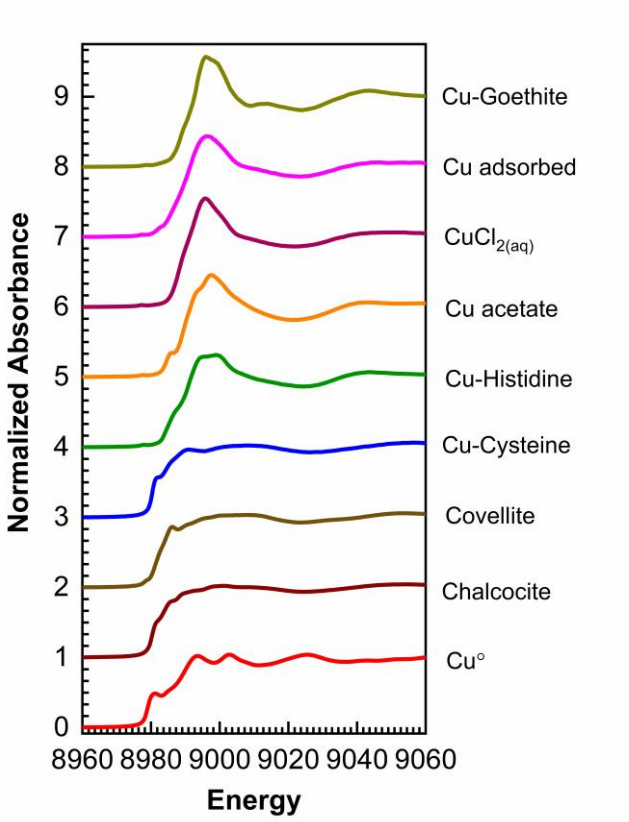

Figure B-2: Cu Standards used for XANES analysis for estimating the speciation of added metals onto the soils. Chalcocite (Cu_2S) was purchased from Alfa Aesar; Covellite (CuS) was purchased from Fisher Scientific; $CuCl_2$ was purchased from Sigma Aldrich; Cu(II)-Histidine, Cu(II)-Cysteine and Cu(II) adsorbed to Goethite were synthesized and Cu metal spectra was obtained from Exafs materials database.

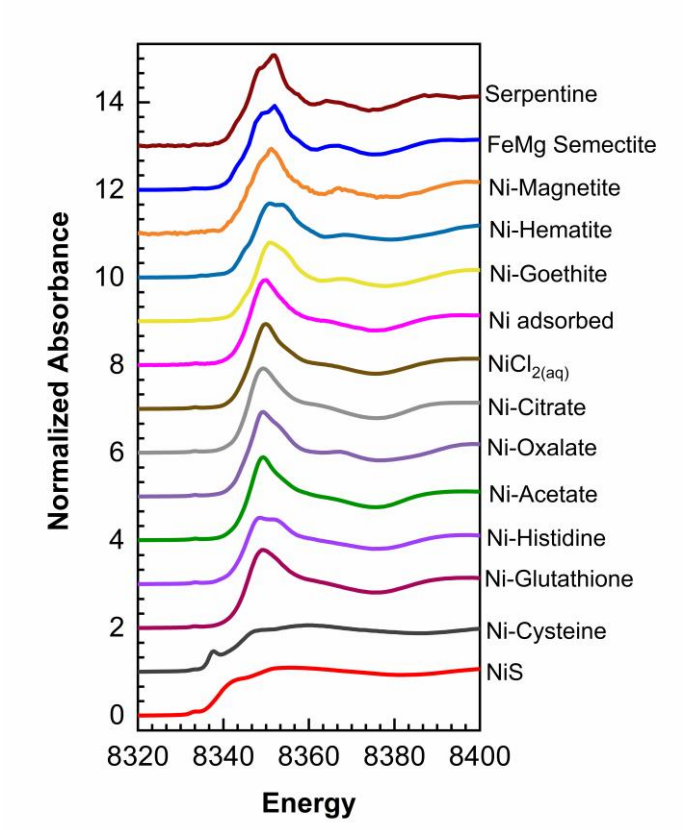

Figure B-3: Ni Standards used for XANES analysis for estimating the speciation of added metals onto the soils. Ni(II) Histidine, Ni(II) Cysteine, Ni(II) Glutathione complexes and Ni-substituted Magnetite were synthesized; Ni-substituted Serpentine and Ni adsorbed to Goethite were synthesized; $NiCl_2$ was purchased from Sigma Aldrich; Ni(II) Sulfide was purchased from Alfa Aesar and Ni(II) Acetate was purchased from Acros Organics.

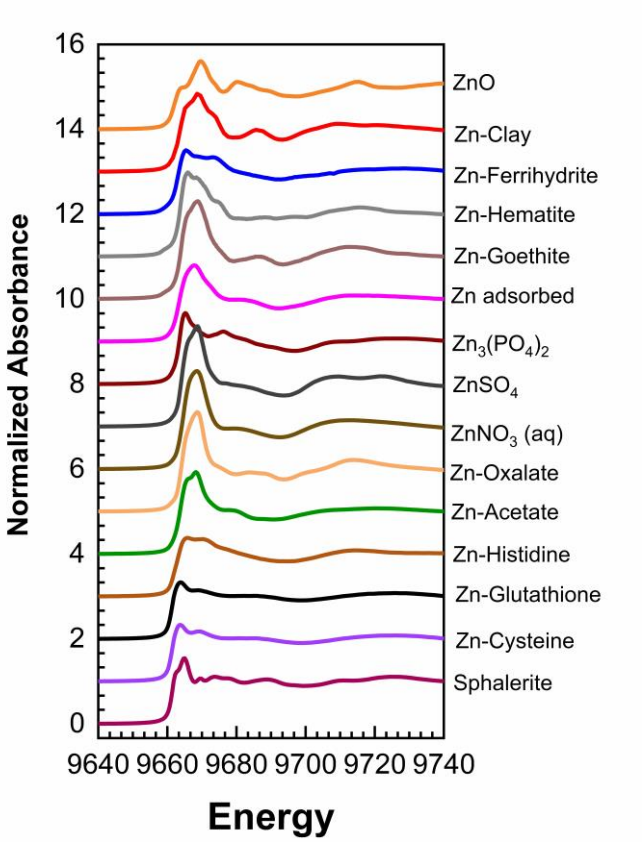

Figure B-4: Zn Standards used for XANES analysis for estimating the speciation of added metals onto the soils. Zn(II)-Glutathione, Zn(II)-Histidine, Zn(II)-Cysteine and Zn adsorbed to goethite were synthesized; Zn(II) Sulfate and $Zn(NO_3)_2$ salt were purchased from J.T. Baker; Zinc(II) Oxide and Sphalerite spectra was obtained from Luo et al[352]; Zn(II) Acetate and Zn(II) Phosphate were purchased from Fisher Scientific and Zn-Ferrihydrite and Zn-Clay- Source were synthesized.

Table B-2: Categories used for XANES analysis for Cu

Category	Standards included
CuS	Covellite
Cu_2S	Chalcocite
Amine bound	Cu-Histidine
Thiol bound	Cu-Cysteine
Adsorbed	Cu adsorbed to goethite and $CuCl_{2(aq)}$
Cu°	Cu foil

Table B-3: Categories used for XANES analysis for Ni

Category	Standards included
NiS	NiS
Amine bound	Ni-Histidine
Thiol bound	Cu-Cysteine
Adsorbed	Ni adsorbed to goethite, Ni-Acetate, and $NiCl_{2(aq)}$
Clay structures	FeMg Smectite and Serpentine

Table B-4: Categories used for XANES analysis for Zn

Category	Standards included
ZnS	Sphalerite
Thiol bound	Zn-Cysteine and Zn-Glutathione
ZnO	Zinc Oxide
Adsorbed	Zn adsorbed to goethite, $ZnSO_4$, $Zn_3(PO_4)_3$, $Zn(NO_3)_{2(aq)}$, Zn-Ferrihydrite, and Zn-Acetate
Clay structures	Zn-Clay

Table B-5: Properties of soils and sediments from different sites

Parameter	Marsh 1	Marsh 2	Stream 1	Stream 2	Riparian 1	Riparian 2
Cu (nmol/g)	730	400	150	80	30	200
Ni (nmol/g)	420	280	300	160	40	110
Zn (nmol/g)	2100	1700	600	300	100	300
Organic carbon (%)	11	9.8	0.4	1.8	1.4	4.0
Specific surface area (m^2/g)	8.2	6.2	7.9	22.0	2.2	6.8
Iron content (mg/g)	23	24	20	35	3	26
Sulfur content (mg/g)	2.6	3.1	1.7	0.8	0.9	1.7

B.3 Previous Characterization of Soils and Sediments

Mineral Composition

The mineralogy of all the samples was dominated by quartz, and some differences in minor phases were observed.[113] Smectite, illite, kaolinite and plagioclase feldspar were the minor phases detected in the soils of Marsh 1, and the stream sediments contained K-feldspar, chlorite, smectite, kaolinite, and illite as minor phases. The Riparian 2 wetland soils had minor K-feldspar, kaolinite, chlorite, and gibbsite, and trace illite; however, only trace amounts of kaolinite, chlorite, and gibbsite were detected in Riparian 1 wetland soils.[113]

Water Sample Characterization

Detailed information on the pH, temperature, conductivity, and element concentrations in the water samples from the selected sites can be found in our earlier study.[113] The pH at marsh wetland sites and stream sediment sites ranged between 7.5-8.1, whereas the pH at riparian wetland sites was lower (~5.0). The dissolved Cu concentration in water samples ranged from 20-80 nM with no distinct trend among the different sites.[113] The dissolved concentration of Ni in the water samples collected from marsh wetlands, stream sediments and Riparian 2 lie in the range of 30-60 nM, and Riparian 1 samples contained less dissolved Ni (~12 nM).[113] The dissolved Zn concentrations were higher than Cu and Ni and varied in the range of 46 - 230 nM.

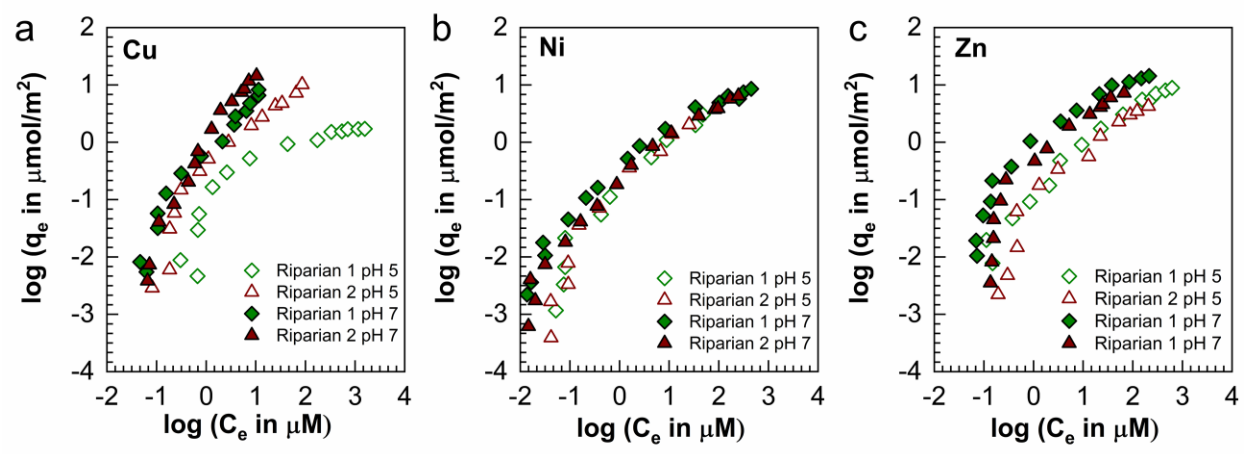

Figure B-5: Effect of difference in pH between 5 and 7 on uptake of (a) Cu, (b) Ni, and (c) Zn on riparian wetland soils.

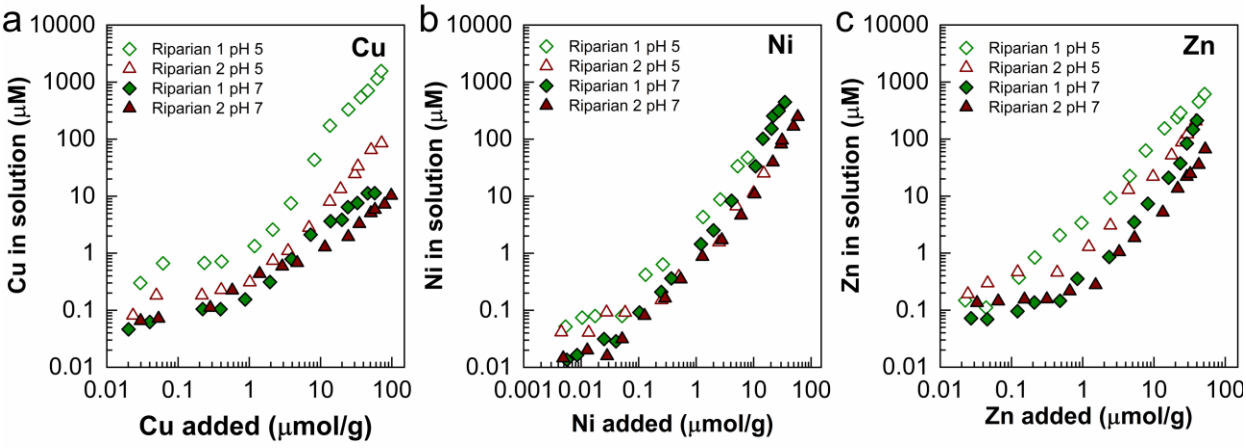

Figure B-6: Concentration of (a) Cu (b) Ni and (c) Zn remaining in the supernatant at the end of uptake experiment in riparian wetland soils at pH 5 and 7.

Table B-6: K_D values at low and high loading for trace metal uptake at different sites

Site	K_D (L/m^2)					
	Cu		Ni		Zn	
	1 µmol/g	10 µmol/g	1 µmol/g	10 µmol/g	1 µmol/g	10 µmol/g
Stream 1	13.5	20.6	0.36	0.1	3.57	1.29
Stream 2	5.06	8.38	0.08	0.01	0.61	0.15
Marsh 1	0.20	0.28	0.14	0.08	0.18	0.11
Marsh 2	0.31	0.57	0.21	0.12	1.16	0.26
Riparian 1	2.53	1.5	0.36	0.12	0.38	0.49
Riparian 2	0.46	1.32	0.25	0.13	0.8	0.37

To account for SSA in determining K_D $\left(\frac{\text{solid-phase concentration}}{\text{solute concentration}}\right)$, the solid phase concentrations were calculated in terms of µmol/m^2 and solute concentration in µmol/L.

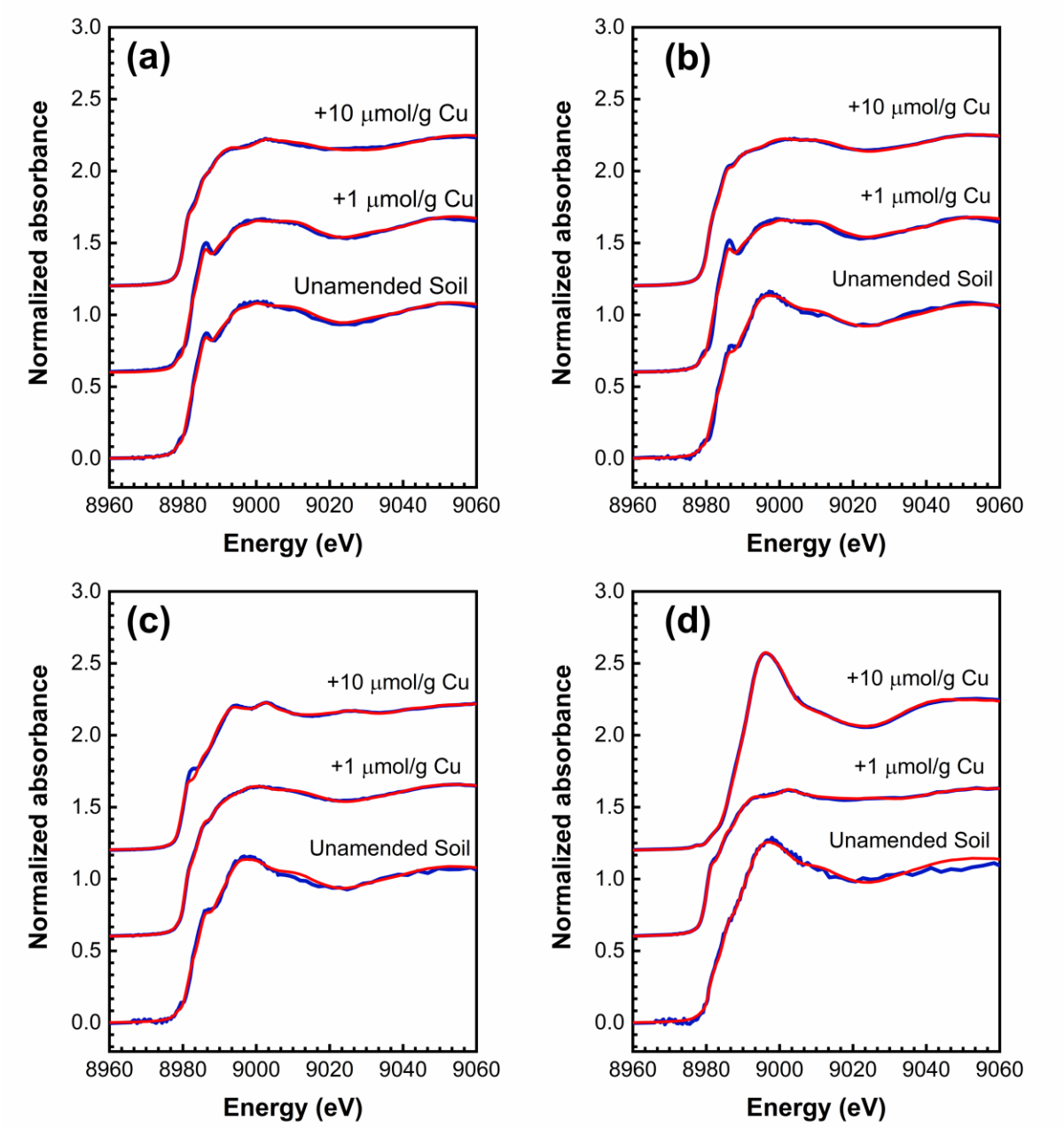

Figure B-7: Spectra obtained using XAS along with fitting results (data in blue and fit in red) for Cu in (a) Marsh 1 (b) Stream 1 (c) Riparian 2 and (d) Riparian 1

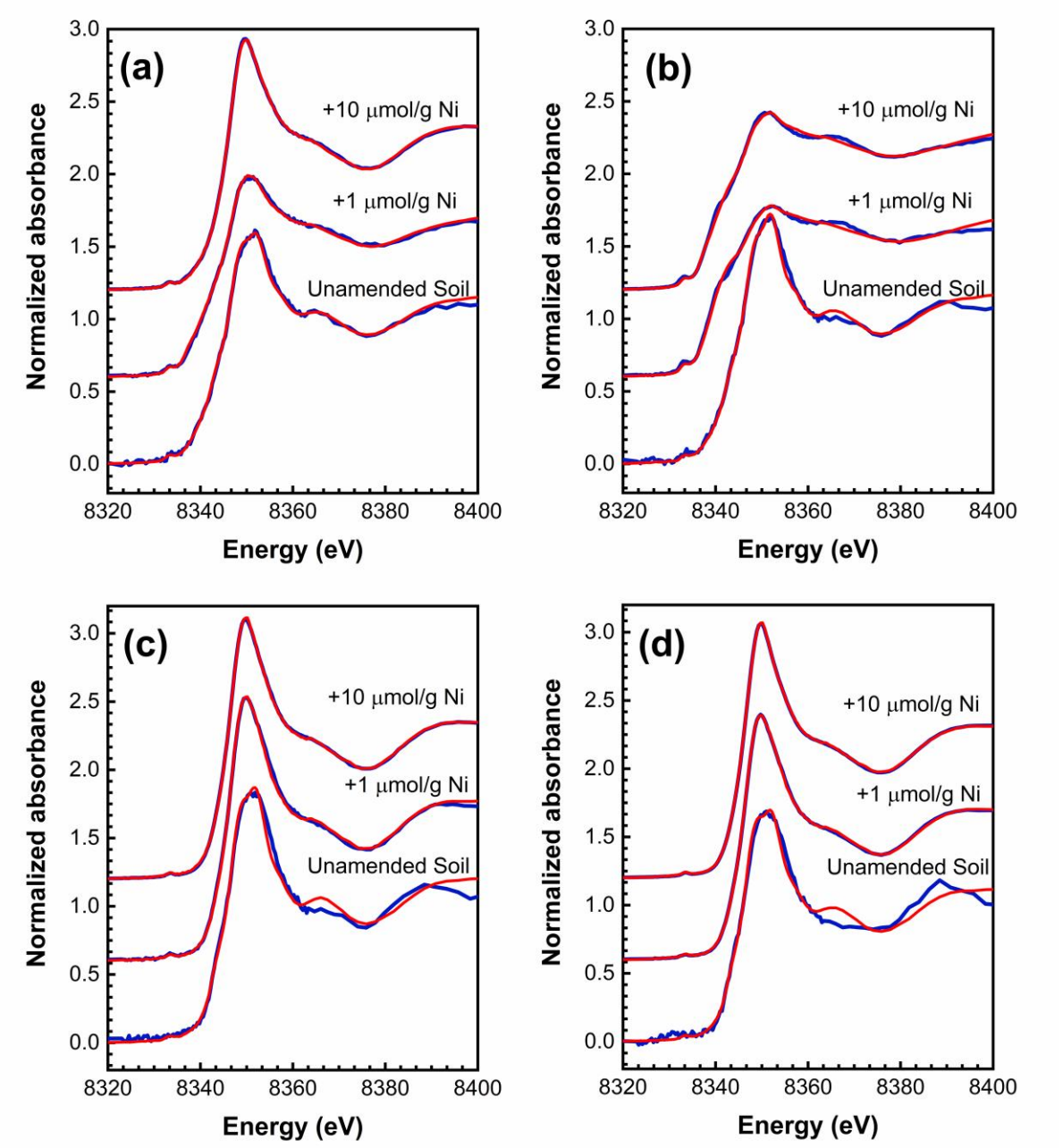

Figure B-8: Spectra obtained using XAS along with fitting results (data in blue and fit in red) for Ni (a) Marsh 1 (b) Stream 1 (c) Riparian 2 and (d) Riparian 1

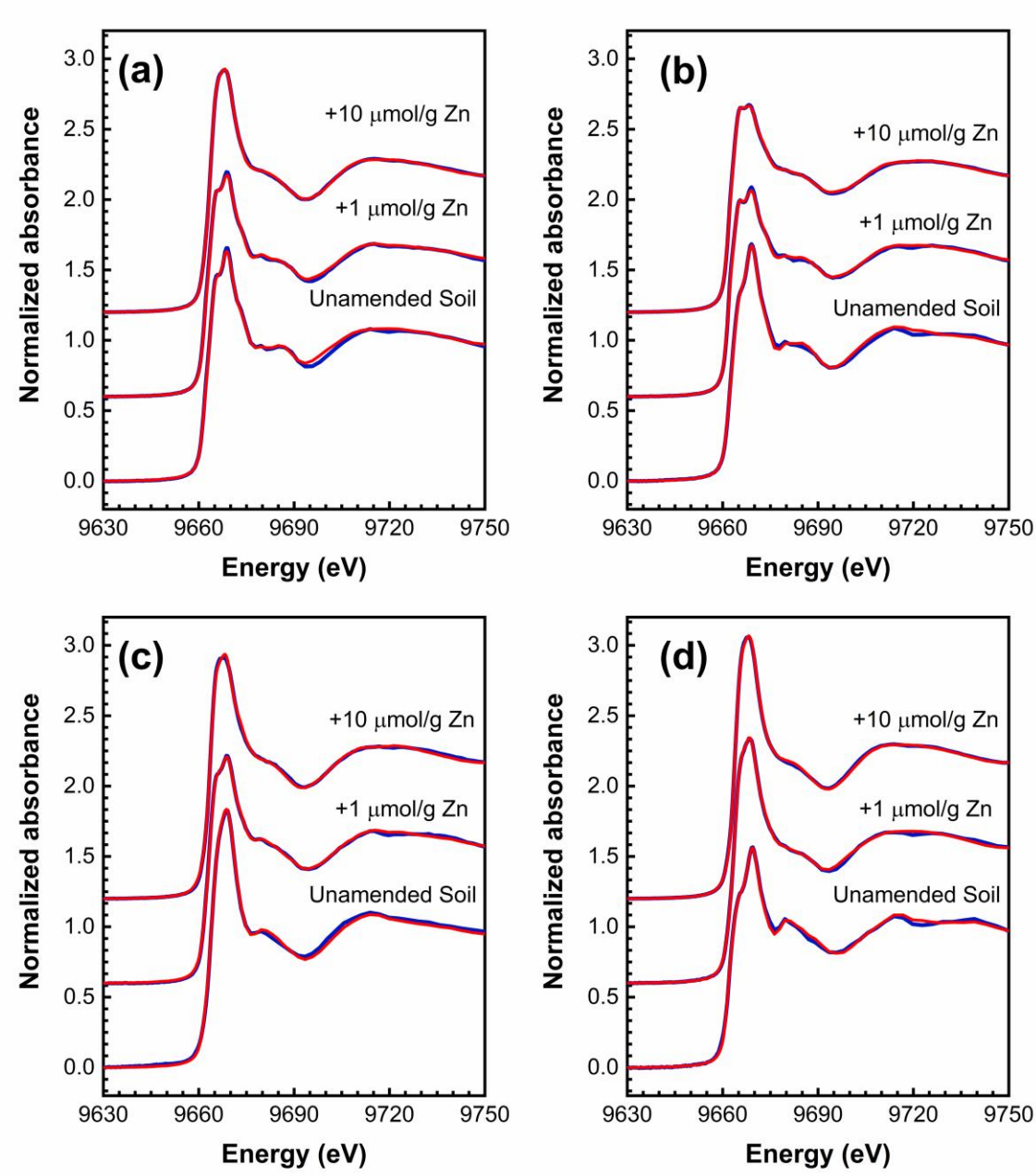

Figure B-9: Spectra obtained using XAS along with fitting results for Zn (data in blue and fit in red) in (a) Marsh 1 (b) Stream 1 (c) Riparian 2 and (d) Riparian 1

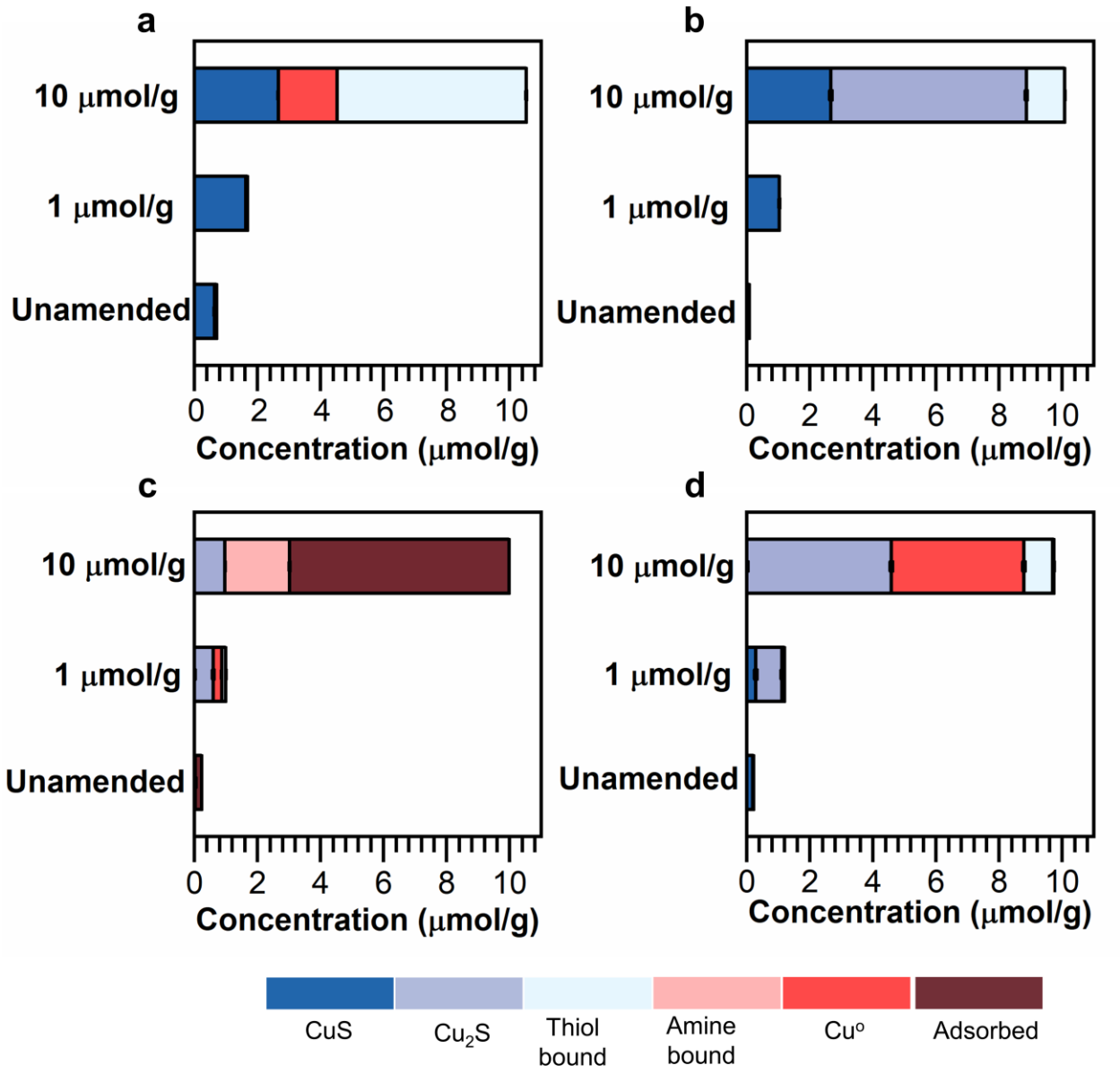

Figure B-10: Total amounts of metals in unamended soils and sediments and after uptake for Cu for the Marsh 1 marsh wetland soils (a), Stream 1 stream sediments (b), Riparian 1 soils (c), and Riparian 2 soils (d). Total amounts in each category of species are calculated from measured total amounts of metals in the soils/sediments and fractions in each category determined from fitting of XANES spectra.

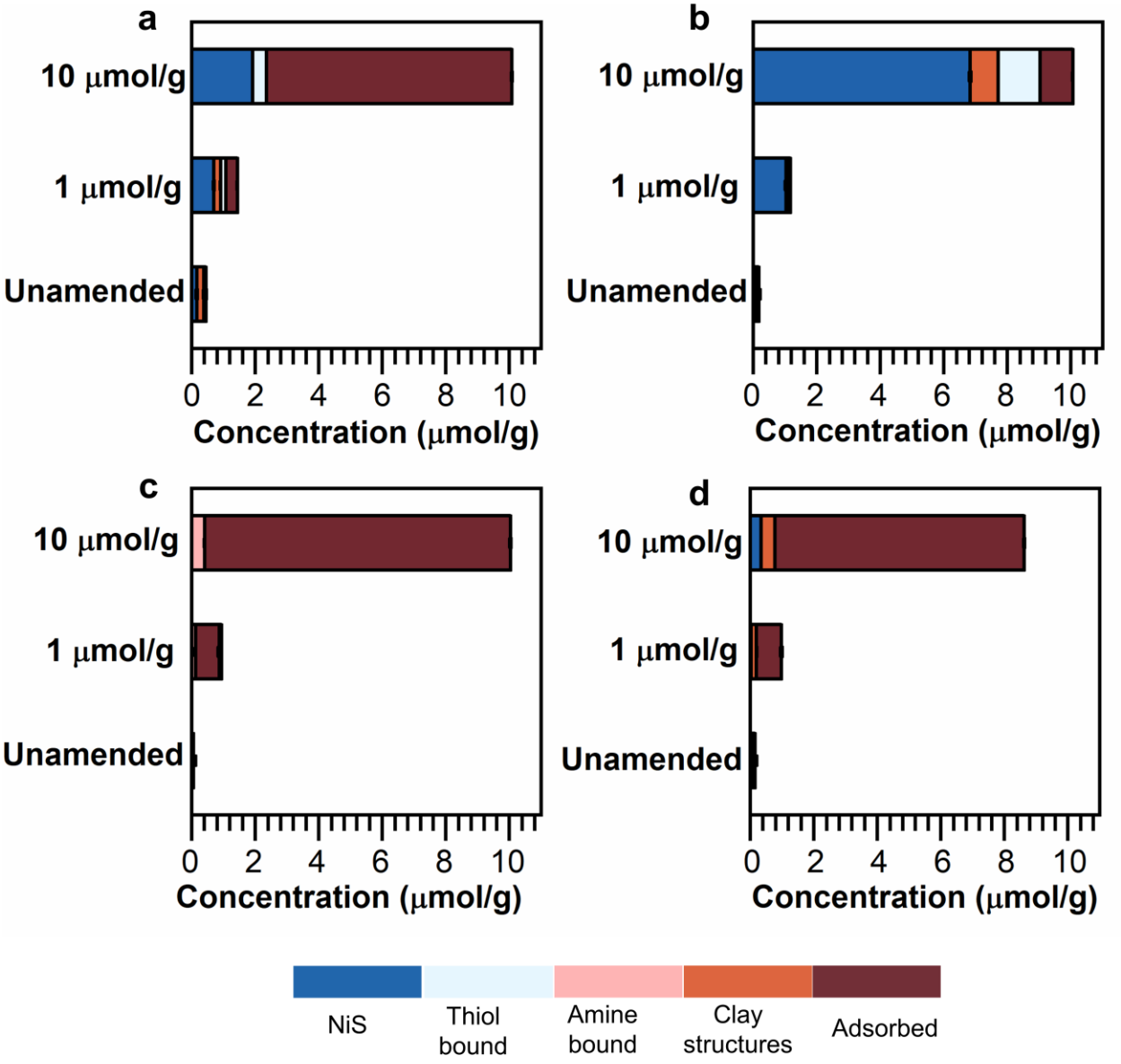

Figure B-11: Total amounts of metals in unamended soils and sediments and after uptake for Ni for the Marsh 1 marsh wetland soils (a), Stream 1 stream sediments (b), Riparian 1 soils (c), and Riparian 2 soils (d). Total amounts in each category of species are calculated from measured total amounts of metals in the soils/sediments and fractions in each category determined from fitting of XANES spectra.

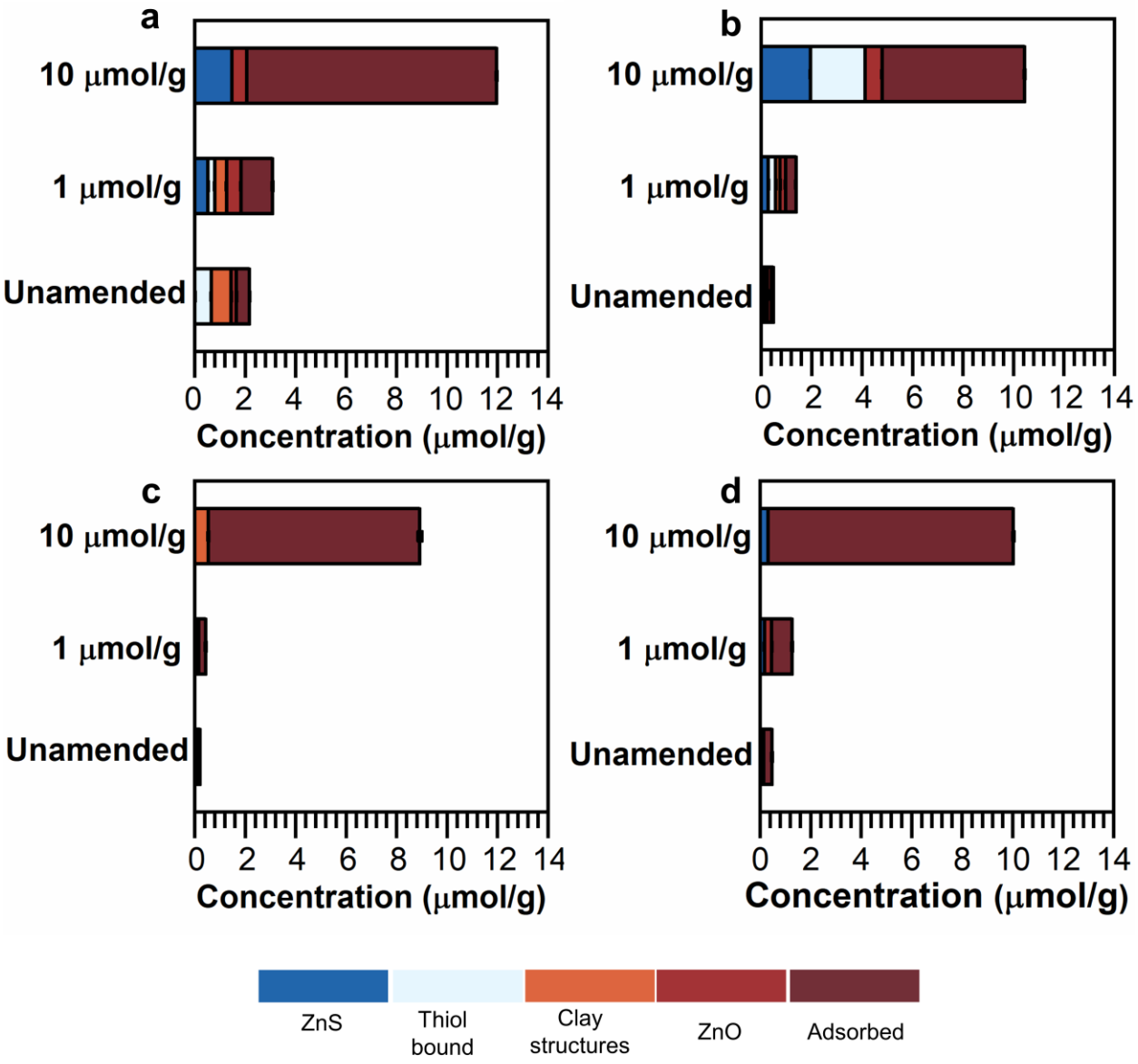

Figure B-12: Total amounts of metals in unamended soils and sediments and after uptake for Zn for the Marsh 1 marsh wetland soils (a), Stream 1 stream sediments (b), Riparian 1 soils (c), and Riparian 2 soils (d). Total amounts in each category of species are calculated from measured total amounts of metals in the soils/sediments and fractions in each category determined from fitting of XANES spectra.

B.4 Presence of ZnO Component in Soils and Sediments

We observed a significant fraction of zinc oxide (10 to 54%) in nearly all the samples after Zn uptake as well as in all the unamended samples (Figure 3.4). Prior studies indicate that ZnO formed in oxic soil cores does not persist under anoxic conditions and dissolves and transforms to other phases.[132,353–355] These considerations suggest that ZnO in our samples may be due to contamination during sampling or X-ray data collection**.** ZnO introduced during field sampling is unlikely to have persisted under anoxic storage conditions. Thus, the ZnO component in our XANES results is likely due to beamline components, such as cellulose acetate tape.[113] Notably, the ZnO contribution generally decreases in relative proportion as total zinc content increases following uptake. This suggests that an approximately fixed ZnO content is present in all samples and is diluted by added zinc, consistent with this being an artifact and not an actual species in the samples.

Table B-7: Dominant solid phase speciation of trace metals at the selected sites

	Condition	Marsh 1	Stream 1	Riparian 1	Riparian 2
Cu	Unamended	CuS	CuS	CuS	CuS, Cu_2S & adsorbed
	1 µmol/g	CuS	CuS	Cu_2S	CuS
	10 µmol/g	CuS, thiol bound, and Cu(0)	CuS and Cu_2S	Amine bound and adsorbed	CuS & Cu(0)
Ni	Unamended	Clay structures	Clay structures	Clay structures	Clay structures
	1 µmol/g	NiS and adsorbed	NiS	Adsorbed	Adsorbed
	10 µmol/g	NiS and adsorbed	NiS and thiol bound	Adsorbed	Adsorbed
Zn	Unamended	Clay structures, thiol bound, and adsorbed	Clay structures and thiol bound	ZnS	Adsorbed
	1 µmol/g	ZnS and adsorbed	ZnS and adsorbed	Adsorbed	Adsorbed
	10 µmol/g	ZnS and adsorbed	Thiol bound, ZnS and adsorbed	Adsorbed	Adsorbed

Appendix C. Supporting Materials for

Chapter 4

Table C-1: Concentration of major elements and species in the simulated site water used for uptake studies and microcosm experiments

Parameter	ANL	ORNL	TB
pH	7.0	7.6	5.0
Ionic Strength	1.7 mM	7.0 mM	0.30 mM
	Concentration (µM)		
Na^+	170	450	60
K^+	170	71	5.3
Ca^{2+}	370	1100	25
Mg^{2+}	290	390	27
Cl-	490	2700	160
SO_4^{2-}	580	260	7.6
NO_3^-	8	70	0
NH_4^+	0	0.2	0
PO_4^{3-}	0	4	0

Table C-2: Characterization of soils and sediments collected from different aquatic systems

Site	Cu (nmol/g)	Mn (nmol/g)	Fe (µmol/g)	C (%)	S (%)	NH_4^+ (µmol/g)	NO_2^- (µmol/g)	NO_3^- (µmol /g)
Riparian 1	48	220	47	1.3	0.02	1.1	BDL	0.14
Riparian 2	260	701	460	6.0	0.09	2.7	BDL	0.00
Stream 1	160	3200	204	3.0	0.10	2.7	BDL	0.14
Stream 2	98	5600	420	0.46	0.02	2.8	BDL	0.43
Marsh 1	280	1960	420	9.0	0.24	21	BDL	0.36

Here, nutrients represent the extractable values from soils and sediments. Total Cu, Mn, and Fe concentrations present in soils and sediments were obtained using microwave-assisted digestion technique. Carbon and sulfur percent were estimated using CHNS analyzer. The detection limit of NO_2^- is 0.02 µmol/g.

C.1 Dissolved Cu Speciation in Microcosms

Two different binding sites are considered in the NICA model, type 1 and type 2, corresponding to carboxylic (low affinity) and phenolic (high affinity) sites respectively [197].

$$Q_i = \frac{n_{i,1}}{n_{H,1}} Q_{\max 1,H} \frac{(\acute{K}_{i,1} c_i)^{n_{i,1}}}{\sum(\acute{K}_{i,1} c_i)^{n_{i,1}}} \frac{\left[\sum(\acute{K}_{i,1} c_i)^{n_{i,1}}\right]^{p_1}}{1+\left[\sum(\acute{K}_{i,1} c_i)^{n_{i,1}}\right]^{p_1}} + \frac{n_{i,2}}{n_{H,2}} Q_{\max 1,H} \frac{(\acute{K}_{i,2} c_i)^{n_{i,2}}}{\sum(\acute{K}_{i,2} c_i)^{n_{i,2}}} \frac{\left[\sum(\acute{K}_{i,1} c_i)^{n_{i,2}}\right]^{p_2}}{1+\left[\sum(\acute{K}_{i,1} c_i)^{n_{i,2}}\right]^{p_2}}$$

Eq S1

where, c_i (mol. L^{-1}) is the concentration of metal; Q_i is the amount of bound ion described by two identical binding expressions, one each for the carboxylic- (1) and phenolic-type (2) site distributions. $Q_{max1,H}$ and $Q_{max2,H}$ are the maximum proton binding capacity of humic substances within each distribution (mol kg^{-1}); p_1 and p_2 account for intrinsic heterogeneity of humic substances; $\acute{K}_{i,1}$ and $\acute{K}_{i,2}$ are median values for affinity distributions for ion, and $n_{i,1}$ and $n_{i,2}$ are used to describe the nonidealities of the ion-binding to each distribution. The ratios $\frac{n_{i,j}}{n_{H,j}}$ with j = 1 or 2 reflect the average stoichiometry of ion binding.

The charge on humic substances is neutralized by the nonspecific binding of counter-ions and exclusion of co-ions within the Donnan volume, V_D ($L \cdot kg^{-1}$), as described by the empirical relationship.

$$logV_D = b(1 - logI) - 1 \qquad \text{Eq S2}$$

Here, I is ionic strength and b is an empirical parameter describing the variation of Donnan volume with ionic strength [198]. The values of parameters used in estimating Cu speciation are listed in Table S3.

Humic substances are normally assumed to be the main binding substances [171], and their concentrations were determined from the dissolved organic carbon (DOC) concentrations. Humic substances account for 60% of DOC in natural water systems [350,356], and they comprise 50% carbon, so concentration of HS was assumed to be 1.2 times the DOC concentration. The pH, temperature, total dissolved elements (Na, Mg, K, Ca, Cl, NO_3, SO_4, and PO_4) (Table EA1), and dissolved Cu, Fe, and Mn were used as the input parameters for determining Cu speciation.

Table S3: Parameters used in NICA-Donnan model for determining Cu speciation in the presence of DOC[203]

Parameter	Value
b	0.57
$Q_{\max 1,H}$	5.88
p_1	0.59
$log\acute{k}_{H,1}$	2.34
$n_{H,1}$	0.66
$log\acute{k}_{Cu,1}$	0.26
$n_{Cu,1}$	0.53
$Q_{\max 2,H}$	1.86
p_2	0.70
$log\acute{k}_{H,2}$	8.60
$n_{H,2}$	0.76
$log\acute{k}_{Cu,2}$	8.26
$n_{Cu,2}$	0.36

C.2 Estimation of Organic Carbon Requirements for Complete Reduction of Nitrate

$$\mathbf{CH_2O + H_2O \rightarrow CO_2 + 4e^- + 4H^+} \qquad \text{Eq S3}$$

$$\mathbf{NO_3^- + 5e^- + 6H^+ \rightarrow \frac{1}{2} N_2 + 3H_2O} \qquad \text{Eq S4}$$

$$\mathbf{5CH_2O + 4H^+ + 4NO_3^- \rightarrow 5CO_2 + 2N_2 + 7H_2O} \qquad \text{Eq S5}$$

Total nitrate available=0.05 mmol

Total organic carbon (OC) requirement = 0.0625 mmol

Table C-3: Organic carbon required for complete nitrate reduction

Site	Organic Carbon (%)	Total organic carbon (mmol)	$\frac{TOC}{OC_{required}}$
Riparian 2	6.0	13	208
Riparian 1	1.3	2.7	43
Stream 1	3.1	6.3	101
Stream 2	0.46	0.77	12
Marsh 1	9.0	19	304

*Here, total organic carbon represents the total amount of organic carbon present in the solid phase (2.5 g of soil/sediment) used for incubation experiments.

Table C-4: Estimated labile concentrations of Cu in the microcosms using NICA-Donnan model

Site	Estimated labile concentration (nM)*		
	Control	Low Cu	High Cu
Riparian 1	2.8 ± 0.9	150 ± 20	1200 ± 80
Riparian 2	1.4 ± 0.8	8.9 ± 3	350 ± 60
Stream 1	0.55 ± 0.3	7.2 ± 2	28 ± 4
Stream 2	4.8 ± 0.9	38 ± 3	560 ± 4
Marsh 1	7.6 ± 5	35 ± 30	150 ± 100

*Labile Cu concentration is the sum of Cu, $CuOH^+$, and $Cu(OH)_2$. The values represent the average of the labile concentrations between the pH range studied. pH varied between 5-6 in wetland soils; 7.6-8.6 in stream sediments, and 7-8 in marsh wetland soils.

C.3 Estimation of Nitrate Requirements for Abiotic Reaction with Fe(II)

$$NO_3^- + 5Fe^{2+} + 12H_2O \rightarrow \frac{1}{2}N_{2(g)} + 5Fe(OH)_3 + 9H^+$$

Riparian 1:

Decrease in Fe : 7.1 µmol

NO_3^- required: 1.4 µmol

Riparian 2:

Decrease in Fe concentration: 72 µmol

NO_3^- required: 14 µmol

Stream 1:

Decrease in Fe concentration: 0.084 µmol

NO_3^- required: 0.017 µmol

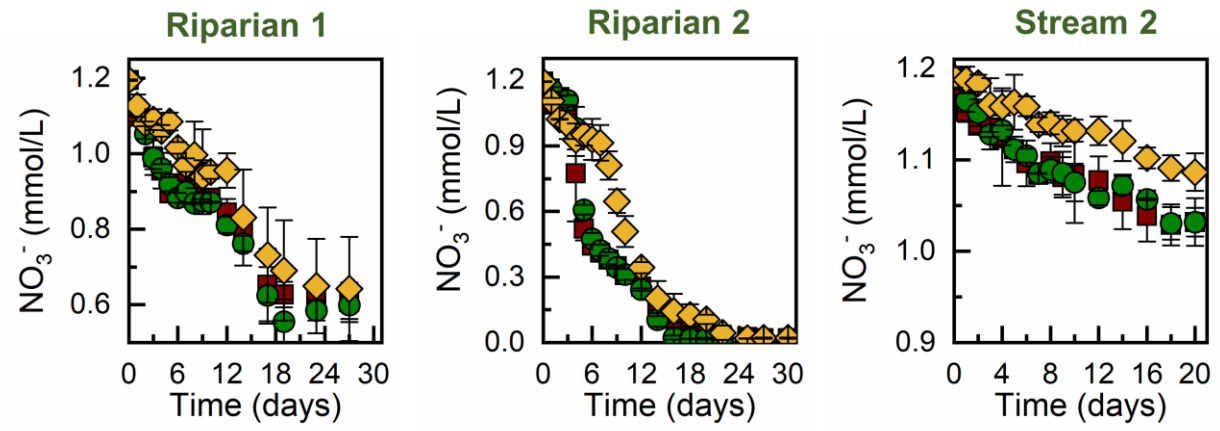

Figure C-1: Variation in the concentration of NO_3^- during incubation period at different sites studied. The scale on the plots is selected to show changes in in NO_3^- for the earliest reaction times.

C.4 One-way Analysis of Variance (ANOVA) on Michaelis-Menten Parameters

One-way ANOVA was used to determine whether there are any significant differences between the means of Michaelis-Menten parameters obtained for control, low Cu loading and high Cu loading for different natural aquatic systems. The data were transformed by taking the logarithm of the values to make them normally distributed. The transformed data satisfied the assumption of homogeneity of variances i.e. the population variances in each group were equal.

Null Hypothesis: $\mu_{control} = \mu_{low\ Cu} = \mu_{high\ Cu}$

Alternate Hypothesis: $\mu_{control} \neq \mu_{low\ Cu} \neq \mu_{high\ Cu}$

Case 1: For $K_{NO_3^-}$ (mmol L^{-1})

	Control	Low	High
Riparian 1	1.08	1.04	1.18
Riparian 2	0.04	0.04	0.23
Stream 1	-0.41	-0.39	-0.31
Stream 2	1.59	1.60	1.85
Marsh 1	-0.33	-0.26	-0.42

Summary for One-Way ANOVA

Source of	*SS*	*df*	*MS*	*F*	*P-value*	*F crit*
Between Groups	0.036	2	0.018	0.022	0.97	3.88
Within Groups	10.09	12	0.84			
Total	10.12	14				

For 95% confidence interval, $F < F_{crit}$ and $p > 0.05$. Hence, there is not enough evidence to reject the null hypothesis. Hence, there is not enough evidence to suggest that Cu addition altered NO_3^- reduction in all the systems studied.

Case 2: For $K_{NO_2^-}$ (mmol L^{-1})

	Control	Low	High
Riparian 1	-1.14	-1.14	-1.17
Riparian 2	-0.17	-0.66	-0.48
Stream 1	0.96	0.99	0.98
Stream 2	-1.10	-2.17	-2.46
Marsh 1	-1.24	-1.17	-1.33

Summary for One-Way ANOVA (mmol L^{-1})

Source of	*SS*	*df*	*MS*	*F*	*P-value*	*F crit*
Between Groups	0.35	2	0.17	0.14	0.87	3.88
Within Groups	15	12	1.3			
Total	15	14				

For 95% confidence interval, $F < F_{crit}$ and $p > 0.05$. Hence, there is not enough evidence to reject the null hypothesis. Hence, there is not enough evidence to suggest that Cu addition altered NO_2^- reduction in all the systems studied.

Case 3: For k_{ab} (mmol L^{-1})

	Control	Low	High
Riparian 1	2.00	2.00	1.99
Riparian 2	0.34	0.34	0.34
Stream 1	-0.16	-0.15	-0.19
Stream 2	-1.82	-1.82	-1.82
Marsh 1	-3.62	-3.57	-3.54

Summary for One-Way ANOVA

Source of	*SS*	*df*	*MS*	*F*	*P-value*	*F crit*
Between Groups	0.00042	2	0.0002	4.71E-	0.99	3.88
Within Groups	54	12	4.53			
Total	54	14				

For 95% confidence interval, $F < F_{crit}$ and $p > 0.05$. Hence, there is not enough evidence to reject the null hypothesis. Hence, there is not enough evidence to suggest that Cu addition altered abiotic reduction of NO_2^- to N_2 in all the systems studied.

Case 4: For K_{N_2O} (mmol L^{-1})

	Control	Low	High
Riparian 1	3.84	1.38	0.54
Riparian 2	4.04	-0.32	-0.68
Stream 1	0.57	-0.14	-3.11
Stream 2	-2.07	-2.62	-2.49
Marsh 1	-0.85	-1.43	-1.74

Summary for One-Way ANOVA

Source of Variation	*SS*	*df*	*MS*	*F*	*P-value*	*F crit*
Between Groups	17.5	2	8.7	2.2	0.15	3.8
Within Groups	47	12	3.9			
Total	65	14				

For 95% confidence interval, $F < F_{crit}$ and $p > 0.05$. Hence, there is not enough evidence to reject null hypothesis. As indicated in the ANOVA table, the variation within the groups is greater than the variation between groups. The natural systems evaluated varied substantially in terms of mineralogy, total trace metal concentrations, initial pH concentrations, organic matter, and sulfur contents. Hence, we think that it will be inappropriate to conduct ANOVA on all the systems together, because of their inherent variability.

Appendix D. Supporting Materials for

Chapter 5

Table D-1: Details of different redox conditions and time intervals considered under each cycle of redox fluctuation

Condition	Time (in days)
Anoxic	6
Anoxic-Oxic	8 (6+2)
Anoxic-Oxic- Anoxic	14 (6+2+6)
Anoxic-Oxic-Anoxic-Oxic	16 (6+2+6+2)
Anoxic-Oxic-Anoxic-Oxic-Anoxic	22 (6+2+6+2+6)
Anoxic-Oxic-Anoxic-Oxic-Anoxic-Oxic	24 (6+2+6+2+6+2)

D.1 Estimation of Labile Concentration of Metals using DGTs

The resin gel strongly binds metal species, and the flux of the metals (F in mol/m^2-s) towards the resin gel is calculated using Fick's law of diffusion (equation 1), where D is the diffusion coefficient (m^2/s) of the labile trace metal species in the diffusion layer, Δg is gel thickness (m) and C_i is the interfacial concentration of labile trace metal species (mol/m^3).

$$\mathbf{F(t)} = \frac{\mathbf{DC_i}}{\mathbf{\Delta g}} \qquad \mathbf{1}$$

The total mass of trace metal accumulated on the resin gel (M) upon diffusion through area (A) of the sampler over the deployment time (t) is shown in equation (2). M is determined analytically by measuring the concentration of the metals (C_e) bound to the resin gel (Eq 3).

$$\mathbf{M} = \frac{\mathbf{DC_i}\boldsymbol{tA}}{\mathbf{\Delta g}} \qquad \mathbf{2}$$

$$\mathbf{M} = \frac{\mathbf{C_e}\left(\mathbf{V_{HNO_3}} + \mathbf{V_e}\right)}{\mathbf{f_e}} \qquad \mathbf{3}$$

where, V_{HNO_3} is the volume of HNO_3 used for eluting the metals attached to the resin (m^3), C_e is the concentration of metals measured analytically using inductively coupled plasma mass spectrometry (ICP-MS) (mol/m^3), V_e is the resin gel volume (m^3), and f_e is the elution factor. The elution factor (f_e) is the ratio of the extracted metal to the bound metal. Based on previous studies, an elution factor of 0.8 was adopted for the calculation of trace metal concentrations in bulk solution.[298,357] The time-averaged DGT concentration is then obtained by equation (4), where A is the exposure area (m^2), and t is the time of deployment (s).

$$\mathbf{C_{DGT}} = \mathbf{C_i} = \frac{\mathbf{M\Delta g}}{\mathbf{DtA}} \qquad \mathbf{4}$$

Table D-2: Recipe for simulated site water for microcosm experiments conducted on wetland soils and stream sediments

Parameter	ORNL	TB
pH	7.6	5
Ionic Strength	7 mM	0.3 mM
	Concentration (µM)	
Na^+	450	60
K^+	70	5
Ca^{2+}	1100	25
Mg^{2+}	400	30
Cl-	2700	150
SO_4^{2-}	256	8
NO_3^-	70	0
NH_4^+	0.2	0
PO_4^{3-}	4	0

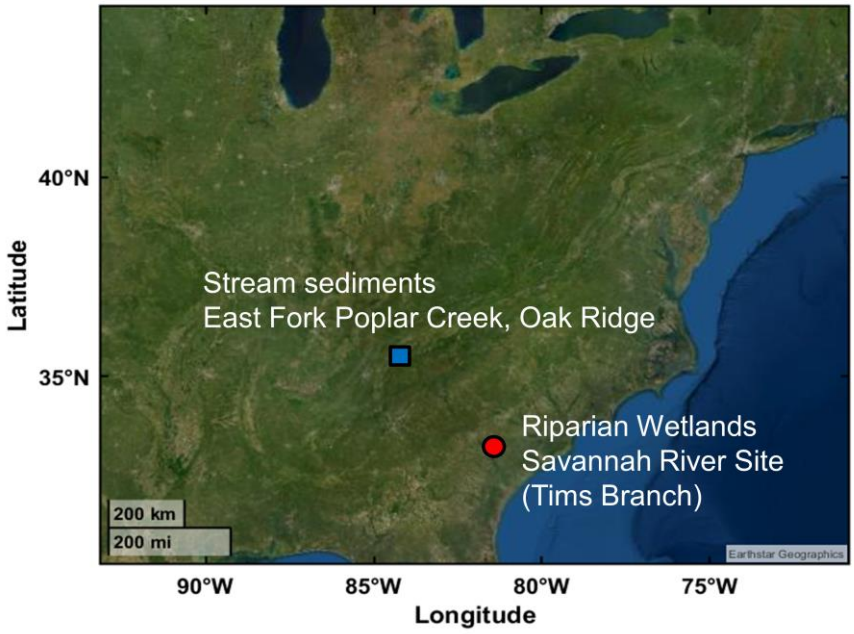

Figure D-1: Locations of the sites selected for collecting soils and sediments for redox fluctuations experiments

D.2 Total concentrations of Metals, Carbon, and Sulfur in Samples

Total carbon, and sulfur contents were determined using the dried soil and sediment samples by combustion elemental analysis using an Elementar vario MACRO cube CHNS analyzer.[113] The total metal concentrations in the soils and sediments were estimated using a microwave digestion analysis method. Specifically, 3 mL of concentrated trace metal grade HNO_3 and 0.3 mL of 30% hydrogen peroxide (H2O2) were added to 0.030 g of dried soil or sediment in a PTFE microwave digester vessel. Samples were left to react at room temperature in the fume hood for 30 minutes and then digested in a CEM MARS6 microwave digestion system. The temperature was ramped from ambient to 175 °C over 10 min and then maintained at 175°C for 15 min to promote complete digestion. After the vessels cooled, samples were filtered using 0.22 µm MCE filters followed by dilution to 2% HNO_3. Triplicate digestions were prepared for each soil or sediments. The concentration of Fe was determined using a Thermo Scientific iCap 7400 Duo inductively-coupled plasma optical emission spectrometer (ICP-OES). The concnetration of trace metals (CU, Ni, Zn, and Co) and Mn were determined by inductively-coupled plasma mass spectrometry (ICP-MS, PerkinElmer NexION 2000).

Table D-3: Total concentration of metals, carbon, and sulfur content at the selected sites

Component	Wetland Soil (TB)	Stream Sediment (ORNL)
Cu (nmol/g)	470 ± 50	320 ± 40
Ni (nmol/g)	150 ± 20	290 ± 50
Co (nmol/g)	20 ± 4	170 ± 30
Zn (nmol/g)	440 ± 40	1300 ± 200
Mn (µmol/g)	0.74 ± 0.09	6.4 ± 0.8
Fe (µmol/g)	190 ± 50	400 ± 100
C (µmol/g)	3000 ± 400	2500 ± 800
S (µmol/g)	18 ± 3	31 ± 5

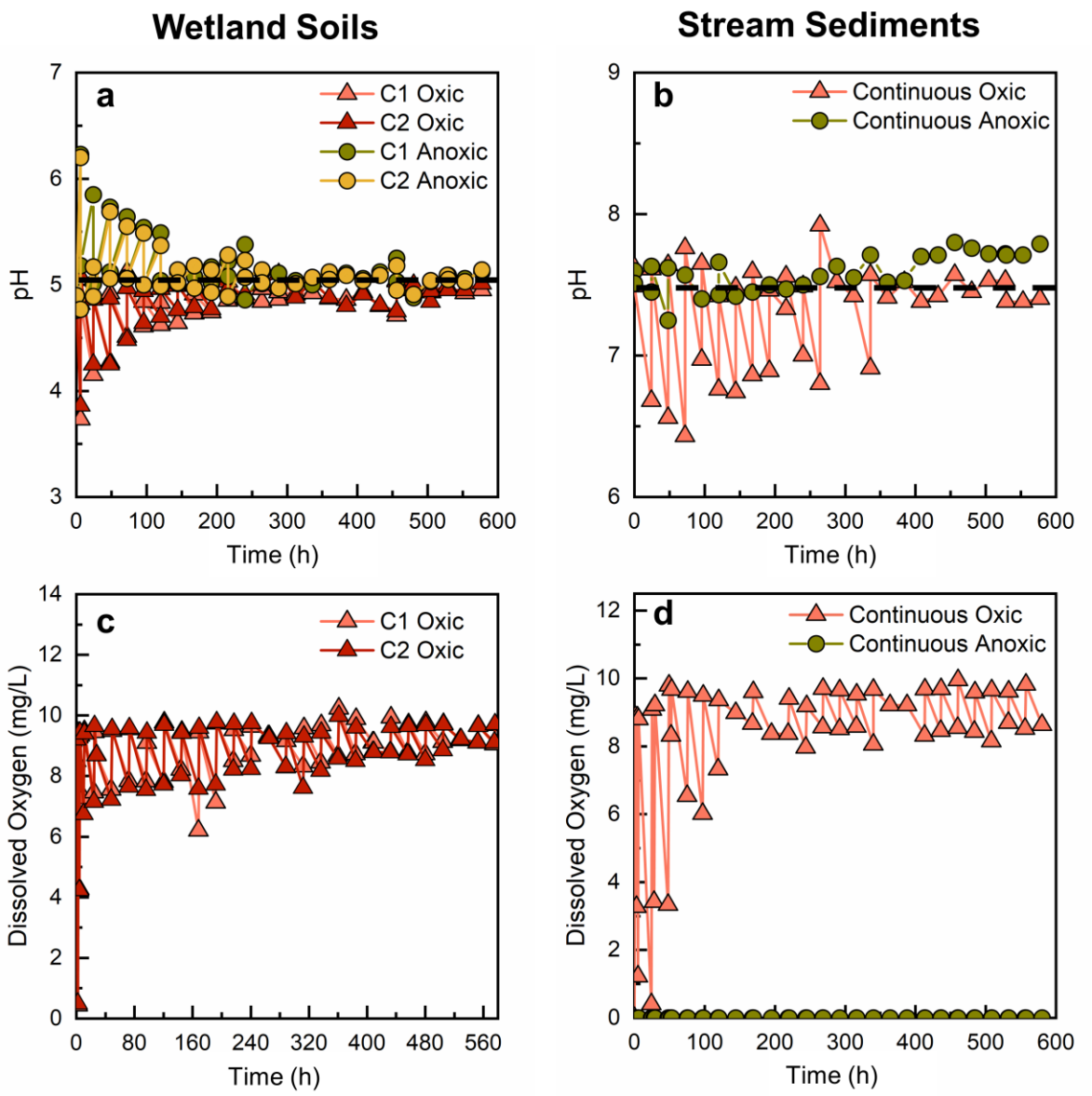

Figure D-2: Effect of anoxic and oxic fluctuations on the pH (a-b) and dissolved oxygen (c-d) in the always anoxic and always oxic controls initiated with riparian wetland soils and streams sediments. C1 and C2 indicate the duplicate microcosms initiated under continuous oxic and anoxic conditions. "Continuous" label represents sustained oxic and anoxic microcosms. The dashed line represents the pH at which microcosms were initiated and readjusted every 24 h.

Table D-4: Average initial and final pH values after adjustment in the microcosms during the redox fluctuation experiments

Wetland Soils			Stream Sediments		
Time (h)	Initial pH	Final pH	Time (h)	Initial pH	Final pH
24	6.0	5.0	24	7.6	7.6
48	6.0	5.0	48	7.7	7.6
72	5.6	5.0	72	7.6	7.7
96	5.8	5.0	96	7.7	7.7
120	5.6	5.1	120	7.6	7.6
144	5.6	5.1	144	7.7	7.6
145	3.7	4.9	145	7.4	7.6
147	3.8	5.0	169	7.5	7.6
150	3.9	5.0	193	7.4	7.6
169	4.3	5.0	216	7.7	7.6
175	4.7	5.0	240	7.7	7.6
193	4.8	5.0	264	7.7	7.6
194	5.1	5.0	288	7.7	7.6
212	5.2	5.1	312	7.7	7.5
224	5.3	5.1	336	7.7	7.6
248	5.4	5.1	360	7.2	7.6
272	5.7	5.0	384	7.3	7.5
296	5.5	4.9	408	7.6	7.6
320	5.5	5.0	432	7.6	7.6
344	5.5	5.1	456	7.6	7.6
345	4.1	5.0	480	7.7	7.6
348	4.1	5.0	504	7.6	7.5
353	4.6	5.1	528	7.6	7.6
369	4.8	5.0	552	7.3	7.5
375	5.0	5.0	576	7.3	7.6
394	5.2	4.9	592	7.4	7.6
400	5.1	5.1			
424	5.3	5.0			
448	5.4	4.9			
472	5.4	4.9			
496	5.4	4.9			
520	5.5	5.0			
545	3.9	5.0			
548	4.0	5.0			
552	4.5	5.1			
575	4.7	5.0			
583	4.8	4.9			

Table D-5: Change in ionic strength over different cycles of redox fluctuations in wetland soils and stream sediments

Condition	Change in ionic strength (μM)	
	Wetland soils	Stream sediments
Cycle 1 Anoxic	49	0.02
Cycle 1 Oxic	213	0.04
Cycle 2 Anoxic	39	0.03
Cycle 2 Oxic	173	0.06
Cycle 3 Anoxic	36	0.01
Cycle 3 Oxic	155	0.07
Total change	665	0.23

Table D-6: Oxygen consumed (minimum and maximum) in different oxic cycles of wetland soils and stream sediments.

Condition	Oxygen demand (mg L^{-1} h^{-1})	
	Wetland Soils	Stream Sediments
Cycle 1 Oxic	1.8-7.6	1.2-7.2
Cycle 2 Oxic	0.83-5.7	0.62-5.2
Cycle 3 Oxic	0.18-4.5	0.12-2.6

D.3 Dissolved Cu Speciation in Microcosms

Two different binding sites are considered in the NICA model, type 1 and type 2, corresponding to carboxylic (low affinity) and phenolic (high affinity) sites respectively.[197]

$$Q_i = \frac{n_{i,1}}{n_{H,1}} Q_{\max 1,H} \frac{(\acute{K}_{i,1} c_i)^{n_{i,1}}}{\sum(\acute{K}_{i,1} c_i)^{n_{i,1}}} \frac{\left[\sum(\acute{K}_{i,1} c_i)^{n_{i,1}}\right]^{p_1}}{1+\left[\sum(\acute{K}_{i,1} c_i)^{n_{i,1}}\right]^{p_1}} + \frac{n_{i,2}}{n_{H,2}} Q_{\max 1,H} \frac{(\acute{K}_{i,2} c_i)^{n_{i,2}}}{\sum(\acute{K}_{i,2} c_i)^{n_{i,2}}} \frac{\left[\sum(\acute{K}_{i,1} c_i)^{n_{i,2}}\right]^{p_2}}{1+\left[\sum(\acute{K}_{i,1} c_i)^{n_{i,2}}\right]^{p_2}}$$

Eq S1

where, c_i (mol. L-1) is the concentration of metal; Q_i is the amount of bound ion described by two identical binding expressions, one each for the carboxylic- (1) and phenolic-type (2) site distributions. $Q_{max1,H}$ and $Q_{max2,H}$ are the maximum proton binding capacity of humic substances within each distribution (mol kg^{-1}); p_1 and p_2 account for intrinsic heterogeneity of humic substances; $\acute{K}_{i,1}$ and $\acute{K}_{i,2}$ are median values for affinity distributions for ion, and $n_{i,1}$ and $n_{i,2}$ are used to describe the nonidealities of the ion-binding to each distribution. The ratios $\frac{n_{i,j}}{n_{H,j}}$ with j = 1 or 2 reflect the average stoichiometry of ion binding.

The charge on humic substances is neutralized by the nonspecific binding of counter-ions and exclusion of co-ions within the Donnan volume, V_D ($L \cdot kg^{-1}$), as described by the empirical relationship.

$$logV_D = b(1 - logI) - 1 \qquad \text{Eq S2}$$

Here, I is ionic strength and b is an empirical parameter describing the variation of Donnan volume with ionic strength [198]. The values of parameters used in estimating Cu speciation are listed in Table S3.

Humic substances are normally assumed to be the main binding substances [171], and their concentrations were determined from the dissolved organic carbon (DOC) concentrations. Humic substances account for 60% of DOC in natural water systems [350,356], and they comprise 50% carbon, so concentration of HS was assumed to be 1.2 times the DOC concentration. The pH, temperature, total dissolved elements (Na, Mg, K, Ca, Cl, NO_3, SO_4, and PO_4) (Table EA1), and dissolved Cu, Fe, and Mn were used as the input parameters for determining Cu speciation.

Table D-7: Comparison of dissolved trace metal concentrations in stream sediments with NICA-Donnan speciation model

Condition	Metal	Concentration (nM)		
		Dissolved	C_{DGT}	$C_{NICA\text{-}Donnan}$
Cycle 1 Anoxic	Cu	5.0	1.6	0.69
	Ni	21	6.6	17
	Co	7.3	5.9	6.6
	Zn	17	15	15
Cycle 1 Oxic	Cu	8.3	5.2	0.76
	Ni	42	30	35
	Co	3.9	2.5	3.2
	Zn	13	12	12
Cycle 2 Anoxic	Cu	7.3	2.7	0.23
	Ni	51	31	41
	Co	11	9.1	9.5
	Zn	29	21	26
Cycle 2 Oxic	Cu	18	5.4	4.7
	Ni	41	18	34
	Co	3.6	1.9	3.2
	Zn	10.8	10.4	9.9
Cycle 3 Anoxic	Cu	9.7	1.7	1.6
	Ni	51	22	44
	Co	16	6.9	14
	Zn	37	20	34
Cycle 3 Oxic	Cu	20	11	6.4
	Ni	37	34	32
	Co	4.5	4.3	4.1
	Zn	11	9.7	10

Table D-8: Comparison of dissolved trace metal concentrations in wetland soils with NICA-Donnan speciation model

Condition	Metal	Concentration (nM)		
		Dissolved	C_{DGT}	$C_{NICA\text{-}Donnan}$
Cycle 1 Anoxic	Cu	7.1	0.34	0.13
	Ni	370	110	310
	Co	120	18	90
	Zn	610	190	500
Cycle 1 Oxic	Cu	15	13	6.1
	Ni	33	28	30
	Co	9.2	5.6	7.1
	Zn	260	210	230
Cycle 2 Anoxic	Cu	24	1.2	0.24
	Ni	248	83	170
	Co	74	15	63
	Zn	1200	220	980
Cycle 2 Oxic	Cu	23	13	6.8
	Ni	30	28	30
	Co	7.7	5.9	6.6
	Zn	240	230	216
Cycle 3 Anoxic	Cu	26	11	2.6
	Ni	270	76	220
	Co	88	9.3	67
	Zn	1500	200	1280
Cycle 3 Oxic	Cu	45	24	14
	Ni	52	47	49
	Co	17.4	9.7	15
	Zn	480	380	430

$C_{NICA\text{-}Donnan}$ indicates freely available trace metal in the solution.

D.4 Details on Selective Extraction Technique used for Determining Oxidizable and Reducible Phases

For each extraction, a wet mass equivalent to 0.5 g dry mass of soil was added to a 15 mL polypropylene tube followed by the addition of a selected extractant. The dry mass was determined on a separate portion of soil by drying at 120°C until a constant mass was achieved. To estimate the fraction of metals bound to reducible forms, 10 mL of 0.040 M NH_2OH-HCl in 25% HOAc was used as an extractant. The tubes were stored at a temperature of 96°C in an oven for 6 h, and then the supernatant was cooled down to room temperature, filtered, diluted, and acidified to determine the dissolved concentration of metals. For estimating the metals bound to oxidizable phases, 1.5 mL of 0.020 M HNO_3 and 2.5 mL of 30% H_2O_2 were added to 0.5 g of soil or sediment. After 2 h, the tubes were placed in an oven maintained at a temperature of 96 °C for 24 h followed by the addition of another 1.5 mL of 30% H_2O_2 solution. The tubes were stored in the oven for an additional 24 h after which 2.5 mL of NH_4OAc (3.2 M) was added to the samples. The samples were then mixed on an end-over-end rotator for 30 min at room temperature, and the supernatant was filtered and stored for dissolved metal analysis. In the above-mentioned extraction step, H_2O_2 can reduce manganese oxides to Mn(II), and the presence of manganese oxides can result in decreased efficiency of organic matter oxidation by H_2O_2.[358,359] In our samples, the solid-phase associated manganese concentration was low relative to the concentration of organic matter (Table S3), and the presence of such low concentrations of Mn was not expected to interfere with the oxidation of organic matter

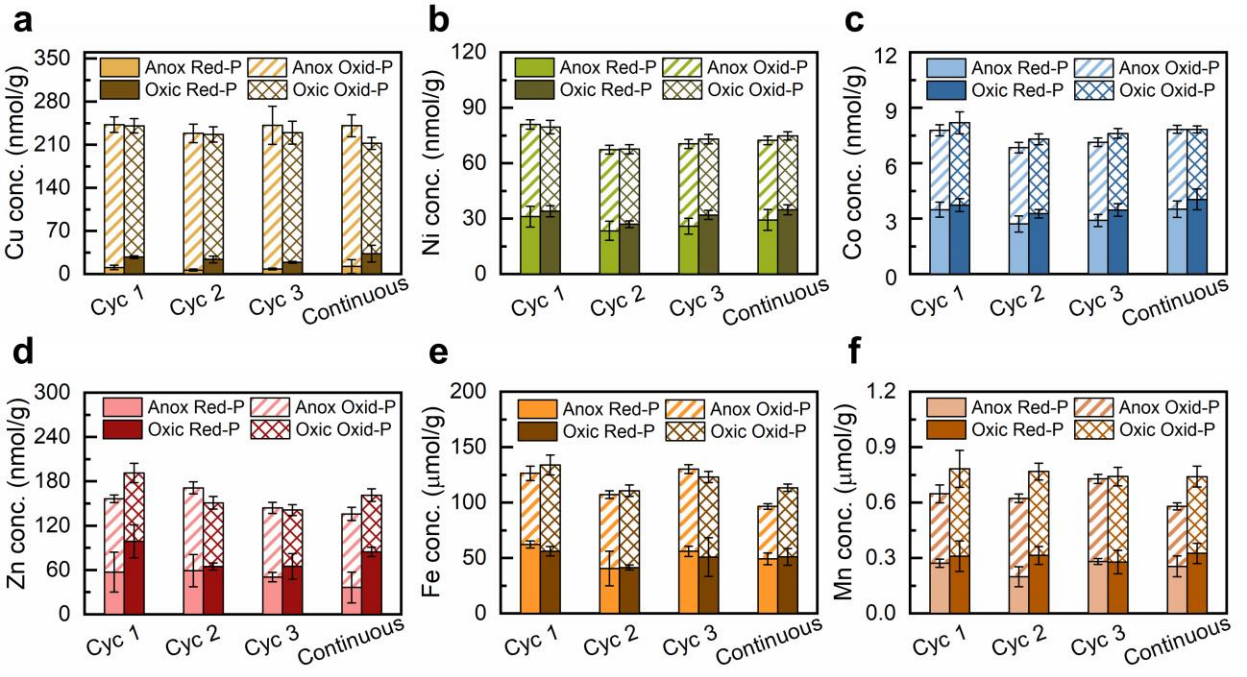

Figure D-3: Change in the concentration of (a) Cu (b) Ni (c) Co (d) Zn (e) Fe and (f) Mn bound to reducible phases (Red-P) and bound to oxidizable phases (Oxid-P) upon redox fluctuations in a wetland soil. The results labeled "Continuous" are from the parallel microcosms that were sustained at oxic and anoxic conditions. Error bars indicate the standard deviation in the duplicate microcosms. The data was obtained using selective extractions procedure as indicated in materials and methods of the manuscript. The amount bound to reducible forms were extracted using 0.040 M NH_2OH-HCl in 25% HOAc, and the oxidizable phases were extracted using 0.020 M HNO_3,30% H_2O_2, and 3.2 M NH_4OH solution.

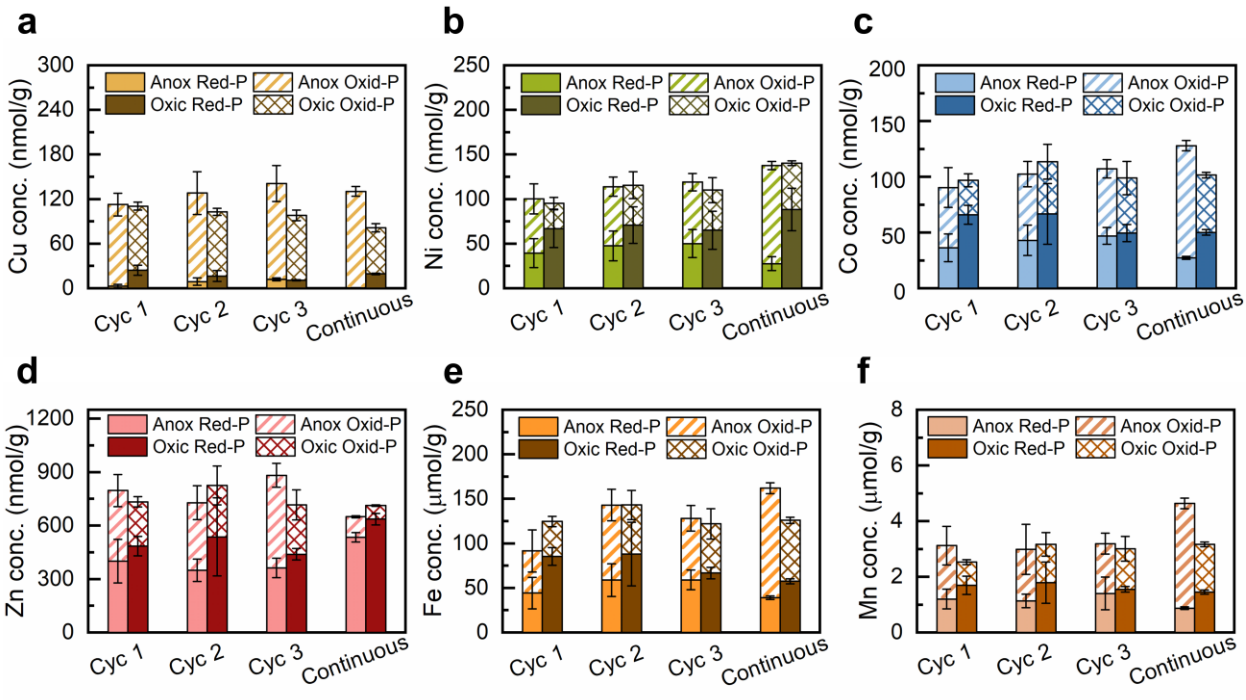

Figure D-4: Change in the concentrations of (a) Cu (b) Ni (c) Co (d) Zn (e) Fe and (f) Mn bound to reducible phases (Red-P) and bound to oxidizable phases (Oxid-P) upon redox fluctuations in sediments collected from a stream. The results labeled "Continuous" are from the parallel microcosms that were sustained at oxic and anoxic conditions. Error bars indicate the standard deviation in the duplicate microcosms. The data was obtained using selective extractions procedure as indicated in materials and methods of the manuscript.

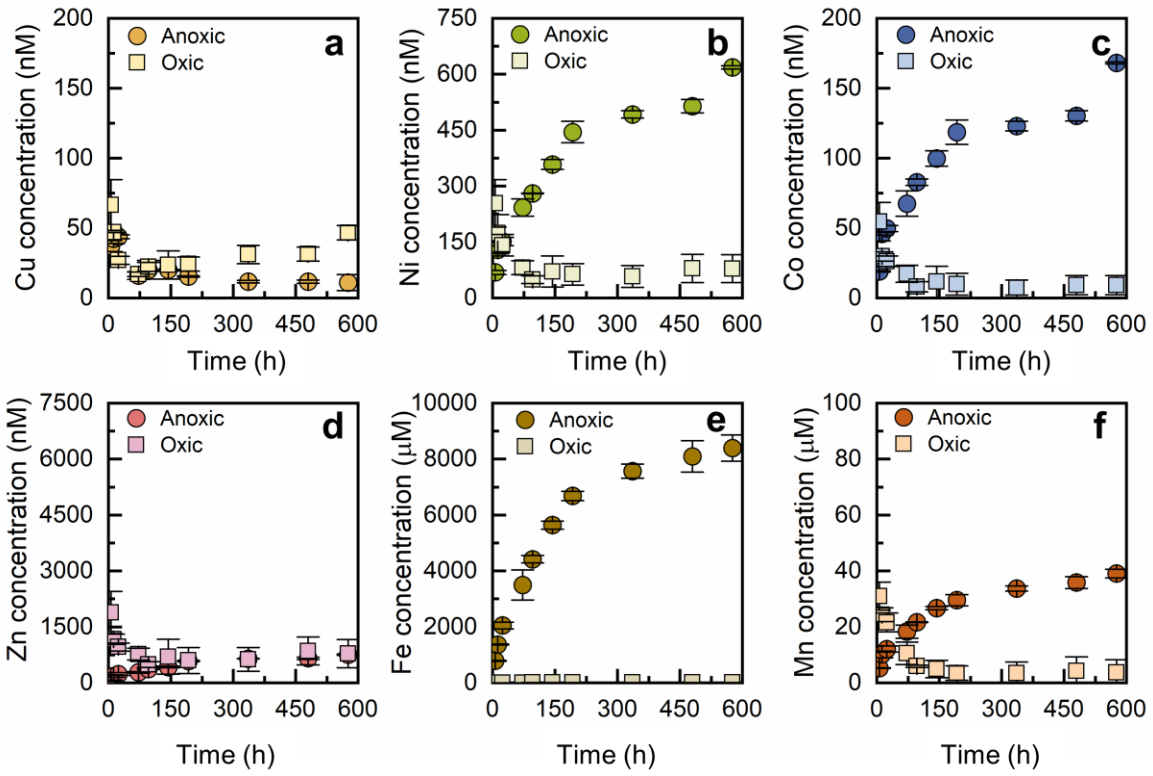

Figure D-5: Concentration of (a) Cu (b) Ni (c) Co (d) Zn (e) Fe and (f) Mn in always oxic and always anoxic controls initiated with riparian wetland soils during the time span of 24 days. Error bars indicate the standard deviation in the duplicate microcosms.

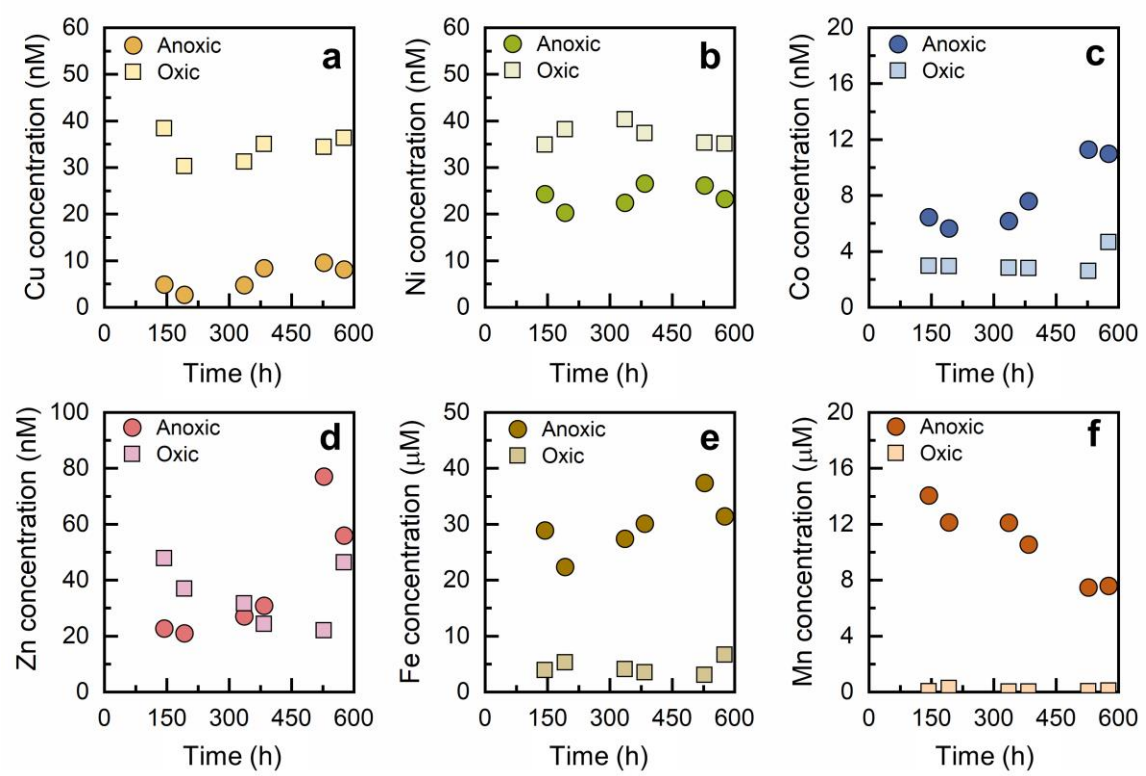

Figure D-6: Concentration of (a) Cu (b) Ni (c) Co (d) Zn (e) Fe and (f) Mn in always oxic and always anoxic controls initiated with stream sediments during the time span of 24 days.

Table D-9: Ratio of DGT estimated concentration to dissolved concentration (C_{DGT}/C_{diss}) after each redox fluctuation

Site	Condition	Cu	Ni	Co	Zn
Wetland soils	Cyc 1 Anoxic	0.05	0.28	0.15	0.31
	Cyc 1 Oxic	0.88	0.83	0.61	0.79
	Cyc 2 Anoxic	0.05	0.29	0.20	0.18
	Cyc 2 Oxic	0.54	0.93	0.77	0.99
	Cyc 3 Anoxic	0.29	0.28	0.11	0.13
	Cyc 3 Oxic	0.53	0.91	0.56	0.80
Stream sediments	Cyc 1 Anoxic	0.31	0.32	0.80	0.86
	Cyc 1 Oxic	0.63	0.70	0.65	0.88
	Cyc 2 Anoxic	0.37	0.60	0.85	0.71
	Cyc 2 Oxic	0.31	0.44	0.53	0.97
	Cyc 3 Anoxic	0.32	0.44	0.44	0.55
	Cyc 3 Oxic	0.53	0.91	0.97	0.87

Table D-10: Percent (%) of total trace metals in the solid phase released to water in different cycles of redox fluctuations in wetland soils and stream sediments

Site	Condition	Cu (%)	Ni (%)	Co (%)	Zn (%)
Wetland soils	Cyc 1 Anoxic	0.005	0.830	1.932	0.461
	Cyc 1 Oxic	0.010	0.074	0.153	0.198
	Cyc 2 Anoxic	0.017	0.551	1.226	0.925
	Cyc 2 Oxic	0.016	0.067	0.128	0.180
	Cyc 3 Anoxic	0.018	0.603	1.471	1.137
	Cyc 3 Oxic	0.032	0.115	0.291	0.366
Stream sediments	Cyc 1 Anoxic	0.005	0.024	0.014	0.004
	Cyc 1 Oxic	0.009	0.048	0.008	0.003
	Cyc 2 Anoxic	0.008	0.059	0.021	0.007
	Cyc 2 Oxic	0.018	0.046	0.007	0.003
	Cyc 3 Anoxic	0.010	0.058	0.030	0.009
	Cyc 3 Oxic	0.021	0.043	0.009	0.003

Appendix E. Trace metal bioaccessibility in freshwater sediments

E.1 Introduction

Trace metals can be present in dissolved form or associated with various phases in sediments. Sediment-associated forms include trace metals adsorbed to or incorporated in organic matter and in minerals that include carbonates, iron oxides, sulfides and aluminosilicates.[7,101] The free metals (M^{n+}) possess greater diffusive transport because of their small size and are the most biologically and chemically active fractions of trace metals.[298] Strong organic metal-chelates, such as complexes with humic acids and fulvic acids, are inert and hence not readily bioavailable, but inorganic hydroxy and carbonate complexes are labile.[52,166–168]The sum of the amount of labile metals in the aqueous phase and the amount retained by the solid phase that can be easily transferred to the aqueous phase forms the part of the bioavailable fraction of metals. Information on the chemical speciation of metals in natural aquatic systems is essential to understand their biogeochemical cycling, bioavailability, and toxicity.[360] The estimation of the bioavailable fraction of metals in the sediments will also help evaluate if the natural metal concentrations are limiting key biogeochemical processes. The bioavailability of trace metals in sediments is dependent upon the characteristics of solid phases (minerals, particulate organic matter, iron and sulfur content) and overlying porewater attributes (pH, redox potential, dissolved organic carbon).[7,362] To evaluate the availability of trace metals in the porewater of wetland soils and sediments, in-situ passive samplers can be used.

The diffusive gradient in thin films (DGT) technique is widely used for *in situ* measurements of trace metals in soils, sediments and water systems.[298,360,361,363,364] The samplers based on this technique consist of three layers, a membrane, diffusion layer and a binding gel layer (Figure E-1).[357,365] This arrangement provides a pathway for the diffusion of ions from the bulk solution to the binding layer. The binding gel strongly binds labile metal species, and the flux of the metals towards the resin gel can be calculated using Fick's Law.[357,366]

The objective of this study was to estimate the bioavailable fraction of metals in the porewater of sediments and the water column of East Fork Poplar Creek located at Oak Ridge National Laboratory, Tennessee by using DGT samplers. An extensive field study was conducted in November 2020 at the site. The methods and results are discussed below.

E.2 Materials and Methods

E.2.1 DGT Development

The diffusion gel and the resin gels were prepared according to the procedure published by Zhang and Davison.[298] The gel solution used for preparing diffusion and binding gels contained 15% by volume acrylamide and 0.3% by volume bis (N, N-methylene-bis-acrylamide) crosslinker. Freshly prepared ammonium persulfate (10%) was used as initiator for polymerization and N, N, N, N tetramethylenediamine served as a catalyst. For the preparation of 10 mL of diffusion gel, 70 µL of ammonium persulfate and 20 µL of N,N,N',N'-tetramethylethylenediamine (TEMED)were added. The resin gel contained 2 g of Chelex 100 (Na form, 200-400 mesh) in 10 mL of gel solution. Less ammonium persulfate (50 µL) and TEMED (15µl) were added in the resin gel solution to prolong the setting process and allow them to settle by gravity. After 45 minutes of setting time, the gels were removed from the casting assembly and hydrated in ultrapure water for

24 hours. The water was periodically changed to remove any contamination of trace metals. The diffusion gels were stored in $NaNO_3$ (0.01 M), and binding gels were stored in ultrapure water at 4℃. Prior to storage, the gels were cut into the desired size for use in DGT samplers.

DGT samplers were assembled 4-5 days prior to shipping them to Oak Ridge National Laboratory (ORNL), and they were stored in re-sealable zipper storage bags along with a few drops of 0.01 M NaCl to prevent the desiccation of the gels. The assembled DGT samplers along with the sample holders were shipped to ORNL in a cooler with ice packs.

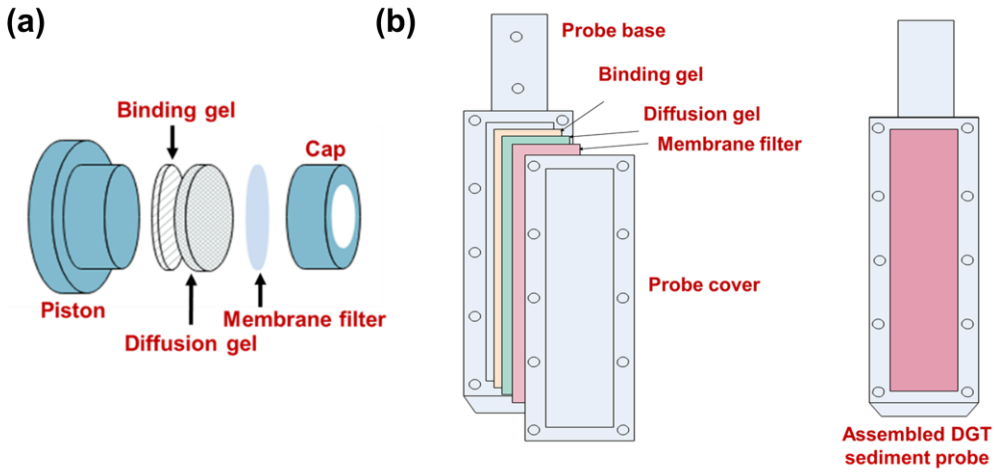

Figure E-1: DGT devices (a) a piston device, for water deployments; and (b) a planar device, designed for sediment deployments.

Table E-1 Details of the samplers deployed at different locations at ORNL

	Deployment time	Location	No of Samplers
Solution Samplers	24, 48 and 72	5.4 Loc 1	9
		5.4 Loc 2	9
		22-23 Loc 1	9
		22-23 Loc 2	9
Sediment Probes	6, 12, 24, 48 and 72	5.4 Loc 1	10
		5.4 Loc 2	10
		22-23 Loc 1	10
		22-23 Loc 2	10

E.2.2 DGT Deployment

Two sites, ORNL 5.4 and ORNL 22-23 were selected for conducting the study (Figure E-2-Figure E-3). At each site (ORNL 5.4 and 22-23), DGT solution samplers (Figure E-1a) and sediment probes (Figure E-1b) were deployed at two different locations. At each location, for water systems, nine DGT samplers (*three for each deployment time i.e., 12, 24 and 48 h*) were deployed in the water column. For sediments, DGT sediment probes were deployed for 6, 12, 24, 48 and 72 hours (in duplicate). The multiple time periods were selected to understand the response of sediments to the localized sink induced by the probes at each location, and to obtain the kinetic parameters associated with adsorption/desorption of metals from the sediments. DGT field blanks were used to assess the possible contamination from storage, deployment and retrieval procedures and transport. The field blanks were assembled and shipped along with the other DGT samplers. They were not deployed at the sites but were washed with deionized water used for cleaning deployed DGTs upon retrieval. The selected locations for deploying the samplers were sufficiently far from each other and were not intended to be replicates right next to each other. The details of the number of DGT samplers deployed and times of deployments are shown in Table E-1**.** The pH, temperature, dissolved oxygen and conductivity of the surface waters were also measured before and after DGT deployment (Table E-2

Table E-3). After removal, DGTs were washed with DI water to remove soil particles and were stored in the refrigerator in air-tight plastic bags with trace amounts of 0.01 M NaCl to prevent the gels from drying out.

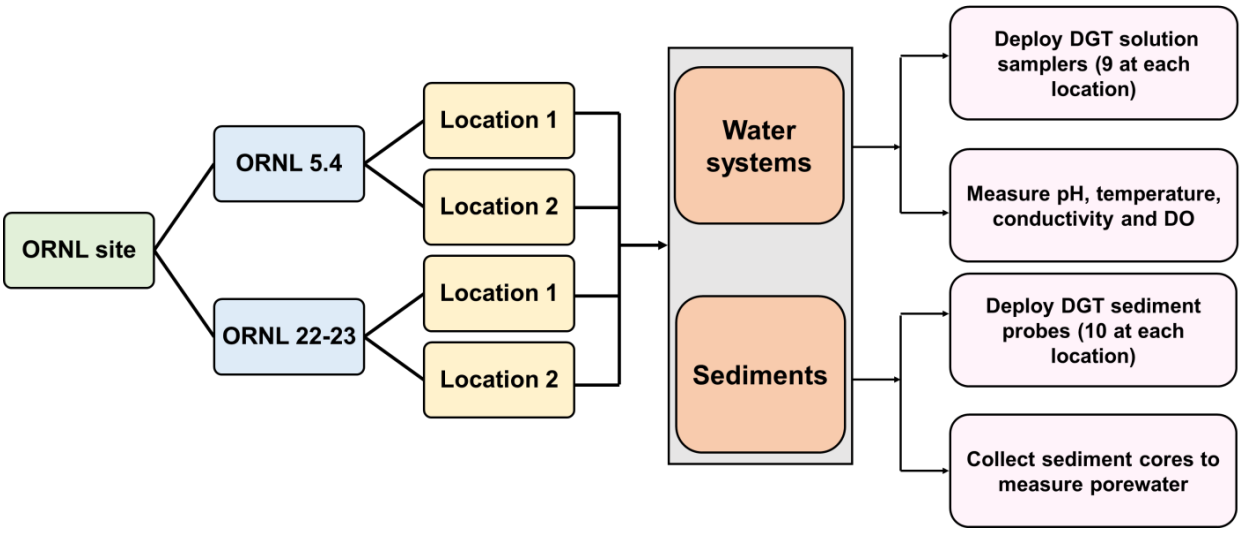

Figure E-2: DGT deployment plan at East Fork Poplar Creek at ORNL

Table E-2: Field site conditions before and after deployment of DGT solution samplers

Site	Parameter	Deployment Time		
		24	48	72
5.4 Location 1	pH	8.01	7.84	7.84
	DO (mg/L)	9.83	10.06	9.87
	Temperature (˚C)	9.65	9.1	9.37
	Conductivity (µS/cm)	289.6	306.5	330.2
5.4 Location 2	pH	8.01	7.91	7.81
	DO (mg/L)	9.85	10.04	9.82
	Temperature (˚C)	9.75	9.18	9.49
	Conductivity (µS/cm)	288.5	305.1	329.3
22-23 Location 1	pH	8.07	8.01	8.00
	DO (mg/L)	10.55	10.59	10.37
	Temperature (˚C)	11.51	11.25	12.49
	Conductivity (µS/cm)	326.4	337.5	359.0
22-23 Location 2	pH	7.86	7.84	7.82
	DO (mg/L)	9.50	9.53	9.21
	Temperature (˚C)	11.58	11.45	12.54
	Conductivity (µS/cm)	326.4	339.9	362.1

Table E-3: Conditions of the water column before and after deployment of DGT sediment probes at the selected locations

Site	Parameter	Deployment Time				
		6	12	24	48	72
5.4 Location 1	pH	7.9	7.9	8.0	7.8	7.8
	DO (mg/L)	10.1	9.4	9.8	10.1	9.9
	Temperature (˚C)	11.7	11.3	9.6	9.1	9.4
	Conductivity (µS/cm)	297	293	290	307	330
5.4 Location 2	pH	8.0	8.0	8.0	8.0	7.9
	DO (mg/L)	10.1	9.5	9.8	10.0	9.8
	Temperature (˚C)	11.75	11.31	9.75	9.18	9.49
	Conductivity (µS/cm)	295.2	292.2	288.5	305.1	329.3
22-23 Location 1	pH	8.1	8.06	8.07	8.01	8.00
	DO (mg/L)	9.87	9.48	10.55	10.59	10.37
	Temperature (˚C)	13.77	12.65	11.51	11.25	12.49
	Conductivity (µS/cm)	336	332.9	362.4	337.5	359
22-23 Location 2	pH	8.06	7.95	7.86	7.84	7.82
	DO (mg/L)	9.46	8.84	9.50	9.53	9.21
	Temperature (˚C)	13.41	12.63	11.58	11.45	12.54
	Conductivity (µS/cm)	332.4	334.2	326.4	339.9	362.1

Water samples were also collected from the deployed locations after 6 hours and 72 hours to determine the concentrations of dissolved metals in the stream. The water samples were stored at 4°C prior to shipment. Sediment cores from each location were also collected to determine the porewater concentration of metals.

E.2.3 DGT Sampler Analysis

Retrieved DGT samplers along with water samples and sediments were shipped to Washington University in St. Louis in a cooler with ice packs. DGT solution samplers and sediment probes were stored in the refrigerator prior to analysis. Water samples were immediately filtered and acidified to determine the dissolved concentration of metals in the water streams. The sediments

obtained from ORNL were centrifuged at 5000 rpm for 10 minutes to obtain the porewater. The porewater was filtered and acidified to determine the concentration of metals in the porewater.

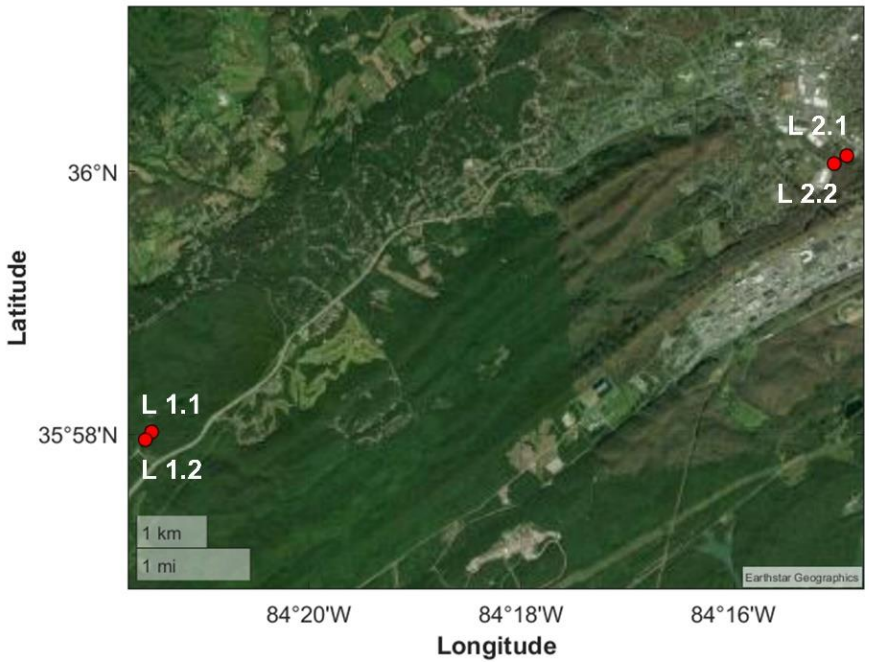

Figure E-3: Sites selected for DGT deployment at Oak Ridge National Laboratory

DGT solution samplers were opened using a screwdriver (Figure E-4) to obtain the resin gel. The resin gel was immersed in 1 mL of 1 M HNO_3 for 24 hours to extract the metals bound to the gel. After 24 hours, the acid was diluted and filtered to determine the concentration of metals using ICP-MS. For sediment probes, the gels and the filter membranes were cut along the window edges without disassembling the probe (Figure E-4). The filter membrane and diffusion gel were removed, and the resin gel was cut into 1 cm x 3 cm rectangular slices using a Teflon-coated blade. The metals were extracted from the resin gel slices by using the same procedure as mentioned above for solution samplers.

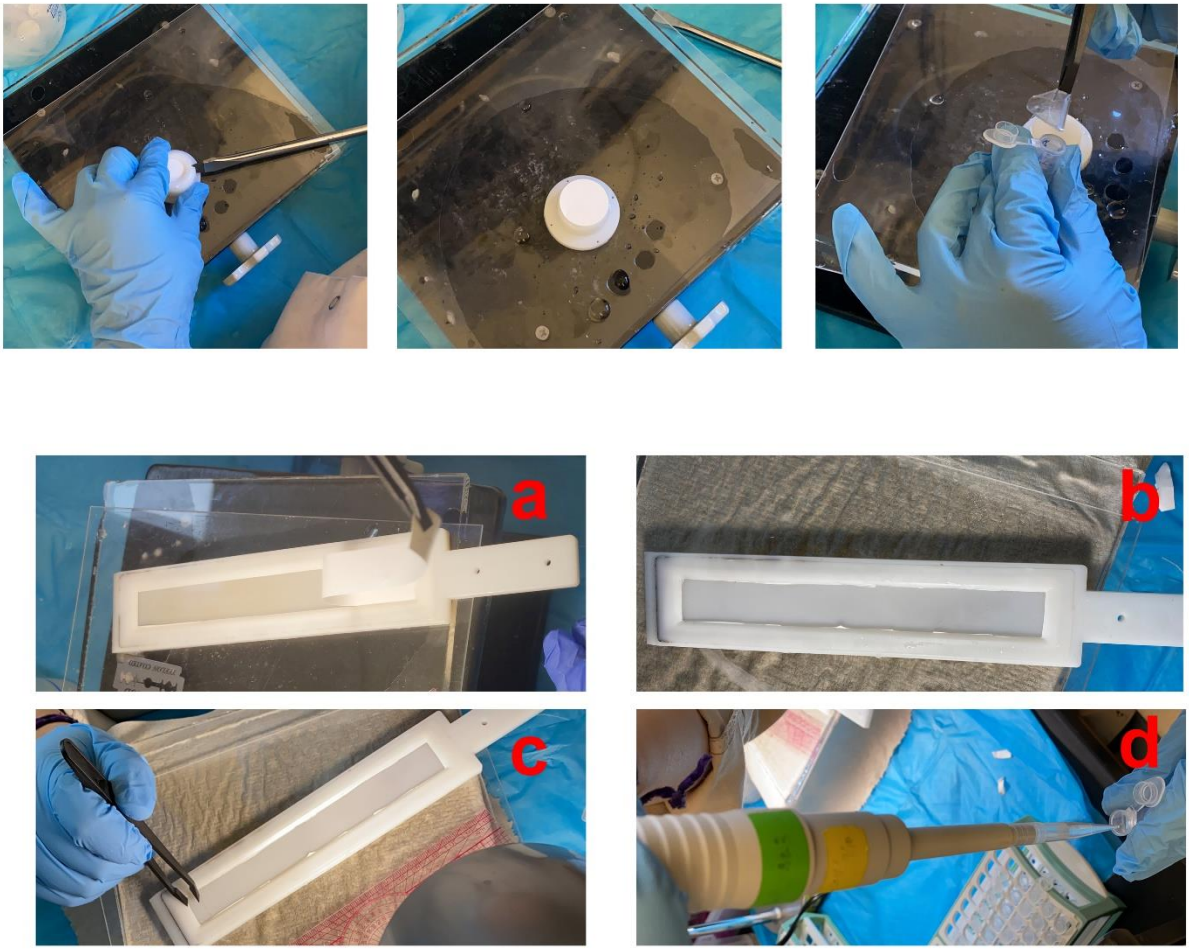

Figure E-4: Procedure for retrieval of resin gels from DGT solution samplers and sediment probes

E.2.4 DGT Calculations

The resin gel strongly binds metal species, and the flux of the metals (F in mol/m^2-s) towards the resin gel is calculated using Fick's law of diffusion (equation 1), where D is the diffusion coefficient (m^2/s) of the labile trace metal species in the diffusion layer, Δg is gel thickness (m) and C_i is the interfacial concentration of labile trace metal species (mol/m^3).

$$\mathbf{F(t)} = \frac{\mathbf{DC_i}}{\mathbf{\Delta g}} \qquad \mathbf{1}$$

The total mass of trace metal accumulated on the resin gel (M) upon diffusion through area (A) of the sampler over the deployment time (t) is shown in equation (2). M is determined analytically by measuring the concentration of the metals (C_e) bound to the resin gel (Eq 3).

$$\mathbf{M} = \frac{\mathbf{DC_i}\boldsymbol{tA}}{\mathbf{\Delta g}} \quad \mathbf{2}$$

$$\mathbf{M} = \frac{\mathbf{C_e}\left(\mathbf{V_{HNO_3}} + \mathbf{V_e}\right)}{\mathbf{f_e}} \quad \mathbf{3}$$

where, V_{HNO_3} is the volume of HNO_3 used for eluting the metals attached to the resin (m^3), C_e is the concentration of metals measured analytically using inductively coupled plasma mass spectrometry (ICP-MS) (mol/m^3), V_e is the resin gel volume (m^3), and f_e is the elution factor. The elution factor (f_e) is the ratio of the extracted metal to the bound metal. Based on previous studies, an elution factor of 0.8 was adopted for the calculation of trace metal concentrations in bulk solution.[298,357] The time-averaged DGT concentration is then obtained by equation (4), where A is the exposure area (m^2), and t is the time of deployment (s).

$$\mathbf{C_{DGT}} = \mathbf{C_i} = \frac{\mathbf{M\Delta g}}{\mathbf{DtA}} \quad \mathbf{4}$$

E.3 Results and Discussion

E.3.1 Water Column Samples

The dissolved metal concentration of metals in the water samples collected after 6 hours and 72 hours were averaged, and the results obtained are shown in Figure E-5. The trace metal concentrations in the water streams followed the trend Zn > Ni > Cu. Co was not detected in any of the samples. We also monitored if the concentration of metals in the water column fluctuated over the deployment period of 72 h (Table E-4).

The concentration of Zn, Ni and Fe almost remained constant at all the locations throughout the deployment span of 72 hours, however, the concentration of Mn increased significantly at both the locations of ORNL 22-23 site (200% at location 1 and 100% at location 2) (Table E-4). The concentration of Cu also fluctuated at all the locations, except 22-23 location 1.

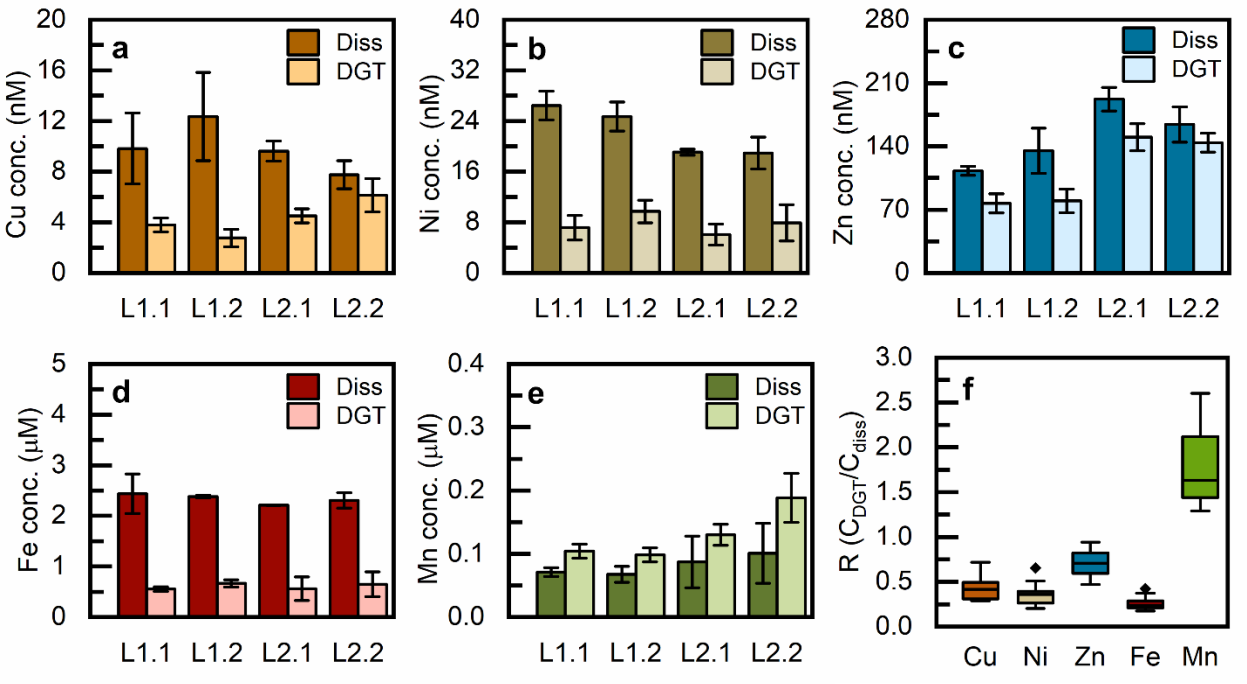

Figure E-5: Dissolved and labile concentrations of (a) Cu (b) Ni (c) Zn (d) Fe and (e) Mn in surface water. The concentration of Co was below detection limit at all the locations. The concentrations are averaged for three deployment time periods (24 h, 48 h, and 72 h). Subplot (f) represents the boxplot for the R values observed for metals at all the locations.

DGT-estimated concentrations of metals (C_{DGT}) in the water column of the stream for 24-hour deployment periods are shown in Figure E-5, and the mass accumulated on the resin gel throughout the deployment span is shown in **Error! Reference source not found.**. C_{DGT} values f ollowed the same trend as observed for dissolved metal concentration in the water streams with Zn > Ni > Cu. The ratio of DGT estimated and initial dissolved metal concentrations, as shown in Figure E-7, suggests that the ORNL 22-23 location 2 had a higher fraction of labile trace metals

than all the other locations. C_{DGT}/C_{stream} for Cu and Ni lies in the range of 0.3-0.8, however, this ratio for Zn was significantly higher (0.60 – 0.95). The low fraction of DGT estimated Cu and Ni concentration at all the locations, except at 22-23 location 2, shows that these metals exist in forms associated with organic complexes that are not readily bioavailable.[360] The ratio of bioavailable Fe to dissolved Fe was low (0.2-0.4), suggesting that a high proportion may be complexed by less mobile humic substances.[367] The higher ratios of C_{DGT} and C_{stream} for Mn (1.5-5.2) indicate that Mn may be predominantly present as free Mn(II) that can readily diffuse and bind to the resin gel in DGT.[368] Also, the Mn concentration fluctuated over a time span of 72 hours, and hence comparing DGT-estimated Mn concentrations with initial Mn concentration in the water stream might not be relevant.

Table E-4: Concentration of dissolved metals in the water samples collected after 6 hours and 72 hours of deploying DGT solution samplers. All the concentrations are in nM.

	5.4 Loc 1		5.4 Loc 2		22-23 Loc 1		22-23 Loc 2	
	6 hr	72 hr	6 hr	72 hr	6 hr	72 hr	6 hr	72 hr
Cu	11.8	7.8	7.8	16.9	10.2	9.1	10.7	4.9
Ni	28.1	24.8	23.1	26.3	19.4	18.7	17.1	20.7
Zn	116.2	109.3	152.9	117.5	201.3	182.9	165.0	123.3
Fe	2711.0	2161.6	2398.4	2361.8	2206.4	2210.2	2198.9	2412.1
Mn	75.8	65.8	58.7	76.4	28.4	85.9	67.1	134.2

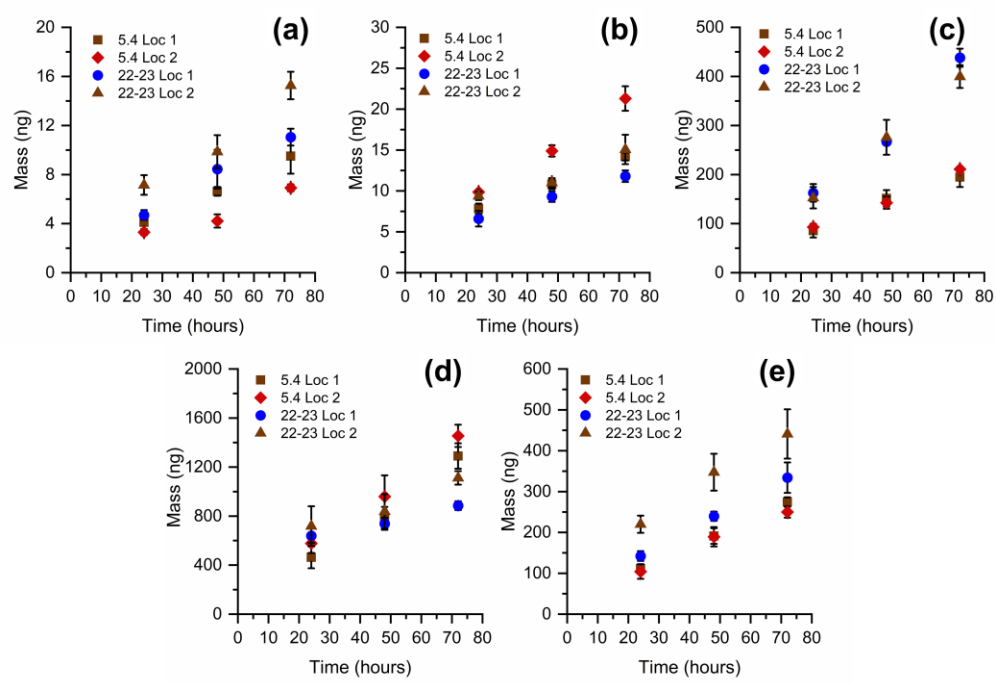

Figure E-6: Mass of (a) Cu (b) Ni (c) Zn (d) Fe and (e) Mn accumulated on the resin gels of solution samplers deployed in the streams for different time periods.

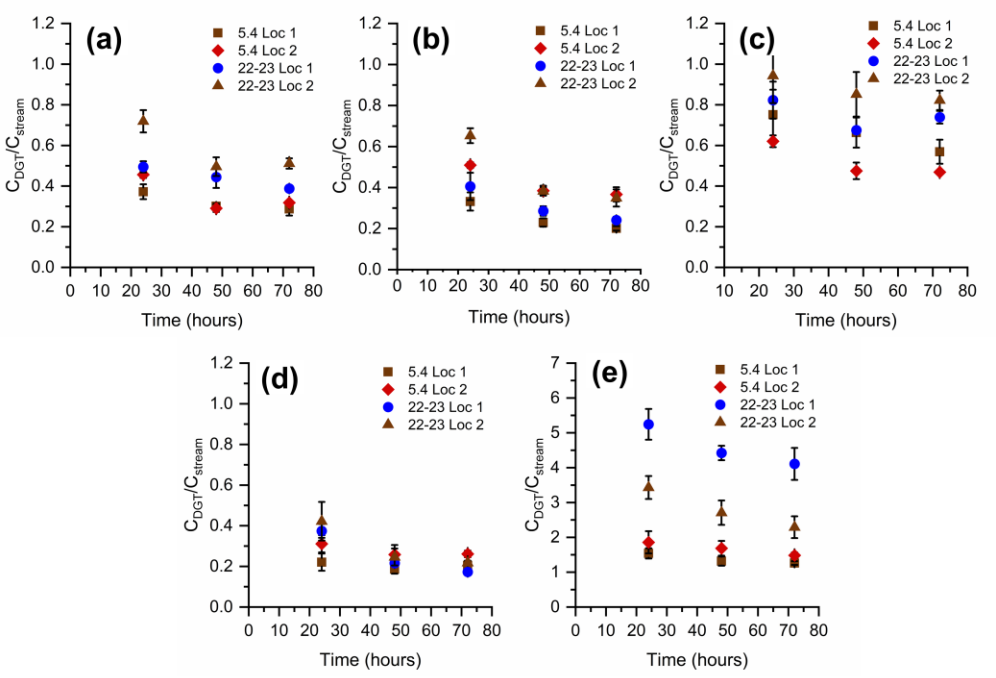

Figure E-7: The ratio of DGT estimated concentration to concentration of metals in the streams for (a) Cu (b) Ni (c) Zn (d) Fe and (e) Mn.

E.3.2 Sediments

The porewater concentration (C_{pw}) of metals in the sediments is shown in Figure E-8**.** The concentration of trace metals in the porewater followed the trend of 22-23 location 1 > 5.4 location 1 > 5.4 location 2 > 22-23 location 2. The concentration of Fe was similar across all the locations, except at 22-23 location 2, where the concentration was significantly lower. The concentration for Mn in the porewater has the trend 5.4 loc 1≈ 22-23 loc 1 > 5.4 loc 2 ≈ 22-23 loc 2. Previous studies have observed similar concentrations of metals in the porewater of uncontaminated sediments.[369–372]

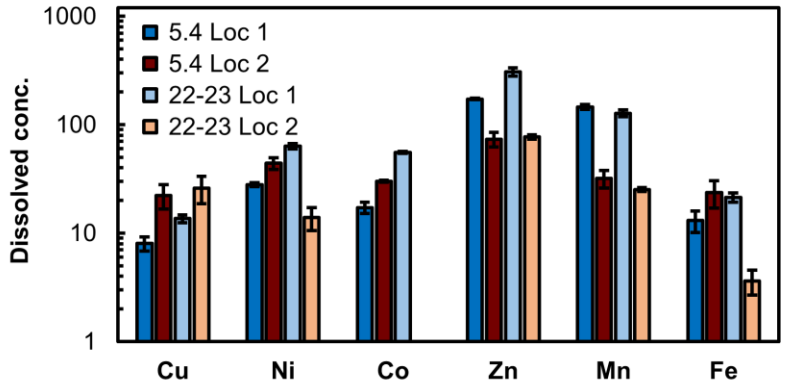

Figure E-8: Porewater concentration of metals obtained on centrifuging sediments. The trace metal concentrations are in nM and the concentration of Fe and Mn are in µM.

DGT sediment probes were used to obtain high-resolution profiles of labile trace metals in the sediments at the four selected locations **(**Figure E-9-Figure E-12**)** for deployment periods of 6, 12, 24, 48 and 72 hours. The mass accumulated on the resin gels was also plotted to understand if the concentration of metals in the porewater were depleted with time **(**Figure E-13-Figure E-16**).** For all locations, the rate of mass accumulation on the resin gels decreased after 24 hours for all the metals, which indicates that the metals in the porewater are not fully replenished from the sediments after the 24-hour deployment period. Hence, a 24-hour time period was selected to

compare the labile concentration of metals at the selected locations **(**Error! Reference source not f ound.**).**

The Cu concentration did not vary substantially across all the locations and was in the range of 3-9 nM **(**Figure E-17a**).** The ratio of C_{DGT} and C_{pw} for Cu is low (0.15-0.50), suggesting that Cu is mostly unavailable at the studied sites. For 5.4 location 1 and location 2, Cu showed a relatively stable profile down to 10 cm depth, however, the labile concentration increased at depths > 10 cm. This trend corresponds well with Fe concentrations at 5.4 locations 1 and 2, where the labile Fe concentration increased with depth and could be due to the dissolution of Fe oxides/hydroxides under anoxic conditions.[373] For 22-23 locations, a slight increase in the Cu concentration was observed at depths between 5-8 cm which can be attributed to the dissolution of Mn oxides **(**Error! R eference source not found.f**).** The decrease in the concentration of Cu at depths > 8 cm can be due to association with stable sulfides in anoxic regions.[7,373]

The labile Ni concentration remained almost constant at all the depths at locations 5.4 location 1 and 22-23 location 2 **(**Figure E-17b**).** At 5.4 location 2, there was an increase in Ni concentration between depths 6-8 cm that relates well with the increase in Fe and Mn concentration observed at the same depths **(**Figure E-17 e,f); however, the Ni concentration decreased at greater depths indicating its associations with organic matter and sulfide moieties.[367] The trend observed for labile Ni concentration at 22-23 location 1 varied significantly from other locations. The concentration increased with depth and reached as high as 40 nM. This could be due to two reasons: (i) the majority of Ni is bound to Fe/Mn oxides/hydroxides, and the dissolution of these oxides/hydroxides might have resulted in the release of Ni in the porewater, and (ii) a change in the redox state of sediments caused the instability of sulfides resulting in the release of Ni into the porewater. Previous studies have seen the release of S and heavy metals at depths below 11

cm.[361,363,374] Overall, the ratio of C_{DGT} to C_{pw} for Ni varied between 0.2-0.5 indicating that the stream sediments effectively bind Ni at the studied locations.

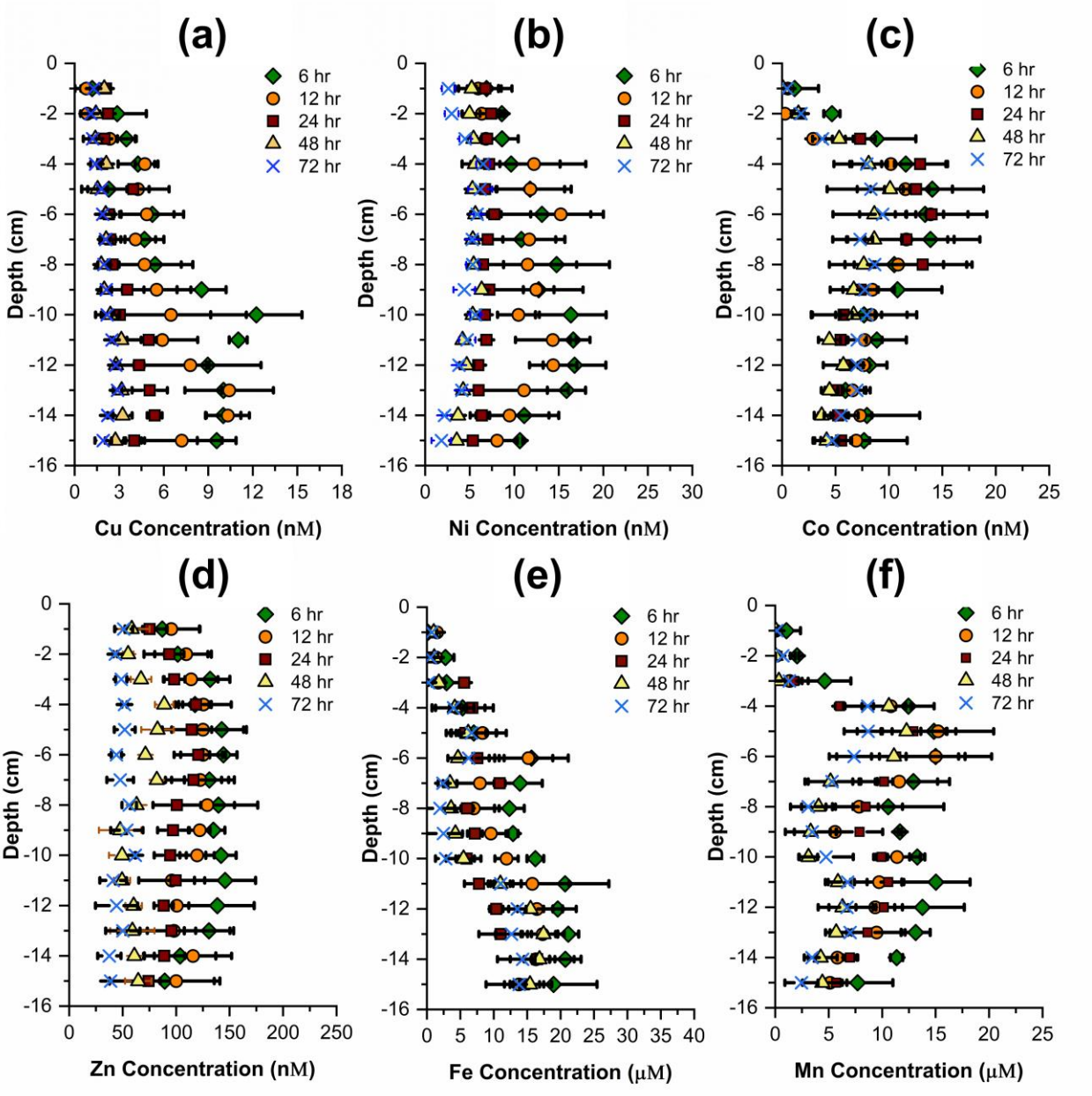

Figure E-9: DGT estimated concentrations for metals (a) Cu (b) Ni (c) Co (d) Zn (e) Fe and (f) Mn at 5.4 location 1 for deployment period of 6, 12, 24,48 and 72 hours.

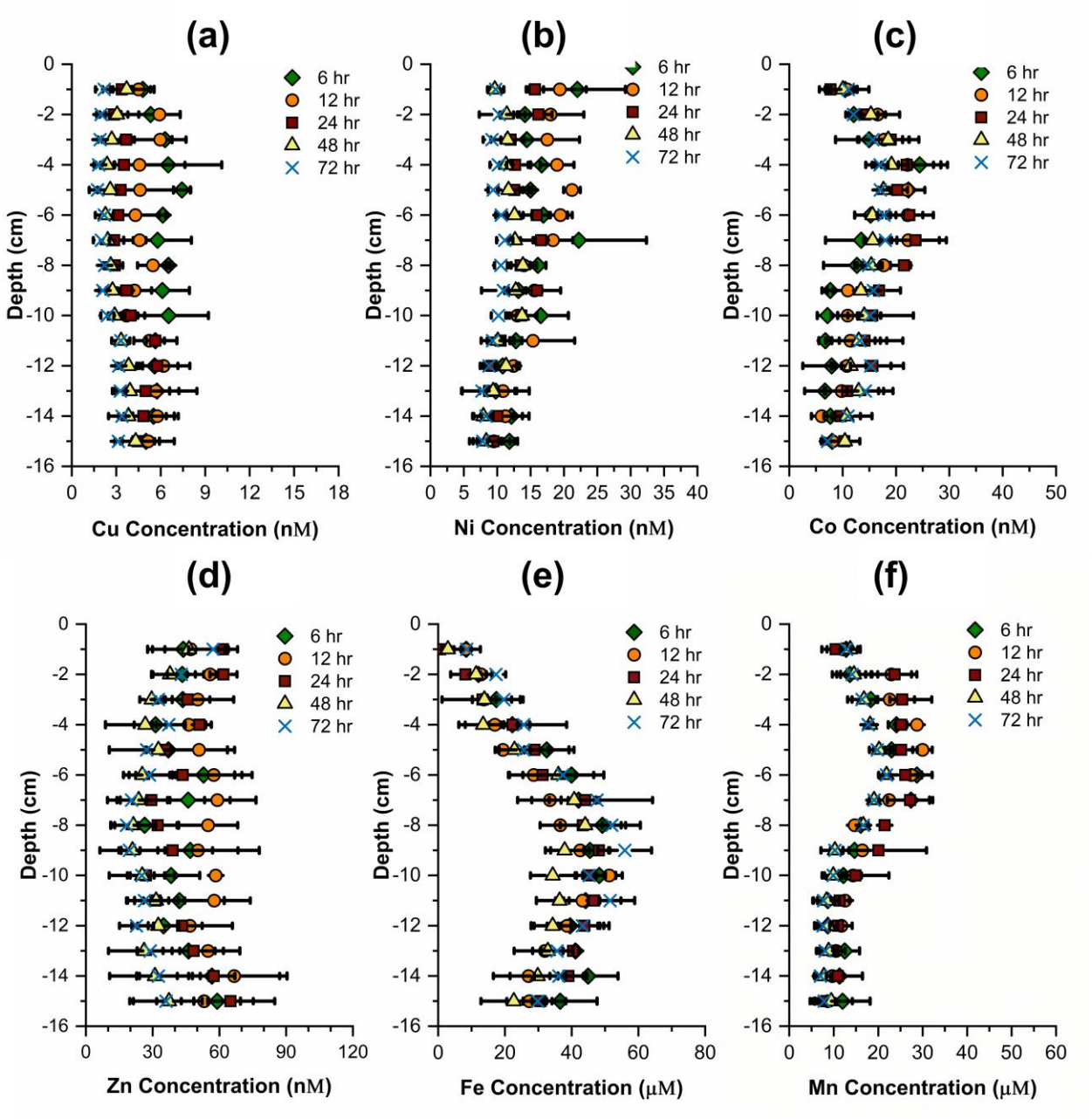

Figure E-10: DGT estimated concentrations for metals (a) Cu (b) Ni (c) Co (d) Zn (e) Fe and (f) Mn at 5.4 location 2 for deployment period of 6, 12, 24, 48 and 72 hours.

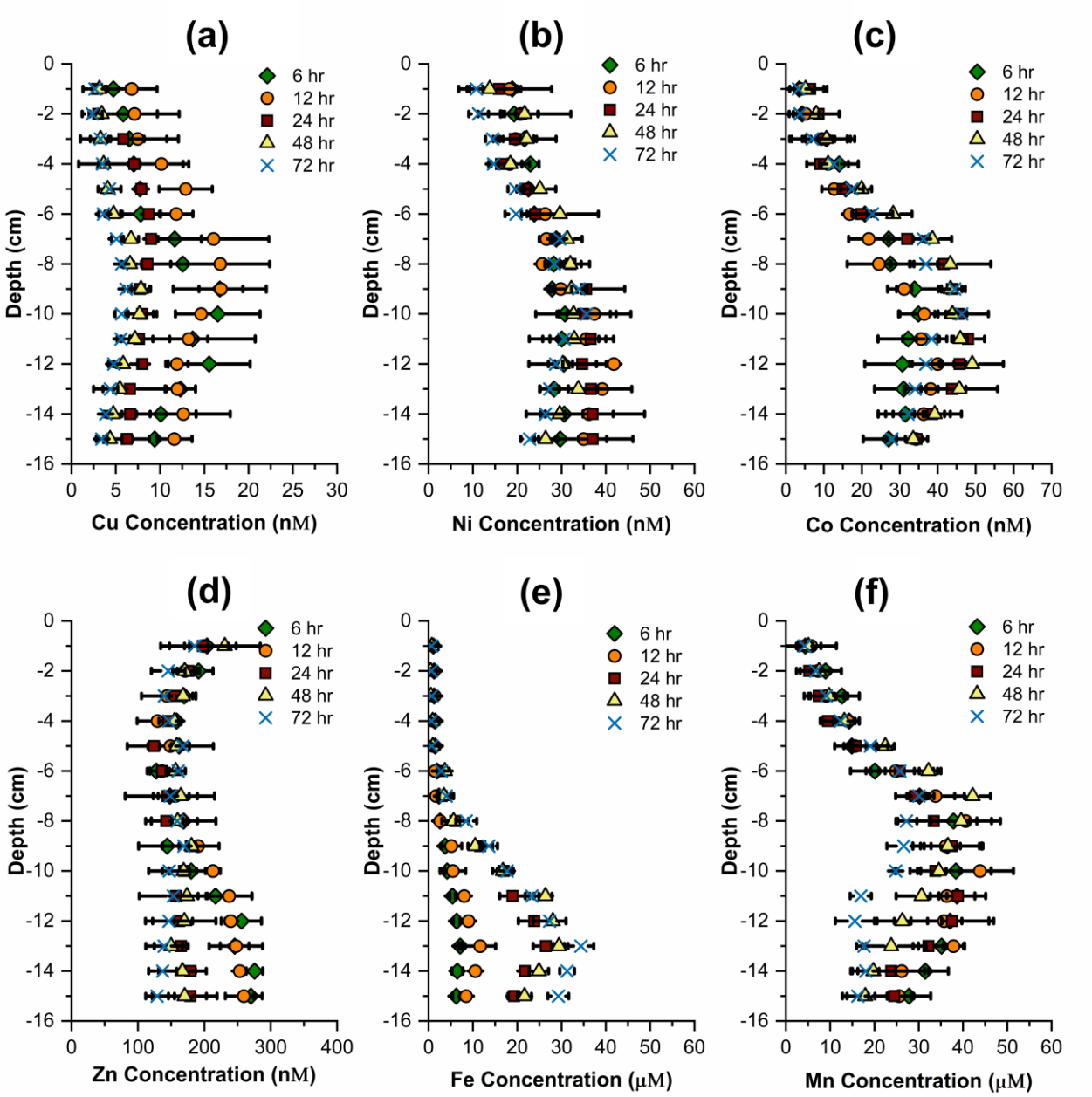

Figure E-11: DGT estimated concentrations for metals (a) Cu (b) Ni (c) Co (d) Zn (e) Fe and (f) Mn at 22-23 location 1 for deployment period of 6, 12, 24, 48 and 72 hours.

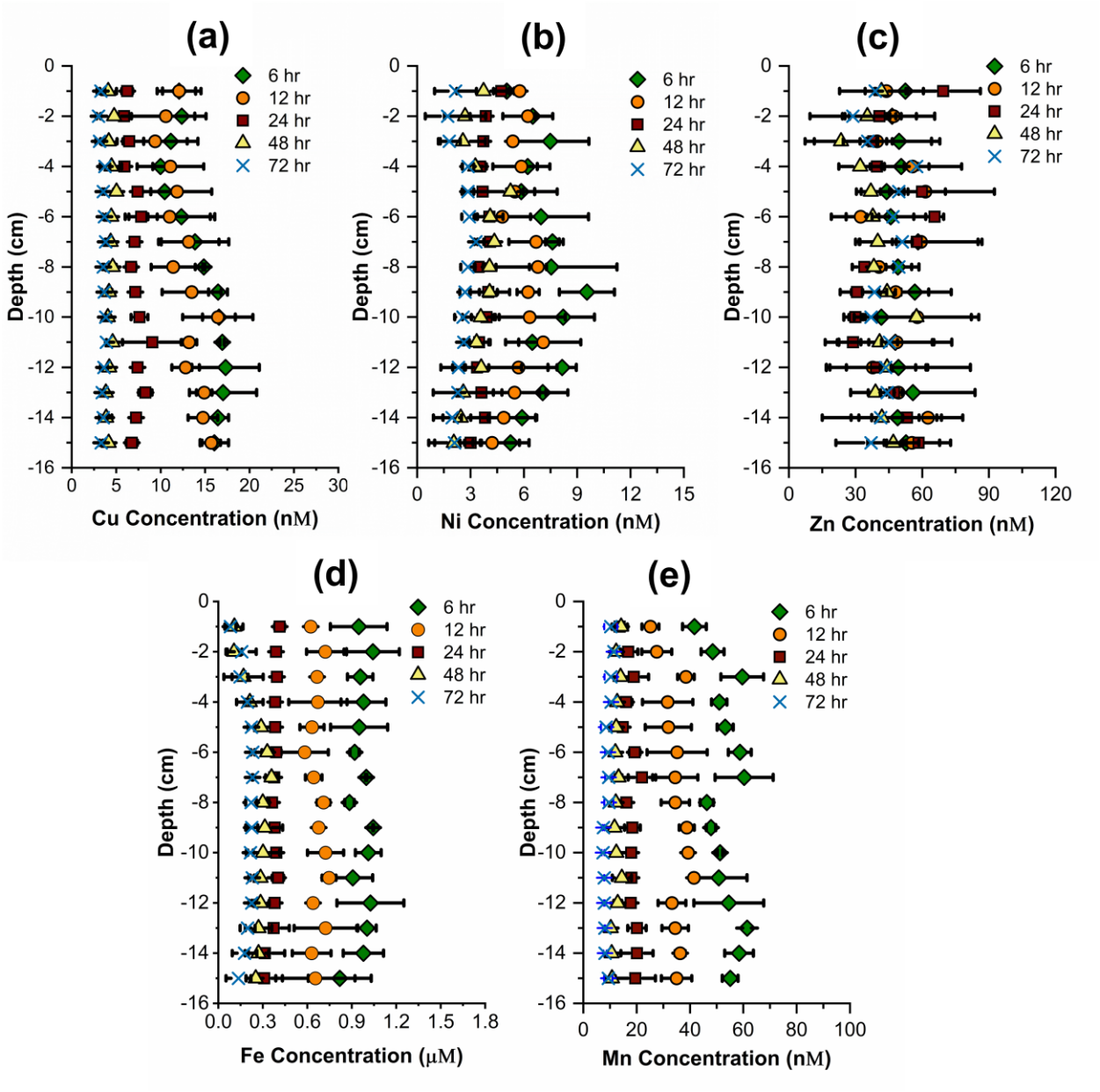

Figure E-12: DGT estimated concentrations for metals (a) Cu (b) Ni (c) Zn (d) Fe and (e) Mn at 22-23 location 2 for deployment period of 6, 12, 24, 48 and 72 hours.

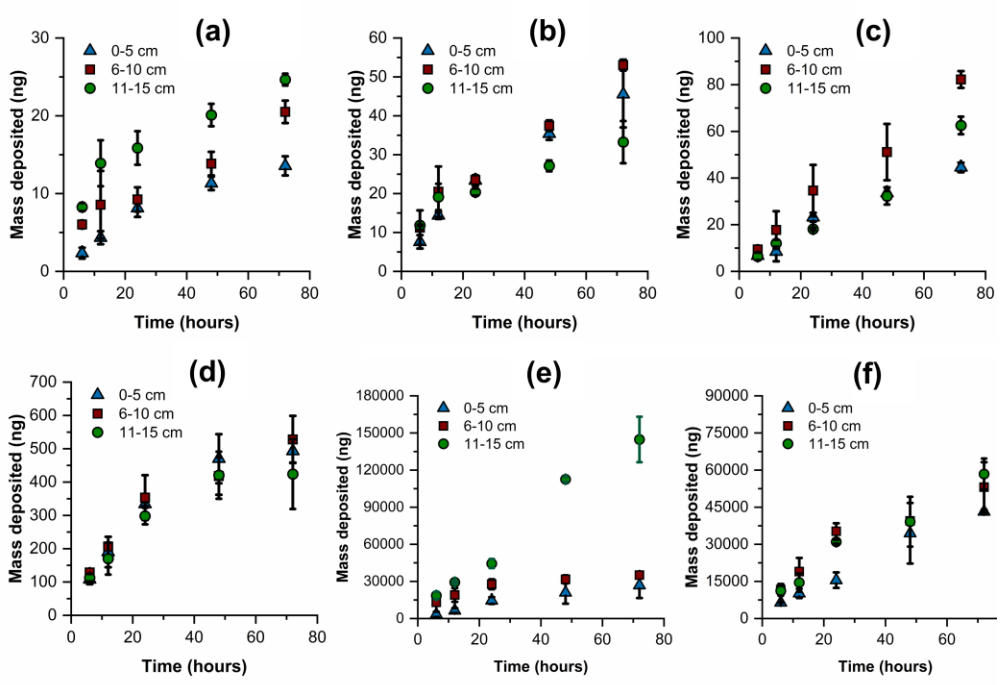

Figure E-13: Mass deposited on the resin gels with time for metals (a) Cu (b) Ni (c) Co (d) Zn (e) Fe and (f) Mn at 5.4 location 1.

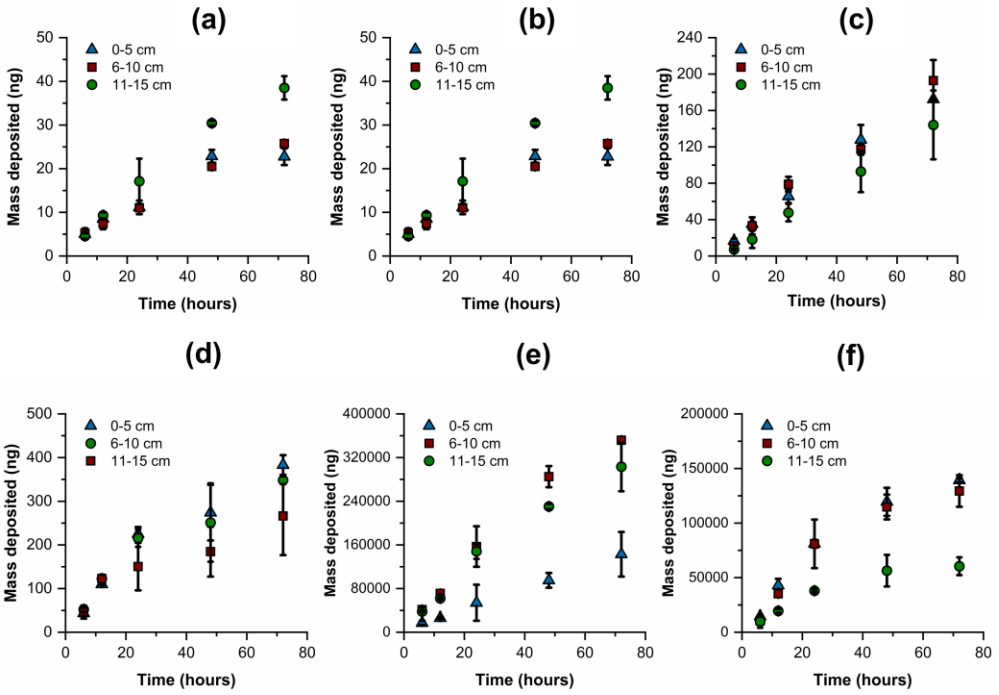

Figure E-14: Mass deposited on the resin gels with time for metals (a) Cu (b) Ni (c) Co (d) Zn (e) Fe and (f) Mn at 5.4 location 2.

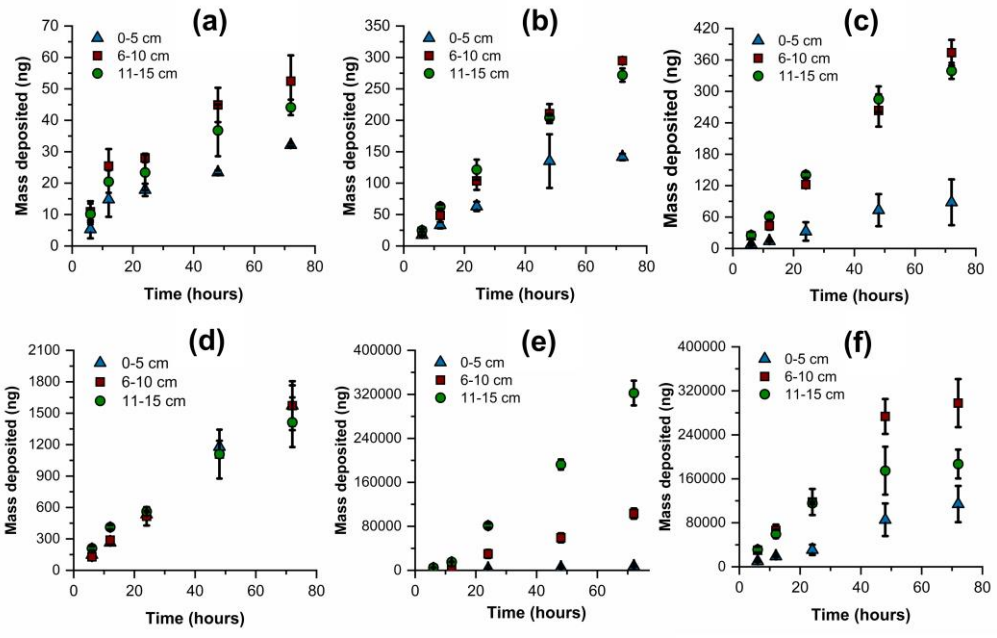

Figure E-15: Mass deposited on the resin gels with time for metals (a) Cu (b) Ni (c) Co (d) Zn (e) Fe and (f) Mn at 22-23 location 1.

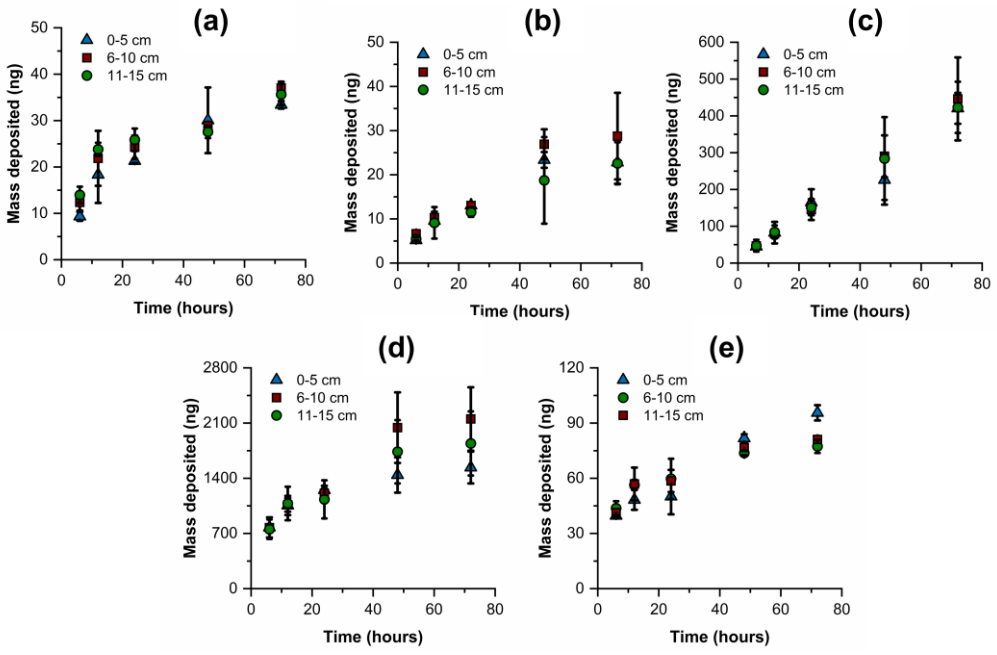

Figure E-16: Mass deposited on the resin gels with time for metals (a) Cu (b) Ni (c) Zn (d) Fe and (e) Mn at 22-23 location 2.

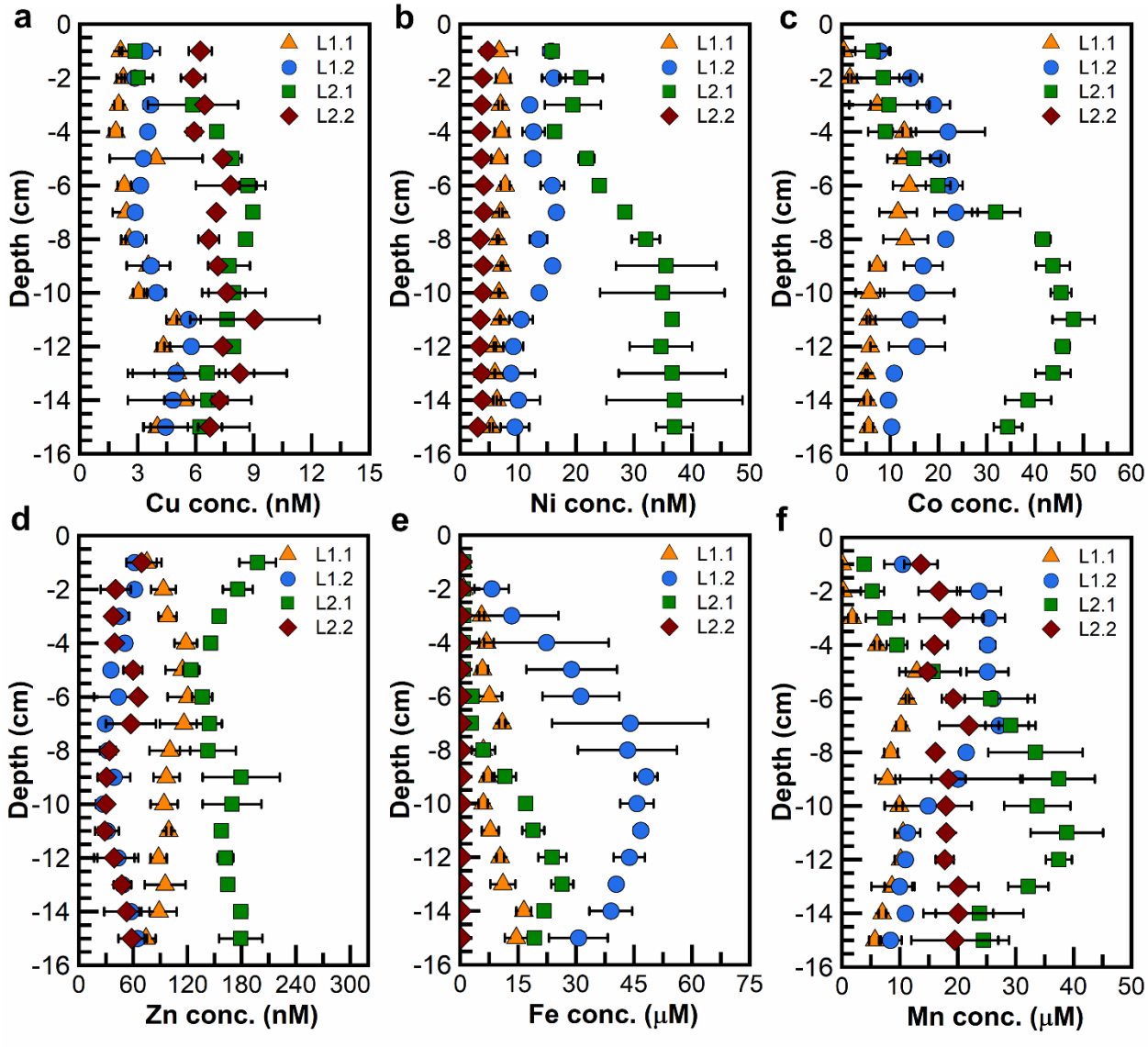

Figure E-17: DGT estimated concentration of metals (a) Cu (b) Ni (c) Co (d) Zn (e) Fe and (f) Mn at different locations for a deployment period of 24 hours.

Labile Co followed the same profile at 5.4 location 1 and 5.4 location 2, and the concentration varied at values below 25 nM at these locations **(**Figure E-17c). The trend relates well to the Mn profile at these locations suggesting that Co has strong associations with Mn oxides/hydroxides present at these locations **(**Figure E-17f). A dominant relationship between Co and Mn has also been observed in previous studies.[375,376] The decrease in Co concentration with

depth can be due to the formation of, or incorporation into, sulfide phases.[7,369] At 22-23 location 1, the Co concentration increased at depths > 5 cm, again similar to the profile obtained for Mn at that location. Co was not detected at 22-23 location 2. The ratio of C_{DGT} to C_{pw} goes as high as 0.9 at the studied locations indicating its high mobility.

The concentration change with depth for Zn is shown in Figure E-17d. The labile Zn concentration varied between 30 - 200 nM at the locations. The concentration profiles of Zn at 5.4 location 2 and 22-23 location 2 were quite similar, almost constant until 11 cm and then with a slight increase in the concentration below that depth. The increase in the Zn concentration below 11 cm can be due to the instability of sulfides caused by the change in the redox state of the sediments.[363,377] At 5.4 location 1, the Zn profile corresponds well with the Mn profile at the location indicating that reductive dissolution of Mn oxides could have resulted in the release of Zn to the porewater.[7,377,378] The profile obtained for Zn at 22-23 location 1 is different from the other locations, as the Zn concentration decreased up to 8 cm depth and then increased. The decrease in the Zn concentration could have been due to the associations with organic matter or sulfides in the sediments[364,377,378], however, the increase at depths > 8 cm could be due to microbial decomposition of organic matter, which could result in the release of Zn into the porewater.[378–381]

DGT-estimated Fe concentrations **(**Figure E-17e) remained almost negligible up to 7 cm depth at 22-23 location 1, indicating that Fe is bound in the form Fe oxy/hydroxides; however, the concentration increased between depths 8-13 cm which suggests the onset of reducing conditions resulting in the dissolution of Fe oxides. At depths > 13 cm, a decrease in Fe concentration was observed at 22-23 location 2. The lower level of Fe in deeper layers may be attributed to the formation of stable crystalline pyrite.[382–384] A similar trend was observed at 5.4 location 1. Labile Fe concentrations at 5.4 location 2 were significantly higher than all the other locations; however,

the trend was similar to other locations as the Fe concentration first increased down to 10 cm depth and then decreased. Very low labile Fe concentrations were detected at 22-23 location 2. Even the porewater concentration of Fe **(**Figure E-8**)** obtained by centrifuging the sediments was lower than at other locations. This suggests that the Fe present at 22-23 location 2 is not bioavailable and is present in the oxidized state in the form of Fe oxides/hydroxides.

C_{DGT} for Mn followed the same trend as observed for Fe as the concentration first increased and then decreased at all the locations, except at 22-23 location 2. The increase in concentration can be due to the dissolution of Mn oxides, and the decrease in concentration can be attributed to the incorporation of Mn into sulfides in deeper layers.[7,385] At 22-23 location 2, the labile Mn concentration almost remained constant throughout the entire depth.

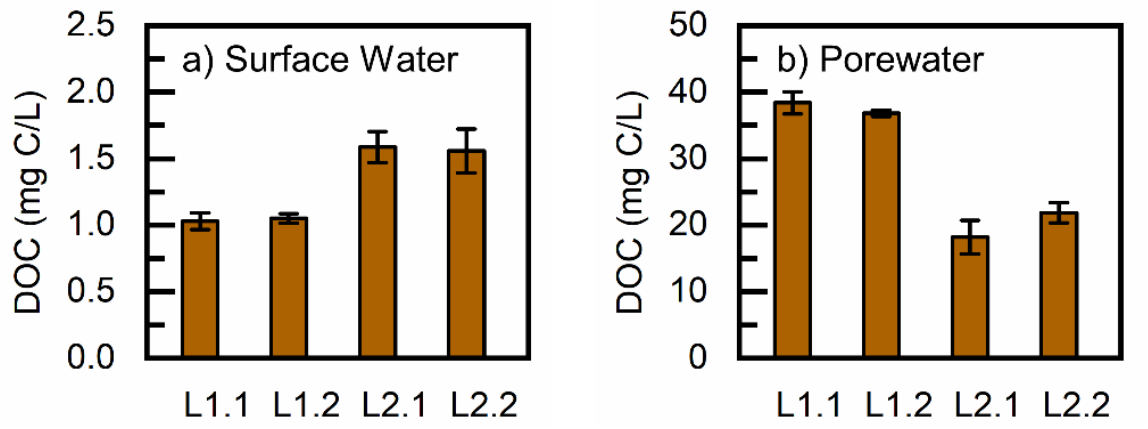

Figure E-18: Concentration of dissolved organic carbon concentrations in surface water and porewater of sediments

E.4 Key Findings

- Deploying DGT solution samplers and sediment probes for an extended period of time can lead to underestimation of the bioavailable fraction of metals at uncontaminated sites like ORNL.
- Depth profiles of metals vary substantially across different metals as well as locations. Variability in sediment characteristics and redox potential at different locations could drive these differences in metal depth profiles.
- The optimum concentration of Cu required for N_2O conversion to N_2 in denitrification lies in the range 4-10 nM.[3] Cu_{DGT} concentration at the selected locations is 3-9 nM and hence N_2O accumulation might not occur in the stream sediments at ORNL. Optimal methanogenic growth occurs at 0.2–2 μM Ni and 0.1–2 μM Co.[3] DGT-estimated Ni and Co concentrations are less than the optimum values, which indicates that these trace metals can play an important role in limiting methane emissions from stream sediments at ORNL.
  The trace metals in the porewater are not fully replenished from the sediments after DGT uptake, which suggests that the solid-phase pool of metals is not easily mobilized under a local sink induced due to DGT samplers.